

HYDROGEN AND METHANOL ACTIVATION BY SOME TERTIARY
PHOSPHINE RUTHENIUM COMPLEXES

By

CASHMAN ROGER STIRLING MASON HAMPTON

B.Sc., University of Victoria, 1967
M.Sc., Simon Fraser University, 1970

A THESIS SUBMITTED IN PARTIAL FULFILLMENT OF
THE REQUIREMENTS FOR THE DEGREE OF
DOCTOR OF PHILOSOPHY

in

THE DEPARTMENT OF CHEMISTRY

We accept this thesis as conforming
to the required standard

THE UNIVERSITY OF BRITISH COLUMBIA

September 1989

© Cashman Roger Stirling Mason Hampton, 1989

In presenting this thesis in partial fulfilment of the requirements for an advanced degree at the University of British Columbia, I agree that the Library shall make it freely available for reference and study. I further agree that permission for extensive copying of this thesis for scholarly purposes may be granted by the head of my department or by his or her representatives. It is understood that copying or publication of this thesis for financial gain shall not be allowed without my written permission.

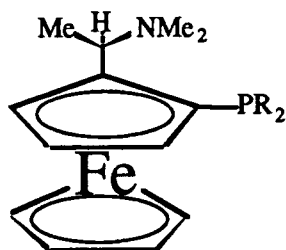
Department of Chemistry

The University of British Columbia
Vancouver, Canada

Date Nov 9, 1989

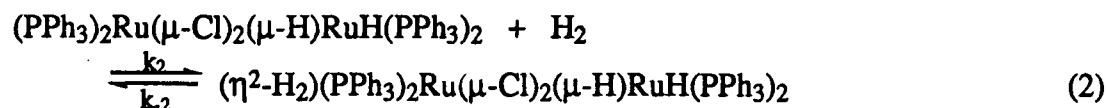
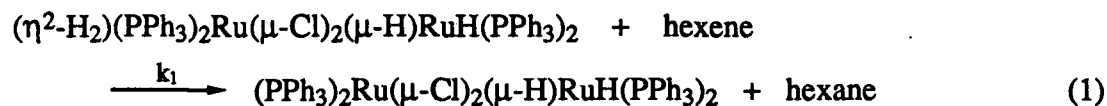
Abstract

The previously known complexes, $\text{Ru}_2\text{H}_4\text{Cl}_2(\text{PR}_3)_4$, have now been correctly reformulated as the $\eta^2\text{-H}_2$ species $(\eta^2\text{-H}_2)(\text{PR}_3)_2\text{Ru}(\mu\text{-Cl})_2(\mu\text{-H})\text{RuH}(\text{PR}_3)_2$ ($\text{R} = \text{Ph}$, $p\text{-tol}$), **1a** and **1b**, and it is confirmed that in solution they are dimeric and undergo no ligand dissociation. Also, a new analogue of complexes of type **1** is reported: the complex $(\eta^2\text{-H}_2)(\text{isoPFA})\text{Ru}(\mu\text{-Cl})_2(\mu\text{-H})\text{RuH}(\text{PPh}_3)_2$, **4**, is formed from the reaction of $\text{RuCl}_2(\text{PPh}_3)(\text{isoPFA})$, **3b**, with H_2 in methanol/benzene, and a crystal structure of **4** shows the $\eta^2\text{-H}_2$ ligand; isoPFA and PPFA (see below) are ferrocene based, chelating P-N ligands, with the structures:



$\text{R} = \text{Pr}^i$ and Ph for isoPFA and PPFA, respectively. Complexes **1a**, **1b** and **4** all react with 1-hexene to give hexane; the main ruthenium phosphine product in the case of **1** is the corresponding $\text{RuHCl}(\text{PR}_3)_3$ complex, while **4** reacts to give a complex mixture of ruthenium phosphine complexes, including **3b**. The amount of hexane formed from the reaction of **4** with hexene is quantified as 2 mol/mol **4**.

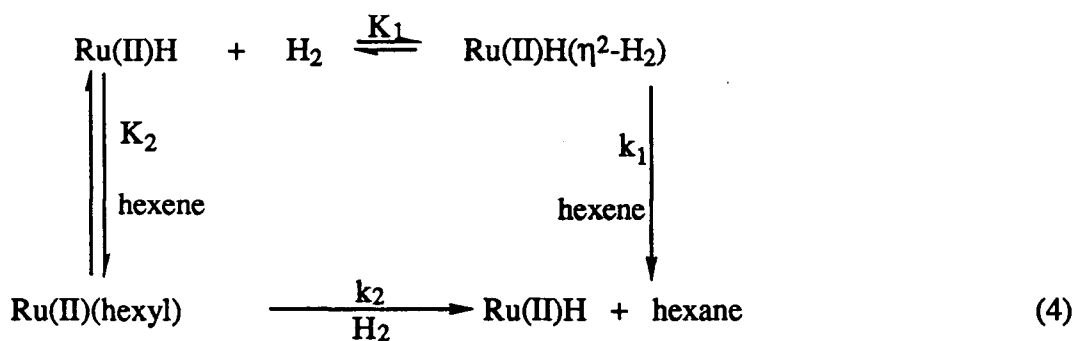
The hydrogenation of 1-hexene catalyzed by **1a** is re-interpreted as occurring via the mechanism:



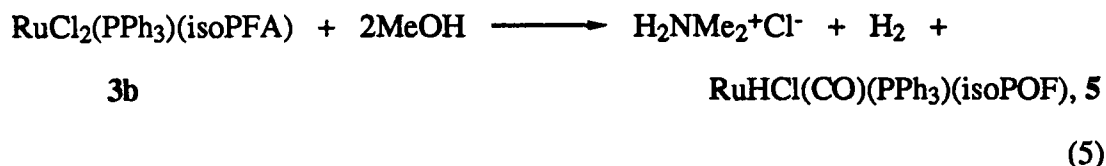
Reactions of $\text{RuCl}_2(\text{PPh}_3)(\text{PPFA})$, **3a**, and $\text{RuCl}_2(\text{PPh}_3)(\text{isoPFA})$, **3b**, with H_2 have been further studied, in connection with earlier mechanistic studies on the

hydrogenation of organic substrates catalyzed by complex **3a**. The complex **3a** reacts with 2 - 8 atm H₂ in *n*-butanol to give ruthenium phosphine products including **1a**. The complex **3b** reacts with H₂ in methanol/benzene to give **4**, as mentioned above, as well as a number of unidentified hydrides; in DMA, the reaction of **3b** with H₂ gives **1a**, **4**, RuHCl(PPh₃)(isoPFA) (**7**), RuHCl(PPh₃)₃ and other unidentified ruthenium phosphine complexes. The product H₂NMe₂⁺Cl⁻ was also isolated from the methanol/benzene reaction mixture, and this product provides evidence that the amine functionality of the P-N ligands is involved in the promotion of the heterolytic cleavage of dihydrogen to give a proton and a hydride (H₂ \longrightarrow H⁺ + H⁻).

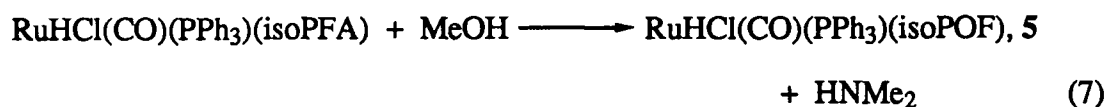
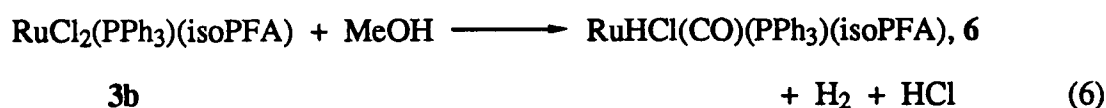
Kinetic studies on the hydrogenation of 1-hexene catalyzed by **3a**, and by **3b** in the present work, are now interpreted according to the mechanism:



Reactions involving **3b** and methanol have also been studied, and **3b** is also active for the transfer hydrogenation (from methanol) of ketones and activated olefins. The reaction of **3b** with methanol in the absence of base is proposed to occur with the stoichiometry:

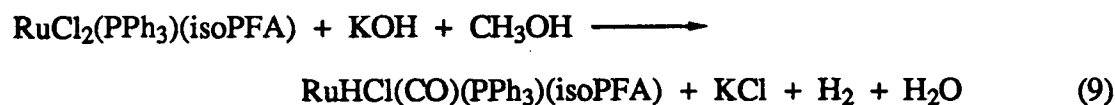


where the ligand isoPOF is formed from isoPFA by replacement of the NMe₂ group on isoPFA by a methoxy group; reaction 6 could occur via the following steps:



A mechanism for reaction 7 is presented and invokes reversible attack by MeOH with replacement of Cl⁻, followed by reversible deprotonation of coordinated MeOH to give successively methoxy, formaldehyde and formyl intermediates, and finally the hydrido-carbonyl, **6**.

The reaction of **3b** with methanol in the presence of KOH is proposed to occur according to the stoichiometry:



and two pathways have been identified, one base-independent, identical to that proposed for reaction 7, and one showing a second-order dependence on KOH. The latter pathway invokes initial reversible attack on RuCl₂(PPh₃)(isoPFA), **3b**, by MeO⁻, replacing Cl⁻ to give RuCl(OMe)(PPh₃)(isoPFA), and subsequent reversible replacement of PPh₃ by OH⁻, followed by concerted loss of OH⁻ and hydride transfer from coordinated OMe⁻ to give a

hydrido-formaldehyde complex $\text{RuHCl}(\eta^2\text{-CH}_2\text{O})(\text{isoPFA})$. A subsequently formed formyl intermediate reacts via intramolecular hydride transfer from the formyl to the metal, H_2 loss, and phosphine coordination to give the hydrido-carbonyl **6**.

Table of Contents

Abstract.....	ii
List of Tables	xiv
List of Figures.....	xvi
List of Symbols and Abbreviations	xxiii
Acknowledgements	xxviii
Chapter 1 Introduction	1
Chapter 2 General experimental.....	5
2.1 General procedures.....	5
2.2 Instrumentation	8
2.3 NMR studies	11
2.4 Materials.....	12
Solvents	12
Gases	12
Phosphines.....	12
Olefin and ketone substrates	12
Other materials	13
Ruthenium complexes	13
$(\eta^2\text{-H}_2)(\text{PR}_3)_2\text{Ru}(\mu\text{-Cl})_2(\mu\text{-H})\text{RuH}(\text{PR}_3)_2$ (R = Ph, p-tol),	
1a, 1b.	13

$\text{Ru}_2\text{Cl}_4(\text{PR}_3)_4$ (R = Ph, p-tol), 2a , 2b	14
$\text{RuCl}_2(\text{PPh}_3)(\text{PPFA})$, 3a	15
$\text{RuCl}_2(\text{PPh}_3)(\text{isoPFA})$, 3b	16
$(\eta^2\text{-H}_2)(\text{isoPFA})\text{Ru}(\mu\text{-Cl})_2(\mu\text{-H})\text{RuH}(\text{PPh}_3)_2$, 4	17
$\text{RuHCl}(\text{CO})(\text{PPh}_3)(\text{isoPOF})$, 5	18
$\text{RuHCl}(\text{CO})(\text{PPh}_3)(\text{isoPFA})$, 6	19
$\text{RuHCl}(\text{PPh}_3)(\text{isoPFA})$, 7	20

Chapter 3 Characterization and reactivity of some dinuclear ruthenium(II)

phosphine complexes containing $\eta^2\text{-H}_2$	22
3.1 Introduction.....	22
Historical background.....	22
Factors affecting the stability of $\eta^2\text{-H}_2$ complexes of the transition metals.....	23
Theoretical considerations.....	24
Criteria for recognition of dihydrogen complexes.....	27
Dinuclear, $\eta^2\text{-H}_2$ complexes reported in the present work.....	32
3.2 Experimental.....	36
Crystal structures.....	36
Visible spectrophotometry.....	36
NMR spectra.....	36
Reactions of 1a and 1b with 1-hexene.....	37
Reactions of $(\eta^2\text{-H}_2)(\text{isoPFA})\text{Ru}(\mu\text{-Cl})_2(\mu\text{-H})\text{RuH}(\text{PPh}_3)_2$, 4	37
Preparation and observation of dihydrogen adducts of 2a and 2b <i>in situ</i>	37
3.3 Results.....	38
Complexes 1a , 1b and 4	38

Dihydrogen adducts of $\text{Ru}_2\text{Cl}_4(\text{PR}_3)_4$ ($\text{R} = \text{Ph}, \text{p-tol}$), 2a and 2b	67
3.4 Discussion	67
Complexes 1a , 1b and 4	67
Dihydrogen adducts of the complexes, $\text{Ru}_2\text{Cl}_4(\text{PR}_3)_4$ ($\text{R} = \text{Ph}, \text{p-tol}$), 2a and 2b	79
 Chapter 4 Mechanistic studies on hydrogenation catalyzed by tertiary phosphine complexes of ruthenium(II)	81
4.1 Introduction	81
Hydrogenation of 1-hexene catalyzed by 1a	83
Hydrogenation systems catalyzed by 3a and 3b	86
Hydrogenation systems catalyzed by 3a	87
Hydrogenation systems catalyzed by $\text{RuCl}_2(\text{PPh}_3)(\text{isoPFA})$, 3b	91
4.2 Experimental	91
Reactions of $\text{RuCl}_2(\text{PPh}_3)(\text{PPFA})$, 3a , with H_2 in toluene- d_8 , toluene- d_8 /butanol and butanol	91
Reactions of $\text{RuCl}_2(\text{PPh}_3)(\text{isoPFA})$, 3b , with hydrogen in DMA, DMA/ C_6D_6 , and benzene/methanol	93
Catalytic hydrogenations of prochiral substrates using $\text{RuCl}_2(\text{PPh}_3)(\text{PPFA})$, 3a , and $\text{RuCl}_2(\text{PPh}_3)(\text{isoPFA})$, 3b	95
NMR studies of the catalytic hydrogenation of 1-hexene by 3a , 3b and $(\eta^2\text{-H}_2)(\text{PPh}_3)_2\text{Ru}(\mu\text{-Cl})_2(\mu\text{-H})\text{RuH}(\text{PPh}_3)_2$, 1a	95
Hydrogen-uptake measurements for 1-hexene hydrogenation.....	96
4.3 Results	96
Reactions of $\text{RuCl}_2(\text{PPh}_3)(\text{PPFA})$, 3a , with hydrogen in toluene- d_8 , toluene- d_8 /butanol and butanol.....	96

Reactions of $\text{RuCl}_2(\text{PPh}_3)(\text{isoPFA})$, 3b , with hydrogen in DMA, DMA/ C_6D_6 , and benzene/methanol	109
In the presence of added PPh_3	109
In the absence of added PPh_3	109
Catalytic hydrogenations of prochiral substrates catalyzed by (<i>S,R</i>)- $\text{RuCl}_2(\text{PPh}_3)(\text{PPFA})$, 3a and (<i>S,R</i>)- $\text{RuCl}_2(\text{PPh}_3)(\text{isoPFA})$, 3b	115
NMR studies of the catalytic hydrogenation of 1-hexene by $(\eta^2\text{-H}_2)(\text{PPh}_3)_2\text{Ru}(\mu\text{-Cl})_2(\mu\text{-H})\text{RuH}(\text{PPh}_3)_2$, 1a , $\text{RuCl}_2(\text{PPh}_3)(\text{PPFA})$, 3a and $\text{RuCl}_2(\text{PPh}_3)(\text{isoPFA})$, 3b	115
The 1a system.....	115
The 3a system.....	118
The 3b system.....	119
Kinetic data from hydrogen-uptake measurements for 1-hexene hydrogenation.....	120
using $(\eta^2\text{-H}_2)(\text{PPh}_3)_2\text{Ru}(\mu\text{-Cl})_2(\mu\text{-H})\text{RuH}(\text{PPh}_3)_2$, 1a , as catalyst.....	120
using compound A as catalyst, prepared from $\text{RuCl}_2(\text{PPh}_3)(\text{PPFA})$, 3a , and H_2 in butanol.....	120
using $\text{RuCl}_2(\text{PPh}_3)(\text{isoPFA})$, 3b as catalyst.....	121
using $(\eta^2\text{-H}_2)(\text{isoPFA})\text{Ru}(\mu\text{-Cl})_2(\mu\text{-H})\text{RuH}(\text{PPh}_3)_2$, 4 as catalyst.....	123
4.4 Discussion	123
The $(\eta^2\text{-H}_2)(\text{PPh}_3)_2\text{Ru}(\mu\text{-Cl})_2(\mu\text{-H})\text{RuH}(\text{PPh}_3)_2$, 1a 1-hexene hydrogenation system.....	123
Hydrogenations involving $\text{RuCl}_2(\text{PPh}_3)(\text{PPFA})$, 3a	127
Reactions of 3a with H_2	127
Hydrogenation systems catalyzed by 3a	130

Hydrogenations involving RuCl ₂ (PPh ₃)(isoPFA), 3b	132
Hydrogenation of 1-hexene catalyzed by	
RuCl ₂ (PPh ₃)(isoPFA), 3b	132
Hydrogenation of prochiral substrates catalyzed by	
RuCl ₂ (PPh ₃)(PPFA), 3a , and RuCl ₂ (PPh ₃)(isoPFA), 3b	133
 Chapter 5 Reactions of RuCl ₂ (PPh ₃)(isoPFA) and derivatives with methanol	135
5.1 Introduction	135
Mechanistic Studies	142
5.2 Experimental	147
Experiments on the effects of various solvents, added PPh ₃ and air,	
respectively, on visible spectra of RuCl ₂ (PPh ₃)(isoPFA), 3b , in	
solution	147
Experiment on the effect of styrene on 3b in solution	147
Reactions of RuCl ₂ (PPh ₃)(isoPFA), 3b , and the derivative,	
RuHCl(CO)(PPh ₃)(isoPOF), 5 , with methanol in the absence of	
added base.....	148
Catalytic activity of 5 and 3b	148
Reactions of RuCl ₂ (PPh ₃)(isoPFA), 3b , and derivatives with	
methanol in the presence of added base.....	149
With Proton Sponge [®] as base.....	149
With KOH as base	150
Experiments on the reaction of RuCl ₂ (PPh ₃)(isoPFA), 3b , with	
KOH/methanol, in THF in the presence or absence of styrene	151
Monitoring changes in the ³¹ P{ ¹ H} NMR spectrum	153
Monitoring changes in the visible spectrum.....	153
Monitoring changes in the styrene/ethylbenzene ratio.....	154

Monitoring gas evolution.....	155
Detection of KCl produced in the reaction of RuCl ₂ (PPh ₃)(isoPFA), 3b , with KOH/MeOH.....	158
Formaldehyde detection	158
Experiment to detect gas phase CO by GC.....	159
² D NMR experiments on distillates from reactions of 3b with KOH/MeOH-d ₄ and MeOH-d ₁	159
An experiment to determine what would happen to CH ₂ O generated in a solution similar to those used for the reactions of 3b with KOH/MeOH	160
Reactions of RuHCl(CO)(PPh ₃)(isoPFA), 6 , with methanol in the absence and presence of base	160
5.3 Results	161
Experiments on the effects of various solvents, added PPh ₃ and air, respectively, on visible spectra of RuCl ₂ (PPh ₃)(isoPFA), 3b , in solution	161
Experiment on the effect of styrene on 3b in solution	161
Reactions of RuCl ₂ (PPh ₃)(isoPFA), 3b , and RuHCl(CO)(PPh ₃)(isoPOF), 5 , with methanol in the absence of base	163
Reactions of RuCl ₂ (PPh ₃)(isoPFA), 3b , with methanol in the presence of added base	170
With Proton Sponge [®] as added base	170
With KOH as base	175
Reactions of RuHCl(CO)(PPh ₃)(isoPFA), 6 , with methanol in the absence and presence of base	184

Experiments on the reaction of RuCl ₂ (PPh ₃)(isoPFA), 3b , with KOH/methanol, in THF in the presence or absence of styrene	185
Experiment to determine the reactivity of THF with methanolic KOH.....	185
Monitoring the ³¹ P{ ¹ H} NMR spectrum.....	185
Work-up of THF/MeOH reaction mixtures	188
Gas evolution experiment results.....	189
Monitoring the THF/MeOH reaction by visible spectrophotometry.....	191
Detection of KCl.....	209
Formaldehyde detection	210
Experiment to detect gas phase CO by GC.....	210
² D NMR experiments on distillates from reactions of 3b with KOH/MeOH-d ₄ and MeOH-d ₁	210
An experiment to determine what would happen to CH ₂ O generated in a solution similar to those used for the reactions of 3b with KOH/MeOH	213
5.4 Discussion.....	214
Solution behaviour of RuCl ₂ (PPh ₃)(isoPFA), 3b	214
Reactions of RuCl ₂ (PPh ₃)(isoPFA), 3b , and derivatives with methanol in the absence of added base.....	214
Reactions of RuCl ₂ (PPh ₃)(isoPFA), 3b , with methanol in the presence of added base	218
With Proton Sponge [®] as added base	218
With KOH as added base.....	222
Experiments on the reaction of RuCl ₂ (PPh ₃)(isoPFA), 3b , with KOH/methanol, in THF in the presence or absence of styrene	223

Organic and gaseous products from high [KOH] reactions	233
The base-independent mechanism and the reaction of RuCl ₂ (PPh ₃)(isoPFA), 3b with methanol in the presence of Proton Sponge [®]	233
The base-independent mechanism and the reaction of RuCl ₂ (PPh ₃)(isoPFA), 3b , with methanol in the absence of base.....	234
 Chapter 6 Summary and suggestions for further work	 235
 Bibliography	 241

List of Tables

Table 3.1 Transition metals which have been found in molecular hydrogen complexes.....	23
Table 3.2 Electronic configurations and oxidation states of examples of η^2 -H ₂ complexes.....	24
Table 3.3 Coordination numbers of η^2 -H ₂ complexes, according to electron configuration.....	24
Table 3.4 Vibrational frequencies, $\nu_{\text{HH}}(\text{cm}^{-1})$, for dihydrogen complexes.....	26
Table 3.5 Some ¹ H NMR HD coupling constants (Hz) for η^2 -H ₂ resonances.....	29
Table 3.6 Selected T ₁ (minimum) values for various hydride and dihydrogen complexes.....	31
Table 3.7 Selected bond angles and distances for crystal structures of 1a and 1b	39
Table 3.8 Selected bond angles and distances for the crystal structure of 4	41
Table 3.9 Spectroscopic data for 1a	72
Table 4.1 T ₁ (300 MHz) values for upfield ¹ H NMR resonances observed for the reaction of RuCl ₂ (PPh ₃)(PPFA), 3a , with H ₂ in toluene-d ₈ /butanol at ambient temperature.....	101
Table 4.2 Hydrogenation results for various substrates using (<i>S,R</i>)-RuCl ₂ (PPh ₃)(PPFA), 3a and (<i>S,R</i>)-RuCl ₂ (PPh ₃)(isoPFA), 3b as catalysts.....	116
Table 5.1 Selected bond distances for complexes RuHCl(CO)(PPh ₃)(isoPOF), 5 , RuHCl(CO)(PPh ₃)(isoPFA), 6 , and RuHCl(PPh ₃)(isoPFA), 7	165
Table 5.2 Selected bond angles associated with the bond distances shown in Table 5.1.....	166
Table 5.3 Catalytic hydrogen transfer from methanol, catalyzed by RuCl ₂ (PPh ₃)(isoPFA), 3b , in neat methanol at 105 °C in the absence of base.....	170
Table 5.4 Colour changes of reaction mixtures and rates of hydrogen transfer from methanol to styrene to give ethylbenzene, as a function of time and initial [KOH].....	177
Table 5.5 Selected molecular structure parameters for RuH ₂ (CO)(PPh ₃) ₃	182
Table 5.6 Some kinetic data for the reaction of RuCl ₂ (PPh ₃)(isoPFA), 3b , with KOH/MeOH in the absence of styrene.....	197
Table 5.7 Some kinetic data for the reaction of RuCl ₂ (PPh ₃)(isoPFA), 3b , with KOH/MeOH showing dependence on [styrene].....	198

Table 5.8 Summary of kinetic data from the GC experiments used to follow styrene hydrogenation during the reaction of 3b with KOH/MeOH in the presence of styrene.....	204
Table 5.9 Comparison of structural parameters of RuHCl(PPh ₃)(isoPFA), 7 , and RuHCl(PPh ₃) ₃	221

List of Figures

Figure 1.1 Structure of FA, PPFA and isoPPFA	3
Figure 2.1 Apparatus for filling tubes with pressures up to 10 atm.....	6
Figure 2.2 Glass apparatus used for manipulating materials under elevated hydrogen pressures, up to 10 atm.....	7
Figure 2.3 Visible spectrophotometer cell (5 cm).....	9
Figure 2.4 Visible spectrophotometer cell (1 mm).....	9
Figure 3.1 Orbital diagrams showing the contributions to the bonding for the M- $(\eta^2\text{-H}_2)$ structure.....	26
Figure 3.2 The skeletal structure of 1a	40
Figure 3.3 The skeletal structure of 1b	40
Figure 3.4 The molecular structure of 4 showing the positions of hydrogen ligands.....	42
Figure 3.5 The visible spectrum of 1a	43
Figure 3.6 Observed and calculated, variable temperature $^{31}\text{P}\{^1\text{H}\}$ NMR of 1a	44
Figure 3.7 Eyring plot for rate constants for phosphine exchange in 1a	45
Figure 3.8 Observed and calculated, variable temperature ^1H NMR spectra of 1a	46
Figure 3.9 General hydrogen ligand exchange model used to simulate hydrogen ligand exchange within 1a , 1b and 4	47
Figure 3.10 Plot of ^1H NMR chemical shifts versus temperature for terminal and bridging hydride ligands in 1a , with extrapolation to 20 °C.....	47
Figure 3.11 Plot of ^1H NMR T_2 values versus temperature for the $\eta^2\text{-H}_2$ ligand of 1a	47
Figure 3.12 Eyring plot for rate constants for hydrogen ligand exchange in 1a	48
Figure 3.13 Plot of T_1 values versus temperature for hydrogen ligands of 1a	49
Figure 3.14 Observed and calculated variable temperature ^1H NMR spectra for hydrogen ligands of 1b	50
Figure 3.15 Plot of ^1H NMR chemical shifts versus temperature for the $\eta^2\text{-H}_2$ and terminal hydride ligands of 1b , including extrapolation to 20 °C.....	51

Figure 3.16 Plot of ^1H NMR T_2 values versus temperature for the $\eta^2\text{-H}_2$ ligand of 1b , including extrapolation to 20 °C.....	52
Figure 3.17 Eyring plot for rate constants for hydrogen ligand exchange in 1b	53
Figure 3.18 Inversion-recovery method plot for ^1H NMR T_1 measurements for the hydrogen ligands of 1b	54
Figure 3.19 Plot of ^1H NMR T_1 values versus temperature for the hydrogen ligands of 1b	54
Figure 3.20 The $^{31}\text{P}\{^1\text{H}\}$ NMR spectrum of 4	56
Figure 3.21 The ^1H NMR spectrum of 4	57
Figure 3.22 Observed and calculated variable temperature ^1H NMR data for 4	58
Figure 3.23 ^1H NMR T_2 values versus temperature for the $\eta^2\text{-H}_2$ ligand of 4 , with extrapolation to higher temperatures.	59
Figure 3.24 Dependence of the ^1H NMR chemical shift on temperature for the $\mu\text{-H}$ ligand of 4	60
Figure 3.25 Eyring plot for the k_1 values ($\eta^2\text{-H}_2/\mu\text{-H}$ exchange) for 4	61
Figure 3.26 Inversion-recovery plot for ^1H NMR T_1 measurements for the hydrogen ligands of 4	61
Figure 3.27 Plot of ^1H NMR T_1 values versus temperature for the hydrogen ligands of 4	62
Figure 3.28 ^1H NMR spectrum of 1b , after two weeks under vacuum at ambient temperature.....	64
Figure 3.29 $^{31}\text{P}\{^1\text{H}\}$ NMR spectrum of 1b , after two weeks under vacuum at ambient temperature.....	65
Figure 3.30 Slow exchange structure showing proposed hydrogen ligand positions for 1b , reported as a classical tetrahydride.....	69
Figure 3.31 $^{31}\text{P}\{^1\text{H}\}$ NMR coupling pattern for complex 1a	71
Figure 3.32 The $^{31}\text{P}\{^1\text{H}\}$ NMR coupling pattern for complex 4	78
Figure 4.1 Uptake plots for the 1a -catalyzed hydrogenation of 1-hexene.....	84
Figure 4.2 Dependence of maximum rate of hydrogenation on total Ru concentration (1a) in DMA at 30 °C	84
Figure 4.3 Dependence of maximum rate of 1a -catalyzed hydrogenation on 1-hexene concentration.....	84

Figure 4.4 Dependence of maximum rate of 1a -catalyzed hydrogenation on hexene concentration, plotted according to equation 4.18.....	84
Figure 4.5 Dependence of maximum rate of 1a -catalyzed hydrogenation on hydrogen concentration.....	85
Figure 4.6 Dependence of maximum rate of 1a -catalyzed hydrogenation on hydrogen concentration, plotted according to equation 4.19.....	85
Figure 4.7 Dependence of maximum rate of 1a -catalyzed hydrogenation on added triphenylphosphine concentration.	85
Figure 4.8 Dependence of the maximum rate of 1a -catalyzed hydrogenation on $[\text{PPh}_3]^{-1}$	85
Figure 4.9 Dependence of maximum rate of 1a -catalyzed hydrogenation on added lithium chloride concentration.....	86
Figure 4.10 Dependence of maximum rate of 3a -catalyzed hydrogenation on total Ru concentration.....	89
Figure 4.11 Dependence of maximum rate of 3a -catalyzed hydrogenation on 1-hexene concentration.....	89
Figure 4.12 Dependence of maximum rate of 3a -catalyzed hydrogenation on partial pressure of H_2	89
Figure 4.13 Inverse dependence of maximum rate of 3a -catalyzed hydrogenation on added phosphine concentration.	89
Figure 4.14 $^{31}\text{P}\{^1\text{H}\}$ NMR spectrum of the <i>in situ</i> products of the reaction of 3a with H_2	98
Figure 4.15 $^{31}\text{P}\{^1\text{H}\}$ NMR spectrum of the reaction mixture formed from the reaction of 3a with H_2	99
Figure 4.16 The upfield ^1H NMR spectrum of <i>in situ</i> products from the reaction of 3a with H_2	100
Figure 4.17 $^{31}\text{P}\{^1\text{H}\}$ NMR spectrum of the yellow precipitate from the reaction of 3a with H_2 in <i>n</i> -butanol	102
Figure 4.18 ^1H NMR spectra of the yellow precipitate from the reaction of 3a with H_2 in <i>n</i> -butanol.....	103
Figure 4.19 ^1H NMR spectra of the yellow precipitate from the reaction of 3a with H_2 in <i>n</i> -butanol, within a) 1 h, and b) 6 h of making up the solution.....	105
Figure 4.20 Variable temperature ^1H NMR spectra of the yellow deposit from the reaction of 3a with hydrogen in benzene/hexane/methanol	108
Figure 4.21 The ^1H NMR spectrum of 3b	110

Figure 4.22 The $^{31}\text{P}\{^1\text{H}\}$ NMR spectrum of a solution obtained after ~6 h from mixing 3b in $\text{C}_6\text{D}_6/\text{DMA}$	111
Figure 4.23 The ^1H NMR spectrum of the residue obtained by removal of solvent from the supernatant of the reaction of 3b with H_2	112
Figure 4.24 The EI mass spectrum of the white crystals of dimethylammonium chloride isolated from the reaction of 3b with H_2	113
Figure 4.25 The $^{31}\text{P}\{^1\text{H}\}$ NMR spectrum of the blackish red crystals of complex Y isolated from the reaction of 3b with H_2	114
Figure 4.26 The ^1H NMR spectrum of Y	114
Figure 4.27 The $^{31}\text{P}\{^1\text{H}\}$ NMR spectrum of the 1a -catalyzed hydrogenation solution containing 0.04 M 1-hexene.....	117
Figure 4.28 The $^{31}\text{P}\{^1\text{H}\}$ NMR spectrum of the 1a -catalyzed hydrogenation solution containing 1.0 M 1-hexene.....	117
Figure 4.29 The $^{31}\text{P}\{^1\text{H}\}$ NMR spectrum acquired during the second hour since the start of the 1a -catalyzed hydrogenation reaction with 1.0 M 1-hexene.....	118
Figure 4.30 The $^{31}\text{P}\{^1\text{H}\}$ NMR spectrum of a 3a -catalyzed hydrogenation solution.....	119
Figure 4.31 The $^{31}\text{P}\{^1\text{H}\}$ NMR spectrum of a 3b -catalyzed hydrogenation solution.....	119
Figure 4.32 H_2 uptake plot for 1-hexene hydrogenation catalyzed by 3b	120
Figure 4.33 Dependence of maximum rate of hydrogenation on total Ru concentration (3b).....	121
Figure 4.34 Dependence of maximum rate of hydrogenation on the square root of the total Ru concentration (3b).....	121
Figure 4.35 Hexene dependence of maximum rate of 3b -catalyzed hydrogenation in DMA.....	122
Figure 4.36 Hydrogen dependence of maximum rate of 3b -catalyzed hydrogenation in DMA.....	122
Figure 4.37 PPh_3 dependence of the reciprocal of the maximum rate of 3b -catalyzed hydrogenation of 1-hexene.....	122
Figure 5.1 Scheme proposed in reference 145 for the dehydrogenation of methanol catalyzed by $\text{RuCl}(\text{OAc})(\text{PPh}_3)_3$	145
Figure 5.2 Glass tube used to monitor changes in the styrene/ethylbenzene ratio during transfer hydrogenation of styrene.....	152

Figure 5.3 a) A 25 mL, modified gas evolution flask for following reactions between $\text{RuCl}_2(\text{PPh}_3)(\text{isoPFA})$, 3b , in THF, and a small volume of KOH/methanol solution. b) Similar apparatus, for use with larger volumes of KOH/methanol solution.	156
Figure 5.4 The visible spectrum of 3b in CHCl_3 solution under nitrogen in the presence and absence of added PPh_3	163
Figure 5.5 The visible spectrum of $\text{RuCl}_2(\text{PPh}_3)(\text{isoPFA})$, 3b , in CHCl_3 solution under nitrogen and on exposure to air, respectively.....	164
Figure 5.6 The X-ray structure of $\text{RuHCl}(\text{CO})(\text{PPh}_3)(\text{isoPOF})$, 5	164
Figure 5.7 The ^1H NMR spectrum of 5	167
Figure 5.8 The ^1H NMR spectrum of a deuteriated sample of 5	168
Figure 5.9 The X-ray structure of $\text{RuHCl}(\text{CO})(\text{PPh}_3)(\text{isoPFA})$, 6	171
Figure 5.10 A stereoscopic view of the structure of 6	171
Figure 5.11 The ^1H NMR spectrum of $\text{RuHCl}(\text{CO})(\text{PPh}_3)(\text{isoPFA})$, 6	172
Figure 5.12 The X-ray structure of $\text{RuHCl}(\text{PPh}_3)(\text{isoPFA})$, 7	174
Figure 5.13 The $^{31}\text{P}\{^1\text{H}\}$ NMR spectrum of 6 after ~1 wk in solution under nitrogen in an NMR tube	176
Figure 5.14 The $^{31}\text{P}\{^1\text{H}\}$ NMR spectrum of the supernatant of a reaction mixture formed by heating $\text{RuCl}_2(\text{PPh}_3)(\text{isoPFA})$, 3b , in dry methanol in the presence of KOH under nitrogen.....	178
Figure 5.15 The ^1H NMR spectrum of the residue obtained from the solution used for the $^{31}\text{P}\{^1\text{H}\}$ NMR spectrum given in Figure 5.14	179
Figure 5.16 The visible spectrum of the CDCl_3 solution used for the ^1H NMR spectrum given in Figure 5.15.....	179
Figure 5.17 The upfield ^1H NMR spectrum of $\text{RuH}_2(\text{CO})(\text{PPh}_3)_3$	180
Figure 5.18 The X-ray structure of $\text{RuH}_2(\text{CO})(\text{PPh}_3)_3$	181
Figure 5.19 The ^1H NMR spectrum of the residue obtained from the eluted second red band, containing complex X , obtained on chromatography of a worked-up supernatant from a $\text{RuCl}_2(\text{PPh}_3)(\text{isoPFA})$, 3b /KOH/methanol reaction mixture.	183
Figure 5.20 Variable time $^{31}\text{P}\{^1\text{H}\}$ NMR spectra of a 3b /THF/styrene/KOH/MeOH reaction mixture obtained within 66 min of starting the reaction	186
Figure 5.21 Variable temperature spectra for the same solution described for Figure 5.20	187

Figure 5.22 The $^{31}\text{P}\{^1\text{H}\}$ NMR spectrum of the red reaction solution formed after 2 d for a reaction similar to that used for Figure 5.20.....	189
Figure 5.23 Gas evolution plot for a reaction between a solution of 3b in THF and a KOH/MeOH solution.....	190
Figure 5.24 Straight-line semi-log plot for Figure 5.23 indicative of first-order gas evolution, based on total mol gas evolved.....	190
Figure 5.25 The changes in the visible spectrum during a 20 °C reaction of 3b with basic methanol in THF under nitrogen with styrene present.....	192
Figure 5.26 Changes in the visible spectrum during the second stage (intermediate [KOH], yellow \longrightarrow red) of a reaction between 3b and methanol in THF in the presence of KOH with styrene absent.	193
Figure 5.27 Plot of the change in absorbance (605 nm) with time during a reaction of 3b with KOH/MeOH in THF at intermediate [KOH] (reaction 8, Table 5.6).	193
Figure 5.28 Plot of $\log(A_t - A_\infty)$ vs time (t) for the data of Figure 5.27, showing behaviour that is first-order in [3b].	194
Figure 5.29 Plot of the change in absorbance (605 nm) with time during a reaction of 3b with KOH/MeOH in THF at high [KOH] (reaction 10, Table 5.6).....	195
Figure 5.30 Plot of $\log(A_t - A_\infty)$ vs time (t) for the data of Figure 5.29, showing behaviour that is first-order in [3b].	196
Figure 5.31 Dependence of k_{obs} , from visible spectrophotometric measurements, on [KOH] for the reaction of 3b with KOH/MeOH in THF (Table 5.6).....	199
Figure 5.32 Plot of k_{obs} , from spectrophotometric measurements, versus [styrene] at two different [KOH] values (Table 5.7).	199
Figure 5.33 Conventional salt effect plot, showing the effect of LiNO_3 on the k_{obs} for the first step of the reaction of 3b with KOH/MeOH in THF	200
Figure 5.34 Plot of k_{obs} , from spectrophotometric measurements, and corrected for salt effect, versus $[\text{KOH}]^2$, for the reaction of 3b with KOH/MeOH in THF.....	201
Figure 5.35 Plot of the percentage of styrene, $\{[\text{styrene}]_t/[\text{styrene}]_0\} \times 100\%$, present at time (t), during reaction 8, Table 5.8.	202
Figure 5.36 Semi-log plot derived from the data of Figure 5.35	203
Figure 5.37 Plot of the percentage of styrene, $\{[\text{styrene}]_t/[\text{styrene}]_0\} \times 100\%$, present at time (t), during reaction 6, Table 5.8.	205
Figure 5.38 Plot of the percentage of styrene, $\{[\text{styrene}]_t/[\text{styrene}]_0\} \times 100\%$, present at time (t), during reaction 7, Table 5.8.	205

Figure 5.39 Semi-log plot, showing the first-order behaviour of the primary hydrogenation process, derived from the data of Figure 5.37	207
Figure 5.40 Semi-log plot, showing the first-order behaviour of the primary hydrogenation process, derived from the data of Figure 5.38	207
Figure 5.41 Plot showing [KOH] dependence of k'_{obs} for styrene hydrogenation, in the reaction of 3b with methanol in the presence of styrene and KOH in THF (Table 5.8)	208
Figure 5.42 Plot showing [styrene] dependence of k'_{obs} for styrene hydrogenation, in the reaction of 3b with methanol in the presence of styrene and KOH in THF (Table 5.8).	208
Figure 5.43 ^2D NMR spectra of deuteriated ethylbenzene obtained by hydrogen transfer from (a) MeOH-d_4 and (b) MeOH-d_1 to styrene during the reaction of $\text{RuCl}_2(\text{PPh}_3)(\text{isoPFA})$, 3b , with MeOH-d_4 and MeOH-d_1 , respectively, in the presence of KOH in THF.	211
Figure 5.44 ^2D NMR spectrum of a) an acetone/styrene solution, and b) an acetone/ethylbenzene solution.....	212
Figure 5.45 Plot of $[\text{OMe}^-]$ versus $[\text{OH}^-]$ based on the equilibrium constant, $K = 18$, for the reaction of NaOH with MeOH at $20\text{ }^\circ\text{C}$	227
Figure 5.46 Proposed mechanism for the second-order base-dependent pathway for reaction 5.30 via methoxide attack on 3b	228
Figure 5.47 Base-independent pathway for the reaction of 3b with KOH/MeOH in THF.....	231

List of Symbols and Abbreviations

[]	molar concentration
[] ₀	initial concentration
[] _T	total concentration
[] _t	concentration at time t
[] _∞	final concentration
[α] _D ^T	specific rotation at temperature T and at the light wavelength of 589 nm from the sodium D line
α	adjacent position on a carbon chain
Å	Ångstrom(s)
A ₀	initial absorbance
Anal.	elemental analysis
A _t	absorbance at time t
atm	atmosphere(s) (pressure unit)
A _∞	final absorbance
bipy	bipyridyl
bq	7,8-benzoquinolate
br s	broad singlet
Bu ^t	tertiary butyl
Calcd.	calculated
Chap.	chapter
cm	centimetre(s)
cm ⁻¹	wavenumber unit
Cp	cyclopentadienyl
Cy	cyclohexyl

Δ	difference
Δ	heat
δ	chemical shift
$^1\text{H}\delta$	^1H NMR chemical shift
$^{31}\text{P}\delta$	$^{31}\text{P}\{^1\text{H}\}$ chemical shift
d	day(s)
d	doublet
ΔG^\ddagger	free energy of activation
ΔH	enthalpy change
ΔH°	standard enthalpy change
ΔH^\ddagger	enthalpy of activation
diop	-O-isopropylidene-2,3-dihydroxy-1,4-bis(diphenylphosphino)butane
DMA	<i>N,N</i> -dimethylacetamide
dppb	1,4-bis(diphenylphosphino)butane
dppe	1,2-bis(diphenylphosphino)ethane
dppm	bis(diphenylphosphino)methane
dppp	1,3-bis(diphenylphosphino)propane
ΔS^\ddagger	entropy of activation
ϵ	extinction coefficient
e.e.	enantiomeric excess
EI	electron impact
Et	ethyl
Fc	ferrocenyl
FID	flame ionization detector
Fig.	Figure
G C	gas chromatography

GCMS	gas chromatography-mass spectrometry
h	hour(s)
η^n	hapticity of degree n
Hz	Hertz
IR	infrared
isoPFA	1-[α - <i>N,N</i> -dimethylaminoethyl]-2-diphenylphosphino-ferrocene
isoPOF	1-[α -methoxyethyl]-2-diisopropylphosphinoferrocene
J	coupling constant
J	Joule(s)
K	equilibrium constant
k	rate constant
kJ	kilojoule(s)
k_{obs}	observed rate constant
Λ	equivalent conductance
λ	wavelength
lit.	literature
λ_{max}	wavelength of an absorbance maximum
log	common logarithm
M	metal atom
M	molar
μ	bridging position between two metal atoms in a molecule
m	multiplet
m/z	mass/charge ratio
Me	methyl

meso-tetraphos-1	(Ph) ₂ P(CH ₂ CH ₂)PPh(CH ₂ CH ₂)- PPh(CH ₂ CH ₂)PPh ₂
μg	microgram(s)
mg	milligram(s)
MHz	megahertz
μL	microlitre(s)
mm	millimetre(s)
mmol	millimole(s)
mol	mole(s)
v	vibrational frequency
nm	nanometre(s)
NMR	nuclear magnetic resonance
OAc	acetyl
P-N	chelating ditertiary phosphine-amine
P-P	chelating ditertiary phosphine
Ph	phenyl
PPFA	1-[α- <i>N,N</i> -dimethylaminoethyl]-2- diisopropylphosphino-ferrocene
PR ₃	tertiary alkyl or aryl phosphine
Pr ⁱ	isopropyl
PS	Proton Sponge [®]
p-tol	<i>para</i> -tolyl
q	quartet
R	residual index
R _w	weighted residual index
s	second(s)
s	singlet

sect.	section
str	strong
TCD	thermal conductivity detector
t	time
t	triplet
T_1	longitudinal relaxation time
$t_{1/2}$	half-life
T_2	transverse relaxation time
tetraphos-2	$P(CH_2CH_2PPh_2)_3$
THF	tetrahydrofuran
TMS	tetramethylsilane
UV-vis	ultraviolet-visible
v br s	very broad singlet
v/v	volume-to-volume ratio
ω	Larmor frequency
w	weak
$w_{1/2}$	halfwidth
{ 1H }	broadband proton-decoupled
{phenyl- 1H }	phenyl proton-decoupled

Acknowledgments

I am grateful to those who have assisted me during the course of my work and in the preparation of this thesis. In particular, valuable help and guidance has been received from my supervisors Dr. B.R. James and Dr. W.R. Cullen. I have appreciated helpful comments from members of my guidance committee: Dr. M. Fryzuk, Dr. P. Legzdins and Dr. A. Merer. Assistance in many practical matters has come from many members of both research groups. Indispensable assistance has been provided by members of the support services, including those working in the analytical, electronic, glass blowing, illustration, mechanical and NMR divisions of the chemistry department.

My wife and children have endured my frequent absence and lateness most graciously. Thanks are also due to my parents, as well as to my wife, for their encouragement.

Chapter 1

Introduction

Homogeneous catalysis holds practical importance for organic synthesis^{1,1b} and also for inorganic reactions.^{1c} The generally mild conditions required for such catalysis, and its amenability to study are other factors which have helped generate the tremendous growth in interest in homogeneous catalytic systems in the past thirty years.

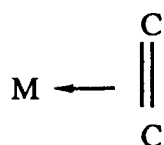
Hydrogenation systems for organic substrates have received particular interest,^{2,3,4} not only for their ease of study, and practical usefulness, but also for the relative simplicity, in selectivity for, organic products. Attractive features notwithstanding, homogeneous hydrogenation systems have received limited commercial interest, because of (a) problems with catalyst/product separation and recovery following the catalytic process and (b) phosphine degradation of phosphine containing catalysts, which occurs under reducing conditions.^{1b}

Catalytic hydrogenation of organic substrates usually involves activation of both dihydrogen and the substrate by bonding to a metal atom, so that these molecules therefore undergo reactions which they would not undergo in the uncomplexed state. Activation of dihydrogen involves formation of an active metal hydride species, and this species can transfer a hydride to a coordinated substrate, which has been rendered, by virtue of coordination, susceptible to nucleophilic attack by the hydride ligand. Hydrogen activation has been proposed to occur via either homolytic (eq. 1.1a, b) or heterolytic (eq. 1.2) cleavage of H₂.





Recent reports of $\eta^2\text{-H}_2$ complexes (discussed in Chapter 3) have provided structural precedents for an intermediate or transition state for reaction 1.1. Structural precedents for a transition state or intermediate for reaction 1.2 (via direct heterolytic cleavage, rather than by oxidative addition to give MXH_2 and subsequent elimination of HX) are not available, apart from Ozin's claim of matrix-isolated, "ligand-free" $\text{Pd}(\eta^1\text{-H}_2)$.⁵ Mechanistic pathways proposed for olefin hydrogenation, by mono- or dihydride species, have usually involved η^2 -olefin coordination:



with subsequent hydride transfer giving an alkyl species; further hydride transfer or, in the case of monohydride catalysts, possibly protonolysis or reaction with another metal hydride gives the alkane. Eisenschmid *et al.*, however, have recently reported evidence for "pairwise" hydrogen transfer to olefinic substrates, which implies catalysis via a dihydride intermediate, with hydrogen transfers being fast compared to relaxation of the hydrogen nuclear spins in *para* hydrogen.^{6,7}

Numerous other hydrogen sources for hydrogenation have been employed (summarized in sect. 5.1), and methanol is one such, little studied, example. Hydrogenation employing dihydrogen and methanol as hydrogen sources is reviewed in more detail in the chapters to follow. Chapter 3 focusses on dihydrogen complexes relevant to the H_2 hydrogenation systems of Chapter 4, which involve ruthenium phosphines and ferrocenyl phosphines. Chapter 5 is devoted to the activation of methanol, mainly by $\text{RuCl}_2(\text{PPh}_3)(\text{isoPFA})$ (isoPFA = chelated 1,2-(α -*N,N*-dimethylaminoethyl)(diisopropylphosphino)ferrocene, Fig. 1.1) and hydrogenation systems are described where hydrogen is transferred from methanol to an unsaturated organic substrate. Most of the present work is related to systems involving ferrocenyl

ligands. A wide variety of ferrocenyl ligands containing phosphine,^{8,9,10,11} arsine,^{8,11,12} sulfide^{8,11-13} and aminoalkyl functions^{8,10,11,14,15,16} has been prepared. A planar element of chirality is conferred by disubstitution of one of the ferrocene rings. In 1970, Gokel and Ugi reported on a simple optical resolution of α -*N,N*-dimethylaminoethylferrocene, FA (Fig. 1.1).¹⁶ Phosphine derivatives of FA can be prepared via lithiation of FA and subsequent reaction with the appropriate chlorophosphine.^{8,10,11,17,18} Fortunately, the lithiation is highly stereoselective, the non-resolved FA giving the (*S,R*)- and (*R,S*)-1,2-(α -*N,N*-dimethylaminoethyl)(phosphino)ferrocene in 96% yield. (In, for example, the (*S,R*)- enantiomer, *S* refers to the centre of chirality at the α -carbon atom of the aminoethyl group, and *R* refers to the planar chirality conferred by the disubstitution of one of the ferrocene rings.) Replacement of the NMe_2 group¹⁰ by hydroxyl, alkoxy or other functions, provides yet other variations on this type of ligand. The variety of derivatives and the accessibility of chiral derivatives have in large part been the reason for the interest in these ligands. Also, they are reasonably stable in air and orange-coloured and can thus be readily chromatographed; they are also readily recrystallized. Fig.

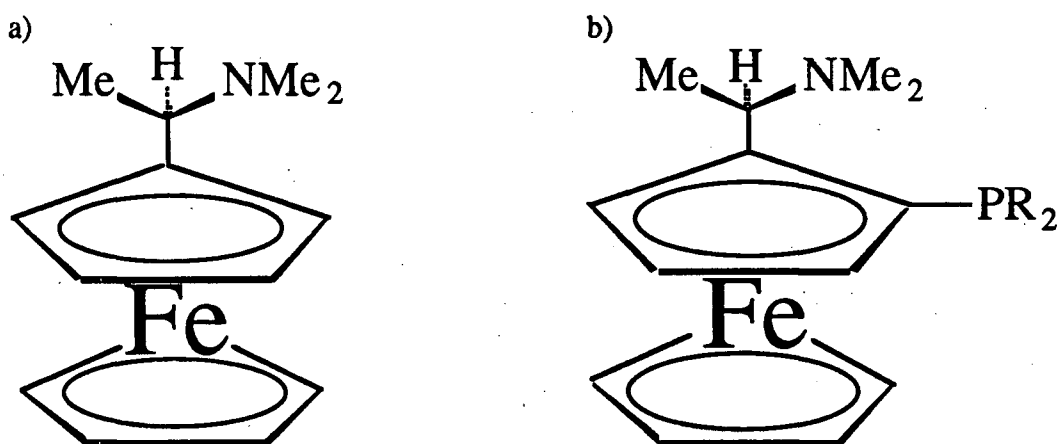


Figure 1.1 a) FA; b) PPFA (R = Ph) and isoPFA (R = Prⁱ)

1.1 shows the main ferrocenyl phosphines used in this work, PPFA and isoPPFA.

Chapter 2

General experimental procedures

2.1 General procedures

Unless otherwise specified, air sensitive reagents and products were manipulated under a nitrogen atmosphere, by using a single or double-manifold vacuum system and Schlenk techniques.

Some reactions described in the chapters to follow, and requiring inert or hydrogen atmospheres, were carried out in glass tubes sealed by heating with a torch, or by closing a valve. For sealing glass tubes (including NMR tubes) under a hydrogen or nitrogen atmosphere, a single-manifold vacuum line connected to a hydrogen or nitrogen source, and also to a manometer, was used. The tube to be sealed was fitted with a ground-glass joint, and a Teflon valve, if desired. Any required solids were placed in the tube, which was then evacuated on the vacuum line. Any required liquids (freeze/thaw-degassed) were then vacuum-transferred into the tube, over a drying agent when desired. With the tube partially immersed in liquid nitrogen, the vacuum-line manifold and the tube were filled with hydrogen or nitrogen to the desired pressure, as indicated on the manometer. If the pressure were about 10 cm Hg below atmospheric pressure, then the pressure in the tube on warming, and after sealing, would be 2-3 atm. A torch was used to seal the tube, at a constriction below the joint, or the Teflon valve was closed, if present. During sealing with a torch, the tube to be sealed was not isolated from the rest of the gas in the manifold; the larger gas volume made for a smaller pressure increase on heating with the torch, thus avoiding positive pressure in the tube during sealing. The larger volume was particularly important if the pressure in the tube during sealing was just under atmospheric pressure.

When pressures of in excess of 3 atm were desired, the set-up shown in Figure 2.1 was used. The gas pressure was adjusted using the pressure gauge, with the tube to be sealed at room temperature, or partially immersed in liquid nitrogen if higher pressures were desired. The Teflon valve (obligatory in this case) attached to the tube was then closed and the tube allowed to warm up to ambient temperature.

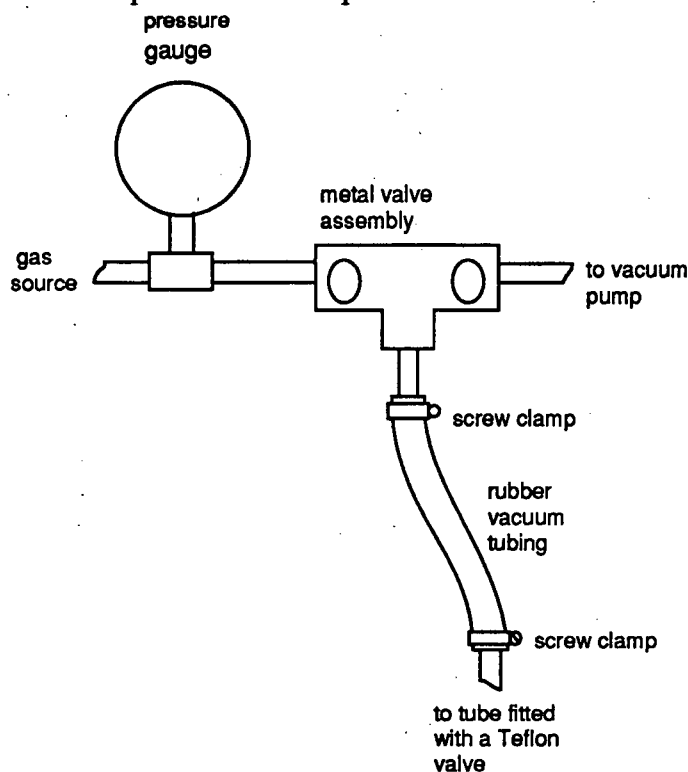


Figure 2.1 Apparatus for filling tubes with pressures up to 10 atm.

For manipulating materials under elevated hydrogen pressures, a tube such as that shown in Fig 2.2 was used. A solid reagent was introduced through the Teflon valve opening, and shaken down to region "A" in the tube, along with a small magnetic stir bar. Solvent was vacuum-transferred into the tube at region "C". With the solvent frozen, the

pressure was then adjusted as described above, the valve on the apparatus (Fig 2.2) was

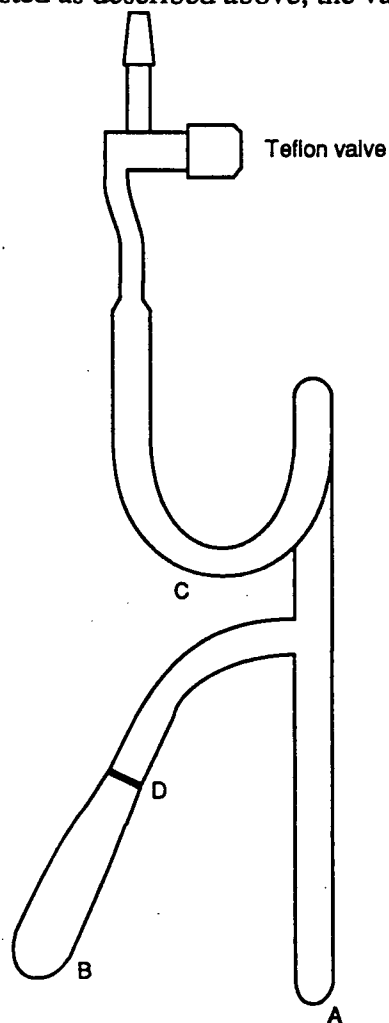


Figure 2.2 Glass apparatus used for manipulating materials under elevated hydrogen pressures, up to 10 atm. The diagram is approximately to scale, and the height of this apparatus is ~40 cm.

closed and the tube allowed to warm to ambient temperature. Solvent and solids were mixed and reaction with hydrogen allowed to occur. Precipitates formed could be filtered under hydrogen by tipping the reaction mixture onto the frit at "D" in the tube and cooling the tube at point "B". The filtered solid could be washed with freeze/thaw-degassed solvent, the wash-solvent, for example, being vacuum-transferred into the tube at point "C" (with filtrate at "B" frozen). In this procedure, filtrates that are unstable in the absence of hydrogen are not visibly affected by the filtration, and solvents for crystallization can also

be layered by vacuum transfer onto the filtrate in section "B" of the tube. The filtered solid can also be shaken, with the filtrate frozen, or moved with the magnetic stir bar into section "A" for recrystallization.

2.2 Instrumentation

Electrical conductance measurements were carried out using a Serfass Conductance Bridge, supplied by the Arthur H. Thomas Co., with a 3403 conductivity cell from the Yellow Springs Instrument Co. Inc.

Infrared spectra were usually recorded on KBr pellets, and solution spectra were recorded using a KBr cell with path length 0.25 mm. Unless otherwise specified, a Nicolet 5DX FTIR spectrophotometer was used.

UV-visible spectra were recorded on a Perkin Elmer 552A spectrophotometer, fitted with either of two thermostatted cell compartments, one for 1.0 cm and 1.0 mm cells, and the other for use with a 5 cm cell. Specially designed cells were used for experiments requiring inert or hydrogen atmospheres (Figs 2.3, 2.4). The spectrophotometer was equipped with both a Hewlett-Packard 7015B X-Y recorder, used for measuring complete spectra from 315 to 900 nm, and a Houston Instruments OmniScribe[®] (continuous feed) recorder, used for following rates for longer periods at a selected wavelength.

Nuclear magnetic resonance spectra were obtained by using Bruker WP80, Bruker WH400, Bruker-Nicolet HXS 270 or Varian XL300 spectrometers. ¹H NMR spectra were recorded as δ (ppm), with positive shifts being downfield from tetramethylsilane. ³¹P{¹H} NMR spectra are recorded as δ (ppm), with positive shifts downfield from 85% H₃PO₄(aq), and with triphenylphosphine used as the external reference (at δ -5.6).

Hexane/hexene isomer ratios in catalytic hydrogenation studies were obtained by using a Varian 6000 gas chromatograph equipped with a column packed with 20% tricresyl phosphate on chromosorb and an FID detector. Heptaldehyde and heptanol were detected

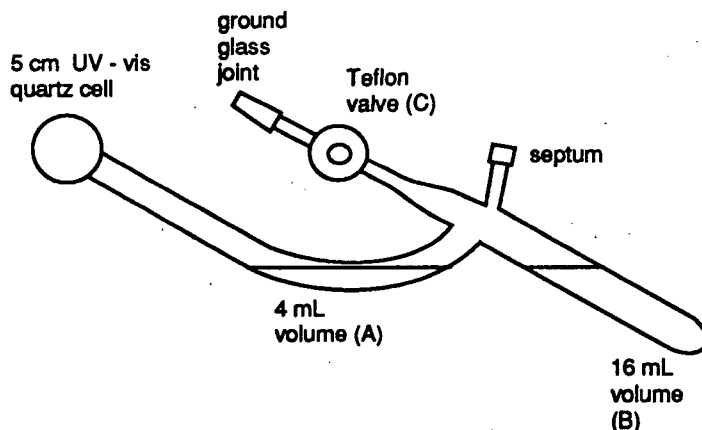


Figure 2.3 Visible spectrophotometer cell used for kinetic studies under nitrogen to monitor the spectral changes in the reaction of $\text{RuCl}_2(\text{PPh}_3)(\text{isoPFA})$ with $\text{KOH}/\text{methanol}$ in THF . A Kontes Teflon valve and F-145 septum plugs, supplied by Alltech Associates, were used for all Teflon valves and septa, respectively, shown in Figs. 2.2, 2.3, 2.4 and 5.2.

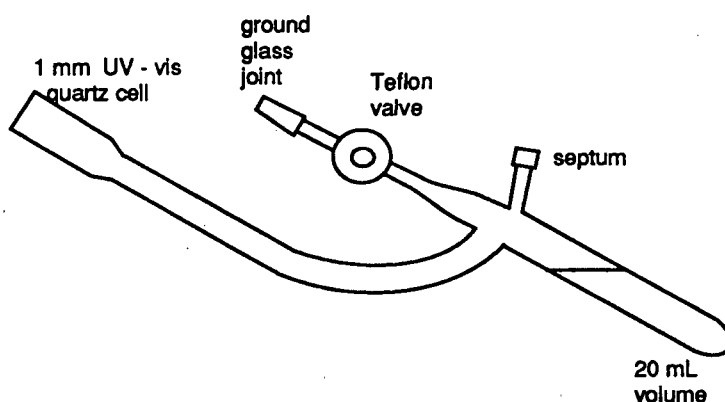


Figure 2.4 Visible spectrophotometer cell used for absorption measurements under a controlled atmosphere.

on the same instrument using an OV-17 column. Styrene/ethylbenzene ratios for kinetic experiments were determined using a Hewlett-Packard 5890 gas chromatograph equipped with a carbowax capillary column, a 3393A integrator and FID detector. Other gas chromatographs used were a Varian 90-P (for preparative GC purposes), and a Hewlett-Packard 5830A, both with TCD detectors. Helium was used as the carrier gas for all gas chromatography.

A constant pressure gas-uptake apparatus for measuring stoichiometric and catalytic absorption (or evolution) of dihydrogen was used as described in detail elsewhere.^{19,20}

Optical rotation measurements were recorded on a Perkin Elmer 141 polarimeter at ambient temperature using a one decimetre pathlength cell which could hold 1mL of solution. The rotations were measured at the sodium-D line (589 nm). The specific rotation of any optically active product, and the optical purity (e.e.) were calculated in a standard manner using the equation:

$$[\alpha]_D^T = \frac{\alpha \times 100}{l \times c} \quad (2.1)$$

where $[\alpha]_D^T$ = specific rotation, at temperature T, measured at the sodium-D line.

α = observed rotation(+) or (-).

l = path length of the cell in decimetres.

c = concentration of solution in g/100 mL.

Optical purity was calculated using the equation:

$$\text{optical purity} = \frac{[\alpha]_{\text{reaction}}}{[\alpha]_{\text{pure}}} \times 100\% \quad (2.2)$$

where $[\alpha]_{\text{reaction}}$ and $[\alpha]_{\text{pure}}$ are equal to the rotation of the reaction product and optically pure compound, respectively.

All mass spectrometry was performed by the UBC mass spectrometry service.

2.3 NMR studies

The T_1 measurements were carried out using a standard inversion-recovery pulse sequence (180° -t- 90°) on a Varian XL-300 spectrometer operating at 300 MHz.

To simulate chemical exchange NMR spectra, the program, DNMR4, QCPE program no. 466, obtained from the Quantum Chemistry Program Exchange, Department of Chemistry, Indiana University, was used. This program was written in the Fortran IV programming language; the DEC 2060 version we received was adapted for the UBC mainframe (UBC computer centre) with assistance from UBC computer centre staff in changing machine-dependent parameters and changing from single to double precision. Sample calculations on test data, obtained from the QCPE, were reproduced, and the calculated spectra were superimposable on those supplied by the QCPE. The T_2 values, required as input for this program, were calculated using the equation:

$$T_2 = \frac{1}{\pi \times w_{1/2}} \quad (2.3)$$

where $w_{1/2}$ is the half-width of the observed peak.

ΔG^\ddagger values were obtained from Eyring plots for the exchange rate constants, k , obtained from simulations over a range of temperatures.

Spin-transfer studies were carried out at 300 MHz on the Varian XL300 spectrometer. To observe spin-transfer between two signals A and B, the decoupler was set at A and decoupler power increased until maximum decrease in integration of signal B was observed, on recording the spectrum at this power. Areas of peaks A and B were monitored with reference to an unaffected peak elsewhere in the spectrum.

2.4 Materials

Solvents

Tetrahydrofuran was distilled from sodium/benzophenone under a nitrogen atmosphere, stored under nitrogen and used within 48 hours. Anhydrous diethylether, hexanes, *n*-hexane and benzene, when referred to as dry, were distilled over CaH₂ prior to vacuum distillation, and stored under nitrogen. DMA was stirred over CaH₂ for at least 24 h, or refluxed for ~1 h prior to distillation under reduced pressure. On one occasion (see section 3.2) DMA was further stirred over RuHCl(PPh₃)₃ (500 mg/L) and distilled a second time to obtain extra pure material.²¹ Dimethylacetamide was used within a day or so of distillation. Alcohols, when referred to as dry, were distilled over Mg/I₂.

Gases

Purified helium, hydrogen, nitrogen, argon, and oxygen, from Union Carbide Canada Ltd., and "syn gas" (H₂/CO, 1:1), from Matheson, were usually used without further purification. Hydrogen used in kinetics experiments was passed through a Matheson Deoxo purifier to remove trace oxygen.

Phosphines

Triphenylphosphine, and tri(*p*-tolyl)phosphine were used as supplied for synthesis work. Triphenylphosphine was recrystallized from methanol for use in hydrogenation kinetics studies. Racemic and optically active PPFA²² and isoPPFA⁸ were synthesized as described elsewhere from FA (Fig. 1.1) and the appropriate ClPR₂.

Olefin and ketone substrates

The substrates, α -*N*-acetamidoacrylic acid, α -*N*-acetamidocinnamic acid and itaconic acid were used as supplied. Styrene, cyclohexene, 1-hexene, vinylmethylketone, ethylmethylketone and acetophenone were passed through 3-5 cm of neutral Al₂O₃ before use, to remove peroxide impurities.

Other materials

Proton Sponge[®], 1,8-bis(dimethylamino)naphthalene was purified as described elsewhere,^{21,23} by chromatographing a hexane solution on alumina.

Ruthenium complexes

Hydrated ruthenium(III) trichloride was obtained on loan from Johnson Matthey Ltd.

Di- μ -chloro- μ -hydrido- η^2 -dihydrogenhydridotetrakis(triarylphosphine)-diruthenium(II), $\text{Ru}_2(\eta^2\text{-H}_2)\text{H}_2\text{Cl}_2(\text{PR}_3)_4$ (aryl = R = phenyl, p-tolyl), **1a**, **1b**.

The DMA-free complexes were prepared as described elsewhere,^{21,23} from $[\text{RuCl}_2(\text{PPh}_3)_2]_2$ and 1 atm H_2 in toluene in the presence of Proton Sponge[®], and from $\text{RuCl}_3(\text{P}(\text{p-tol})_3)_2(\text{DMA})$ and 1 atm H_2 in benzene in the presence of Proton Sponge[®], respectively.

1a: Anal. Calcd. for $\text{C}_{72}\text{H}_{64}\text{Cl}_2\text{P}_4\text{Ru}_2$: C, 65.21; H, 4.86. Found: C, 64.95; H, 4.93. $^{31}\text{P}\{^1\text{H}\}$ NMR (121 MHz, toluene- d_8 , ambient temperature, hydrogen atmosphere) δ 70.5, 46.0 (lit.^{21,23}: $\delta_{\text{C}_6\text{D}_6}$ (ambient temperature) 68, 43). The ^1H NMR spectrum, and further information on the $^{31}\text{P}\{^1\text{H}\}$ NMR spectrum, are presented in section 3.3, as well as the structure, Table 3.7, Fig 3.2.

1b: <5% phosphorus-containing impurity present, based on $^{31}\text{P}\{^1\text{H}\}$ NMR (121 MHz, CD_2Cl_2 , ambient temperature, 2 - 3 atm hydrogen atmosphere) δ 68.8, 44.7 (lit.^{21,23} $\delta_{\text{toluene-}d_8}$ (ambient temperature) 69.2, 44.0). Further information on the $^{31}\text{P}\{^1\text{H}\}$ NMR spectrum, and the ^1H NMR spectrum, is presented in section 3.3.

The preparation of the bis-DMA solvate, $(\eta^2\text{-H}_2)(\text{PPh}_3)_2\text{Ru}(\mu\text{-H})(\mu\text{-Cl})_2\text{RuH}(\text{PPh}_3)_2\cdot 2\text{DMA}$, from $\text{RuCl}_3(\text{PPh}_3)_2(\text{DMA})$ and 1 atm H_2 in DMA in the presence of Proton Sponge[®], has been reported in the literature,^{21,23} but in the present work this complex was prepared by a different route, from $\text{RuCl}_2(\text{PPh}_3)(\text{isoPFA})$, as follows:

$\text{RuCl}_2(\text{PPh}_3)(\text{isoPFA})$ (0.45 g, 0.56 mmol), prepared as described below, was stirred in DMA (3 mL) under hydrogen (10 atm) for 4 d at ambient temperature, in which time an orange precipitate was deposited. This was filtered under hydrogen and washed twice with methanol and once with hexane. The yield was estimated to be ~ 70 (± 20) mg ($\sim 40\%$).

Anal. Calcd. for $\text{C}_{80}\text{H}_{82}\text{O}_2\text{N}_2\text{Cl}_2\text{P}_4\text{Ru}_2$: C, 64.04; H, 5.20; N, 1.87. Found: C, 63.75; H, 5.43; N, 1.64. The $^{31}\text{P}\{^1\text{H}\}$ and ^1H NMR spectra were the same as for the DMA-free complex. IR ν_{KBr} 2129, 1970, 1903, 1822 cm^{-1} , all broad, weak.

Di- μ -chlorodichlorotetrakis(triarylphosphine)diruthenium(II), $\text{Ru}_2\text{Cl}_4(\text{PR}_3)_4$ (R = aryl = phenyl, p-tolyl), **2a**, **2b**

The triphenylphosphine complex was prepared as described elsewhere,^{21,24} from $\text{RuCl}_3(\text{PPh}_3)_2(\text{DMA}) \cdot \text{DMA}$ and 1 atm H_2 in DMA, or by stirring $\text{RuCl}_3(\text{PPh}_3)_2(\text{DMA}) \cdot \text{DMA}$ ^{21,27} (0.5 g, 0.55 mmol) in *n*-butanol (2 mL) under hydrogen (8 atm) for 2 d (further discussion of this preparation is given in sect. 3.4). In the latter procedure, $\text{Ru}_2\text{Cl}_2(\text{PPh}_3)_4$, **2a** was deposited as a light brown solid, which was filtered and washed with methanol. Yield: 0.3 g (76%). Anal. Calcd. for $\text{C}_{72}\text{H}_{60}\text{Cl}_4\text{P}_4\text{Ru}_2$: C, 62.07; H, 4.31. Found: C, 61.44; H, 4.50 (discussed in sect. 3.4). $^{31}\text{P}\{^1\text{H}\}$ NMR (121 MHz, toluene- d_8 , ambient temperature, under vacuum) δ 60.3 (br s), 52.9 (br s); $^{31}\text{P}\{^1\text{H}\}$ NMR (121 MHz, toluene- d_8 , ambient temperature, under 2 - 3 atm hydrogen) δ 60.0 (br s), 52.7 (br s); $\delta(-58^\circ\text{C})$ 60.9 (d), 53.3 (d), $^2J_{\text{PP}} = 42$ Hz (lit.²¹ $\delta_{\text{toluene-}d_8}$ (-40 $^\circ\text{C}$) 60.0 (d), 52.4 (d), $^2J_{\text{PP}} = 42$ Hz; also, lit.²⁴ $\delta_{\text{toluene-}d_8}$ (-70 $^\circ\text{C}$) 58.8 (d), 53.0 (d), $J_{\text{PP}} = 41.5$ Hz).

The tri(p-tolyl)phosphine analogue, $\text{Ru}_2\text{Cl}_4(\text{P}(\text{p-tol})_3)_4$, **2b** was prepared by stirring 0.25 g (0.16 mmol) $\text{RuCl}_3(\text{P}(\text{p-tol})_3)_2\text{DMA} \cdot \text{DMA}$ ^{21,27} in *n*-butanol (3 mL) under hydrogen (7 atm) overnight. To the resulting brown solution, diethyl ether (~ 10 mL), hexanes (~ 15 mL) and methanol (~ 10 mL) were added. Additions of solvent were

interspersed by periods of keeping the solution for several hours in the freezer, at $\sim 30\text{ }^{\circ}\text{C}$, to induce crystallization. Some crystals did form during these periods in the freezer.

Finally, the volume was reduced to 10 mL, and the brown deposit, including the crystals, was filtered and washed with methanol. X-ray photographs of crystals from this sample indicated poor diffraction. Total yield: 0.046 g (23%). Anal. Calcd. for

$\text{C}_{84}\text{H}_{84}\text{Cl}_4\text{P}_4\text{Ru}_2$: C, 64.62; H, 5.38. Found: C, 64.12; H, 5.88. $^{31}\text{P}\{^1\text{H}\}$ NMR (121 MHz, toluene- d_8 , ambient temperature, hydrogen atmosphere) δ 58.8 (br s), 52.0 (br s) (lit.^{21,23} ($-40\text{ }^{\circ}\text{C}$) 60.1 (d), 52.5 (d), $^2J_{\text{PP}} = 42\text{ Hz}$).

Dichloro{1-[α -*N,N*-dimethylaminoethyl]-2-diphenylphosphino-ferrocene}(triphenylphosphine)ruthenium(II), $\text{RuCl}_2(\text{PPh}_3)(\text{PPFA})$, **3a**

This was prepared as described elsewhere,²⁵ except that an improved reagent ratio ($\text{RuCl}_2(\text{PPh}_3)_3$: PPFA) was used (1.24 g, 1.29 mmol : 0.73 g, 1.64 mmol, respectively), thus giving an excess of the soluble reagent, PPFA, in this reaction in which the starting complex, $\text{RuCl}_2(\text{PPh}_3)_3$, and product, $\text{RuCl}_2(\text{PPh}_3)(\text{PPFA})$, **3a**, are suspended solids. Anal. Calcd. for $\text{C}_{44}\text{H}_{43}\text{NCl}_2\text{P}_2\text{FeRu}$: C, 60.36; H, 4.95; N, 1.60. Found: C, 60.54; H, 5.15; N, 1.70. $^{31}\text{P}\{^1\text{H}\}$ NMR (121 MHz, C_6D_6 , ambient temperature, under vacuum) δ 77.5(d), 44.3(d), $^2J_{\text{PP}} = 39\text{ Hz}$. The previously reported²⁵ values, also in C_6D_6 , of δ 170.5, 137.0, "downfield from $\text{P}(\text{OMe})_3$ ", which, in turn, is 141 ppm downfield from 85% H_3PO_4 , are very different from the values given here and must have been misreported. The literature difference in chemical shifts for the two resonances is the same as that given here, as is the coupling constant. A $^{31}\text{P}\{^1\text{H}\}$ NMR peak at δ 23.9 was typically found for solutions of this complex and is identified as OPPh_3 ;^{21,26} this peak was found even when the C_6D_6 had been stirred for $\sim 3\text{ h}$ under vacuum over calcium hydride before vacuum transfer into the NMR tube containing the $\text{RuCl}_2(\text{PPh}_3)(\text{PPFA})$. The optically

active complex was prepared using (*S,R*)- PFFA (optical purity = 84%), which itself was synthesized as described, from FA of the same optical purity²² (see also Chapter 1).

Dichloro{1-[α -*N,N*-dimethylaminoethyl]-2-diisopropylphosphino-ferrocene}(triphenylphosphine)ruthenium(II), RuCl₂(PPh₃)(isoPFA), **3b**

RuCl₂(PPh₃)₃ (0.8 g, 0.8 mmol), prepared from RuCl₃·xH₂O and PPh₃ in methanol as described,²⁷ and racemic isoPFA (0.56 g, 1.5 mmol) prepared as described,⁸ from FA prepared from ferrocene carboxaldehyde, were refluxed overnight under nitrogen in a solvent mixture of hexane or hexanes (50 mL) and CHCl₃ (5 mL). The suspended RuCl₂(PPh₃)₃ gradually reacted to give a green, sparingly soluble product, which was filtered, washed with hexane(s) and dissolved in hot benzene. This solution was filtered and the volume reduced to 10 mL. Hexane(s) (50 mL) was then layered onto this solution under nitrogen and crystallization allowed to occur slowly at -30 °C over several days. The dark green product was isolated by filtration and washed with hexane(s). Yield: 0.43 g 56.66; H, 5.99; N, 1.60. Alternatively, recrystallization of the initially precipitated crude product from CH₂Cl₂/hexane(s) gave a product that was CH₂Cl₂/hexane(s) to give a product that appeared pure by ³¹P{¹H} NMR but which was 0.63% low in carbon. Recrystallization of this latter product from THF resulted in a product with acceptable elemental analysis (C, 56.30; H, 6.06; N, 1.68). Celite[®] was used for the filtrations for recrystallizations in CH₂Cl₂ and THF to remove a very fine black, insoluble material that appeared to be produced in the preparation. ³¹P{¹H} NMR (121 MHz, CDCl₃, ambient temperature, nitrogen atmosphere) δ 96.2(d), 36.6(d), ²J_{PP} = 32 Hz. ¹H NMR (300 MHz, CDCl₃, ambient temperature, nitrogen atmosphere) δ 0.72 (m, 6H, PCHCH₃), 1.18 (dd, 3H, ³J_{PH} = 15 Hz, ³J_{HH} = 7 Hz, PCHCH₃), 1.43 (d, 3H, ³J_{HH} = 7 Hz, FcCHCH₃), 1.75 (dd, 3H, ³J_{PH} = 13 Hz, ³J_{HH} = 7 Hz, PCHCH₃), 2.24, 2.82 (2m, 2H, PCHCH₃), 2.35, 2.44 (2s, 6H, N(CH₃)₂), 4.22 (s, 5H, FeC₅H₅), 4.4

(t, 1H, $J_{\text{HH}} = 3$ Hz, FeC_5H_3), 4.58 (bs, 2H, FeC_5H_3), 6.2 (q, 1H, $^3J_{\text{HH}} = 6$ Hz, FcCHCH_3), 7.37 (m, 9H, Ph *meta, para*), 7.92 (t, 6H, $J = 8$ Hz, Ph *ortho*). The optically active complex was prepared as described above, but using (*S,R*)-isoPFA of optical purity = 84%. This ligand, in turn, was prepared as described,⁸ from FA of the same optical purity. Crystals of $\text{RuCl}_2(\text{PPh}_3)(\text{isoPFA})$, **3b** (with racemic isoPFA), grown by I.R. Butler, were subjected to an X-ray analysis. The data²⁸ reveal a pseudo-octahedral structure with approximately *trans* chlorides, *cis* phosphorus donor atoms and an *ortho* phenyl hydrogen atom in the vicinity of the sixth position.

Di- μ -chloro- μ -hydrido- η^2 -dihydrogenhydridobis(triphenylphosphine){1-[α -*N,N*-dimethylaminoethyl]-2-diisopropylphosphino-ferrocene}diruthenium(II), (η^2 - H_2)(isoPFA) $\text{Ru}(\mu\text{-Cl})_2(\mu\text{-H})\text{RuH}(\text{PPh}_3)_2$, **4**

All manipulations were carried out under a hydrogen atmosphere. A suspension of the starting complex, **3b** (0.334 g, 0.41 mmol) was reacted with H_2 (1-4 atm) at room temperature in a benzene/methanol (10:1) solvent mixture (4 mL) in an apparatus (Fig. 2.2) designed to minimize chances of atmospheric contamination. Reaction occurred in 4 - 10 days to give a brown solution and an orange precipitate. Because of the solubility limitation, larger amounts required longer reaction times. The rate also appeared to depend on methanol concentration. The precipitate was filtered and washed with methanol and benzene. A more detailed description of the experimental procedure is described in sect. 4.2. Yield: 0.094 g (39%). Anal. Calcd. for $\text{C}_{56}\text{H}_{66}\text{NCl}_2\text{P}_3\text{FeRu}_2$: C, 57.29; H, 5.62; N, 1.19. Found: C, 57.37; H, 6.02; N, 1.39. $^{31}\text{P}\{^1\text{H}\}$ NMR (121 MHz, CD_2Cl_2 , ambient temperature, 2 - 3 atm hydrogen atmosphere) δ ~78.5 (two overlapping doublets with $^2J_{\text{PP}} = 25$ or 40 Hz, PPh_3 *trans* to Cl), 77.2 (br s--possibly two br s overlapping, isoPFA), 64.6 (two overlapping doublets with $^2J_{\text{PP}} = 32$ or 40 Hz, PPh_3

trans to μ -H). ^1H NMR (300 MHz, CD_2Cl_2 , ambient temperature, 2 - 3 atm hydrogen atmosphere) δ -18.6 (dd, $^2J_{\text{PH}} = 28, 32$ Hz, Ru-H), -12 to -17 (bs, η^2 -H₂ and μ -H exchanging), 0.3, 0.39, 1.5, 1.8 (4dd, 12H, $^3J_{\text{PH}} = 15$ Hz, $^3J_{\text{HH}} = 7$ Hz, PCHCH₃), 1.48 (d, 3H, $^3J_{\text{HH}} = 7$ Hz, FcCHCH₃), 2.35, 3.1 (2s, 6H, N(CH₃)₂), 4.1 (s, 5H, C₅H₅), 4.08, 4.32, 4.42 (3s, 3H, C₅H₃), 4.50 (q, 1H, $^3J_{\text{HH}} = 7$ Hz, Fc-CH CH₃) (Signal at 4.50 resolved in CDCl_3), 6.9-7.2 (m, 18H, Ph *meta*, *para*), 7.4, 7.55 (2t, 12H, $J_{\text{HH}} = 9$ Hz, Ph *ortho*). Variable temperature experiments (Fig 3.25) and NMR discussion (sects. 3.3, 3.4) are presented later. About 14% of the product appears to comprise two other isomers, with $^{31}\text{P}\{^1\text{H}\}$ signals comparable to those given above, but slightly shifted: 79 (two overlapping doublets), 77.6 (s, possibly two s). IR ν^{KBr} 2109, 2025 cm^{-1} . Crystals of $(\eta^2\text{-H}_2)(\text{isoPFA})\text{Ru}(\mu\text{-Cl})_2(\mu\text{-H})\text{RuH}(\text{PPh}_3)_2\text{C}_6\text{H}_6$ suitable for an X-ray structure determination were obtained by recrystallization from CH_2Cl_2 /hexane/benzene (sect. 4.2). The crystal structure (Table 3.8, Fig. 3.4) is described later.

Carbonylchlorohydrido{1-[α -methoxyethyl]-2-diisopropylphosphinoferrrocene}(triphenylphosphine)ruthenium(II),
 $\text{RuHCl}(\text{CO})(\text{PPh}_3)(\text{isoPOF})$, **5**

A suspension of the starting complex, **3b** (0.245 g, 0.3 mmol), was refluxed under nitrogen in methanol (5 mL) for 7 d. During this time, the green starting complex, itself only sparingly soluble, reacted to give a yellow precipitate. The air-stable precipitate was isolated by filtration and washed with acetone. Yield: 0.16 g (67%). The product was recrystallized from dichloromethane/methanol. Anal. Calcd. for $\text{C}_{38}\text{H}_{45}\text{O}_2\text{ClP}_2\text{FeRu}$: C, 57.93; H, 5.72; N, 0.0; O, 4.07; Cl, 4.5. Found: C, 57.27; H, 5.59; N, 0.0; O, 3.90; Cl, 4.5. $^{31}\text{P}\{^1\text{H}\}$ NMR (121 MHz, CDCl_3 , ambient temperature, nitrogen atmosphere) δ 46.0 (d), 46.4 (d), $^2J_{\text{PP}} = 188$ Hz. ^1H NMR (300 MHz, CDCl_3 , ambient temperature,

nitrogen atmosphere) δ -13.9 (t, 1H, $^2J_{PH} = 19$ Hz, Ru-H), 0.83 (dd, 3H, $^3J_{PH} = 16$ Hz, $^3J_{HH} = 7$ Hz, PCHCH₃), 1.14 (d, 3H, $^3J_{HH} = 8$ Hz, FcCHCH₃), 1.81 (dd, 3H, $^3J_{PH} = 18$ Hz, $^3J_{HH} = 8$ Hz, PCHCH₃), 2.36 (m, 1H, PCHCH₃), 2.38 (s, 3H, OCH₃), 3.3 (m, 1H, PCHCH₃), 4.24, 4.28, 4.30, 4.32 (4s, 8H, FeC₅H₅, FeC₅H₃), 6.52 (q, 1H, $^3J_{HH} = 7$ Hz, FcCHCH₃), 7.38 (m, 9H, Ph *meta, para*), 7.71 (m, 6H, Ph *ortho*). IR $\nu^{KBr}(\text{Ru-H})$: 2007 cm⁻¹(w); $\nu^{KBr}(\text{CO})$ 1923 cm⁻¹(str). Crystals suitable for an X-ray structure determination were obtained and the crystallographic data are given later (Tables 5.1, 5.2, Fig. 5.6).

Carbonylchlorohydrido{1-[α -*N,N*-dimethylaminoethyl]-2-diisopropylphosphinoferrocene}(triphenylphosphine)ruthenium(II), RuHCl(CO)(PPh₃)(isoPFA), **6**

A suspension of the starting complex, **3b** (0.06 g, 0.07 mmol) was refluxed with 25 μ L of a 3 M methanolic solution of KOH (~0.07 mmol) in 2 mL of methanol, till no more solid, sparingly soluble, green starting material was visible and a reddish-yellow solid had been deposited (~30 min). The precipitate was filtered from the red supernatant under an inert atmosphere and washed with methanol. Yield of crude product: 0.018 g (25%). The efficiency of this preparation, in terms of product selectivity, is enhanced if the RuCl₂(PPh₃)(isoPFA), **3b** is very finely ground. Larger crystals are slow to dissolve and take longer to react. Secondary reactions, fortunately 10 to 100 times slower than the formation of **6**, do occur; hence, the reaction must be stopped before significant amounts of the secondary products form, yet after the starting material has disappeared. A sample of the product was recrystallized from methanol/dichloromethane. Anal. Calcd. for C₃₉H₄₆ONClP₂FeRu: C, 58.64; H 5.76; N 1.75; Cl, 4.4. Found: C, 57.52; H, 5.86; N, 1.70; Cl, 5.5. $^{31}\text{P}\{^1\text{H}\}$ (121 MHz, CDCl₃, ambient temperature, nitrogen atmosphere) δ 50.0 (d), 31.9 (d), $^2J_{PP} = 290$ Hz. This coupling is confirmed by both 300

MHz and 400 MHz spectra. The $^{31}\text{P}\{^1\text{H}\}$ NMR spectrum showed another set of doublets, with varying intensity (from ~10% relative to the above, up to almost equal intensity), and with chemical shifts differing by $\delta \sim 0.15$, and with the same $^2J_{\text{PP}}$ value. ^1H NMR (300 MHz, CDCl_3 , ambient temperature, nitrogen atmosphere) δ -15.3 (dd, $^2J_{\text{PH}} = 30, 20$ Hz, Ru-H), 0.82 (dd, 3H, $^3J_{\text{PH}} = 12$ Hz, $^3J_{\text{HH}} = 6$ Hz, PCHCH₃), 1.22 (dd, 3H, $^3J_{\text{PH}} = 12$ Hz, $^3J_{\text{HH}} = 6$ Hz, PCHCH₃), 1.26 (d, 3H, $^3J_{\text{HH}} = 6$ Hz, Fc-CHCH₃), 1.68 (m, 6H, PCHCH₃), 2.3 (br s, 6H, N(CH₃)₂, resolved from 0 °C down to -50 °C into two separate singlets at 2.21, 2.38 ppm), 2.5 (m, 1H, PCHCH₃), 3.28 (m, 1H, PCHCH₃), 4.2 (s, 5H, FeC₅H₅), 4.28, 4.35, 4.41 (3s, 3H, C₅H₃), 5.48 (q, 1H, $^3J_{\text{HH}} = 5$ Hz, Fc-CHCH₃), 7.35 (s, 9H, Ph *meta, para*), 7.72 (m, 6H, Ph *ortho*). Another minor (~10%) high-field ^1H NMR hydride resonance always accompanied that described above: -15.8(t) with $^2J_{\text{PH}} = \sim 23$ Hz. IR $\nu^{\text{KBr}}(\text{Ru-H})$ 2079 $\text{cm}^{-1}(\text{w})$; $\nu^{\text{KBr}}(\text{CO})$ 1879 $\text{cm}^{-1}(\text{str})$. A single crystal X-ray structure determination (Tables 5.1, 5.2, Figs. 5.9, 5.10) was carried out on crystals grown as described below.

Chlorohydrido{1-[α -*N,N*-dimethylaminoethyl]-2-diisopropylphosphinoferrocene}(triphenylphosphine)ruthenium(II), RuHCl(PPh₃)(isoPFA), **7**

The starting complex, **3b** (0.08 g, 0.1 mmol), and Proton Sponge[®] (0.023 g, 0.1 mmol) were placed under nitrogen in methanol (1-2 mL) for 5 months. Large black-red crystals (~20 mg) of **7** grew in this time, as well as yellow crystals of **6**. The amount of **7** was difficult to measure as some red crystals had grown around the crystals of starting material. This mixture of crystals of **3b**, **6**, and **7** was separated from the solution by filtration or decanting and washed with methanol and dried. The large black-red crystals of

7 were then isolated by handpicking them out of the mixture. Anal. Calcd. for $C_{38}H_{48}NCIP_2FeRu$: C, 59.06; H, 6.22; N, 1.81. Found: C, 58.38; H, 6.00; N, 1.80. $^{31}P\{^1H\}$ NMR ($CDCl_3$, 121 MHz, ambient temperature, under vacuum) δ 98.0 (d), 61.5 (d), $^2J_{PP} = 40$ Hz. 1H NMR ($CDCl_3$, 300 MHz, ambient temperature, nitrogen atmosphere) δ -23.1 (dd, $^2J_{PH} = 40, 27$ Hz, RuH). IR $\nu^{KBr}(RuH)$ 2028 $cm^{-1}(w)$; a peak at 1897 $cm^{-1}(w)$ was probably due to the presence of some **6**. A single crystal X-ray structure determination was carried out and is discussed later (Tables 5.1, 5.2, Fig. 5.12).

Chapter 3

Characterization and reactivity of some dinuclear ruthenium(II) phosphine complexes containing $\eta^2\text{-H}_2$

3.1 Introduction

Historical background

The possibility of a transition state, involving dihydrogen molecules interacting with a metal centre, has been considered over the past thirty years.²⁹ In 1976, Ashworth and Singleton³⁰ cited indirect evidence for stable H_2 binding. These workers observed that all the reactions of $\text{RuH}_4(\text{PPh}_3)_3$ and $\text{RuH}_3(\text{dppe})_2^+$ proceeded by initial loss of H_2 , and by analogy with the similar behaviour of reversibly bonded dioxygen compounds, they proposed that these complexes could be regarded as dihydrogen adducts of ruthenium(II). This appears to be a weak analogy, however. Direct proof for such binding in these and other reported systems was lacking until about 1983.²⁹

In 1980, Kubas reported³¹ that the infrared spectra of the complexes, $\text{M}(\text{H}_2)(\text{CO})_3(\text{PR}_3)_2$ ($\text{M} = \text{Mo}, \text{W}$; $\text{R} = \text{Pr}^i, \text{Cy}$), as well as the lability of dihydrogen in these complexes, suggested that the H_2 bonding might be unusual. Eventually, Kubas' group obtained neutron diffraction and X-ray crystal structures of $\text{W}(\text{H}_2)(\text{CO})_3(\text{PCy}_3)_2$, and the neutron structure showed a dihydrogen moiety. The ^1H NMR spectrum of the HD complex showed that the HD coupling constant was large, and similar to that for gaseous HD, thus providing the most convincing evidence for the presence of bound dihydrogen. These NMR and diffraction data were first reported in 1983.^{32,33} The next stable H_2 complex to be reported was $[\text{IrH}(\text{H}_2)(\text{bq})(\text{PPh}_3)_2]^+$, by Crabtree *et al.*³⁴ Their ^1H NMR T_1 measurements indicated the binding of molecular hydrogen. This criterion is discussed below. Subsequently, Morris *et al.* reported³⁵ that the complexes, $[\text{MH}(\text{H}_2)(\text{dppe})_2]^+$ ($\text{M} = \text{Fe}, \text{Ru}$) contained bound dihydrogen; the X-ray crystal structure showed a short H-H distance for the H_2 moiety, and a large HD coupling constant for the HD complex

confirmed the presence of bound dihydrogen (further discussion of this criterion appears below), consistent with Ashworth and Singleton's speculation about the Ru complex.³⁰ Recent articles, including reviews, cite numerous other examples of dihydrogen complexes.^{29,36,37} While some such species are stable only at low temperature, others exist at ambient temperatures. A number of previously known polyhydrides are now recognized as containing the $\eta^2\text{-H}_2$ ligand; among these is $\text{RuH}_2(\text{H}_2)(\text{PPh}_3)_3$,³⁸ again, as previously suggested.³⁰

Factors affecting the stability of $\eta^2\text{-H}_2$ complexes of the transition metals

Molecular hydrogen complexes have thus far been reported for the transition metals shown in Table 3.1,^{29,37} and include examples for the electron configurations shown in Table 3.2. Complexes stable at room temperature, if necessary under 1 atm hydrogen, have been found only for d^2 , d^4 , d^6 and d^8 configurations. The coordination numbers^{29,36,37,39} (counting $\eta^2\text{-H}_2$ as one) for complexes along with their electron

Table 3.1

Transition metals which have been found in molecular hydrogen complexes.

Cr	Fe	Co	Ni	Cu
Mo	Ru	Rh	Pd	
W	Re	Os	Ir	

configurations are shown in Table 3.3. All known dihydrogen complexes (the count being over 50, to date) are 18 electron species, considering $\eta^2\text{-H}_2$ as a 2-electron donor.

Other points to note are:²⁹

all known complexes are neutral or cationic, and none are anionic; all contain π -acceptor ligands, except for the matrix-isolated, "ligand-free" PdH_2 and the small cluster complexes, $\text{Cu}_2\text{H}_2(\text{H}_2)_x$ and $\text{Cu}_3(\text{H}_2)$; and most examples are octahedral.

Table 3.2Electronic configurations and oxidation states of examples of $\eta^2\text{-H}_2$ complexes.

electron configuration	oxidation state	group number	example(s)
d^0	VI	6	$[\text{MoH}_4(\eta^2\text{-H}_2)(\text{dppe})_2]^{2+}$ ³⁹
d^2	V	7	$\text{ReH}_5(\eta^2\text{-H}_2)(\text{PPh}_3)_2$, $\text{ReH}_5(\eta^2\text{-H}_2)(\text{dppe})$ ³⁶
d^4	II	6	$\text{M}(\text{H})(\eta^2\text{-H}_2)\text{Cp}(\text{CO})_2$ ($\text{M} = \text{Mo}, \text{W}$) ⁴⁰
d^4	IV	8	$[\text{OsH}_3(\eta^2\text{-H}_2)(\text{PPh}_3)_3]^+$
d^6	II	8	many examples, ^{29,36,37} e.g., $[\text{MH}(\eta^2\text{-H}_2)(\text{dppe})]^+$ ($\text{M} = \text{Ru}, \text{Fe}$) ³⁵
d^8	I	9	$[\text{Rh}(\eta^2\text{-H}_2)\{\text{P}(\text{CH}_2\text{CH}_2\text{PPh}_2)_3\}]^+$, ⁴¹ $\text{Co}(\eta^2\text{-H}_2)\text{R}(\text{CO})_3$ ($\text{R} = \text{H}, \text{CH}_3$) ⁴²
d^{10}	0	10	$\text{Ni}(\eta^2\text{-H}_2)(\text{CO})_3$ ⁴³

Table 3.3Coordination numbers of $\eta^2\text{-H}_2$ complexes, according to electron configuration

coordination number	electron configuration
9	0 (only one d^0 complex proposed to date)
8	2
7	4 (taking $\eta^5\text{-C}_5\text{H}_5^-$, in $\text{M}(\text{H})(\eta^2\text{-H}_2)\text{Cp}(\text{CO})_2$ ($\text{M} = \text{Mo}, \text{W}$), as occupying three coordination sites)
6	6
5	8
4	10 (exceptions include only the matrix-isolated "ligand-free" $\text{Pd}(\eta^2\text{-H}_2)$ and small clusters, such as $\text{Cu}_3(\eta^2\text{-H}_2)$)

Theoretical considerations

Kubas' group²⁹ has considered the question of whether steric or electronic factors are more important in determining whether H_2 binds as $\eta^2\text{-H}_2$ or as the dihydride. Within the series of complexes, $\text{MoH}_2(\text{CO})_3(\text{L-L})$, where L-L is a chelating, ditertiary phosphine ligand, the basicity of the phosphine (i.e. electronic factors) appears to be more important

in determining the mode of H₂-binding. The more basic, alkyl ditertiary phosphines promoted dihydride formation, whereas dppe (with phenyl groups) permits η²-H₂ coordination. It had been observed that stable dihydrogen complexes contained bulky ligands, and it was earlier thought that steric factors were more important; Kubas, however, concludes from the data on the Mo series that electronic factors are more important. But the fact remains that all room-temperature-stable dihydrogen complexes do contain bulky ligands. It seems reasonable that bulky ligands, in some systems, might promote dihydrogen coordination over dihydride formation if such a reduction in coordination number would better accommodate the bulky ligands. There are insufficient experimental data to discuss the factors meaningfully.

A study⁴⁴ on protonation of the series of complexes, [RuH(Cp)(Ph₂P(CH₂)_nPPh₂)]⁺ (n = 1-3) has demonstrated the importance of chelate ring size in determining whether dihydride or η²-H₂ ligands are produced in this system. The dppm ligand, n = 1, promoted the formation of the dihydrogen complex exclusively, while dppp, n = 3, promoted only dihydride formation. The dppe complex, on protonation, yielded a mixture of the two types.

An insight into how electronic factors might influence the mode of H₂ bonding is provided by theoretical treatments.^{29,45,46,47} The favoured model for the bonding is shown in Fig. 3.1 Molecular orbital calculations⁴⁶ indicated that donation of σ electrons to the metal atom provides the main contribution to the bonding, whereas the contribution of back-bonding from a metal to the σ* orbital of the η²-H₂ moiety is small. In the crystal structure of W(η²-H₂)(CO)₃(P(Prⁱ)₃)₂, the H₂ is oriented so that such π interaction is possible.⁴⁶ Calculations also confirm⁴⁷ that π-acceptor ligands enhance the M←H₂ interaction, whatever the metal, consistent, for example, with the experimental observation for the MoH₂(CO)₃(L-L) complexes. Burdett *et al.*⁴⁷ note, in particular, that a π-acceptor ligand *trans* to the η²-H₂ ligand stabilizes the bonding mode, by reducing the extent of back-bonding into σ*(H₂). However, complexes such as M(η²-H₂)(CO)₅ (M = Cr, Mo)

are unstable with respect to loss of H_2 , in spite of the number of π -acceptor (CO) ligands; the back-bonding to $\sigma^*(H_2)$ may, in these cases, be too small.²⁹ It seems that some back-bonding is necessary for stability.²⁹ Thus, d^0 complexes are expected to be unstable.³⁶

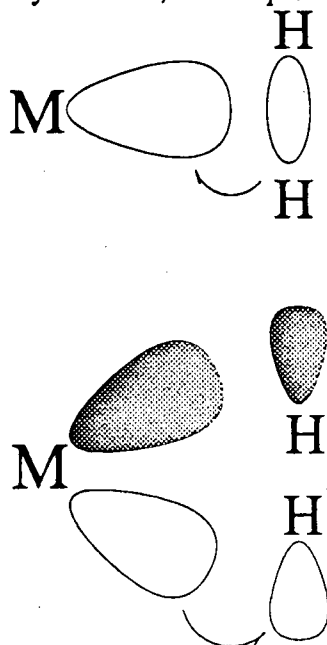


Figure 3.1 Orbital diagrams showing the contributions to the bonding for the $M-(\eta^2-H_2)$ structure.

The following summary may be made of factors determining whether or not a η^2-H_2 complex may be formed:

a) The metal There is not yet sufficient reason to exclude other transition metals (e.g., group IV, V or even XI and XII metals) as candidates for η^2-H_2 complexes, but generalizations are possible. Classical hydrides are more likely for the early transition metals; for example, $WH_6(PR_3)_3$ is classical, but $ReH_7(PR_3)_2$ contains a dihydrogen ligand. Also, classical hydrides are more likely for third-row metals; for example, $OsH_4(PR_3)_3$ is classical, while the Fe and Ru analogues contain dihydrogen.

b) The 18 electron rule It may not be accidental that all η^2-H_2 complexes are 18-electron species. If there were, say, a vacant site on a transient 16-electron dihydrogen complex, a second dihydrogen molecule (if available) would be likely to coordinate,

because any metal centre that can stabilize one $\eta^2\text{-H}_2$ would probably be able to stabilize another. Although not all the $\eta^2\text{-H}_2$ complexes are formed by addition of free H_2 to unsaturated precursors (some are formed by protonation of hydrides), free dihydrogen is always generated *in situ* in these systems. That is, coordinated dihydrogen is labile and the coordination reversible.²⁹ On the other hand, there may have been insufficient attempts to protonate 16-electron hydrides.

c) Electron configuration So far it appears that an even-numbered d^n configuration is required, and d^6 is preferable.

d) Ligand type The presence of π -acceptor ligands helps to stabilize these complexes, and bulky ligands may favour a dihydrogen complex over a dihydride.

f) Structure Octahedral geometry seems to be preferred.

Criteria for recognition of dihydrogen complexes

The ν_{HH} mode in the infrared spectrum has attracted more interest than other IR vibrational modes for the purpose of characterization, but only a few complexes have exhibited the assigned broad weak band in the range 2400 to 3100 cm^{-1} (Table 3.4). Often the band is either obscured by other bands or is too weak to be seen. In a few cases,²⁹ other frequencies have been assigned as due to vibrations of the MH_2 unit (e.g., $\nu_a(\text{MH}_2)$ 1345 - 1568 cm^{-1} , $\nu_s(\text{MH}_2)$ 868 - 960 cm^{-1} , $\delta(\text{MH}_2)$ 400 - 471 cm^{-1}). The usefulness of infrared and Raman spectra has been quite limited.

Prior to the publication⁴⁸ of the structure determined in the present work and shown later in Figure 3.4, neutron and X-ray structure determinations had been successful in locating the $\eta^2\text{-H}_2$ ligand in $\text{W}(\eta^2\text{-H}_2)(\text{CO})_3(\text{PPr}_3)_2$ and $[\text{FeH}(\eta^2\text{-H}_2)(\text{dppe})_2]^+$. In $\text{W}(\eta^2\text{-H}_2)(\text{CO})_3(\text{PPr}_3)_2$, the H-H distance is given as 0.75 Å⁴⁹ by X-ray, 0.84 Å⁴⁹ and 0.82(1) Å^{50,51} by neutron diffraction. In $[\text{FeH}(\eta^2\text{-H}_2)(\text{dppe})_2]\text{BF}_4$, the H-H distance is 0.89(11) Å (X-ray); a neutron diffraction study of a crystal of the BPh_4^- salt yields 0.815(20) Å.^{52,53} The X-ray structure⁴⁸ (Fig. 3.4) of $(\text{isoPFA})(\eta^2\text{-H}_2)\text{Ru}(\mu\text{-H})(\mu\text{-$

Table 3.4

Vibrational Frequencies, $\nu_{\text{HH}}(\text{cm}^{-1})$, for Dihydrogen Complexes

Complex	$\nu_{\text{HH}}(\text{cm}^{-1})$	reference
$\text{W}(\eta^2\text{-H}_2)(\text{CO})_3(\text{PCy}_3)_2^{\text{a}}$	2690	29
$\text{Mo}(\eta^2\text{-H}_2)(\text{CO})_3(\text{PCy}_3)_2^{\text{a}}$	2950 ^d	29
$\text{Mo}(\eta^2\text{-H}_2)(\text{CO})(\text{dppe})_2^{\text{a}}$	2650	29
$\text{W}(\eta^2\text{-H}_2)(\text{CO})_5^{\text{b}}$	2711	29
$\text{Co}(\eta^2\text{-H}_2)(\text{CO})_2(\text{NO})^{\text{c}}$	3100	29
$\text{FeH}_2(\eta^2\text{-H}_2)(\text{PEtPh}_2)_3^{\text{a}}$	2380	36,54
$\text{FeH}_2(\eta^2\text{-H}_2)(\text{PBuPh}_2)_3^{\text{a}}$	2400	58

^aNujol mull.^bLiquid xenon solution at -70 °C.^cXenon matrix at -261 °C.^dCalculated, based on the observed frequency for the D₂ complex.

$\text{Cl})_2\text{RuH}(\text{PPh}_3)_2$, **4** has revealed the $\eta^2\text{-H}_2$ ligand, with an H-H distance of 0.80(6) Å.

There are only three crystal structures to date showing the $\eta^2\text{-H}_2$ ligand; disorder and other problems have frustrated attempts to locate the $\eta^2\text{-H}_2$ unit in other crystal structures.^{23,55,56,57,58}

Data from NMR studies, particularly J_{HD} coupling constants and T_1 measurements, have been used extensively for the study of $\eta^2\text{-H}_2$ complexes. Formation of the corresponding $\eta^2\text{-HD}$ species using HD instead of H₂ in the synthesis, or using deuteration of an $\eta^2\text{-H}_2$ complex, allows for observation of the HD coupling constant (Table 3.5). The value of J_{HD} is an order of magnitude larger than that for compounds containing classical, non-linked hydride and deuteride ligands, and is comparable to that for HD gas (43.2 Hz). The value of J_{HD} has been also used as a measure of the interaction of the HD molecule with the metal centre, lower values of J_{HD} being indicative of stronger interaction. Sometimes, however, in fluxional complexes, this coupling is obscured, and Crabtree's

Table 3.5

Some ^1H NMR HD Coupling Constants (Hz) for $\eta^2\text{-H}_2$ Resonances^a

Complex	J_{HD}	reference
$\text{W}(\text{HD})(\text{CO})_3(\text{PPr}^i_3)_2$	33.5	49
<i>trans</i> - $[\text{OsH}(\text{HD})(\text{meso-tetraphos-1})]\text{BPh}_4$	26.4	37
<i>trans</i> - $[\text{FeH}(\text{HD})(\text{meso-tetraphos-1})]\text{BF}_4$	32.3	37
$[\text{Rh}(\text{HD})(\text{tetraphos-2})](\text{O}_2\text{CCF}_3)$	18	54
$\text{Mo}(\text{HD})(\text{CO})(\text{dppe})_2$	34	57
$\text{Ru}(\text{HD})\text{Cp}(\text{dmpe})$	22	59
$[\text{Ru}(\text{HD})\text{Cp}(\text{PPh}_3)(\text{CNBu}^t)]\text{PF}_6$	28.6	60
$[\text{Ru}(\text{HD})\text{Cp}(\text{dppe})]\text{PF}_6$	24.9	44
$[\text{Ru}(\text{HD})\text{Cp}(\text{dmpe})]\text{PF}_6$	21.9	44
$[\text{RuD}(\text{HD})(\text{dppe})]^+$	32.9	61
$[\text{RuD}(\text{HD})(\text{depe})]^+$	32	61
$[\text{FeD}(\text{HD})(\text{dppe})]^+$	30	61
$[\text{FeD}(\text{HD})(\text{depe})]^+$	28	61
$[\text{Ru}(\text{HD})\text{Cp}(\text{CO})(\text{PR}_3)]^+$ ($\text{PR}_3 = \text{PPh}_3, \text{PMe}_3,$ $\text{PMe}_2\text{Ph}, \text{PCy}_3$)	28-30	59
$[\text{IrH}(\text{HD})(\text{bq})(\text{PPh}_3)_2]^+$	29.5	62
$[\text{IrH}(\text{HD})(\text{bq})(\text{PCy}_3)_2]^+$	29	62
$[\text{FeD}(\text{HD})(\text{Ph}_2\text{PCH}_2\text{CH}_2\text{PEt}_2)]^+$	32	63

^acf. HD gas, 43.2 Hz⁴⁹. The J_{HD} values for deuteride-hydride complexes are an order of magnitude smaller (e.g., $J_{\text{HD}} < 1$ Hz for $[\text{RuHDCp}(\text{dppe})]^+$ ⁴⁴).

coupling is obscured, and Crabtree's group^{36,62} introduced the use of another NMR criterion, the ^1H NMR longitudinal relaxation time, T_1 , for the $\eta^2\text{-H}_2$ resonance.

Because the H-H distance, r_{HH} , for the $\eta^2\text{-H}_2$ ligand is relatively short, the NMR relaxation time, T_1 , is also short (<100 ms.) The relaxation mechanism is usually "dipole-dipole" for protons less than 2 Å apart³⁶, and for this mechanism, the rate of relaxation, $R(\text{DD})$, is related to the internuclear distance generally by the equation:³⁶

$$R(\text{DD}) = [T_1(\text{DD})]^{-1} = 0.3\gamma^4 h^2 r^{-6} (2\pi)^{-2} J(\omega)$$

$$R(DD) = [T_1(DD)]^{-1} = 0.3 \gamma^4 h^2 r^{-6} (2\pi)^{-2} \left[\frac{\tau_c}{(1 + \omega^2 \tau_c^2)} + \frac{4\tau_c}{(1 + 4\omega^2 \tau_c^2)} \right] \quad (3.1)$$

where $J(\omega)$ = spectral density,

γ = gyromagnetic ratio,

h = Planck's constant,

r = internuclear distance,

τ_c = rotational correlation time

and ω = Larmor frequency.

Thus, T_1 is proportional to r_{HH}^6 and the range of T_1 values for η^2 -H₂ atoms is roughly an order of magnitude less than the range for coordinated hydride ligands.

Equation 3.1 predicts a T_1 minimum when the Brownian motion is best matched with the Larmor frequency, ω ; ie., when:

$$\tau_c = 0.63/\omega \quad (3.2)$$

where τ_c is a measure of the Brownian motion. Thus, if a T_1 minimum can be observed, by a series of T_1 measurements at various temperatures, τ_c can be calculated by using equation 3.2, and hence, r_{HH} can be calculated, the other factors being known.³⁶ Table 3.6 lists some T_1 and r_{HH} values³⁶ estimated by this method, which assumes dipole-dipole relaxation to be the only mechanism. Thus, the T_1 value is both diagnostic for showing the presence of the η^2 -H₂ ligand and useful for estimating r_{HH} for it.

Morris *et al.*⁵² have discussed the need for a refinement of the minimum T_1 method, because of the effect on the T_1 by contribution of another mechanism in addition to that related to the tumbling of the complex. The refinement is an attempt to include the effect, via dipole-dipole relaxation, of the rotation of the H₂ molecule about the M-H₂ bond axis, and defines two correlation times: τ_H , for the tumbling of the complex as a whole, and τ_{H_2} , for the additional motion of the spinning H₂. The H-H (H₂) distances for the two complexes, $[\text{FeH}(\text{H}_2)(\text{dppe})_2]^+$ and $\text{W}(\text{H}_2)(\text{CO})_3(\text{PPr}_3)_2$, for which solid state H-H

Table 3.6

Selected T_1 (minimum) values^a for various hydride and dihydrogen complexes

complex	temperature (K)	T_1 (ms) (minimum)	r_{HH} (Å) (from T_1)	r_{HH} (Å) (from solid state)
classical hydrides:				
$\text{WH}_6(\text{PMe}_2\text{Ph})_3$	235	181	1.74C ^b	
$\text{WH}_5(\text{PMePh}_2)$	240	179	1.74C	
$[\text{IrH}_2(\text{CO})_2(\text{PPh}_3)_2]^+$	210	245	1.81C	
$[\text{ReH}_8(\text{PPh}_3)]^-$	200	245	1.83C	
dihydrogen complexes:				
$[\text{FeH}(\eta^2\text{-H}_2)(\text{dppe})_2]^+$	210	< 8.5	< 1.05C	0.89(11) ^c , 0.815(20) ^d
$\text{W}(\eta^2\text{-H}_2)(\text{CO})_3(\text{PPr}_i)_2$	193	< 5	< 0.96C	0.75(16) ^c , 0.82(1) ^d
$\text{RuH}_2(\eta^2\text{-H}_2)(\text{PPh}_3)_3$	266	30	1.16C	
$[\text{IrH}(\text{H}_2)(\text{bq})(\text{PPh}_3)_2]^+$	200	8	1.04C	0.92 ^e
$\text{ReH}_5(\eta^2\text{-H}_2)(\text{PPh}_3)_2$	200	110	1.20C	

^aFrom reference 36; r_{HH} calculated from equation 3.1.^bHamilton and Crabtree³⁶ have introduced the empirical constant C to bring calculated r_{HH} values into line with known solid state values; they have suggested the value 0.9 for dihydrogen complexes and 1.0 for classical hydrides.^cFrom X-ray diffraction data.^dFrom neutron diffraction data.^eFrom solid state NMR data.

distances are known (*vide supra*), were calculated by using the following modified expression for the spectral density, $J(\omega)$, at a particular frequency, $\omega (= 2\pi\nu)$:⁵²

$$J(\omega) = 0.25 \frac{\tau_{\text{H}}}{1 + \omega^2 \tau_{\text{H}}^2} + 0.75 \frac{\frac{\tau_{\text{H}}}{(1 + 2\alpha)}}{1 + \omega^2 \left(\frac{\tau_{\text{H}}}{1 + 2\alpha}\right)^2} \quad (3.3)$$

where $\alpha = \tau_{\text{H}}/\tau_{\text{H}_2}$. (3.4)

Reasonable H-H distances (r_{HH}) for the H_2 moiety are obtained when the correlation time for the spinning motion of the H_2 -ligand is assumed to be much faster than that for the complex as a whole; i.e.:

$$\tau_{H_2} \ll \tau_H, \text{ and } \alpha \approx 0. \quad (3.5)$$

For this case, the spectral density function becomes:

$$J(\omega) = \frac{0.25\tau_H}{1 + \omega^2\tau_H^2} \quad (3.6)$$

The value of r_{HH} , obtained using this expression for $J(\omega)$ in equation 3.1, differed from the result using Crabtree's method, by a factor of $(0.25)^{1/6}$, or ~ 0.8 . Independent evidence for this spinning motion has been reported,^{51,52} and the spin rate was measured for the complex, $W(D_2)(CO)_3(PPr^i_3)_2$, as being >130 kHz.⁵¹

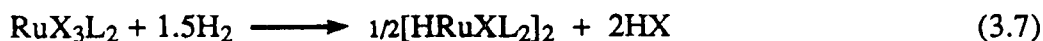
Dinuclear, η^2 - H_2 complexes reported in the present work

Interest in Ru complexes containing monodentate tertiary phosphine ligand systems has grown out of ongoing efforts to characterize possible intermediate hydrides in catalytic olefin hydrogenation systems. Interest in the dinuclear, η^2 - H_2 complexes to be described arose, in particular, out of efforts by others in this department^{25,64,65} to characterize hydrides formed in hydrogenation systems employing $RuCl_2(PPh_3)(PPFA)$, **3a**, and $RuCl_2(PPh_3)(isoPPFA)$, **3b**, as catalyst precursors. Initial efforts by Rodgers *et al.*²⁵ had failed to detect hydrides in the reaction of **3a** with hydrogen at pressures of ≤ 1 atm. This thesis reports the formation of three dihydrogen complexes in various systems, including the complex $(\eta^2-H_2)(PPh_3)_2Ru(\mu-H)(\mu-Cl)_2RuH(PPh_3)_2$, **1a**, previously formulated with all hydrogen ligands as classical hydrides.

The characterization and reactivity of the complexes **1a** and **1b** have been reinvestigated in the present work. Prior to the discovery and initial characterization of

complexes **1**, by Dekleva, Thorburn and James,²³ a monohydride bisphosphine intermediate was believed to be an active species in the hydrogenation of olefins catalyzed by the Ru(II) trisphosphine complex, $\text{RuHCl}(\text{PPh}_3)_3$ ^{2-4,66,67,68,69} (further discussion appears in chapter 4). Related to these studies is the interest in possible hydride intermediates important in the activation of hydrogen by DMA solutions of the Ru(III) complexes, RuX_3L_2 ($\text{X} = \text{Cl, Br; L} = \text{PPh}_3, \text{AsPh}_3$).⁶⁹ A series of hydrides, initially characterized as $[\text{HRuXL}_2]_2$ ($\text{X} = \text{Cl, Br; L} = \text{PPh}_3, \text{AsPh}_3$), were isolated^{69,70} and their catalytic behaviour investigated^{70,71} (again, discussed further in chapter 4).

The preparative reactions were initially⁶⁹ written as equation 3.7, the measured H_2 uptake corresponding to 1.5 moles H_2 per Ru:

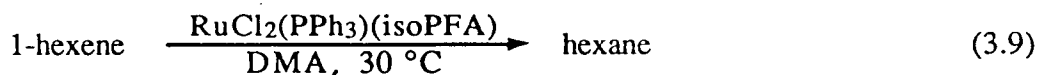


A few years later, Dekleva *et al.*^{21,23} discovered that a subsequent slower H_2 absorption occurred, and that, finally, a total of 2 moles H_2 was absorbed per Ru. The products were consequently formulated, correct in terms of stoichiometry, as $[\text{RuH}_2\text{XL}_2]_2$, and the reactions written as:



A series of chemical reactions supported this formulation and, in addition, a crystal structure of the complex with $\text{X} = \text{Cl}$ and $\text{L} = \text{P}(p\text{-tol})_3$ was obtained,^{21,23,71} although the hydrogen ligands were not located. Dekleva *et al.*²³ also rationalized the ^1H and $^{31}\text{P}\{^1\text{H}\}$ NMR spectra, and the visible spectra, of two of the systems ($\text{X} = \text{Cl; L} = \text{PPh}_3, \text{P}(p\text{-tol})_3$), based on the structure of the *p*-tolyl system (see Fig. 3.3, later). Although in his thesis work, Dekleva²¹ alluded to the possibility that **1b** might be an $\eta^2\text{-H}_2$ complex, no experimental data to verify this were obtained. The present studies, to be described in this chapter, show that this type of complex contains one terminal and one bridged hydride, and a $\eta^2\text{-H}_2$ moiety.

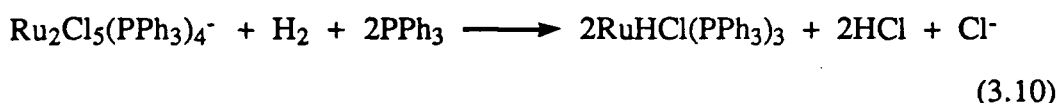
The characterization and reactivity of $(\text{isoPFA})(\eta^2\text{-H}_2)\text{Ru}(\mu\text{-H})(\mu\text{-Cl})_2\text{RuH}(\text{PPh}_3)_2$, **4**, are also presented in this chapter. The discovery of this complex arose out of a search for possible hydride intermediates in the catalytic hydrogenation system:



Chapter 4 contains a detailed account of this search, the background of the work, and the relevance of the findings to the catalytic hydrogenation. In this chapter, the focus is on the complex itself, and its place in the series of dinuclear dihydrogen complexes examined in the present work.

Also presented in this chapter are two newly discovered adducts of dihydrogen and the complexes $\text{Ru}_2\text{Cl}_4(\text{PR}_3)_4$ ($\text{R} = \text{Ph}$, *p*-tol), **2a** and **2b**, respectively, formed *in situ* in solution. The history of the dimeric complexes **2** is closely linked with that of $\text{RuCl}_2(\text{PPh}_3)_3$, which has received considerable attention²⁻⁴ as a catalyst for a wide variety of organic reactions, and as a precursor for $\text{RuHCl}(\text{PPh}_3)_3$. Early reports^{27,72,73} of a solvated, monomeric bisphosphine species, resulting from the dissociation of PPh_3 from $\text{RuCl}_2(\text{PPh}_3)_3$, in various solvents, were later disputed.^{74,75} On the basis of $^{31}\text{P}\{^1\text{H}\}$ NMR evidence ($\delta_{\text{CH}_2\text{Cl}_2}(-97\text{ }^\circ\text{C})$ 58.8 (d), 53.0 (d), $^2J_{\text{PP}} = 41.5$ Hz), Hoffman and Caulton described the bisphosphine species as the dimer; in the non-coordinating solvent, CH_2Cl_2 , a monomer would be expected to be square planar or tetrahedral, thus giving a $^{31}\text{P}\{^1\text{H}\}$ NMR singlet.²⁶ These workers also suggested the possibility of a polymeric species in the solid state,²⁶ and other workers^{76,77} have discussed the possibility of polymeric species in concentrated solution. James and coworkers^{24,70,78} subsequently reported the isolation of this species, from the reaction of $\text{RuCl}_3(\text{PPh}_3)_2(\text{DMA})\cdot\text{DMA}$ with hydrogen in DMA; the DMA-free complex **2a** was precipitated by addition of methanol. A

molecular weight measurement in toluene (Calcd.: 1390; Found: 1200) confirmed the dimeric formulation. In DMA at 25 °C, **2a** exhibited a singlet at δ 66.7 in the $^{31}\text{P}\{^1\text{H}\}$ NMR spectrum, and this singlet was initially interpreted^{24,70} as indicating a monomeric species, $\text{RuCl}_2(\text{DMA})_2(\text{PPh}_3)_2$; Dekleva²¹ later showed that at low temperature an ABCD spin pattern was the major feature of the $^{31}\text{P}\{^1\text{H}\}$ NMR spectrum ($\delta_{\text{DMA/toluene-d}_8}(-70\text{ }^\circ\text{C})$ 52.88 (d, P_A), 48.34 (d, P_B), 42.67 (d, P_C), 42.22 (d, P_D), $J_{\text{AB}} = 29.9$ Hz; $J_{\text{CD}} = 36.8$ Hz), and he attributed this pattern to the complex, $\text{Ru}_2\text{Cl}_4(\text{DMA})(\text{PPh}_3)_4$, thought to be a triply chloro-bridged dinuclear molecule, with DMA coordinated and both Ru atoms being six-coordinate. In the **2a** preparation described above, the DMA evidently dissociates during the methanol precipitation. Studies in this department have been carried out on the reactions of $\text{RuCl}_2(\text{PPh}_3)_3$ with hydrogen to give $\text{RuHCl}(\text{PPh}_3)_3$ and, because of the complicated solution behaviour of $\text{RuCl}_2(\text{PPh}_3)_3$, studies were also done in the presence of excess phosphine and/or chloride. In the presence of excess chloride, solutions of $\text{RuCl}_2(\text{PPh}_3)_3$ contain the triply chloro-bridged $\text{Ru}_2\text{Cl}_5(\text{PPh}_3)_4^-$ as the main species.^{21,23} To "probe the intermediate stages" of the reaction:



Dekleva²¹ studied the reactivity of **2a** toward hydrogen in the absence of PPh_3 , and he reported this complex, in the absence of added base and in a non-basic solvent, to be inert toward hydrogen; but in the presence of Proton Sponge[®] in DMA or toluene- d_8 , the reaction proceeded to give $[\text{RuH}_2\text{Cl}(\text{PPh}_3)_2]_2$, now known to be a $\eta^2\text{-H}_2$ complex (*vide supra*):



This reaction in toluene was used in the present work to synthesize the DMA-free complex. In the course of the present work, it was discovered that the complexes **2a** and **2b** do show some reactivity toward H_2 at 2 - 3 atm in toluene solution.

3.2 Experimental

Crystal structures

$(\eta^2\text{-H}_2)(\text{PPh}_3)_2\text{Ru}(\mu\text{-H})(\mu\text{-Cl})_2\text{RuH}(\text{PPh}_3)_2\text{-toluene-d}_8\text{-DMA}$:

Dark red crystals of this complex grew in a NMR tube containing a toluene- d_8 solution of the bis-DMA solvate of the complex under 2 - 3 atm H_2 . Anal. Calcd. for a toluene- d_8 -DMA solvate, $\text{C}_{83}\text{H}_{81}\text{ONCl}_2\text{P}_4\text{Ru}_2$: C, 65.89; H, 5.36; N, 0.93. Found: C, 65.73; H, 5.47; N, 0.00. The bis-DMA solvate was prepared from $\text{RuCl}_2(\text{PPh}_3)(\text{isoPFA})$, **3b**, as described in section 2.4. A single crystal X-ray diffraction study was carried out by J. Simpson, University of Otago, New Zealand, in the hope of finding the $\eta^2\text{-H}_2$ ligand.⁵⁵

$(\eta^2\text{-H}_2)(\text{isoPFA})\text{Ru}(\mu\text{-H})(\mu\text{-Cl})_2\text{RuH}(\text{PPh}_3)_2\text{-C}_6\text{H}_6$:

Crystals of the benzene solvate of **4**, suitable for X-ray analysis, were obtained by means of the procedure described in section 4.2. The crystal structure determination was performed by J.-P. Charland at N.R.C., in Ottawa, and the structure has been published.⁴⁸

Visible spectrophotometry

To confirm the reported visible spectrum of **1a**,²³ specially purified DMA (distilled from $\text{RuHCl}(\text{PPh}_3)_3$,²¹ see section 2.4) was used for extinction coefficient measurements. The DMA-free complex, **1a**, was prepared as described (section 2.4).

NMR spectra

Complex **1a**:

For variable temperature ^1H NMR and $^{31}\text{P}\{^1\text{H}\}$ NMR spectra for simulation purposes, the complex, **1a**, was generated *in situ* under hydrogen from **2a** and Proton Sponge[®] (*cf.* section 2.4). Low temperature T_1 measurements for the hydrogen ligands were carried out on the bis-DMA solvate in toluene- d_8 solution under hydrogen using the inversion-recovery method. The T_1 measurements above 0 °C were carried out on the *in situ*-species generated both from **3a** in butanol/toluene under hydrogen (section 4.2) and from **2a** with Proton Sponge[®] in toluene- d_8 under hydrogen (section 2.4).

Complex 1b:

The complex, **1b**, was prepared as described in section 2.4, and isolated prior to recording the NMR spectra.

Reactions of 1a and 1b with 1-hexene

The solvate-free complex, **1a**, ($\sim 10^{-3}$ M) was mixed with a ten to twenty-fold excess of hexene in toluene- d_8 in a NMR tube under vacuum at ambient temperature. The ^1H NMR spectrum was recorded both after 3 h from time of mixing and after 9 d. The vacuum distillate of the solution was then analyzed by gas chromatography.

For the analogous reaction of 1-hexene with **1b**, the complex ($\sim 10^{-2}$ M) was mixed with an approximately ten-fold excess of 1-hexene in CD_2Cl_2 in a NMR tube under vacuum at ambient temperature. The ^1H NMR spectrum was recorded both after 7 h from time of mixing and after 9 d. The vacuum distillate of the solution was then analyzed by gas chromatography.

*Reactions of $(\eta^2\text{-H}_2)(\text{isoPFA})\text{Ru}(\mu\text{-Cl})_2(\mu\text{-H})\text{RuH}(\text{PPh}_3)_2$, **4***

To test the stability of **4** in CD_2Cl_2 solution under vacuum, the complex, (~ 10 mg, 0.01 mmol) was dissolved in CD_2Cl_2 in a 5 mm NMR tube, and the tube was sealed under vacuum. The ^1H NMR spectrum was recorded within six hours and after three weeks in the NMR tube, kept mostly at -30 °C but also for several days at ambient temperature.

Reaction with 1-hexene was studied by mixing **4** (5 mg, 0.0043 mmol) with 1-hexene (0.040 mmol) under vacuum in CD_2Cl_2 (1 g) at ambient temperature. The ^1H NMR spectrum was recorded after 8 h and both ^1H NMR and $^{31}\text{P}\{^1\text{H}\}$ NMR spectra recorded after two weeks. The vacuum distillate of this solution was then analyzed by gas chromatography.

Preparation and observation of dihydrogen adducts of 2a and 2b in situ

The complexes, **2a**, prepared by stirring $\text{RuCl}_3(\text{PPh}_3)_2(\text{DMA})\cdot\text{DMA}$ under hydrogen (several atm) in *n*-butanol (sect. 2.4), and **2b**, prepared as described in section 2.4, were

each dissolved in toluene- d_8 under 2 - 3 atm H_2 and the NMR spectra recorded of the respective solutions containing the resulting H_2 adducts.

3.3 Results

Complexes 1a, 1b and 4

An elemental analysis of a sample of the crystals of **1a**, $(\eta^2-H_2)(PPh_3)_2Ru(\mu-Cl)_2(\mu-H)RuH(PPh_3)_2 \cdot \text{toluene-}d_8 \cdot \text{DMA}$, submitted for X-ray analysis, shows a C and H content consistent with a DMA·toluene- d_8 solvate; the nitrogen result of 0.0 % is perhaps in error as only a small sample was available (0.29 mg). Although toluene was found in the crystal structure, there appeared to be other solvent molecules present, possibly disordered, which could not be refined. Consequently, the hydrogen ligands could not be located. The complex was nevertheless shown to be a chloro-bridged dimer, with an arrangement of Ru, Cl and P atoms almost identical to that of the analogous tri(*p*-tolyl)phosphine structure obtained earlier (see Figs. 3.2, 3.3; Table 3.7).

For complex **4**, the crystallographic data are of excellent quality and refinement proceeded well to reveal the hydrido and dichloro-bridged dinuclear complex pictured in Fig. 3.4. Structural parameters are summarized in Table 3.8 and may be compared with the data for the two other analogous structures of **1a** and **1b** (Table 3.7). The skeletal atoms of all three structures are numbered in an analogous manner to highlight their similarities, except that the nitrogen atom of the isOPFA ligand in **4** replaces P(4) of **1a** and **1b**. It should be noted that the skeleton structure of **4** is not superimposable on its mirror image, and thus has this element of chirality, in addition to the chirality of the isOPFA ligand, which may be *R,S* or *S,R*.

The dihydrogen ligand bond length, H(1)-H(2), is 0.80(6) Å, and this ligand is symmetrically coordinated, "side-on", to the Ru atom bearing the isOPFA ligand.

Table 3.7

Selected bond angles and distances for crystal structures of
 $(\eta^2\text{-H}_2)(\text{PR}_3)_2\text{Ru}(\mu\text{-Cl})_2(\mu\text{-H})\text{RuH}(\text{PR}_3)_2$ (R = Ph, p-tol), **1a** and **1b**

	1a^a	1b^b
Distances (Å)		
Ru(1)-Ru(2)	2.83	2.80(0)
Ru(1)-P(1)	2.22	2.23(1)
Ru(1)-P(3)	2.25	2.28(1)
Ru(2)-P(2)	2.27	2.26(1)
Ru(2)-P(4)	2.39	2.39(1)
Ru(1)-Cl(1)	2.48	2.46(1)
Ru(1)-Cl(2)	2.56	2.57(1)
Ru(2)-Cl(1)	2.44	2.47(1)
Ru(2)-Cl(2)	2.47	2.48(1)
Angles (°)		
P(1)-Ru(1)-P(3)		97.6(5)
P(1)-Ru(1)-Cl(1)		166.8(5)
P(1)-Ru(1)-Cl(2)		94.4(5)
P(1)-Ru(1)-Ru(2)		111.9(4)
P(3)-Ru(1)-Cl(1)		95.6(5)
P(3)-Ru(1)-Cl(2)		113.8(4)
P(3)-Ru(1)-Ru(2)		148.4(4)
P(2)-Ru(2)-P(4)		104.1(5)
P(2)-Ru(2)-Cl(1)		92.1(5)
P(2)-Ru(2)-Cl(2)		167.6(5)
P(2)-Ru(2)-Ru(1)		110.0(4)
P(4)-Ru(2)-Cl(1)		102.9(4)
P(4)-Ru(2)-Cl(2)		88.0(4)
P(4)-Ru(2)-Ru(1)		139.3(3)
Ru(1)-Cl(1)-Ru(2)	70.2	69.3(4)
Ru(1)-Cl(2)-Ru(2)	68.4	67.3(3)

^aFrom the present work.⁵⁵

^bFrom reference 23.

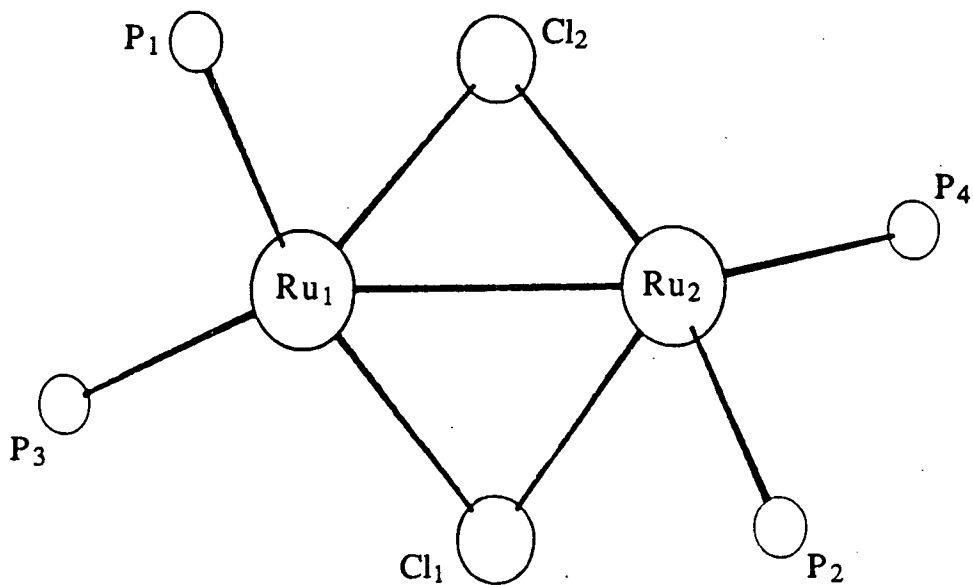


Figure 3.2 The skeletal structure of **1a**, determined by X-ray diffraction.

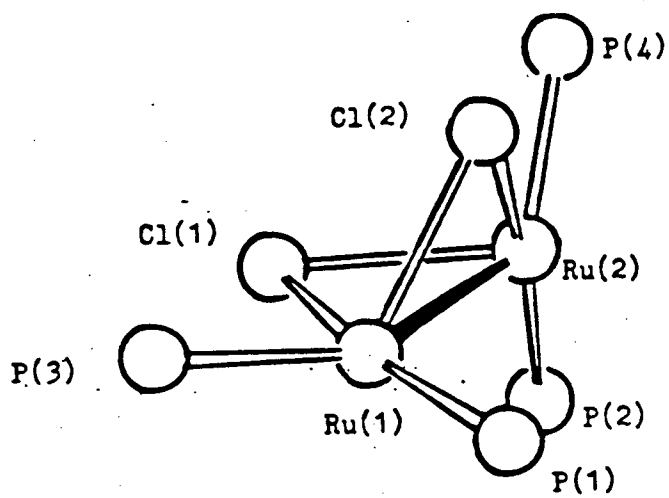


Figure 3.3 The skeletal structure of **1b**, determined by X-ray diffraction. From reference 23.

Table 3.8

Selected bond angles and distances for the crystal structure of



Distances (Å)	
Ru(1)-Ru(2)	2.811(2)
Ru(1)-P(1)	2.229(2)
Ru(1)-P(3)	2.249(2)
Ru(2)-P(2)	2.240(2)
Ru(2)-N	2.300(4)
Ru(1)-Cl(1)	2.453(2)
Ru(1)-Cl(2)	2.620(2)
Ru(2)-Cl(1)	2.435(2)
Ru(2)-Cl(2)	2.528(2)
Angles (°)	
P(1)-Ru(1)-P(3)	96.35(7)
P(1)-Ru(1)-Cl(1)	168.32(4)
P(1)-Ru(1)-Cl(2)	98.02(8)
P(1)-Ru(1)-Ru(2)	114.33(6)
P(3)-Ru(1)-Cl(1)	95.19(7)
P(3)-Ru(1)-Cl(2)	114.36(7)
P(3)-Ru(1)-Ru(2)	148.16(4)
P(2)-Ru(2)-P(4)	96.5(1)
P(2)-Ru(2)-Cl(1)	101.22(8)
P(2)-Ru(2)-Cl(2)	168.54(4)
P(2)-Ru(2)-Ru(1)	113.40(6)
P(4)-Ru(2)-Cl(1)	92.4(1)
P(4)-Ru(2)-Cl(2)	94.7(1)
P(4)-Ru(2)-Ru(1)	138.46(9)
Ru(1)-Cl(1)-Ru(2)	70.20(6)
Ru(1)-Cl(2)-Ru(2)	66.16(6)
Parameters for hydrogen ligands:	
Distances (Å)	
H(1)-H(2)	0.80(6)
Ru(2)-H(1)	1.50(4)
Ru(2)-H(2)	1.47(4)
Ru(2)-H(12)	1.71(4)
Ru(1)-H(12)	1.49(4)
Ru(1)-H(13)	1.50(4)
Angles (°)	
Ru(1)-H(12)-Ru(2)	122(3)
Ru(2)-H(1)-H(2)	72(4)
Ru(2)-H(2)-H(1)	76(4)

H(12)-Ru(1)-H(13)	89(2)
H(12)-Ru(2)-H(2)	108(2)
H(12)-Ru(2)-H(1)	78(2)
Ru(2)-Ru(1)-H(13)	108(1)
Ru(1)-Ru(2)-H(1)	96(2)
Ru(1)-Ru(2)-H(2)	127(2)

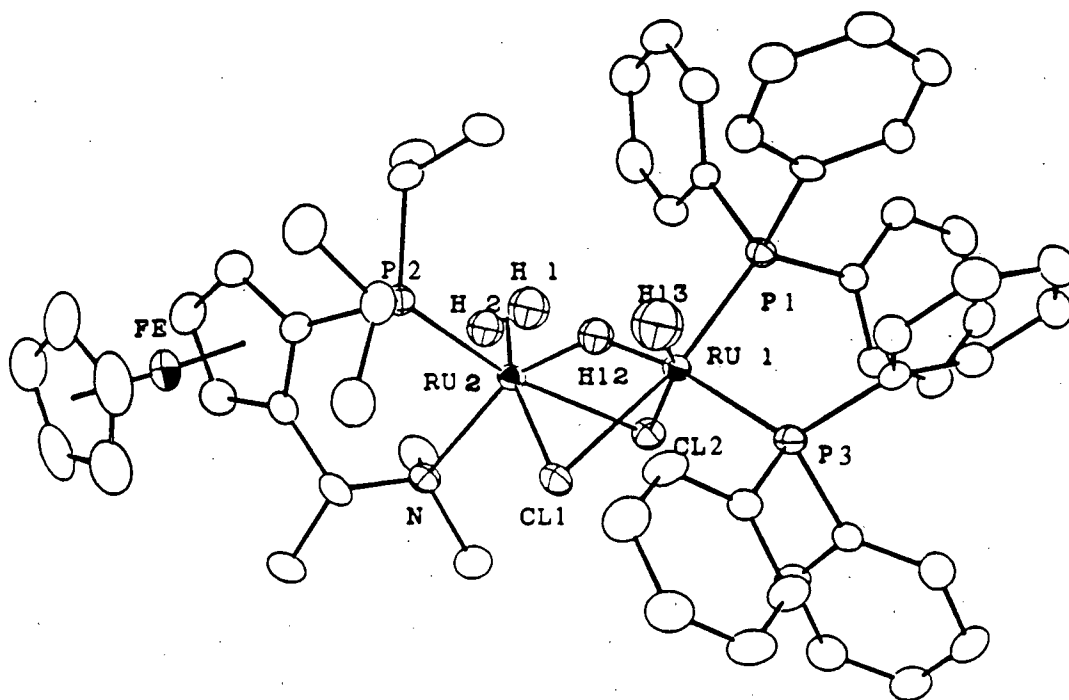


Figure 3.4 The molecular structure of **4**, from X-ray diffraction data, showing the positions of hydrogen ligands.

The bridging hydride is unsymmetrically coordinated: Ru(1)-H(12) 1.49(4) Å, Ru(2)-H(12) 1.71(4) Å, and the Ru-(H₂) distances, Ru(2)-H(1) 1.50(4) Å, Ru(2)-H(2) 1.47(4) Å, are not significantly different from the terminal, Ru(1)-H(13) distance of 1.50(4) Å. The H-H bond is parallel to the Ru(1)-Ru(2) direction, and the plane defined by Ru(2), H(1) and H(2) roughly bisects the P(2)-Ru(1)-N and H(12)-Ru(1)-Cl(1) angles.

Visible spectra of DMA solutions of **1a** (e.g., Fig. 3.5) show a maximum at 495 nm ($\epsilon = 1580 \pm 10 \text{ M}^{-1}\text{cm}^{-1}$) over a range of concentrations ($1.01 \times 10^{-3} \text{ M} < [\text{Ru}]_{\text{T}} < 6.2 \times 10^{-3} \text{ M}$) that roughly correspond to those used in the hexene hydrogenation study by Thorburn.⁷¹ Thorburn's catalysis data will be considered in sect. 4.4.

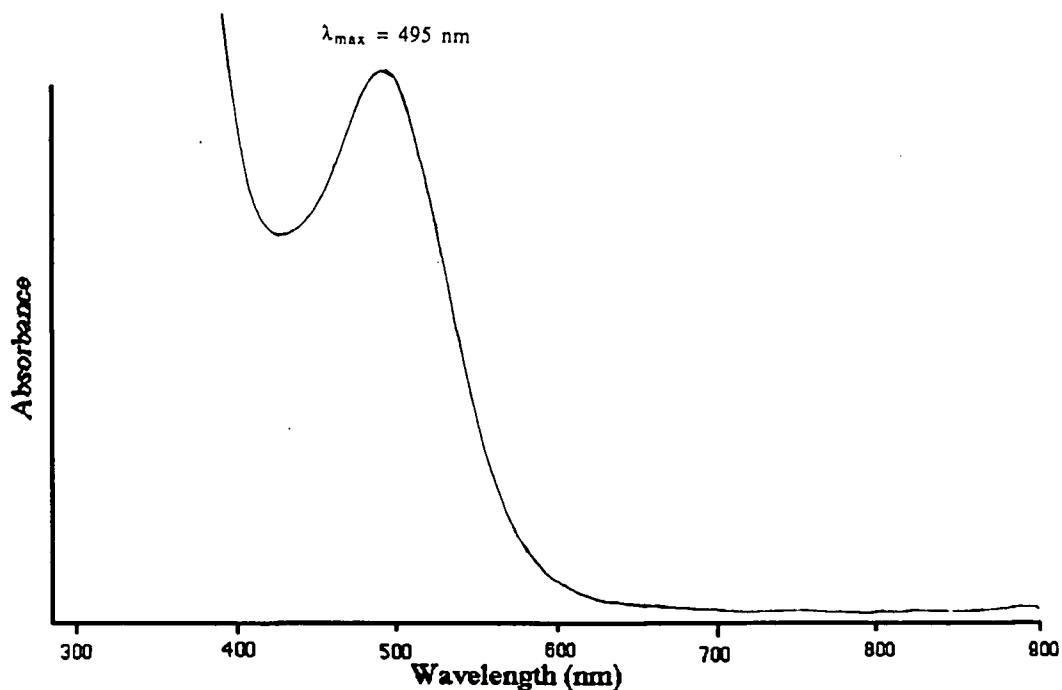


Figure 3.5 The visible spectrum of **1a** in DMA under hydrogen.

The $^{31}\text{P}\{^1\text{H}\}$ NMR spectra of the bis-DMA solvate of **1a** exhibited the same features as the solvate-free complex generated *in situ* under H_2 from **2a** and Proton Sponge[®] (*cf.* sect. 2.4). Peaks at δ 70.5 and 46.0 ppm at ambient temperature broaden on cooling to give four resolved resonances, at $-58\text{ }^\circ\text{C}$, whose chemical shifts (79.5 (s), 63.5 (s), 62 (s), 29.5 (s)) remained temperature invariant down to $-88\text{ }^\circ\text{C}$; there is thus rapid exchange of phosphorus environments at ambient temperature. The calculated (sect. 2.3) and observed $^{31}\text{P}\{^1\text{H}\}$ NMR spectra are shown in Fig. 3.6. No couplings are resolved at 121 MHz, but the variation in broadness of these peaks (at $-68\text{ }^\circ\text{C}$, $w_{1/2} = 78, 47, 94, 100$ Hz, respectively) is consistent with the values of coupling constants reported by Dekleva *et al.*²³ for the 32.4 MHz spectrum (see discussion, sect. 3.4). The model used for the simulation was an $\text{ABCD} \rightleftharpoons \text{BADC}$ exchange system, defined by a first-order rate constant, k . The " T_2 " values were calculated from the above halfwidths ($w_{1/2}$), and T_2 values and chemical shifts were kept constant over the temperature range of the simulation. It is noted that these " T_2 " values were merely input to a computer program for simulation purposes and probably reflect values of coupling constants more than actual T_2 values. The

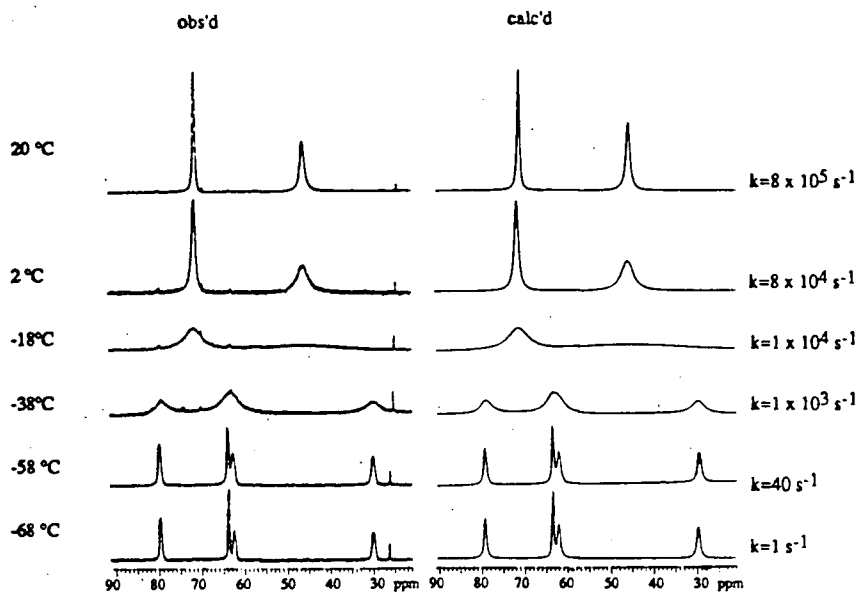


Figure 3.6 Observed and calculated, variable temperature $^{31}\text{P}\{^1\text{H}\}$ NMR data (121 MHz, toluene- d_6) for **1a** measured under H_2 .

exchange constants, also shown in Fig. 3.6, indicate rapid exchange at 20 °C ($k = 8 \times 10^5 \text{ s}^{-1}$). An Eyring⁷⁹ plot (Fig. 3.7) yields values for ΔH^\ddagger ($70 \pm 12 \text{ kJ/mol}$), ΔS^\ddagger ($110 \pm 50 \text{ J/mol/K}$) and ΔG^\ddagger ($38 \pm 3 \text{ kJ/mol}$ at 20 °C) for the phosphine exchange. Errors in k values from these line-shape analyses are greater for very fast and very slow exchange, since line shapes change less with temperature in these regimes than they do in intermediate exchange-rate regimes. These errors are estimated to vary from $\sim 10\%$ for intermediate values of k , up to $\sim 50\%$ for highest and lowest values. These errors were propagated by estimating their effect on the slope and intercept of the Eyring plot to give the errors in the activation parameters.

The ^1H NMR spectrum of **1a** at 20 °C (Fig. 3.8) shows a signal at -12.9 ppm ($w_{1/2} = 75 \text{ Hz}$) which broadened on cooling to -18 °C , while further cooling yielded the slow exchange spectra: eg., at -69 °C : δ -8.6 (d, 1 $\mu\text{-H}$, $^2J_{\text{PH}} = 66 \text{ Hz}$), -12.6 (br s, $w_{1/2} \sim 500 \text{ Hz}$, 2 $\eta^2\text{-H}_2$ protons), -17.2 (t, 1 terminal H, $^2J_{\text{PH}} = 30 \text{ Hz}$). Exchange spectra simulations employed an $\text{A}_2 \rightleftharpoons \text{BX} \rightleftharpoons \text{CXY}$ exchange model (cf. Fig. 3.9) where one proton, B, with a long T_2 exchanges with both two protons, A_2 , with a short T_2 and one other proton, C, with a long T_2 . The observed and calculated upfield ^1H NMR spectra

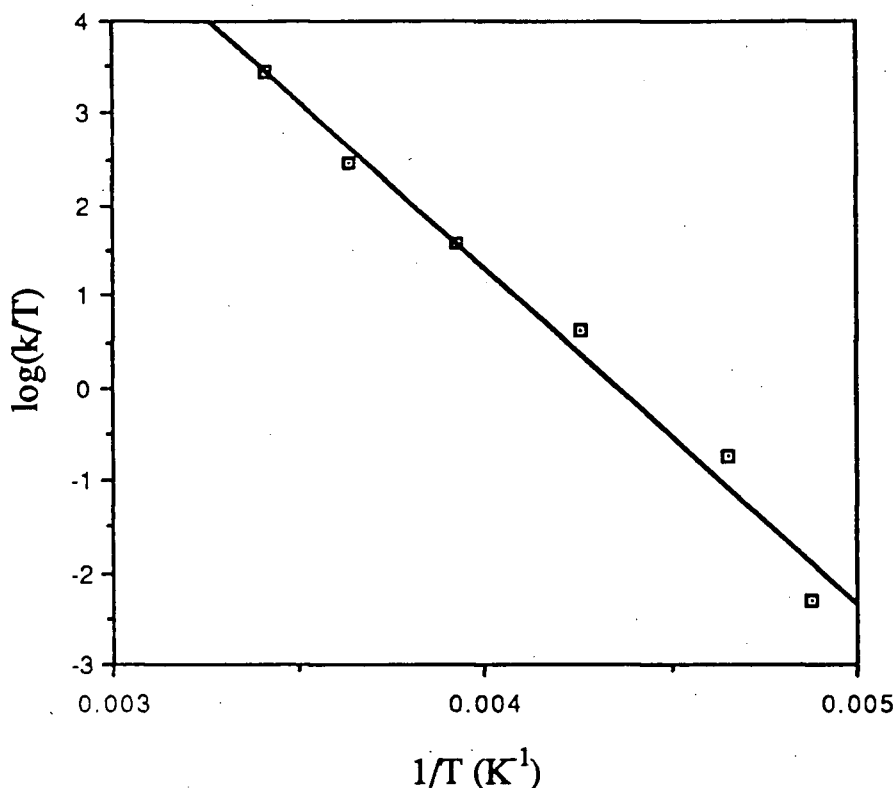


Figure 3.7 Eyring plot for rate constants for phosphine exchange in 1a.

of 1a are shown in Fig. 3.8. The exchange constant for the $A_2 \rightleftharpoons BX$ exchange is k_1 , and for the $BX \rightleftharpoons CXY$ process is k_2 . In order to include the observed temperature dependence of the chemical shifts in the calculation, values for these shifts for the slow exchange spectra were plotted (Fig. 3.10) and extrapolation made to higher temperatures so as to be consistent with fast-exchange-averaged peaks. The chemical shift of the $\eta^2\text{-H}_2$ resonance was held invariant with temperature; this was done rather arbitrarily, as broadening above and below -53°C made observation of any change of chemical shift with temperature difficult. The T_2 values used for the bridging and terminal hydrides were 8 and 12 ms, respectively, for all simulations except for the one for the spectrum at -78°C , where slightly lower values (6 and 8 ms, respectively) were used in order to mimic broadening possibly caused by limitations in solubility at this temperature. Figure 3.11 shows how " T_2 " for the $\eta^2\text{-H}_2$ resonance was allowed to decrease with decreasing

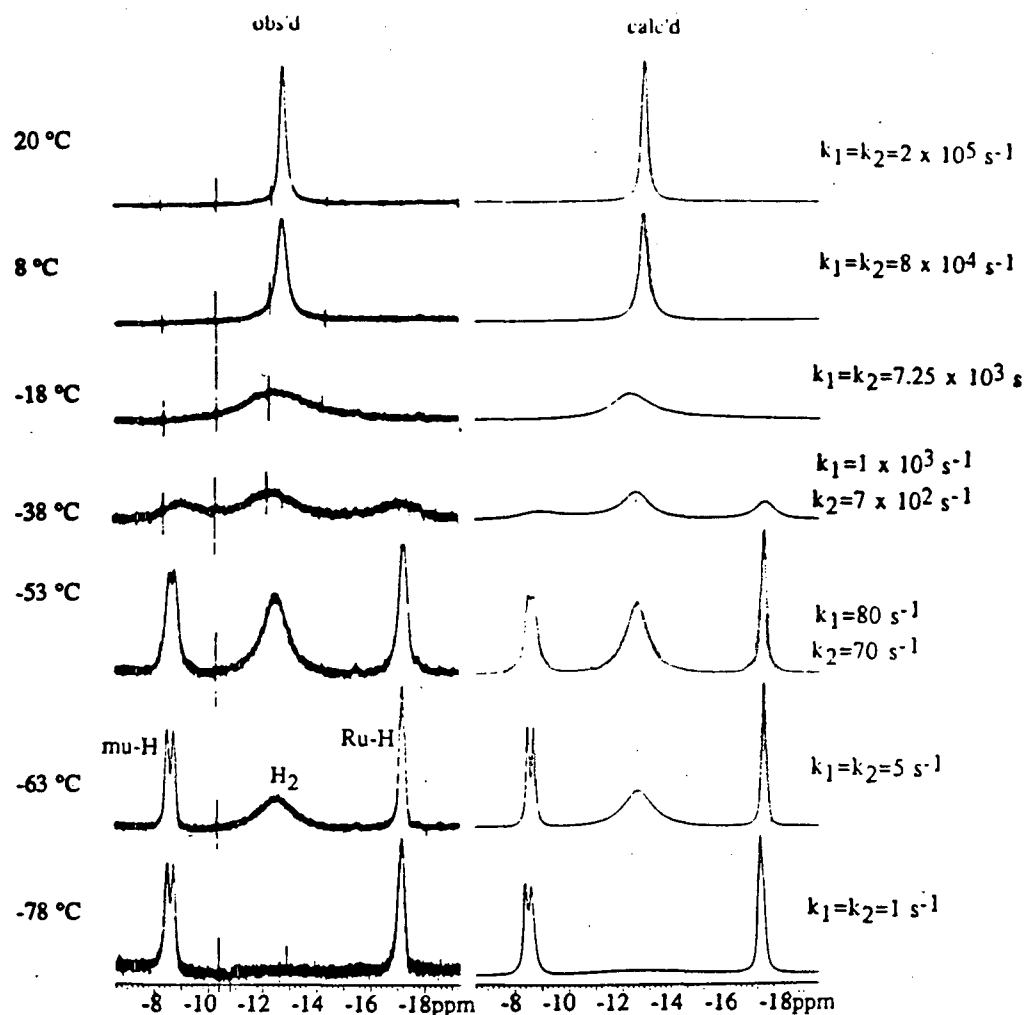


Figure 3.8 Observed and calculated, variable temperature ^1H NMR (300 MHz, toluene- d_8) spectra of 1a measured under H_2 .

temperature; values of " T_2 " were obtained from the half-widths for this resonance in the slow exchange regime and extrapolated to higher temperatures by using a " $\log T_2$ versus T^{-1} " plot. (Such a plot normally gives a straight line with slope of -1, since $T_2^{-1} \propto T^{-1}$ in liquids and gases.^{79b} However, the broadness of dihydrogen resonances in general has not been fully explained, and the extrapolation used in Figure 3.11, and Figures 3.16 and 3.23 which are discussed later, is really empirically based, using the variation of the " T_2 " of the dihydrogen resonance with temperature in the slow exchange regime.) The resonance for $\eta^2\text{-H}_2$ at -78 °C was so broad as to almost disappear, but narrowed on return to higher temperatures; thus, it was difficult to estimate a " T_2 " from the half-width at this

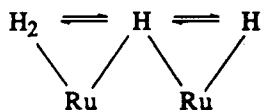


Figure 3.9 General hydrogen ligand exchange model used to simulate hydrogen ligand exchange within 1a, 1b and 4.

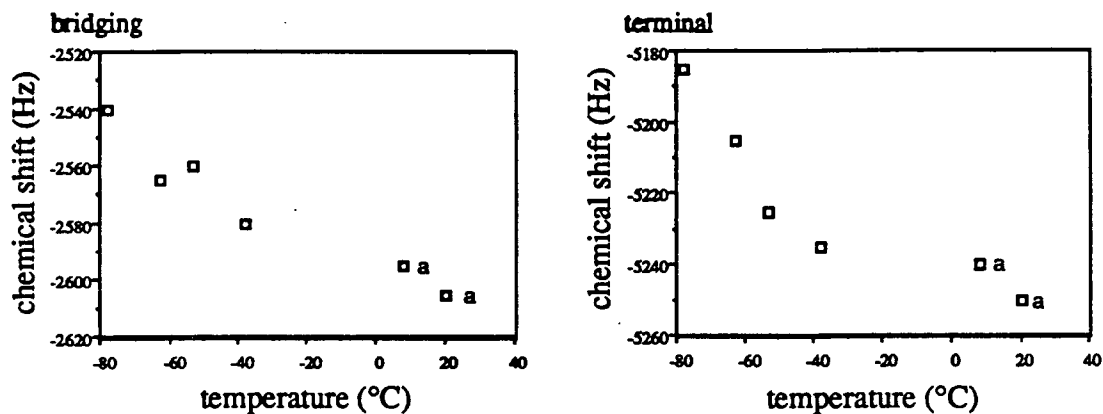


Figure 3.10 Plot of ^1H NMR chemical shifts versus temperature for terminal and bridging hydride ligands in 1a, with extrapolation to 20 °C; data measured under H_2 . Points marked 'a' are estimated as described in the text.

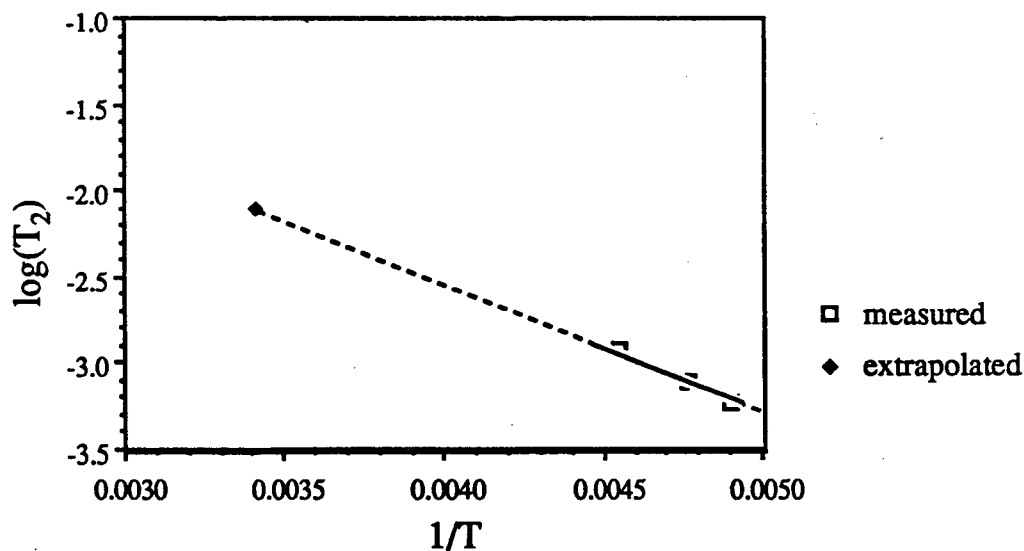


Figure 3.11 Plot of ^1H NMR (300 MHz, toluene- d_8) T_2 values versus temperature for the $\eta^2\text{-H}_2$ ligand of 1a, measured under H_2 , including extrapolation to 20 °C.

temperature. The exchange constants are shown in Fig. 3.8, and quantify the rate of exchange at various temperatures. This rate is rapid at ambient temperature (at 20 °C, k values = $2 \times 10^5 \text{ s}^{-1}$) and slows as the temperature is lowered (at -78 °C, k values = 1 s^{-1}). The constants, k_1 and k_2 , were the same within experimental error. The fit of the simulation to the observed spectra is good;⁸⁰ however, careful comparison of observed and calculated spectra recorded near the coalescence temperature reveals a difficulty experienced in matching the line shapes of the broad peaks in these spectra by simple adjustment of k_1 and k_2 . Figure 3.12 shows the Eyring plot for this system which yields

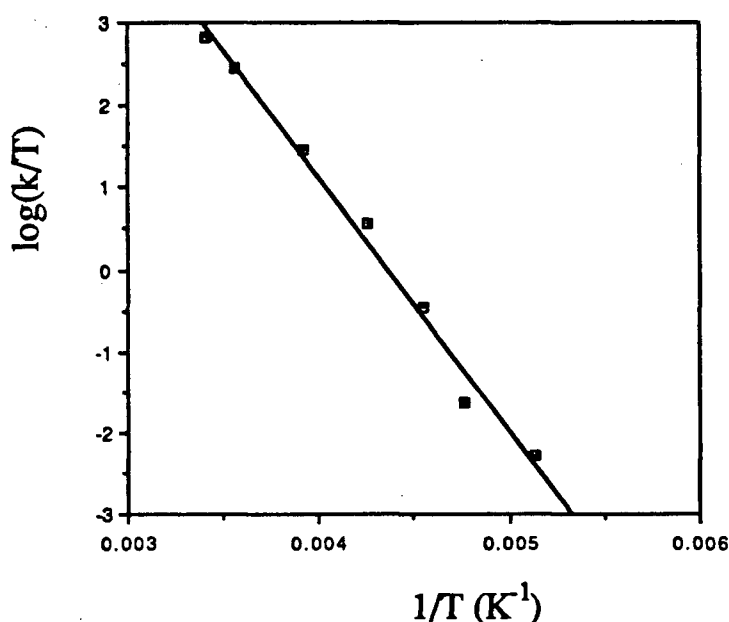


Figure 3.12 Eyring plot for rate constants ($k = (k_1 + k_2)/2$) for hydrogen ligand exchange in 1a.

the values for ΔH^\ddagger , ΔS^\ddagger and $\Delta G^\ddagger(20 \text{ °C})$ of $60 \pm 10 \text{ kJ/mol}$, $60 \pm 40 \text{ J/mol/K}$ and $41 \pm 2 \text{ kJ/mol}$, respectively.

The quality of the spectra used for low temperature T_1 measurements was poor because of the low concentrations used. Errors in T_1 values may be as high as 20%. Figure 3.13 shows the variation of T_1 values with temperature. Because of the exchange processes, minima could not be located. The T_1 values completely average at temperatures

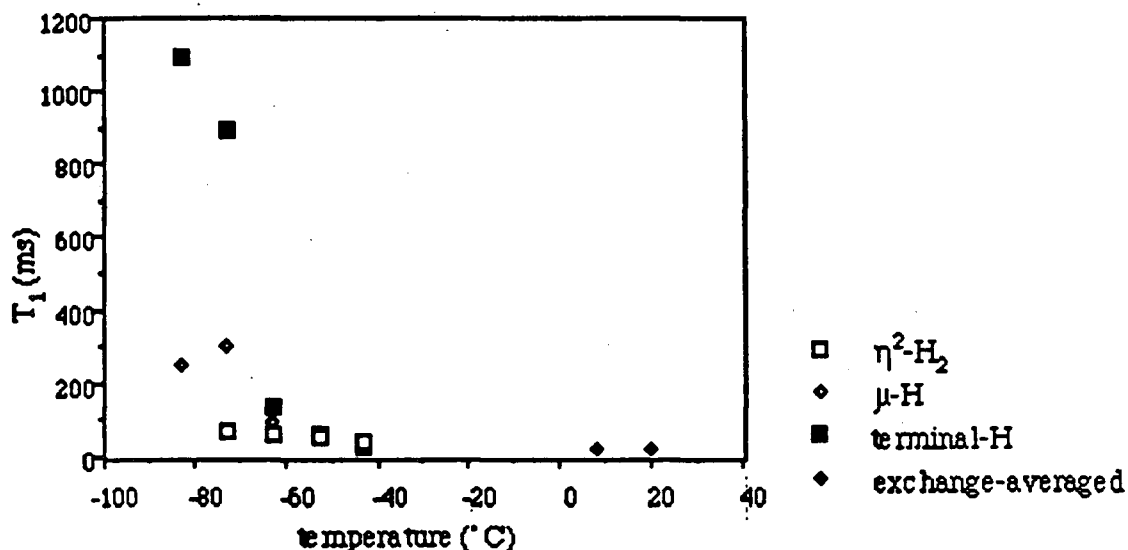


Figure 3.13 Plot of T_1 (300 MHz, toluene- d_6) values versus temperature for hydrogen ligands of **1a**. Values above 0 °C were obtained using a sample generated *in situ* in a NMR tube containing **2a** and Proton Sponge[®] under 2 - 3 atm H_2 .

above ~ -40 °C. However, the values at -73 °C (T_1 in ms, δ : 300, -8.6; 77, -12.6; 900, -17.2) indicate the presence of a $\eta^2\text{-H}_2$ resonance at -12.6 ppm. From -40 °C up to room temperature, the averaged T_1 shows little change, with values of 40 ms at -40 °C, and 20 ms at both 6 °C and 20 °C.

Complex **1b**:

Corresponding ^1H NMR measurements were made on the tri(*p*-tolyl)phosphine analogue of **1a** and the high-field spectra of these two complexes found to be very similar at both high and low temperature. The upfield ^1H NMR spectra of **1b** were recorded from 20 ° down to -94 °C. The 20 ° and -94 °C spectra are virtually the same as 400 MHz spectra reported earlier by Dekleva *et al.*^{21,23} Figure 3.14 shows the observed and calculated spectra over the range, 20 ° to -83 °C. The exchange model used for the simulation is similar to that employed in the simulation for hydrogen ligand exchange in the PPh_3

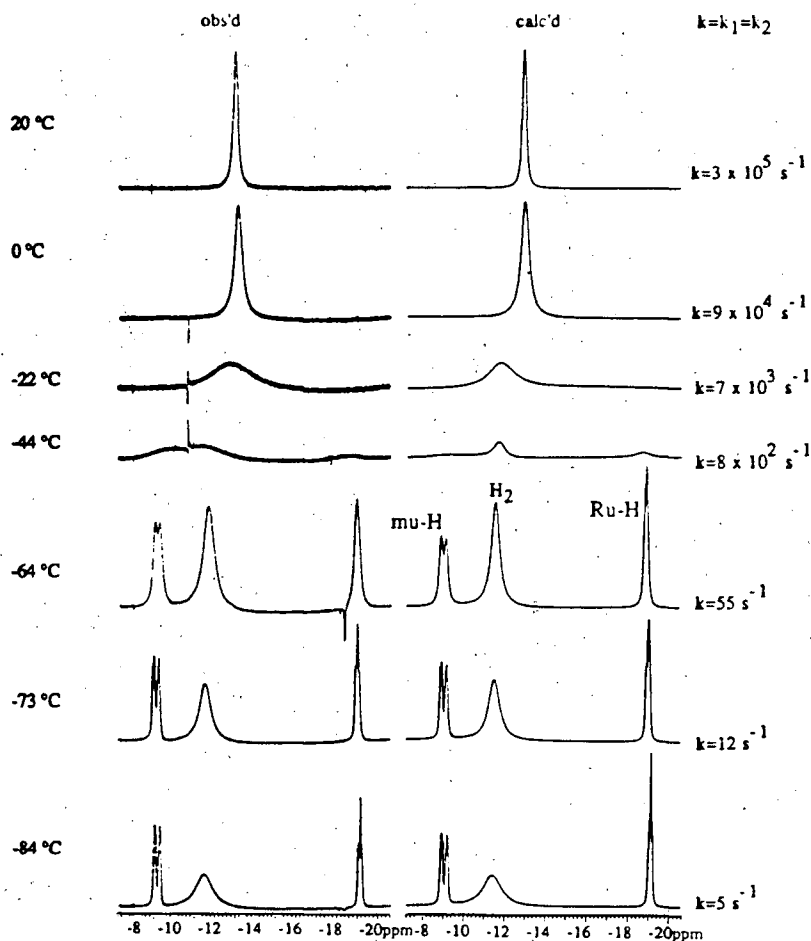


Figure 3.14 Observed and calculated variable temperature ^1H NMR spectra (300 MHz, CD_2Cl_2 , under hydrogen) for hydrogen ligands of **1b**.

analogue, except for incorporation of additional coupling information available from the spectra of the *p*-tol analogue, resolution being better due to higher solubility. The model used, then, is $\text{A}_2 \rightleftharpoons \text{BXYZ} \rightleftharpoons \text{CXY}$, with $k = k_1 \approx k_2$. In the model, a special case of that shown in Fig. 3.9, with indicated coupling constants set to zero, the exchange constant, k_1 , applies to the $\text{A}_2 \rightleftharpoons \text{BXYZ}$ exchange, while the constant k_2 applies to the $\text{BXYZ} \rightleftharpoons \text{CXY}$ exchange. The proton B, with a long T_2 , exchanges with both the A protons, with short T_2 values, and also with the proton C, with a long T_2 . The lowfield resonance is due to B, the high-field resonance due to C and the intermediate resonance due

to A_2 . The coupling constants used in the simulation are: J_{BX} , J_{BY} and J_{BZ} (78, 8, 2 Hz, respectively) and J_{CX} , J_{CY} (both 27 Hz). Figure 3.15 shows how the chemical shifts of the $\eta^2\text{-H}_2$ and terminal hydride resonances vary with temperature. Values of shifts obtained from the slow exchange spectra were plotted against temperature; the extrapolation to higher temperatures is rather arbitrary but consistent with the fast-exchange-averaged peak values, as in the case of the PPh_3 analogue. However, this procedure leads to exchange

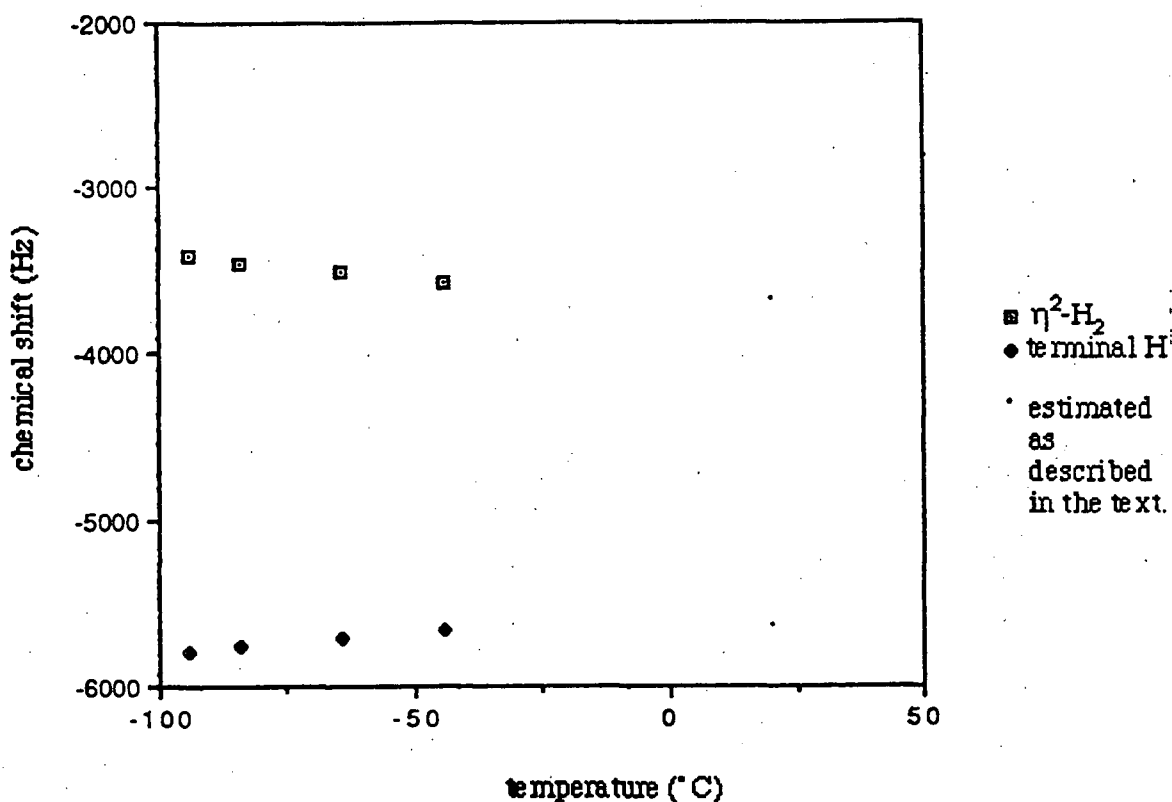


Figure 3.15 Plot of ^1H NMR chemical shifts versus temperature for the $\eta^2\text{-H}_2$ and terminal hydride ligands of **1b**, including extrapolation to 20°C .

constants that are in line with the low temperature exchange rates (see the Eyring plot later, Fig. 3.17). The T_2 values used for the terminal and bridging hydride, "C" and "B", respectively, in the exchange model above, were obtained from the half-widths of resonances in the low-temperature spectra. These T_2 values were held constant, at 20 ms, over the temperature range of the simulation; but the T_2 of the dihydrogen ligand was varied as shown in Fig. 3.16, with the T_2 values from the slow-motion-regime spectra extrapolated to higher temperatures in a manner similar to that used above for the 1a ^1H NMR spectra. Activation parameters obtained from an Eyring plot (Fig. 3.17) of these exchange constants were:

$$\Delta H^\ddagger = 49 \pm 7 \text{ kJ/mol}$$

$$\Delta S^\ddagger = 30 \pm 30 \text{ J/mol/K}$$

$$\Delta G^\ddagger(20 \text{ }^\circ\text{C}) = 41 \pm 2 \text{ kJ/mol}$$

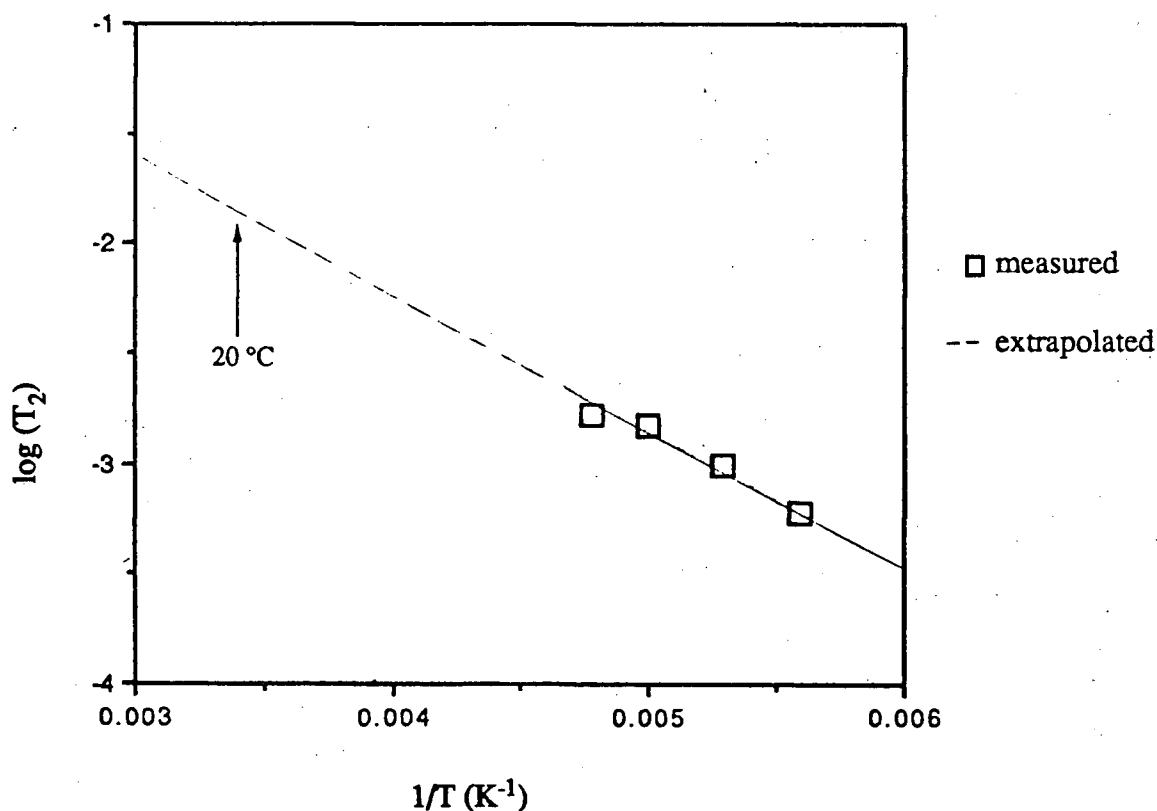


Figure 3.16 Plot of ^1H NMR T_2 values versus temperature for the $\eta^2\text{-H}_2$ ligand of 1b, including extrapolation to $20 \text{ }^\circ\text{C}$.

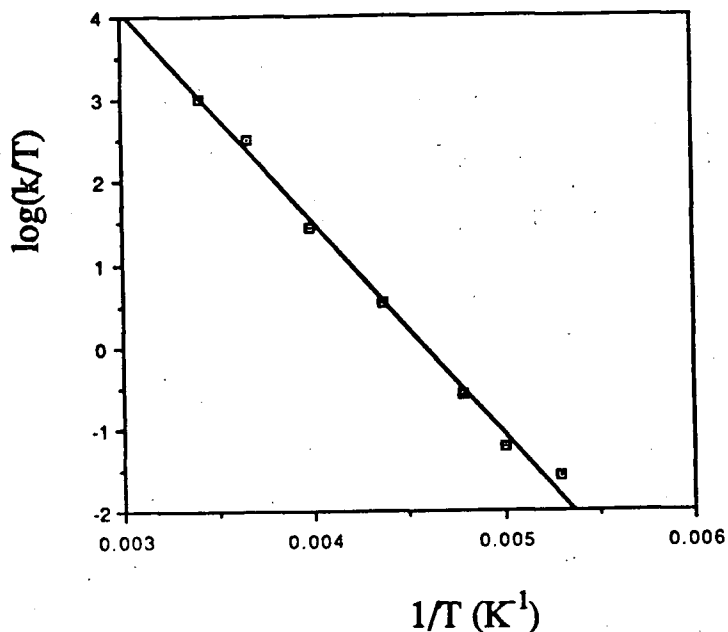


Figure 3.17 Eyring plot for rate constants for hydrogen ligand exchange in **1b**.

A typical inversion-recovery plot for the ^1H NMR T_1 measurements on **1b** is shown in Fig. 3.18. The broad $\eta^2\text{-H}_2$ resonance can be seen to recover more rapidly than the hydride resonances. Values of T_1 measured over the temperature range -94° to -64°C are displayed in Fig. 3.19. At -94°C , $T_1(\text{ms})$ values are 44 ($\eta^2\text{-H}_2$), 120 ($\mu\text{-H}$) and 350 (terminal H); the value for the $\eta^2\text{-H}_2$ resonance is within the range³⁶ (4 - 100 ms) expected for an $\eta^2\text{-H}_2$ ligand.

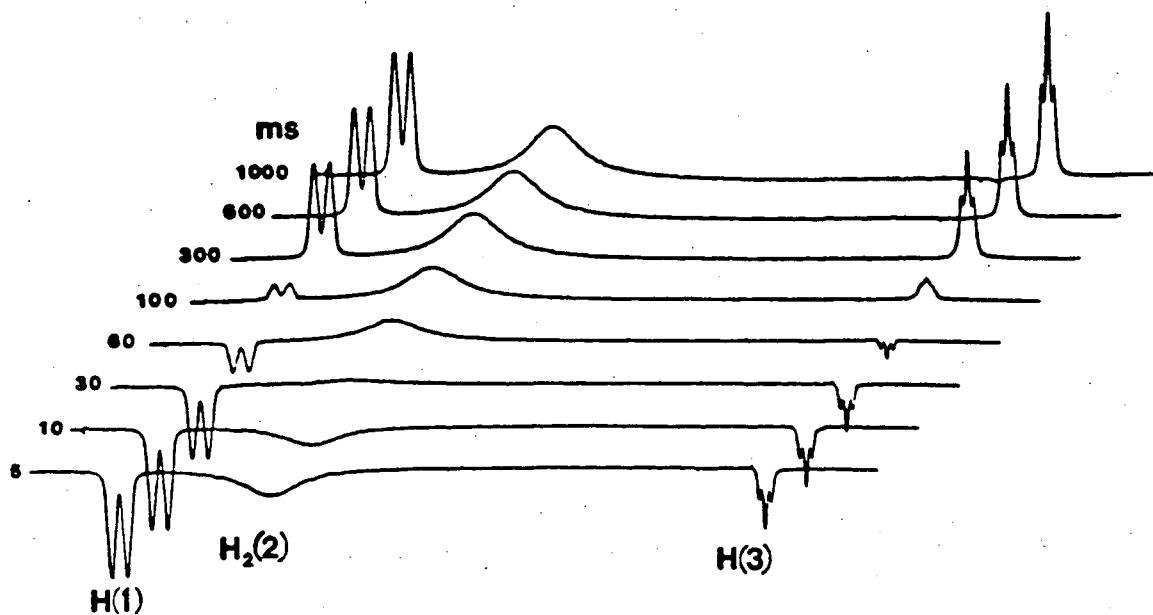


Figure 3.18 Inversion-recovery method plot for ^1H NMR T_1 measurements (300 MHz, CD_2Cl_2 , -83°C , under hydrogen) for the hydrogen ligands of **1b**. Delay times (ms) are given at the left. The $\eta^2\text{-H}_2$ ligand resonance recovers faster than that of the hydrides.

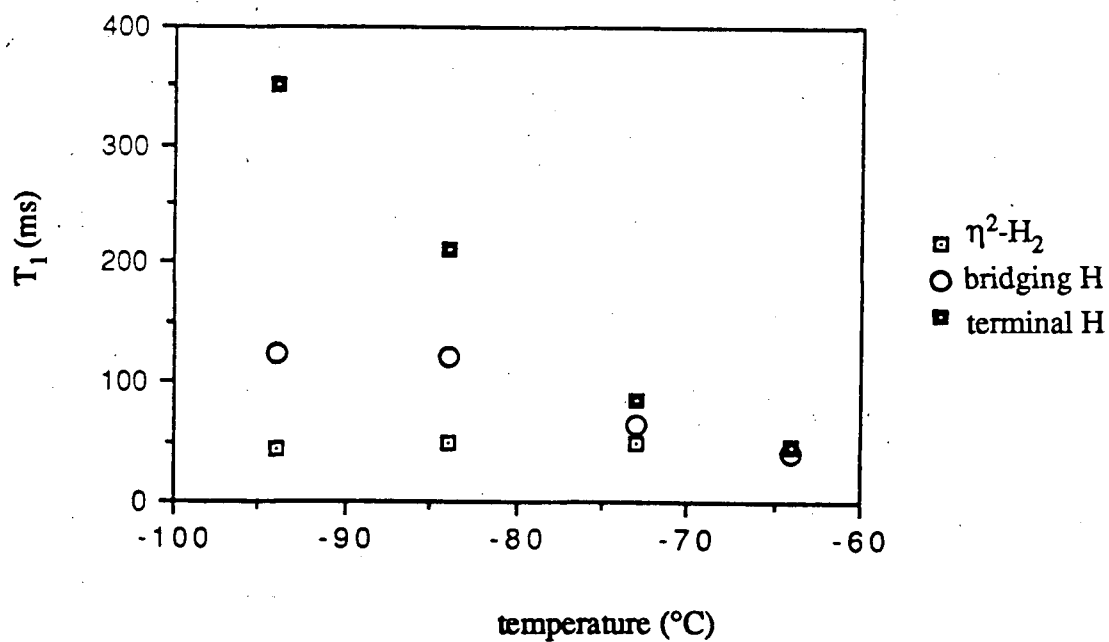


Figure 3.19 Plot of ^1H NMR T_1 values (300 MHz, CD_2Cl_2 , under hydrogen) versus temperature for the hydrogen ligands of **1b**.

The $^{31}\text{P}\{^1\text{H}\}$ NMR spectrum of **4** is shown in Fig. 3.20 and is invariant with temperature. A major set of resonances implies two major isomers or diastereomers: δ 78.5 (two overlapping doublets, P(1) *trans* to Cl), 77.2 (br s, possibly two are overlapping, P(2) of isoPFA), 64.6 (two overlapping doublets, P(3) *trans* to $\mu\text{-H}$). The presence of a second set of $^{31}\text{P}\{^1\text{H}\}$ NMR resonances (Fig. 3.20), of lesser intensity, is probably due to two other minor isomers, perhaps diastereomers.

The region downfield of δ 0 in the 300 MHz ^1H NMR spectrum of **4** in CD_2Cl_2 at 20 ° under hydrogen is shown in Fig. 3.21, and the detailed assignments are given in section 2.4. Signals from δ 6.9 to 7.55 are due to the PPh_3 ligands, while those from δ 0.3 to 4.45 are due to the isoPFA ligand. Two distinct $\text{N}(\text{CH}_3)_2$ peaks at δ 2.35 and 3.1 show the coordination of the nitrogen atom in solution; the free ligand in solution exhibits only a single $\text{N}(\text{CH}_3)_2$ resonance at δ 2.1. Further indication of coordination of the N atom of isoPFA is the position of the Fc-CHCH_3 quartet at δ 4.45, which is shifted downfield from the free ligand value of δ 4.0.⁸ In the upfield region (Fig. 3.22), the main features, at 20 °C, are a broad resonance, and a doublet of doublets at δ -18.6 (see below) which is always accompanied by another minor doublet of doublets some 16 Hz farther downfield. This minor signal is probably results from another less abundant diastereomer, as noted in the $^{31}\text{P}\{^1\text{H}\}$ NMR spectrum. An exchange process occurs mainly at the isoPFA end of the dinuclear molecule between the dihydrogen and bridging hydride ligands; the signals for the dihydrogen and bridging hydride ligands are resolved, though exchange-broadened, at -9 °C, and sharpen on cooling to -48 °C. The upfield region at -61 °C shows δ -18.5 (t, 1H, $^2J_{\text{PH}} \approx 30$ Hz), -17.3 (br s, 1H, $\mu\text{-H}$), -12.8 (br s, 2H, $\eta^2\text{-H}_2$); see also sect. 2.4. The observed and calculated (sect. 2.3) upfield ^1H NMR spectrum is shown in Fig. 3.22. The exchange simulation was carried out using basically the same model (Fig. 3.9) as for the ^1H NMR simulations described earlier, except that in this case, for **4**, $k_1 \gg k_2$; at 20 °C, $k_1 = 4000$ s⁻¹, $k_2 = 40$ s⁻¹. The k_1 constant applies to the exchange process involving the $\eta^2\text{-H}_2$ and $\mu\text{-H}$ ligands, while the k_2 constant applies to

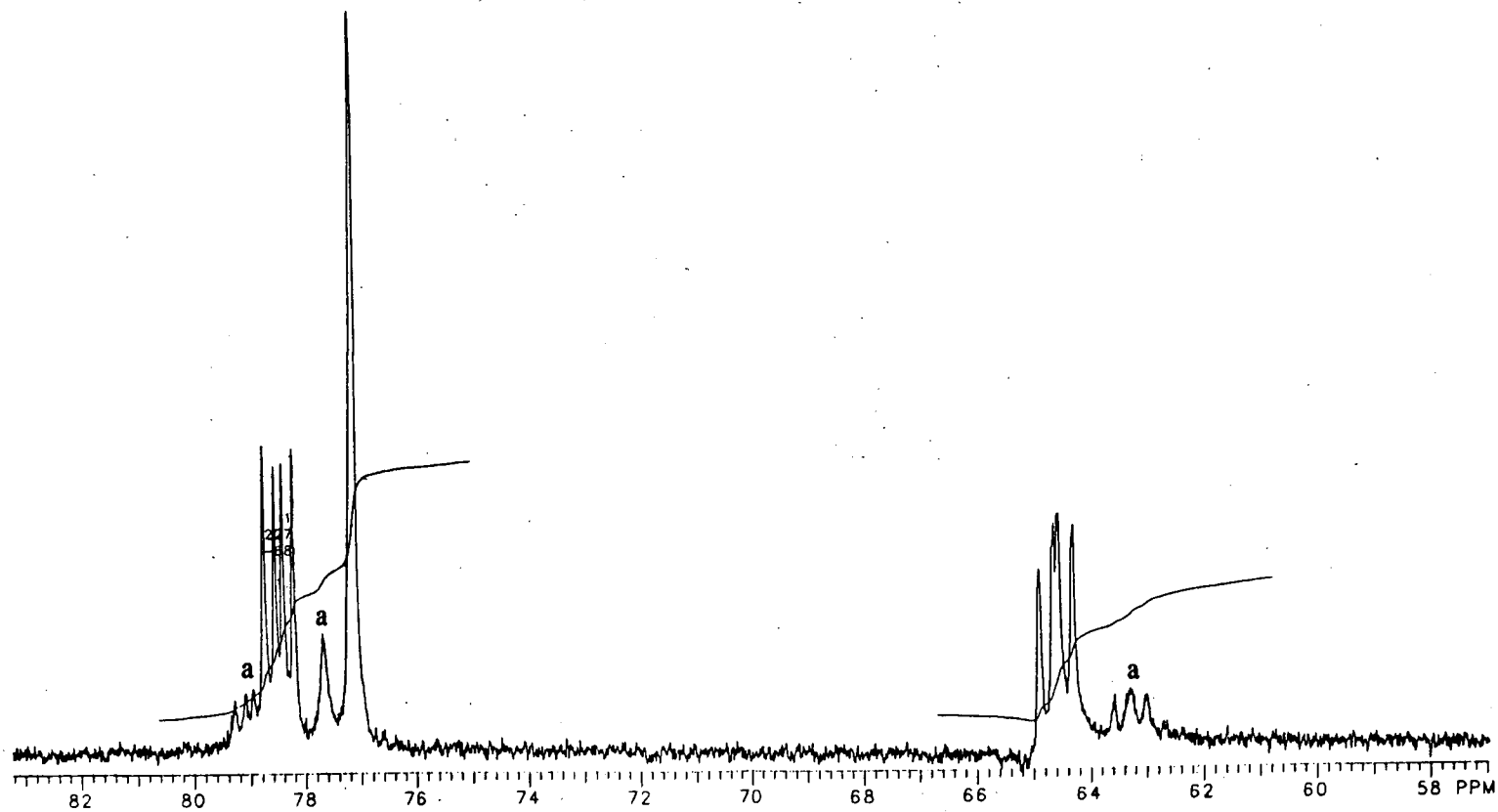


Figure 3.20 $^{31}\text{P}\{^1\text{H}\}$ NMR spectrum (121 MHz, CD_2Cl_2 , ambient temperature, under hydrogen) of **4**. Resonances marked with an 'a' are possibly due to two minor isomers of **4**.

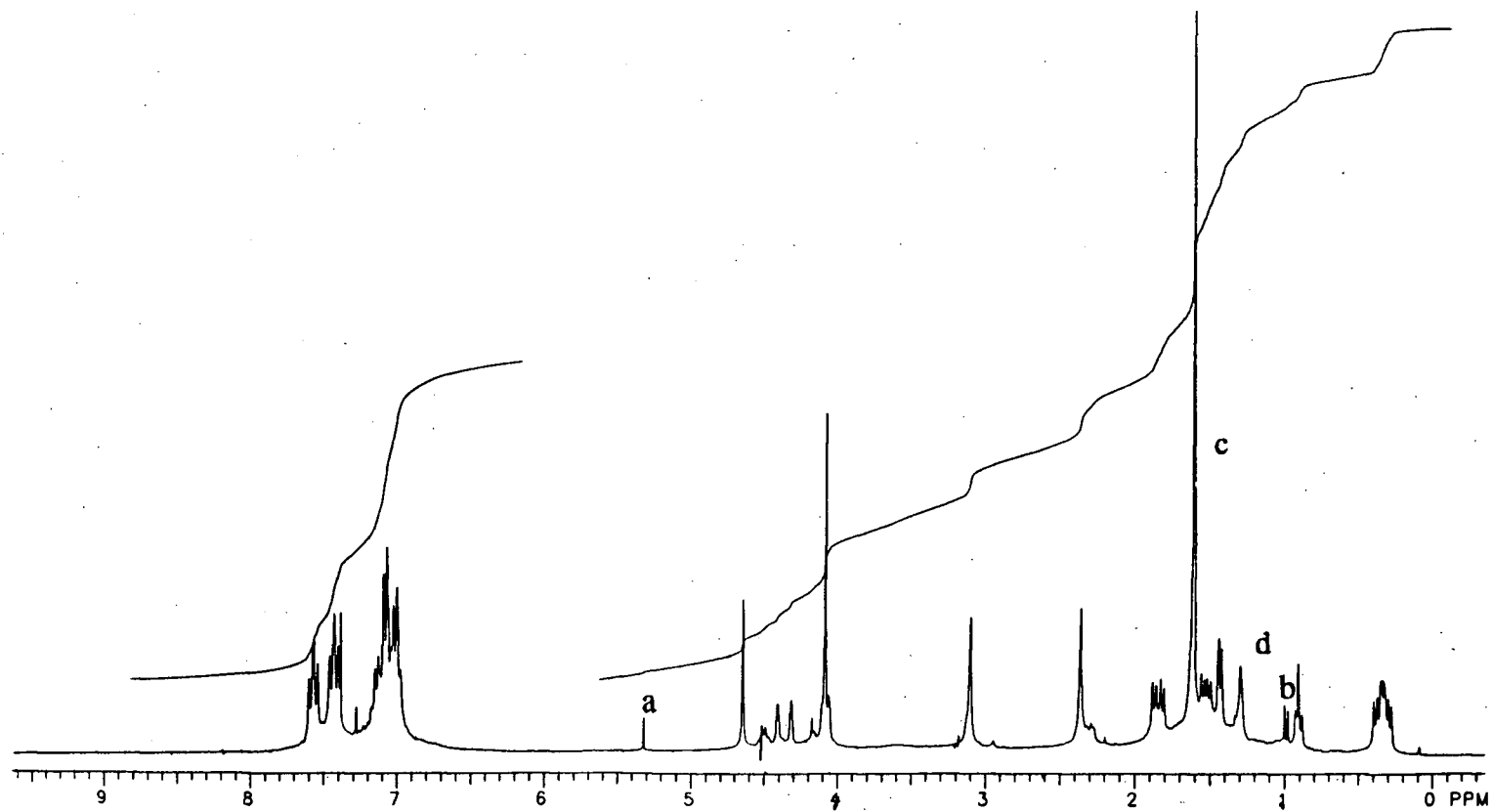


Figure 3.21 The ^1H NMR spectrum (300 MHz, CD_2Cl_2 , ambient temperature, under hydrogen) of 4.

The resonance marked 'a' is due to CD_2Cl_2 ; that marked 'b' is due to an unidentified impurity; the resonance marked 'c' is due to water; that marked 'd' is due to grease

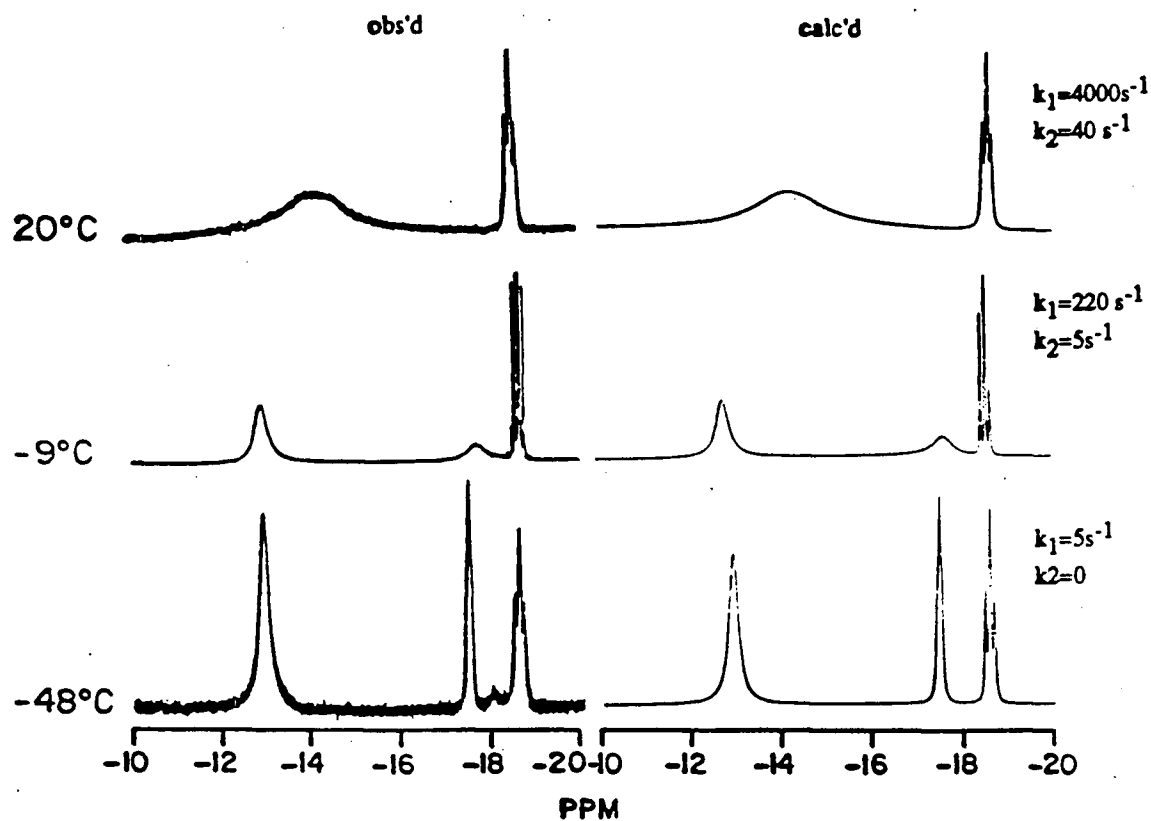


Figure 3.22 Observed and calculated variable temperature ^1H NMR data (300 MHz, CD_2Cl_2 , under hydrogen) for 4.

the exchange process involving the bridging and terminal hydride ligands. The model consists of a BXYZ spin system exchanging rapidly with an A_2XYZ spin system and slowly with a CXYZ system, but only J_{CX} and J_{CY} were allowed to be non-zero. The " T_2 " values for the simulation of the $\eta^2\text{-H}_2$ ligand resonance were permitted to increase with increasing temperature by means of extrapolation from the low temperature values (see Fig. 3.23). The input " T_2 " values for the -9° and 20°C simulations of the other hydride resonances were given the value of 90 ms, obtained from the halfwidth of the terminal hydride resonance, at δ -18.5, from the -9°C spectrum; for the -48°C simulation, values of

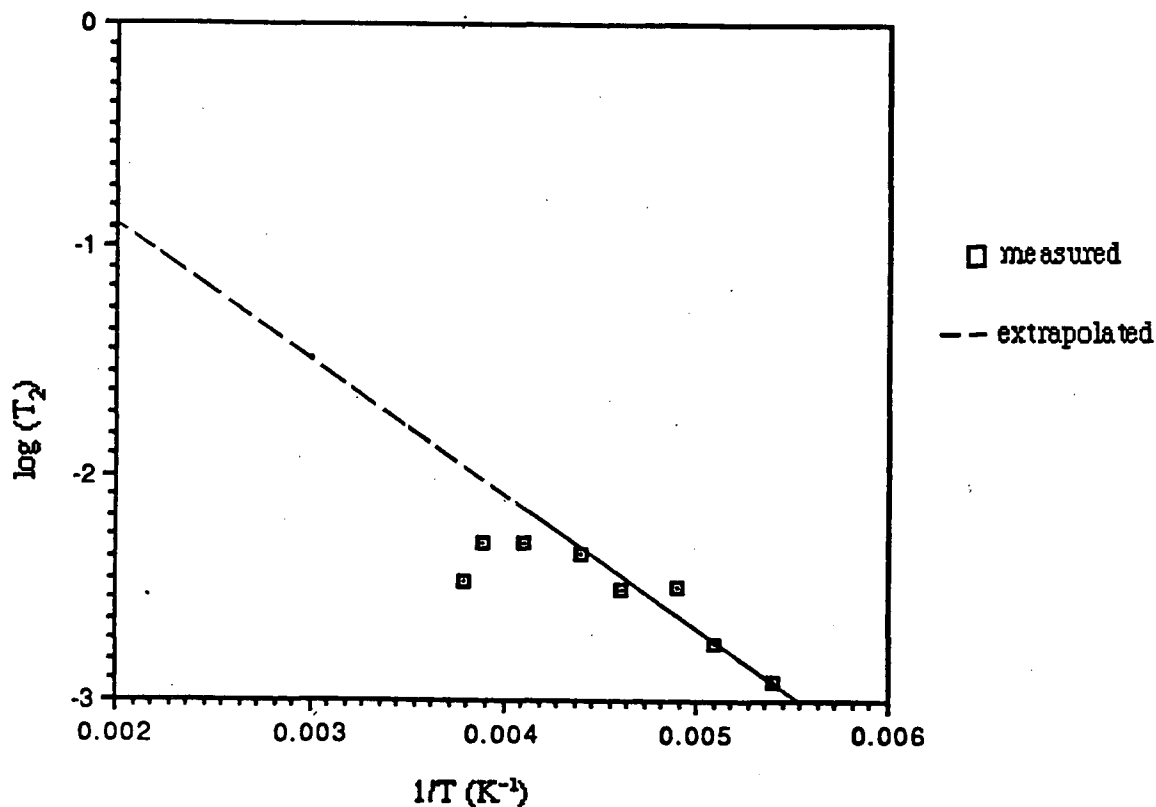


Figure 3.23 ^1H NMR T_2 values versus temperature for the $\eta^2\text{-H}_2$ ligand of 4, with extrapolation to higher temperatures.

25 ms were used, to simulate hydride peak broadening in the rather poor quality spectrum recorded at -48°C . The chemical shift of the $\mu\text{-H}$ resonance was permitted to shift slightly upfield with decreasing temperature (Fig. 3.24). The activation parameters obtained from an Eyring plot (Fig. 3.25) of the k_1 values, for the $\eta^2\text{-H}_2/\mu\text{-H}$ exchange, are:

$$\Delta H^\ddagger = 51 \pm 8 \text{ kJ/mol,}$$

$$\Delta S^\ddagger = -3 \pm 30 \text{ J/mol/K and}$$

$$\Delta G^\ddagger = 52 \pm 1 \text{ kJ/mol at } 20^\circ\text{C.}$$

The inversion-recovery method was used to obtain T_1 measurements (sect. 2.3) for the ^1H NMR upfield resonances; these measurements were carried out at 300 MHz, under hydrogen and over a range of temperatures. The inversion recovery plot for the -70°C measurement, shown in Fig. 3.26, and a plot of the measured T_1 values, over the range,

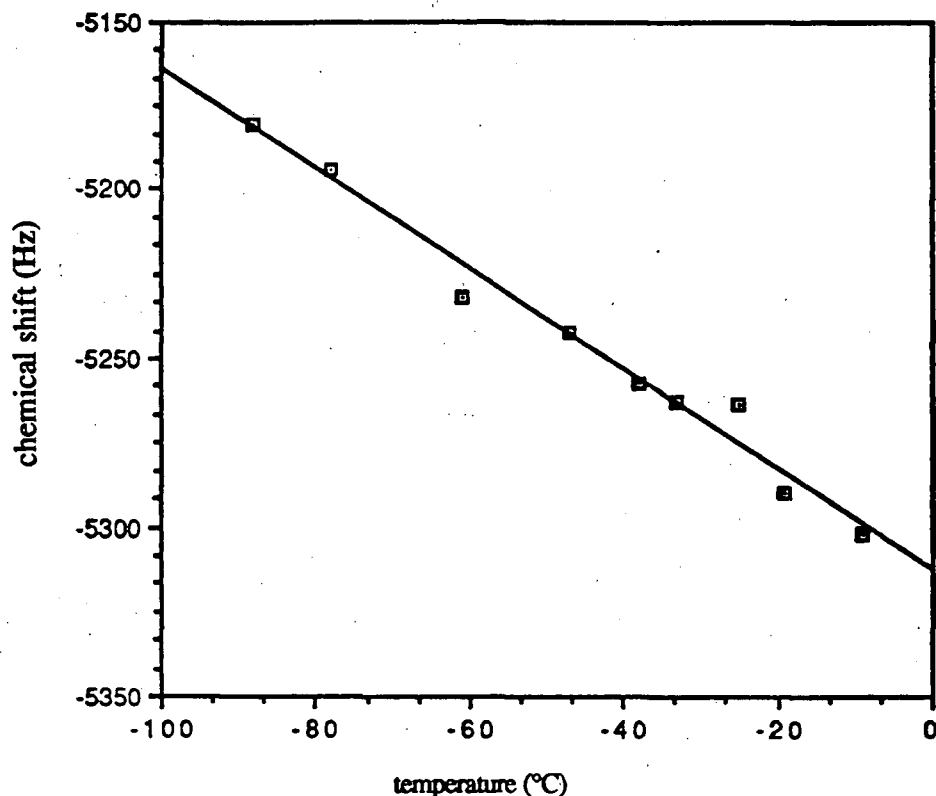


Figure 3.24 Dependence of the ^1H NMR chemical shift on temperature for the $\mu\text{-H}$ ligand of 4. The shifts for the $\eta^2\text{-H}_2$ and terminal H ligands were taken as constant at -3898 and -5572 Hz, respectively.

-88 to 20 $^\circ\text{C}$, is shown in Fig. 3.27. The T_1 values show the presence of one $\eta^2\text{-H}_2$ ligand (e.g., at -60 $^\circ\text{C}$, for the resonance at $\delta -12.8$, $T_1 = 13.8(3)$ ms) and two hydrides (at -60 $^\circ\text{C}$, for the resonances at $\delta -17.3$ ($\mu\text{-H}$) and -18.5 (terminal), the T_1 values are $182(6)$ ms and $251(5)$ ms, respectively). In general for exchanging systems, the T_1 values begin to average when the exchange time becomes less than the T_1 of a given state;⁶² in the present case the T_1 's of the $\eta^2\text{-H}_2$ and $\mu\text{-H}$ ligands begin to average at about -50 $^\circ\text{C}$, where the exchange time $= 1/k_1 = 1/(5 \text{ s}^{-1}) = 200$ ms, and the T_1 of the ligand at this temperature is about 200 ms (Fig. 3.27). The terminal Ru-H T_1 begins to average with the T_1 's of the other hydrogen ligands at about -10 $^\circ\text{C}$, and since the terminal Ru-H T_1 at this temperature is 230 ms, an estimate of k_2 from the T_1 measurements would be about 4 s^{-1} ; this is consistent with the estimate, from the line shape simulation, of $k_2 = 5 \text{ s}^{-1}$ at -9 $^\circ\text{C}$. The T_1 values of the resonances for the $\mu\text{-H}$ and $\eta^2\text{-H}_2$ ligands are completely averaged at -9 $^\circ\text{C}$.

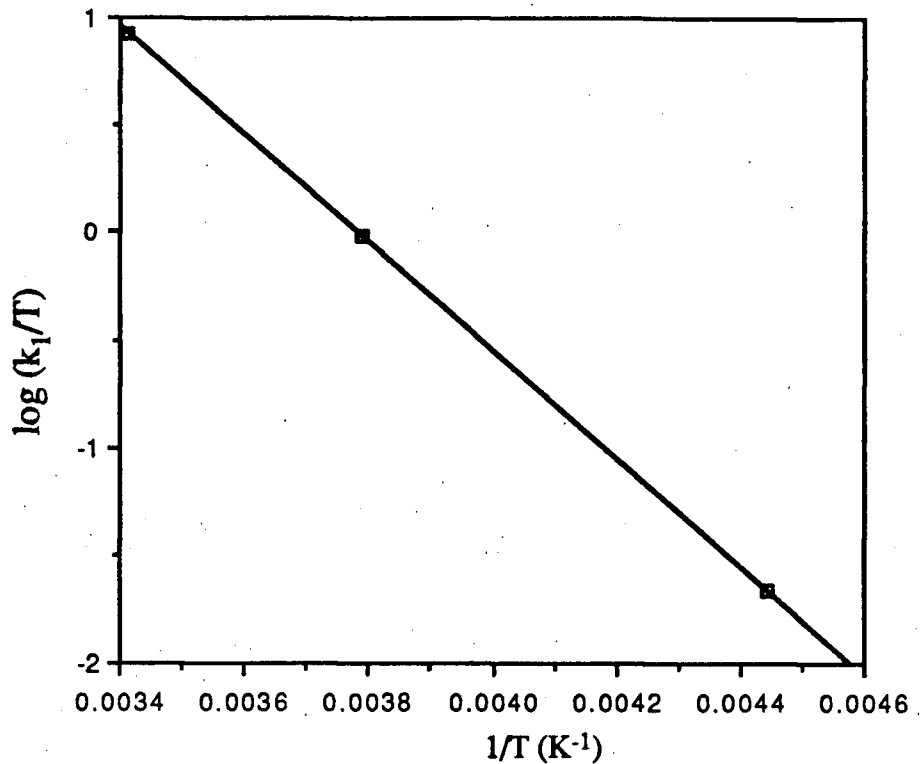


Figure 3.25 Eyring plot for the k_1 values ($\eta^2\text{-H}_2/\mu\text{-H}$ exchange) for 4.

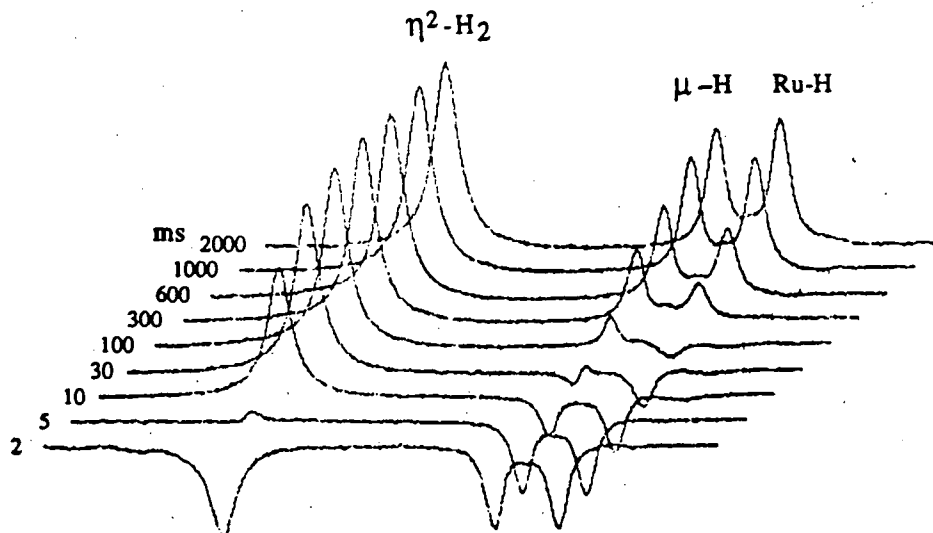


Figure 3.26 Inversion-recovery plot for ^1H NMR T_1 measurements (300 MHz, CD_2Cl_2 , -70°C , under hydrogen) for the hydrogen ligands of 4. Delay times (ms) are shown at the left.

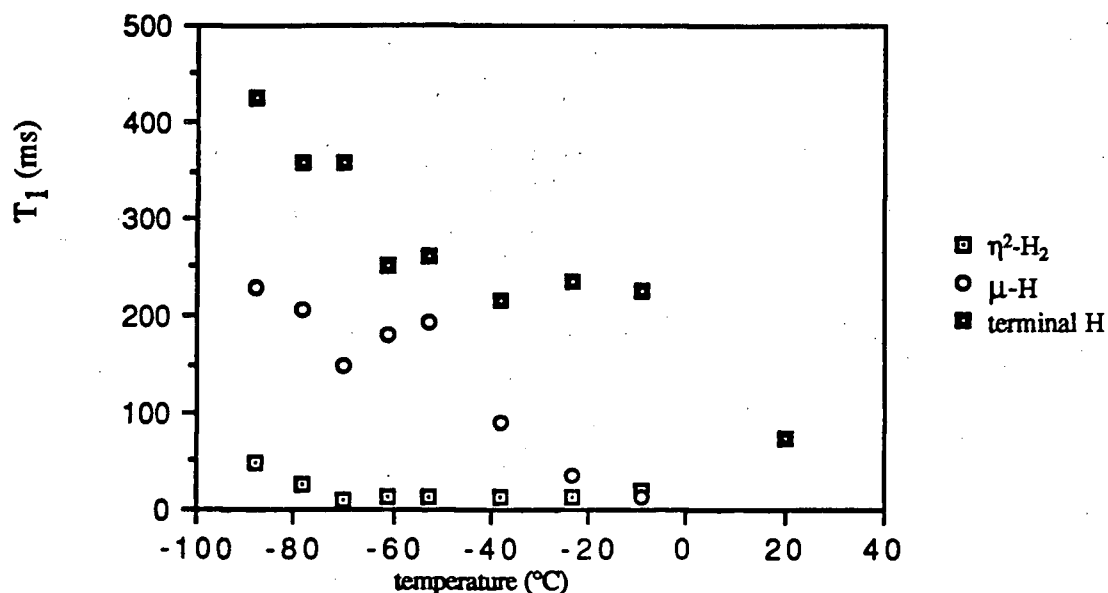


Figure 3.27 Plot of ^1H NMR T_1 values (300 MHz, CD_2Cl_2 , under hydrogen) versus temperature for the hydrogen ligands of **4**.

Spin-saturation transfer studies at 300 MHz, under hydrogen, revealed no spin transfer between the three upfield resonances at $-48\text{ }^\circ\text{C}$; however, at $-9\text{ }^\circ\text{C}$, irradiation of the $\eta^2\text{-H}_2$ resonance caused collapse of the $\mu\text{-H}$ resonance, although irradiation of the $\mu\text{-H}$ resonance decreased the $\eta^2\text{-H}_2$ resonance by only 60%. When the $\mu\text{-H}$ resonance was irradiated, there was also a slight reduction in the terminal Ru-H peak area by $< 20\%$, and when the terminal Ru-H resonance was irradiated, there was approximately 50% reduction in the $\mu\text{-H}$ resonance.

Reactions of **1a** and **1b** with 1-hexene:

Both complexes reacted with 1-hexene under vacuum to give hexane, isomerized hexenes and the respective $\text{RuHCl}(\text{PR}_3)_3$ complexes.

Complex **1a**:

Three hours after mixing, the only hydride signal observed in the ^1H NMR spectrum was that of $\text{RuHCl}(\text{PPh}_3)_3$ ($\delta(\text{ambient temperature}) -17.4$ (q, $^2J_{\text{PH}} = 26$ Hz), in agreement with the literature.⁸¹ After 9 d, the ^1H NMR spectrum still exhibited only the

same hydride resonance. The gas chromatogram of the distillate of this solution showed the presence of hexane, 1-hexene and 2-hexene (*cis* and *trans*) in a 10:1:100 ratio. Thus, only 1% of the original hexene remained, most being isomerized.

Complex 1b:

The ^1H NMR spectrum taken after 7 h shows unreacted 1b (δ -13.28(br s), *cf.* sect. 2.4) and $\text{RuHCl}(\text{P}(\text{p-tol})_3)_3$ (δ -18.0 (q, $^2J_{\text{PH}} = 26$ Hz), *cf.* lit.⁸²) and a barely visible triplet at δ -15.8. After 9 d, the only hydride signal observed in the ^1H NMR spectrum was the quartet due to $\text{RuHCl}(\text{P}(\text{p-tol})_3)_3$. The gas chromatogram of the distillate of this solution showed the presence of hexane and 2-hexene (*cis* and *trans*) in a 1:3 ratio; less than 1% of the original 1-hexene remained.

Reactivity of 1a and 1b under vacuum and under nitrogen

Complex 1a:

The NMR spectra of the complex in toluene- d_8 under vacuum in an NMR tube showed partial decomposition had occurred after 9 d. The $^{31}\text{P}\{^1\text{H}\}$ NMR spectrum was of poor quality because of low concentration, and peaks at δ 70.5 and 46.0, due to the original complex, dominated the spectrum. In the ^1H NMR spectrum, two hydride signals at δ -12.9(br s) and -17.4 (q, $^2J_{\text{PH}} = 26$ Hz) in a ratio of 6:1 indicated a mole ratio of 1a : $\text{RuHCl}(\text{PPh}_3)_3$ of 1.5:1. The ^1H NMR spectrum of a similar solution, but left under nitrogen for 9 d shows the *same* two hydrides to be present, suggesting that the *same* decomposition process occurred.

Complex 1b:

A solution of this complex in CD_2Cl_2 under vacuum in an NMR tube was largely unchanged after 10 h, as indicated by the ^1H NMR spectrum. But after 2 weeks, the integration of the ^1H NMR upfield signals (δ -13.28 br s, -18.0 q, $^2J_{\text{PH}} = 26$ Hz) indicated a 1b : $\text{RuHCl}(\text{P}(\text{p-tol})_3)_3$ ratio of 1:1. No other major hydride signals were observed (Fig. 3.28). The $^{31}\text{P}\{^1\text{H}\}$ NMR spectrum (Fig. 3.29) showed three main species to be

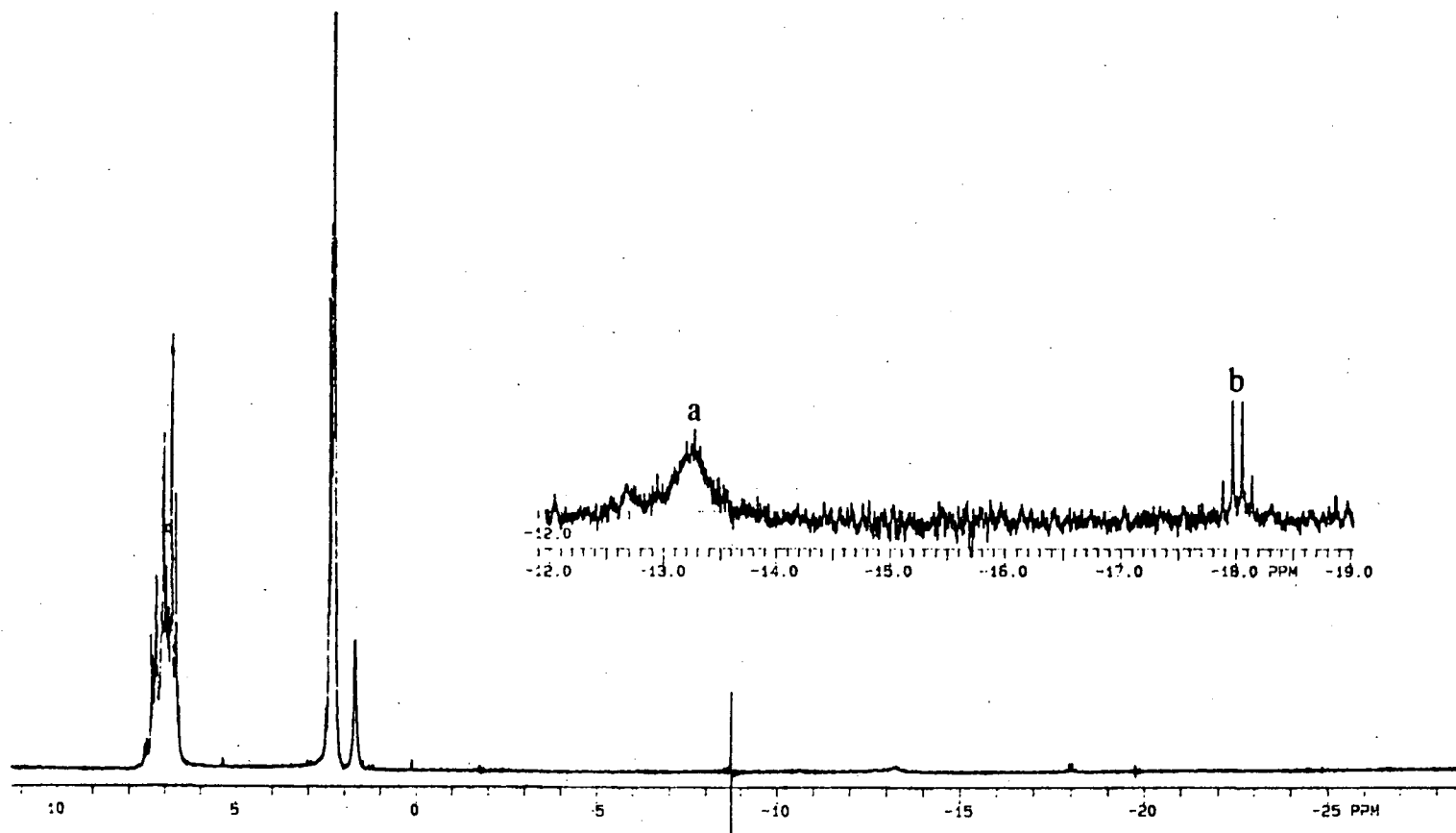


Figure 3.28 ^1H NMR spectrum (300 MHz, CD_2Cl_2 , ambient temperature) of **1b**, after two weeks under vacuum at ambient temperature. The resonance marked 'a' is due to **1b**; resonance 'b' is due to $\text{RuHCl}(\text{P}(p\text{-tol})_3)_3$. An expansion of the upfield region is shown in the inset.

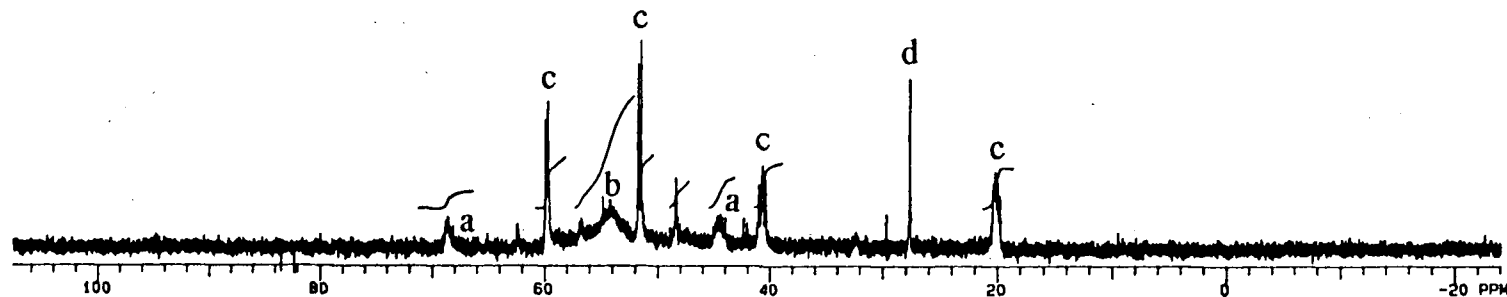


Figure 3.29 The $^{31}\text{P}\{^1\text{H}\}$ spectrum (300 MHz, CD_2Cl_2 , ambient temperature) of **1b**, after 2 wk under vacuum at ambient temperature. Resonances are marked as follows: 'a', **1b**; 'b', $\text{RuHCl}(\text{P}(\text{p-tol})_3)_3$; 'c', the A'B'CD' species described by Dekleva;²¹ 'd', Ph_3PO ; unmarked resonances are unidentified.

present: **1b** ($\delta(20\text{ }^\circ\text{C})$ 68.7 br s, 44.7 br s, *cf.* sect. 2.4), $\text{RuHCl}(\text{P}(\text{p-tol})_3)_3$ (δ 54.2 br s, *cf.* lit.⁸¹) and another complex with a four-spin ABCD system ($\delta(20\text{ }^\circ\text{C})$ 59.8 (d, $J_{\text{PP}} = 23$ Hz), 51.7 (d, $J_{\text{PP}} = 30$ Hz), 40.8 (dd, $J_{\text{PP}} = 42, 30$ Hz) and 20.2 (dd, $J_{\text{PP}} = 42, 23$ Hz), hereinafter referred to as the A'B'C'D'⁸³ complex, to distinguish it from the four-spin, ABCD systems described above. The same products were formed under nitrogen, indicating little, if any, reaction of **1b** with nitrogen.

Reactions of **4**

Stability in CD_2Cl_2 solution under vacuum:

The solution ^1H NMR spectrum showed that **4** was stable as such for hours at $\sim 20\text{ }^\circ\text{C}$. However, after three weeks in the NMR tube, mostly at $-30\text{ }^\circ\text{C}$, but also for several days at ambient temperature, the solution exhibited NMR spectra that indicated $\sim 30\%$ rearrangement to **1a** ($^{31}\text{P}\{^1\text{H}\}$ NMR δ (ambient temperature) 47 (br s), 71 (br s) and δ ($-68\text{ }^\circ\text{C}$) 79.5, 64.5, 61.5 and 35.5 (4 br s); ^1H NMR δ (ambient temperature) -13.1 (br s), and δ ($-68\text{ }^\circ\text{C}$) -8.9 (d), -12.4 (br s), -17.2 (br s)), $\sim 30\%$ residual **4** ($^{31}\text{P}\{^1\text{H}\}$ NMR δ (ambient temperature) 79 (dd), 77.5 (s), 65 (dd); ^1H NMR δ (ambient temperature) -14 (very broad resonance), -18.6 (dd), and δ ($-68\text{ }^\circ\text{C}$) -12.8 (br s), -18 (br s), -18.6 (br s)), and other phosphorus containing products.

Reaction with 1-hexene

The ^1H NMR spectrum of the reaction mixture, after 8 h from mixing, indicated partial reaction to give new hydride signals, δ (ambient temperature) -9.1 (d), -9.8 (bs). After two weeks no high-field (hydride) signals were found and the $^{31}\text{P}\{^1\text{H}\}$ NMR spectrum confirmed that the dihydrogen complex had completely reacted. The NMR spectra indicated the presence of $\text{RuCl}_2(\text{PPh}_3)(\text{isoPFA})$, **3b** ($^{31}\text{P}\{^1\text{H}\}$ NMR: δ (ambient temperature) 94 (d), 35.5 (d), $^2J_{\text{PP}} = 32$ Hz; ^1H NMR δ (ambient temperature) as listed in sect. 2.4, within 0.1 ppm) and other unidentified species. The gas chromatogram of the vacuum distillate showed that 0.010 mmol hexane and 0.030 (*cis* and *trans*) 2-hexene were produced from 0.0043 mmol **4** and 0.040 mmol 1-hexene.

A dihydrogen adduct of [RuCl₂(PPh₃)₂]₂, 2a

The dimer **2a**, prepared by the method of Wang^{24,70} and in *n*-butanol as described earlier (p. 14), was in neither case obtained analytically pure, and the ³¹P{¹H} NMR spectrum of the product from the latter reaction indicated ~10% phosphorus-containing impurity. Also, the identity of the product from the butanol preparation is implied by its fairly clean *in situ* reaction with hydrogen in the presence of Proton Sponge[®] to give **1a**. Figs. 3.6 and 3.8 show the NMR spectra obtained for **1a** produced from the [RuCl₂(PPh₃)₂]₂ from a butanol preparation; the ³¹P{¹H} NMR spectrum of this **1a** solution shows only trace signals at 43.5 and 24.0, the latter being OPPh₃.^{21,26} The NMR data for **2a** under vacuum are given in sect. 2.4. Under hydrogen (2-3 atm), the NMR spectra indicate formation of an adduct with dihydrogen: ¹H NMR (300 MHz, toluene-d₈, ambient temperature) δ -10.3 (br s), T₁ = 17 ms, integrated phenyl: η²-H₂ ratio = 60:1; δ (-58 °C) -10.1 (br s), and a weak signal(s) at δ ~-9, with ~20% of the area of the δ -10.1 signal; ³¹P{¹H} NMR (121 MHz, toluene-d₈, ambient temperature) δ 60.0 (bs), 52.7 (bs); δ (-58 °C) 60.9 (d), 53.3 (d), ²J_{PP} = 42 Hz. Other weak signals in the ³¹P{¹H} NMR spectrum indicate minor amounts of phosphorus-containing impurities.

*A dihydrogen adduct of [RuCl₂(P(*p*-tol)₃)₂]₂, 2b*

Again, the NMR spectra of **2b**, under hydrogen, indicate the presence of a dihydrogen adduct (¹H NMR (toluene-d₈, 300 MHz, ambient temperature) δ -10.1 (br s), T₁ = 17 ms, phenyl: η²-H₂ ratio = 80:1; ³¹P{¹H} NMR (toluene-d₈, 121 MHz, ambient temperature) δ 59 (br s), 52 (br s). Weak ³¹P{¹H} NMR signals in the δ 40 - 50 range again indicate minor amounts of phosphorus containing impurities.

3.4 Discussion

Complexes 1 and 4

On the basis of the low temperature T₁ measurements, the complexes **1a** and **1b** should be reformulated as containing a dihydrogen moiety. These complexes were

reported²³ along with other similar ones ($[\text{RuH}_2\text{XL}_2]_2$; X = Cl, L = AsPh₃; X = Br, L = PPh₃, AsPh₃); all the species showed similar NMR spectra at ambient temperature, and the latter group probably also contain the $\eta^2\text{-H}_2$ ligand.

The crystal structures of the two complexes **1a** and **1b** are almost identical (see Table 3.7 and Figs. 3.2 and 3.3). Corresponding bond lengths in many cases are the same within experimental error. This similarity for skeletal bond lengths is not surprising in view of the similarity of the phosphine ligands in the two complexes. The Ru-Ru distance of 2.83 Å in **1a** is almost the same as (but significantly different from) that in the structure of the P(*p*-tol)₃ analogue (2.80 Å), and is close to the middle of the range generally found for a Ru-Ru single bond, 2.632 to 3.034 Å.^{84,85} (A range of 2.28 to 2.95 Å quoted elsewhere^{21,23} is in error, the value, 2.28 Å, being the length of a multiple bond.^{86,87}) Acute bridging angles (M-B-M, M = metal, B = bridging atom) of about 70° are regarded as being caused by the presence of a metal-metal bond in M₂B₂ systems;⁸⁸ thus, there is further support in this case for Ru-Ru bonding in **1a** from the Ru-Cl-Ru angles: $\angle\text{Ru}(1)\text{-Cl}(1)\text{-Ru}(2) = 70.2^\circ$, $\angle\text{Ru}(1)\text{-Cl}(2)\text{-Ru}(2) = 68.4^\circ$, while corresponding values for the P(*p*-tol)₃ analogue, **1b**, are 69.3 and 67.3°. These may be compared with the "remarkably acute" $\angle\text{Fe-S-Fe} = 68^\circ$ in a Fe₂S₂ system,⁸⁸ presented as evidence for an Fe-Fe bond.

Dekleva *et al.*²³ attributed deviations from "idealized" (C₂) symmetry in the structure of **1b** to the presence of hydride ligands, although, as in the present PPh₃ structure hydride ligands were not located. The probable hydride positions in **1b** (numbered in order of increasing chemical shift) were assigned as shown in Fig. 3.30; the P atoms also were numbered in order of increasing chemical shift in the low temperature ³¹P{¹H} NMR spectrum. Assignment of the hydride ligand positions was based on the low temperature 400 MHz ¹H NMR spectrum (*cf.* the 300 MHz spectrum, Fig. 3.14), the low temperature ³¹P{¹H} and ³¹P{Ph-¹H} spectra (at 32.4 MHz), as well as vacant site positions in the solid state structure. Lengthening of bonds, Ru(1)-Cl(2) and Ru(2)-P(4), compared to other corresponding bond lengths in the **1b** molecule, seemed to confirm the

positions assigned to H(3) and H(1);²³ no such lengthening of Ru(2)-Cl(1) was observed "trans" to an "H(2)" atom. The two "H(2)" atoms are, however, now regarded as the atoms of a symmetrically coordinated $\eta^2\text{-H}_2$ ligand. The T_1 values at $-94\text{ }^\circ\text{C}$: 120 ms (H(1)), 44 ms (H(2), or more correctly, $\text{H}_2(2)$), 350 ms (H(3)) indicate a hydride, a dihydrogen and a hydride ligand, respectively (Figs. 3.18, 3.19). The Ru(2)-Cl(1) bond in **1b**, presumably *trans* to the $\eta^2\text{-H}_2$ ligand, is about the same length as the Ru-Cl bonds *trans* to a phosphine. This suggests, assuming the placing of the $\eta^2\text{-H}_2$ ligand is correct,

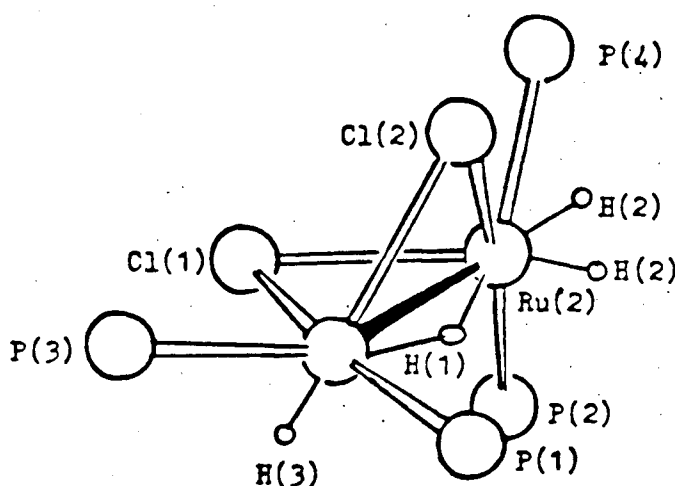


Figure 3.30 Slow exchange structure showing proposed hydrogen ligand positions for **1b**, reported as a classical tetrahydride.²³

that the *trans*-influence of an $\eta^2\text{-H}_2$ ligand is weak relative to that of a hydride.

The low temperature ^1H NMR spectrum of **1b** has been published, but this is the first report of the low temperature ^1H NMR spectrum of the PPh_3 analogue. Dekleva, using CD_2Cl_2 , was not able to observe the low temperature ^1H NMR spectrum because of limitations of solubility.²¹ However, the solubility in toluene- d_6 is sufficient for the purpose. The low temperature ^1H NMR spectrum contains three upfield resonances at $-69\text{ }^\circ\text{C}$, $\delta_{\text{toluene-}d_6}$ -8.6 (d), -12.6 (br s), -17.2 (t), which average at $20\text{ }^\circ\text{C}$ to one broad singlet (δ -12.9). The simulation (Fig. 3.8) confirms that the ratio of areas under these three resonances is 1:2:1, respectively. The T_1 measurements (sect. 3.3) for these resonances

indicate a hydride, a dihydrogen ligand and a hydride, respectively. The T_1 values (Fig. 3.13) are almost completely averaged, on warming to $-43\text{ }^\circ\text{C}$, because of hydride/dihydrogen exchange. The crystal structures and NMR spectra for the two complexes, **1a** and **1b**, are very similar, and the positions of the hydrides of the Ph analogue can be assigned as in the p-tol complex (Fig. 3.30) by similar arguments.²³ Thus, the H(1) resonance at δ -8.6, due to a bridging hydride, is consistent with its position *trans* to two phosphine ligands, P(3) and P(4), as there is a tendency for resonances of hydrides *trans* to ligands of high *trans*-influence to be generally at lower field than those of hydrides *trans* to ligands of low *trans*-influence, *other things being equal*.⁸⁹ The terminal hydride, H(3), which is *trans* to one ligand of low *trans*-influence, Cl(2), resonates at higher field (δ -17.2). The Ru(2) atom is a more likely site for the $\eta^2\text{-H}_2$ ligand because of the close structural correspondences between **1a** and **4** (discussed later), where the $\eta^2\text{-H}_2$ ligand is crystallographically located on Ru(2); and the length of the Ru(1)-Cl(2) bond (2.56 Å), longer than the other Ru-Cl distances by ~ 0.1 Å, is consistent with it being *trans* to the H(3) ligand of high *trans*-influence.⁸⁹ The ^{31}P NMR resonances of phosphines *trans* to hydrides are typically at higher field^{90,91}, and the assignment of the P(3) and P(4) resonances is consistent with their positions being *trans* to the hydride, H(1). The reason for the lengthening of the Ru(2)-P(4) bond relative to other Ru-P bonds in the molecule is not clear; a similar lengthening occurs in the p-tol analogue.

Assignment of these positions in a solid state structure, using solution NMR data, seems valid because, as for **1b**, the low temperature $^{31}\text{P}\{^1\text{H}\}$ NMR spectrum of the PPh_3 complex is consistent with retention, in solution, of the solid state structure. The low temperature 32.4 MHz spectrum reported by Dekleva²¹ (32.4 MHz, CD_2Cl_2): 73.9 (d, $^2J_{\text{PH}} = 40$ Hz, P(1)), 59.4 (dd, $^2J_{\text{PH}} = 20$, 5 Hz, P(2)), 55.4 (td, $^2J_{\text{PH}} = 40$, 5 Hz, P(3)) and 28.0 (dd, $^2J_{\text{PH}} = 40$, 20 Hz, P(4)) exhibits the coupling pattern diagrammed in Fig. 3.31. These $^{31}\text{P}\{^1\text{H}\}$ NMR data are similar to those obtained for **1a** in the present work: (121 MHz, toluene- d_8 , $-58\text{ }^\circ\text{C}$ down to $-88\text{ }^\circ\text{C}$) δ 79.5 P(1), 63.5 P(2), 62.5 P(3), 29.5

P(4). The $^{31}\text{P}\{^1\text{H}\}$ NMR spectrum for the bis-DMA solvate and for the DMA-free complex are the same in toluene- d_6 ; thus, the DMA is not coordinated in solution. Dekleva *et al.*^{21,23} also found the visible spectra in toluene and in DMA to be similar and that **1a** obeyed Beer's Law in DMA, confirming the original work of Wang,⁷⁰ and conformity to Beer's Law is confirmed in the present work. Thus Thorburn's observations (Table 3.9)

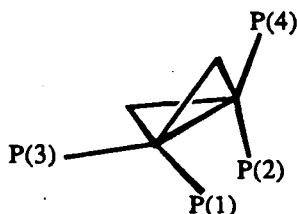
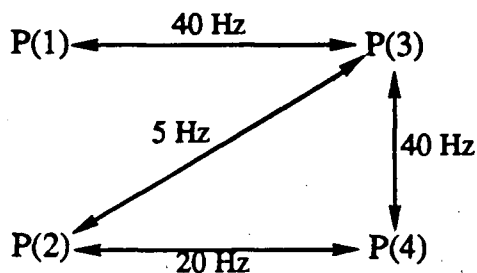


Figure 3.31 $^{31}\text{P}\{^1\text{H}\}$ NMR coupling pattern for complex **1a**.²¹

indicating non-conformity to Beer's Law for **1a** in DMA (perhaps because of impurities in the DMA) are surely in error and there is no evidence for the monomer-dimer⁷¹ equilibrium he suggested. Wang's molecular weight determination⁷⁰ of the bis-DMA solvate in benzene, on a sample analyzing correctly for $[\text{RuHCl}(\text{PPh}_3)_2\cdot\text{DMA}]_2$ (now, more correctly formulated as $(\eta^2\text{-H}_2)(\text{PPh}_3)_2\text{Ru}(\mu\text{-Cl})_2(\mu\text{-H})\text{RuH}(\text{PPh}_3)_2\cdot 2\text{DMA}$) had given an effective value of 500, and was interpreted by invoking dissociation of solvated DMA molecules from the dimer in benzene solution. Thus, the actual value determined experimentally for $(\eta^2\text{-H}_2)(\text{PPh}_3)_2\text{Ru}(\mu\text{-Cl})_2(\mu\text{-H})\text{RuH}(\text{PPh}_3)_2\cdot 2\text{DMA}$ was 1500 (calcd.: 1499). Thus, this molecular weight determination is further confirmation of dinuclearity in benzene solution, and in the light of spectroscopic similarities in DMA and in toluene, implies

Table 3.9

Spectroscopic data for 1a

 $^{31}\text{P}\{^1\text{H}\}$ NMR spectrum

solvent, δ values	temperature ($^{\circ}\text{C}$)	atmosphere	reference
toluene, 69.5, 45.3	-60	not specified	70 ^a
C_6D_6 , 68.0, 43.1	ambient	" "	21
CD_2Cl_2 , 73.9 (d, 40 Hz), 59.4 (dd, 20, 5 Hz), 55.4 (td, 40, 5 Hz), 28.0 (dd, 40, 20 Hz)	-80	" "	21

(see also section 3.3)

 ^1H NMR spectrum

solvent, δ values	temperature ($^{\circ}\text{C}$)	atmosphere	reference
C_6D_6 , 13.8	30	not specified	70
C_6D_6 , 12.81	ambient	" "	21

(see also section 3.4)

Visible spectrophotometric data (DMA solution)

λ_{max} (nm)	ϵ ($\text{M}^{-1}\text{cm}^{-1}$), concentration ($\text{M} \times 10^3$)	atmosphere	temp. ($^{\circ}\text{C}$)	reference
500	1530 ^b (± 200) (Beer's Law obeyed)	not specified	not specified	70
500	700 ^c , 0.4	argon	25 $^{\circ}\text{C}$	71
	750 ^c , 0.9	"	"	"
	900 ^c , 1.3	"	"	"
	1000 ^c , 2.0	"	"	"
	1100 ^c , 4.0	"	"	"
	1200 ^c , 7.5	"	"	"
495	1500 ^b , 0.18 - 12	hydrogen (not appreciably different in the absence of hydrogen)	not specified	21
495	1580, 6.20	hydrogen	25 $^{\circ}\text{C}$	present work
	1570, 3.12	"	"	"
	1580, 1.01	"	"	"

^aThe $^{31}\text{P}\{^1\text{H}\}$ NMR data reported by Wang⁷⁰ were in error; his "-60 $^{\circ}\text{C}$ " spectrum actually looks very much like the room temperature spectrum. The identity of the complex Wang studied is, however, confirmed as 1a by its visible spectrum, as indicated in the table.

^bPresumably, ϵ was calculated based on the concentration of ruthenium, rather than concentration of dimer; this was not made clear by the author.

^cCalculation based on concentration of ruthenium.

dinuclearity in DMA as well. Thus, there is NMR, spectrophotometric and molecular weight evidence for retention of the solid state structure of complexes **1** in solution.

The model (P(1) exchanging with P(2), P(3) exchanging with P(4)) that successfully simulates the exchange process observed in the ^{31}P spectrum of the PPh_3 complex, probably reflects the change in phosphorus environments caused by the hydrogen ligand exchange processes. Thus, for example, P(1) on Ru(1), and P(2) on Ru(2), exchange environments as the $\eta^2\text{-H}_2$ ligand resides on alternate ruthenium centres. This rationalizing of the variable temperature ^{31}P behaviour requires the exchange rate constants from the ^{31}P and ^1H NMR simulations to be equal within experimental error, and this is probably true: the rate constant ($k = 8 \times 10^5 \text{ s}^{-1}$) for the phosphorus exchange at 20°C and that ($k = 2 \times 10^5 \text{ s}^{-1}$) of the hydrogen exchange at 20°C are similar, considering the error estimate of $\pm 50\%$ given above for k values in the fast exchange region.

The ^1H NMR exchange rate constants for hydrogen ligand exchange for the two analogues, **1a** and **1b**, are similar. However, comparison of the ^1H NMR spectra of the PPh_3 complex (-63°C , Fig. 3.8) and the $\text{P}(\text{p-tol})_3$ complex (-64°C , Fig. 3.14) reveals slightly more broadening of signals for the p-tol complex, even though, for the latter complex, resolution is better because of higher solubility of this complex.

The mechanism of exchange may involve coordinated $\eta^3\text{-H}_3$ units, bridging dihydrogen, or both. Involvement of an $\eta^3\text{-H}_3$ unit in hydride/dihydrogen exchange in $[\text{Ir}(\text{H})(\eta^2\text{-H}_2)(\text{bq})(\text{L})_2]^+$ ($\text{bq} = 7,8\text{-benzoquinoline}$; $\text{L} = \text{PPh}_3$) has been suggested,⁶² and the trihydrogen ligand has been shown to exist in the complexes, $[\text{Ir}(\text{H}_3)(\eta^5\text{-C}_5\text{H}_5)(\text{L})]^+$ ($\text{L} = \text{PMe}_3, \text{PPh}_3, \text{AsPh}_3$),⁹² MH_3Cp_2 (where $\text{M} = \text{Nb, Ta}$; $\text{Cp} = \text{C}_5\text{H}_4\text{Me}, \text{C}_5\text{H}_4(\text{SiMe}_3)$ or $\text{C}_5\text{H}_3(\text{SiMe}_3)_2$) and $\text{RuH}_3(\text{C}_5\text{Me}_5)(\text{PR}_3)$.^{93,94} There is no documented precedent for bridging H_2 , although within the complex, $\text{CpRu}(\mu\text{-H})_4\text{RuCp}$,⁹⁵ the $(\mu\text{-H})\text{-}(\mu\text{-H})$ distances in the solid state (X-ray) perhaps indicate two bridging H_2 molecules; the T_1 measurements in solution indicated classical hydrides, but this, of course, does not preclude the existence of $\mu\text{-H}_2$ groups in the solid state.^{95b} Kubas *et al.*⁵¹ have shown that

hydrogen ligands can readily shift back and forth from classical hydrides to a nonclassical dihydrogen ligand in solution.

The suggestion has been made^{61,96} that an N₂ ligand should be replaceable by an η^2 -H₂ ligand when the dinitrogen stretching frequency falls in the range 2060 - 2150 cm⁻¹; examples of replacement of coordinated dihydrogen by dinitrogen have also been observed.^{36,61,62,96} However, no evidence of reaction with nitrogen by the complexes, **1a** and **1b**, was observed; the decomposition of the complexes, **1a** and **1b**, in the absence of hydrogen, was not appreciably affected by the presence of dinitrogen.

The unidentified A'B'C'D' complex, referred to in section 3.3 as a decomposition product of **1b** has been discussed by Dekleva,²¹ who also examined the ³¹P{¹H}, ³¹P{phenyl-¹H} and ¹H NMR of the analogous PPh₃, A'B'C'D' complex. The similarity of the ³¹P NMR spectra of these two A'B'C'D' complexes imply very similar structures. Also, he pointed out that the similarity of the ³¹P{¹H} chemical shifts and coupling patterns for the two complexes, **1b** and the p-tol A'B'C'D' complex, imply a similar dinuclear structure and phosphine-ligand disposition for these two molecules. The chemical shifts of the two upfield ³¹P NMR resonances, P_C and P_D (in order of increasing chemical shift), would allow for two phosphine ligands *trans* to a bridging hydride. Also, a ³¹P{phenyl-¹H} NMR spectrum of the PPh₃ A'B'C'D' complex showed that: the P_D resonance was coupled to only a single hydride with ²J_{PH} = 63 Hz, P_C appeared to be coupled to at least one hydride with ²J_{PH} ≈ 30 Hz, P_B was broadened only slightly, and P_A was possibly coupled to more than one hydride, one of which had ²J_{PH} ≈ 20 Hz.²¹

Dekleva was unable to determine the number of hydrides by NMR; however, from the reaction of the PPh₃ A'B'C'D' complex with PPh₃, he inferred the following reaction:



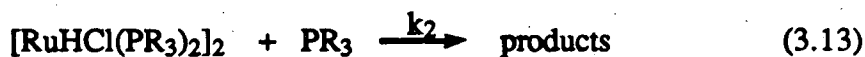
and it was concluded that this A'B'C'D' species had at least one hydride per ruthenium. The formulations Ru₂H₂Cl₂(PPh₃)₄ and Ru₂H₃Cl₃(PPh₃)₄ were considered, but no definite conclusions were drawn. The decomposition of **1b**, under nitrogen or vacuum,

observed in this work, probably proceeds by loss of dihydrogen, followed by disproportionation of $\text{Ru}_2\text{H}_2\text{Cl}_2(\text{P}(\text{p-tol})_3)_4$ to give $\text{RuHCl}(\text{P}(\text{p-tol})_3)_3$ and other unidentified products. Further, it appears from the reaction of **1b** with hexene, under vacuum, that either, or both of **1b** and $\text{Ru}_2\text{H}_2\text{Cl}_2(\text{P}(\text{p-tol})_3)_4$ react with hexene, because the only phosphine-containing product in significant concentration is $\text{RuHCl}(\text{P}(\text{p-tol})_3)_3$.

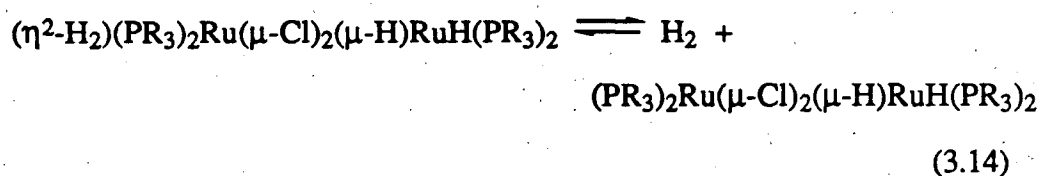
Whether or not the $\eta^2\text{-H}_2$ ligand atoms are actually transferred to hexene in this latter reaction is not yet resolved. The reaction of $\text{RuH}_4(\text{PPh}_3)_3$ with 1-pentene was reported by Cole-Hamilton and Wilkinson,⁹¹ prior to the complex being shown to be a dihydrogen dihydride species.³⁸ The reaction gave an undetermined amount of dihydrogen, 2 moles of pentane and an apparent pentadiene complex, with no Ru-hydride products being detected. Although the mechanism proposed involved initial loss of hydrogen, followed by reaction of an $\text{Ru}(\text{H})_2$ moiety with pentene, the data do not preclude 1-pentene as the source of the observed dihydrogen, with the $\eta^2\text{-H}_2$ and hydride ligand atoms involved in formation of the pentane. In the present work, however, since $\text{RuHCl}(\text{PR}_3)_3$ remains after reaction, with hexene, of both species **1** ($\text{R} = \text{Ph}, \text{p-tol}$), it seems more likely that the dihydrogen is transferred to form the alkane. The question of the fate of the hydrogen ligands in the reaction of **1a** and **1b** with hexene could prove difficult to sort out even by deuteration studies, because isomerization of alkene, and H ligand exchange are both occurring, as well as hydrogen-atom exchange with ortho-phenyl hydrogens.⁷¹

Other reactions of the complexes, $[(\eta^2\text{-H}_2)\text{L}_2\text{Ru}(\mu\text{-X})_2(\mu\text{-H})\text{RuHL}_2]$ ($\text{X} = \text{Cl}, \text{Br}$; $\text{L} = \text{PPh}_3, \text{P}(\text{p-tol})_3, \text{AsPh}_3$), with L , CO and bipy, giving RuHXL_3 , $\text{RuHCl}(\text{CO})_2\text{L}_2$ and $\text{RuHCl}(\text{bipy})\text{L}_2$, respectively, proceed with evolution of 1 mole of dihydrogen per mole of starting complex.²³ Similar evolution of hydrogen has also been observed in related reactions of $\text{RuH}_4(\text{PPh}_3)_3$.^{30,38} Predissociation of the molecular hydrogen ligand has been suggested for all these reactions.^{23,38,56} The kinetics of the reaction of **1a** and **1b** with the respective phosphine have been studied by Thorburn⁷¹ and Dekleva *et al.*^{21,23} The

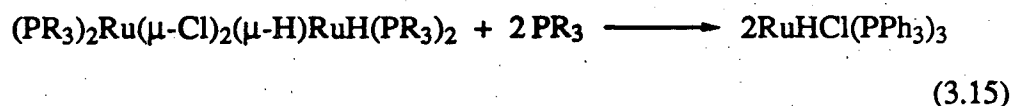
reaction rate showed a direct inverse first-order dependence on dihydrogen, consistent with a pre-dissociation equilibrium involving loss of dihydrogen. This dihydrogen dependence and first-order dependences on both phosphine and ruthenium were interpreted in terms of the following mechanism:



While a value for k_2K could be obtained from the kinetic data at 30 °C, individual k_2 and K values could only be estimated. The estimate for K ($\leq 2 \times 10^{-5}$ M for both systems) is close to that obtained from a re-examination of the kinetic data obtained by Thorburn⁷⁰ (sect. 4.4) for the hydrogenation of 1-hexene catalyzed by 1a. With the new formulation of the tetrahydride dimers as 1, K becomes the dissociation equilibrium constant for the loss of the dihydrogen ligand from the dimer:



which is followed by:



The crystal structure of 4 (Fig. 3.4) is the third reported structure to reveal a $\eta^2\text{-H}_2$ ligand; no other crystal structures of a dinuclear dihydrogen complex have been reported, in which the dihydrogen ligand has been located. The H-H distance, 0.80(6) Å, is similar to those found in the mononuclear complexes (sect. 3.1). The presence of a $\eta^2\text{-H}_2$ ligand is supported by the ¹H NMR T_1 measurements at low temperature, the value of 12 ms (δ -12.8) indicating a very short H-H distance. The exchange exhibited by the hydrogen ligands is unique in that it mostly involves the $\mu\text{-H}$ ligand and $\eta^2\text{-H}_2$ ligand, which is at the

isoPFA end of the molecule. Exchange is slow between the μ -H and the terminal hydride at the other end of the molecule. The linear Eyring plot for k_1 (for the fast process) shows the self-consistency of the results.

Except for the nitrogen atom, the mirror image of the skeleton of this isoPFA structure is approximately superimposable on those of the analogous structures of **1a** and **1b**, even to the point that the bond distances and angles are similar (*cf.* Tables 3.7 and 3.8, and Figs. 3.2, 3.3 and 3.4). For example, distances for Ru(1)-Ru(2) are all between 2.80 and 2.83 Å; distances for Ru(1)-P(1) are 2.22 to 2.23 Å; and for Ru(2)-P(2), 2.24 to 2.27 Å. The Ru(2)-P(4) distances are the longest Ru-P distances in Table 3.7, while the Ru(2)-N distance is longer than all the Ru-P distances in the isoPFA structure (Table 3.8). Such close correlations occur all down the list of bond distances and angles in the Tables 3.7 and 3.8. Furthermore, the effects of *trans* influences, cited in discussion of Table 3.7, are also reflected in the parameters in Table 3.8 for the isoPFA structure. The longest Ru-Cl distance in each of the three structures is the Ru(1)-Cl(2) bond. This is attributed to its position *trans* to a hydride. In the case of the isoPFA structure, the Ru(1)-Cl(2) bond (2.620(2) Å), which is lengthened relative to other Ru-Cl distances in this molecule (2.453(2), 2.435(2) and 2.528(2) Å) is confirmed by the crystal structure to be *trans* to the terminal hydride (H(13)). The ^1H NMR chemical shift of this terminal hydride (δ -18.6) is consistent with its position *trans* to a ligand (Cl) of weak *trans* influence. The magnitudes of the coupling constants for the δ -18.5 resonance are in the range typical of a hydride *cis* to a phosphine ligand.^{89,91} The *trans*-influence of the $\eta^2\text{-H}_2$ ligand (*trans* to Ru(2)-Cl(1), 2.435(2) Å) is weak, and this is the shortest Ru-Cl distance in this molecule. As implied earlier in this section, the Ru(2)-N distance, which corresponds to Ru(2)-P(4) in each of **1a** and **1b**, is anomalously large. This could be attributed to the *trans*-influence of the bridging hydride; but, as in **1a** and **1b**, the Ru(1)-P(3) distance (2.239(2) Å) is comparable to the other Ru-P distances (2.229(2) and 2.240(2) Å) in this molecule, and is evidently only slightly affected by its *trans* relationship to the bridging hydride (H(12)). This is

particularly surprising because in **4** the unsymmetrically bridging hydride, H(12), is bonded more closely to Ru(1) (Ru(1)-H(12): 1.49(4) Å) than to Ru(2) (Ru(2)-H(12): 1.71(4) Å). There is, however, evidence in the $^{31}\text{P}\{^1\text{H}\}$ NMR spectrum of the *trans*-influence of the bridging hydride on P(3). The two doublet-of-doublets must be due to P(1) and P(3), which are *cis* to each other, and have differing structural relationships to P(2) (*cf.* Fig. 3.4). The difference in chemical shifts is undoubtedly due to the *trans*-influence of bridging ligands. The upfield resonance at δ 64.6 is therefore assigned to the P(3) atom, which is *trans* to a bridging hydride, H(12), and the resonance at 78.5 is assigned to the P(1) atom, which is *trans* to a bridging chloride. The relations of the observed couplings to the structure are shown in Figure 3.32, and the $^{31}\text{P}\{^1\text{H}\}$ NMR data for **4** are thus consistent with retention of solid state structure in solution. Although the crystallographically determined H(12) position seems inconsistent with other skeletal bond lengths in the molecule, it is possible to rationalize this using electron counting. The Ru(2)-H(12) bond distance is long, while the Ru(1)-H(12) distance is about the same as other Ru-H distances in the molecule. Thus, if this bridging hydride atom is considered to

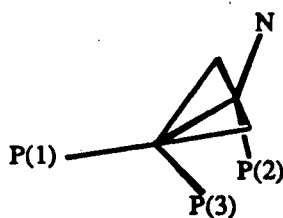
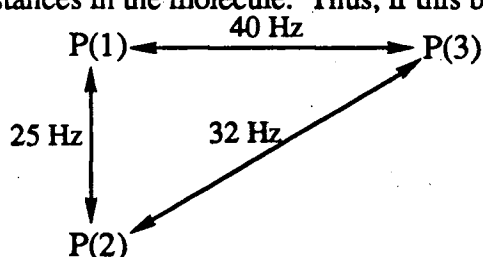


Figure 3.32 The $^{31}\text{P}\{^1\text{H}\}$ NMR coupling pattern for complex **4**. The $\mu\text{-Cl}$ atoms are the only bridging atoms shown in the structure diagram to facilitate the comparison with complexes **1** (See Fig. 3.31). The crystallographically located $\mu\text{-H}$ atom is approximately *trans* to P(3).

be coordinated solely to Ru(1), and assuming the existence of a metal-metal bond, the electron count is 18 at each Ru atom.

The reaction of **4** with 1-hexene to give 2 moles of hexane is again reminiscent of the work of Cole-Hamilton and Wilkinson⁹¹ (*vide supra*) on the similar reaction of $\text{RuH}_4(\text{PPh}_3)_3$ with pentene to give 2 moles of pentane. As in the discussion above, it is not known whether the $\eta^2\text{-H}_2$ ligand is the source of hydrogen for one of the moles of hexane, or whether, in a mechanism similar to the proposal of those workers, the hexene is the source of hydrogen for one mole of hexane, with hexadiene, perhaps coordinated, also produced.

The partial disproportionation of **4** to **1a** under vacuum, in CD_2Cl_2 , occurred slowly, over a period of weeks. Under hydrogen, in CD_2Cl_2 , however, there was no change in the ^1H NMR spectrum for several weeks after mixing the components in a sealed NMR tube. It is not clear whether this disproportionation is the pathway for the formation of **1a** in the reaction of $\text{RuCl}_2(\text{PPh}_3)(\text{isoPFA})$, **3b**, with hydrogen in DMA (see sect. 4.3).

The three dinuclear dihydrogen complexes **1a**, **1b** and **4** described above are analogous to the complex, $(\eta^2\text{-H}_2)(\text{PCy}_3)_2\text{Ru}(\mu\text{-Cl})_2(\mu\text{-H})\text{RuH}(\text{PCy}_3)_2$, reported in the literature.⁹⁶ The only other reported example of a dinuclear dihydrogen complex is the poorly characterized, " $\text{Cu}_2\text{H}_2(\text{H}_2)_x$ ", which was reported at a conference,⁹⁷ and is referred to by Kubas²⁹ in his review.

*Dihydrogen adducts of the complexes, $\text{Ru}_2\text{Cl}_4(\text{PR}_3)_4$ ($R = \text{Ph}, p\text{-tol}$), **2a** and **2b***

Dekleva's attempts²¹ to prepare the complexes **2a** and **2b** in DMA by the method of Wang⁷⁰, produced samples with with unsatisfactory elemental analyses, attributed to a "DMA impurity" (for **2a**, Calc'd for $(\text{C}_{36}\text{H}_{30}\text{Cl}_2\text{P}_2\text{Ru})_2$: C, 62.07; H, 4.34. Found: C, 62.81; H, 5.42; N, 0.87). The carbon analysis for the product obtained from butanol solution in the present work show an improvement in elemental analysis, but is still not entirely satisfactory (sect. 2.4).

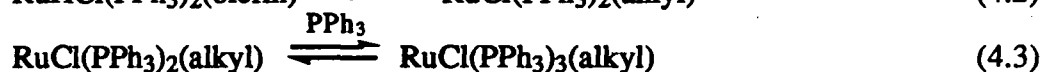
Both complexes **2a** and **2b** largely retain their structure under hydrogen in toluene- d_6 ; however, the broad ^1H NMR resonances at about δ -10, exhibited by both complexes under hydrogen, show T_1 values that indicate the binding of an $\eta^2\text{-H}_2$ ligand. The integrations of these resonances indicate only one $\eta^2\text{-H}_2$ for every two $\text{Ru}_2\text{Cl}_4(\text{PR}_3)_4$ moieties. The suggestion by other workers⁷⁶ of the possibility of polymeric species in concentrated solution was mentioned in section 3.1; oligomeric species, such as $\text{Ru}(\eta^2\text{-H}_2)\text{Cl}(\text{PR}_3)_2\{\text{RuCl}_2(\text{PR}_3)_2\}_6(\eta^2\text{-H}_2)\text{Cl}$ would explain the ^1H NMR integrations in the present case under H_2 . However, the solution $^{31}\text{P}\{^1\text{H}\}$ NMR resonances for **2a** under hydrogen were almost identical to those for **2a** under vacuum (see sects. 3.3 and 2.2), which might perhaps be due to very loose binding of the $\eta^2\text{-H}_2$ ligand. Joshi in this laboratory has recently discovered that $[\text{RuCl}_2(\text{dppb})]_2$ also binds an $\eta^2\text{-H}_2$;⁹⁸ the adduct of this latter complex exhibits a ^1H NMR upfield resonance similar to those described above ($\delta \sim -10$, $T_1 \approx 13$ ms). As discussed earlier, solutions of $\text{RuCl}_2(\text{PPh}_3)_3$ contain, among other species, **2a**, and the discovery of the binding of dihydrogen to this dimer under slightly elevated pressures thus has important implications for the mechanism of the reaction of $\text{RuCl}_2(\text{PPh}_3)_3$ with hydrogen, and the widespread use of $\text{RuCl}_2(\text{PPh}_3)_3$ for catalytic hydrogenation of olefins.

Chapter 4

Mechanistic studies on hydrogenation catalyzed by tertiary phosphine complexes of ruthenium(III)

4.1 Introduction

Interest in homogeneous hydrogenation grew slowly after early reports by Calvin in 1938⁹⁹ on the hydrogenation of benzoquinone catalyzed by cupric acetate, and by Roelen,¹⁰⁰ in 1944, on hydrogenations catalyzed by cobalt carbonyl complexes. Then after foundational work¹⁰¹ by Halpern and coworkers in 1952 - 62, rapid expansion of the field began to take place, mainly in the area of platinum metal catalysts. The history of ruthenium(II) catalysts stems from when Halpern, Harrod and James¹⁰² reported in 1961 that aqueous solutions of chlororuthenate(II) were active catalysts for the hydrogenation of several olefinic compounds, including maleic, fumaric and acrylic acids. In 1965, the complexes, $\text{RuCl}_2(\text{PPh}_3)_3$, and $\text{RuHCl}(\text{PPh}_3)_3$, were reported, by Wilkinson's group,⁶⁶ as extremely effective catalysts for the hydrogenation of terminal olefins. These Ru complexes, as well as the related $\text{RhCl}(\text{PPh}_3)_3$ complex, are widely used now as catalysts in organic syntheses.³ Because of experimental difficulties, Wilkinson's group had not obtained detailed kinetics for the hydrogenations catalyzed by $\text{RuHCl}(\text{PPh}_3)_3$. James' group found that kinetic studies were possible in DMA¹⁰³, and a series of studies^{2,3,4,21,23,69-71,73,78} was initiated in this solvent on this and related complexes. Addition of PPh_3 was found to inhibit hydrogenation, yet there was no observable dissociation of phosphine from $\text{RuHCl}(\text{PPh}_3)_3$ in solution.^{26,72,73} To explain this and other kinetic data, James² proposed the following mechanism as one of the pathways for certain olefinic substrates:





However, Eisenberg *et al.*^{6,7} have recently demonstrated a "pair-wise" addition of hydrogen to olefins, catalyzed by $\text{RuHCl}(\text{PPh}_3)_3$, $\text{Ru}(\text{H}_2)\text{H}_2(\text{PPh}_3)_3$ and $\text{Ru}(\text{N}_2)\text{H}_2(\text{PPh}_3)_3$ (as well as some Rh and Pd catalysts); this discovery of pair-wise addition perhaps contradicts the mechanism suggested above, involving alkyl formation, followed by oxidative-addition of H_2 and subsequent hydride migration to give the alkane with regeneration of the monohydride catalyst. The findings of Eisenberg's data imply catalysis via a dihydride intermediate, with hydrogen transfers being fast compared to relaxation of the hydrogen nuclear spins in *para* hydrogen. Thus, a reinterpretation of some unpublished data obtained by Hui¹⁰³ and Markham⁷² on hydrogenation catalyzed by $\text{RuHCl}(\text{PPh}_3)_3$ should be carried out at some time.

Because of its suggested involvement in reactions 4.1 - 4.3, a bis phosphine species was later isolated by James *et al.*⁶⁹ The species is now known, from the present work, to be $(\eta^2\text{-H}_2)(\text{PPh}_3)_2\text{Ru}(\mu\text{-Cl})_2(\mu\text{-H})\text{RuH}(\text{PPh}_3)_2$, **1a**, (sect. 3.3) and not, as previously thought,⁶⁹ $[\text{RuHCl}(\text{PPh}_3)_2]_2$. Related to the $\text{RuHCl}(\text{PPh}_3)_3$ hydrogenation system, it is noteworthy that the "bis phosphine species", **1a**, appears to be accessible in solutions of $\text{RuHCl}(\text{PPh}_3)_3$. Several workers^{56,104,105} have observed broadening of the ^1H NMR hydride signal of $\text{RuHCl}(\text{PPh}_3)_3$ under a hydrogen atmosphere, and have attributed the broadening to various exchange processes. Dekleva *et al.*^{21,56} also found that, when solutions of $\text{RuHCl}(\text{P}(\text{p-tol})_3)_3$ were warmed under 1 atm hydrogen in toluene- d_8 , the high-field hydride quartet at δ -16.8 broadened and a new weak broad signal at δ -12.8 appeared in the ^1H NMR spectrum; this latter signal corresponds to the averaged, ambient temperature, high-field signal of the $(\eta^2\text{-H}_2)(\text{P}(\text{p-tol})_3)_2\text{Ru}(\mu\text{-Cl})_2(\mu\text{-H})\text{RuH}(\text{P}(\text{p-tol})_3)_2$ species, **1b**. As the "bis phosphine species" was a possible catalytic intermediate,^{70,71,78} James and Wang carried out kinetic studies on the hydrogenation of

acrylamide catalyzed by "[RuHCl(PPh₃)₂]₂" in DMA,⁷⁸ and Thorburn⁷¹ followed this up with a similar study but using 1-hexene as substrate instead of acrylamide.

The present work includes a reconsideration of Thorburn's data⁷¹ on the 1-hexene hydrogenation system using the catalyst **1a**, as it is now reformulated. Also in the present work, catalytic systems based on two analogues of RuCl₂(PPh₃)₃ are considered: (a) the 1-hexene hydrogenation system employing RuCl₂(PPh₃)(PPFA), **3a**, initially investigated by Rodgers *et al.*;²⁵ (b) the 1-hexene hydrogenation system using RuCl₂(PPh₃)(isoPPFA), **3b**, as a catalyst.

Hydrogenation of 1-hexene catalyzed by 1a

The re-interpretation of Thorburn's kinetic data⁷¹ is worthwhile because his analysis was based on a mistaken formulation of the ruthenium complex and on the assumption that the dimer catalyst dissociates in solution to monomers (see sect. 3.4).

The kinetic data presented below are Thorburn's,⁷¹ and the account given rests heavily on Thorburn's description of the work. Data on solution behaviour of **1a** and its reactivity toward hexene come mainly from the present work. Representative uptake plots are given in Figure 4.1, and maximum rates were readily measured. Complete reduction of 1-hexene occurred and the final solution contained the initial Ru complex, now known to be **1a**; isomerization of 1- to 2-hexene was negligible.

The kinetic dependences, together with some reciprocal analysis plots are shown in the appropriate Figures: Ru (Fig. 4.2), 1-hexene (Figs. 4.3, 4.4), H₂ (Fig. 4.5, 4.6), PPh₃ (Figs. 4.7, 4.8) and LiCl (Fig. 4.9).

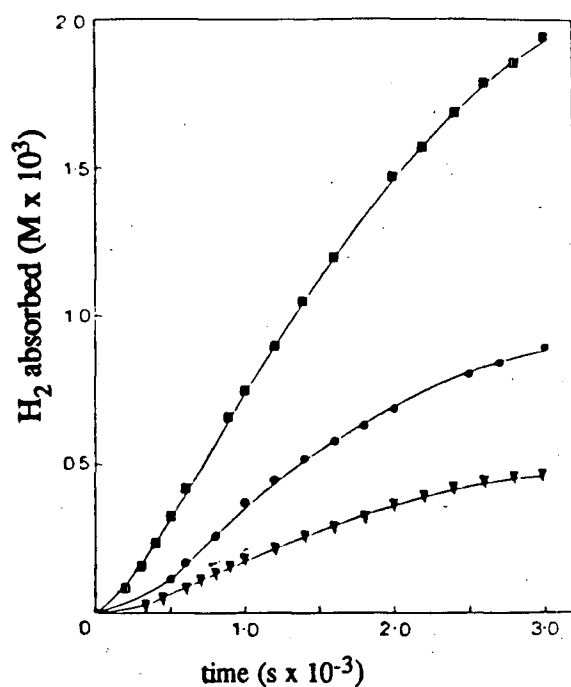


Figure 4.1 Uptake plots for the hydrogenation of 1-hexene in DMA at 30 °C catalyzed by 1a.⁷¹

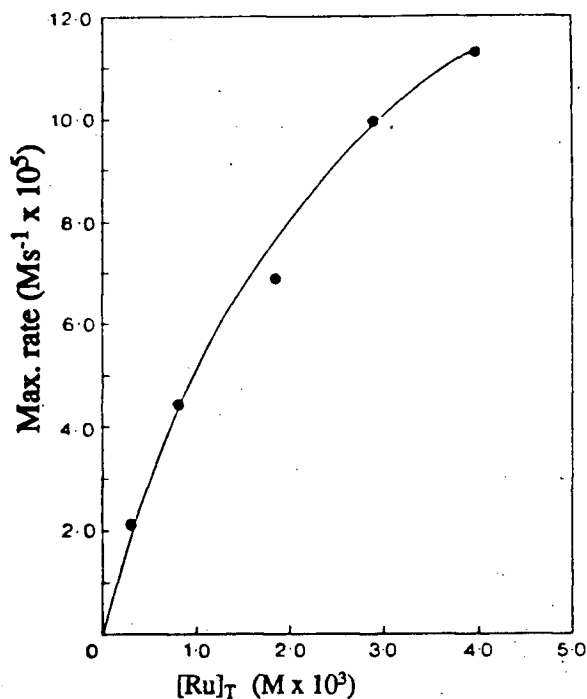


Figure 4.2 Dependence of maximum rate of hydrogenation on total Ru concentration (1a) in DMA at 30 °C with $P_{H_2} = 1$ atm, $[hexene] = 0.2$ M.⁷¹

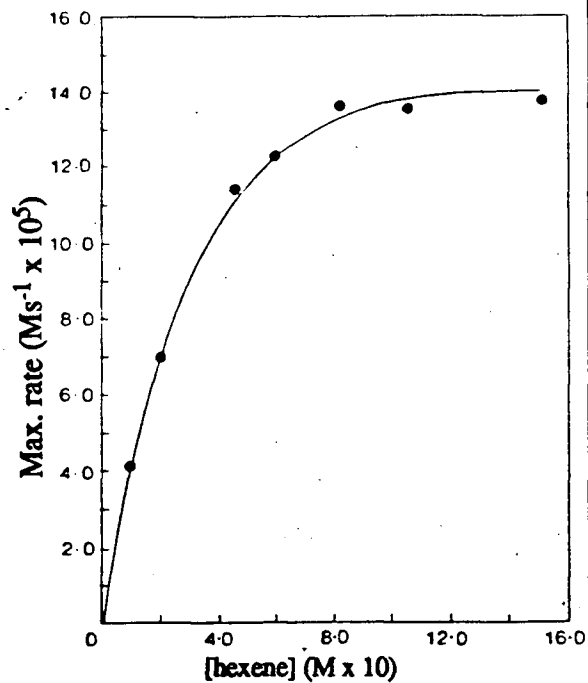


Figure 4.3 Dependence of maximum rate of hydrogenation on 1-hexene concentration in DMA at 30 °C with $P_{H_2} = 1$ atm, $[Ru]_T$, as 1a, = 2×10^{-3} M.⁷¹

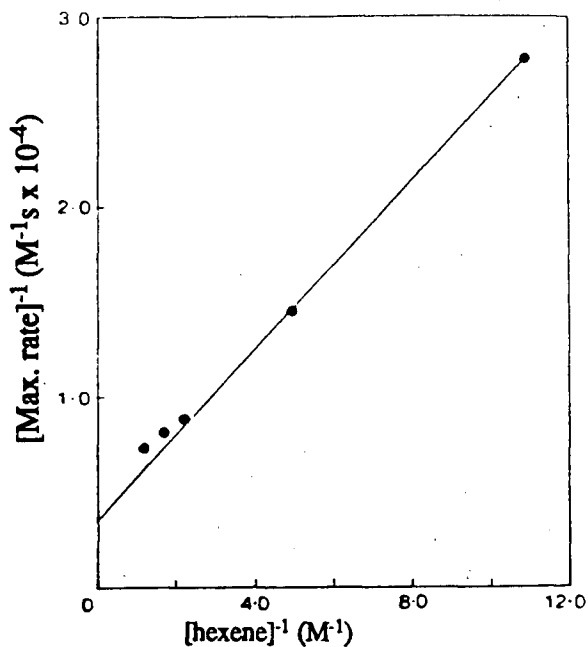


Figure 4.4 Dependence of maximum rate of hydrogenation on 1-hexene concentration as plotted according to equation 4.18 (sect. 4.4).⁷¹

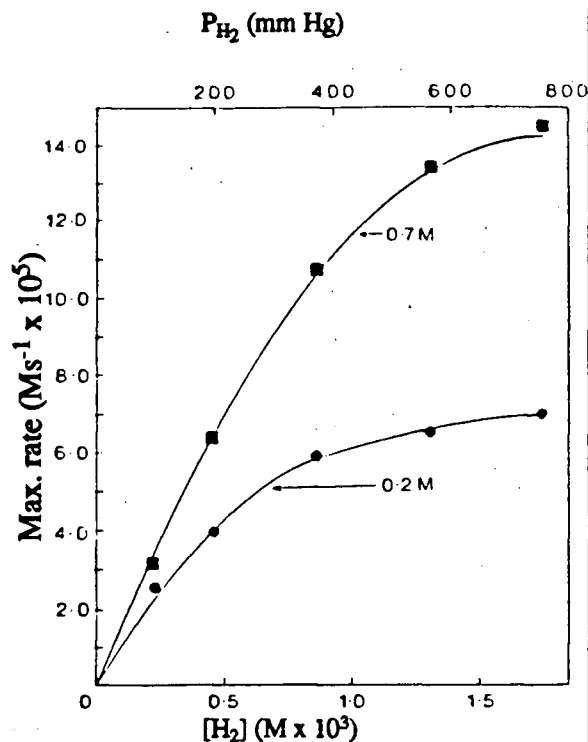


Figure 4.5 Dependence of maximum rate of hydrogenation on hydrogen concentration in DMA at 30 °C with [hexene] = 0.2 M, 0.7 M and $[Ru]_T$, as 1a, = 2×10^{-3} M.⁷¹

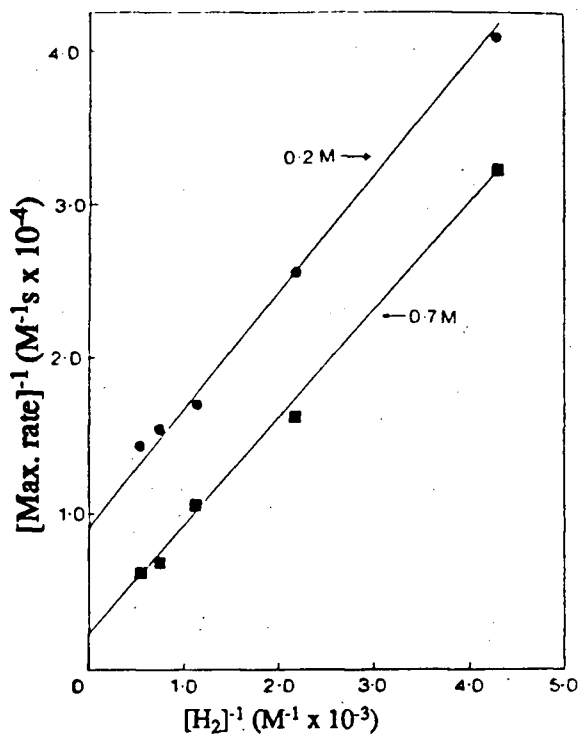


Figure 4.6 Dependence of maximum rate on hydrogen concentration as plotted according to equation 4.19 (sect. 4.4).⁷¹

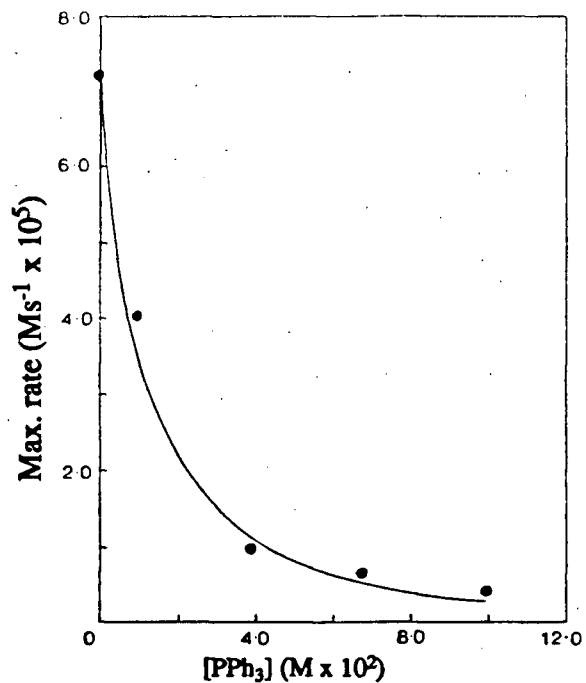


Figure 4.7 Dependence of maximum rate of hydrogenation on added triphenylphosphine concentration in DMA at 30 °C with [hexene] = 0.2 M, 0.7 M and $[Ru]_T$, as 1a, = 2×10^{-3} M.⁷¹

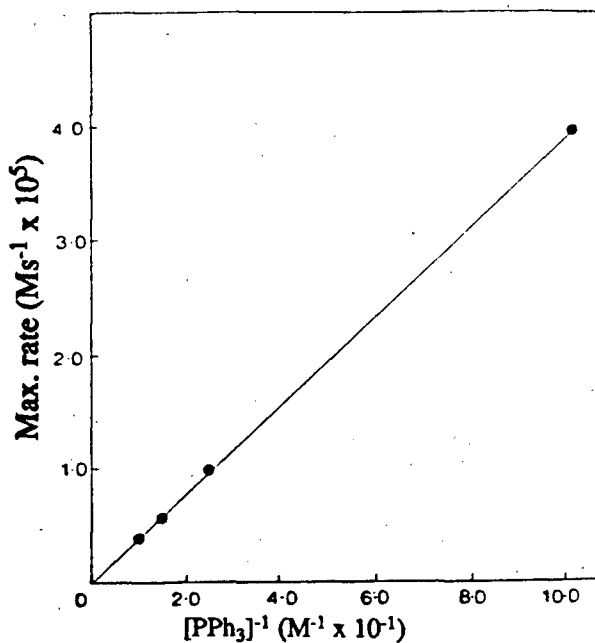


Figure 4.8 Dependence of the maximum rate on $[PPh_3]^{-1}$.⁷¹

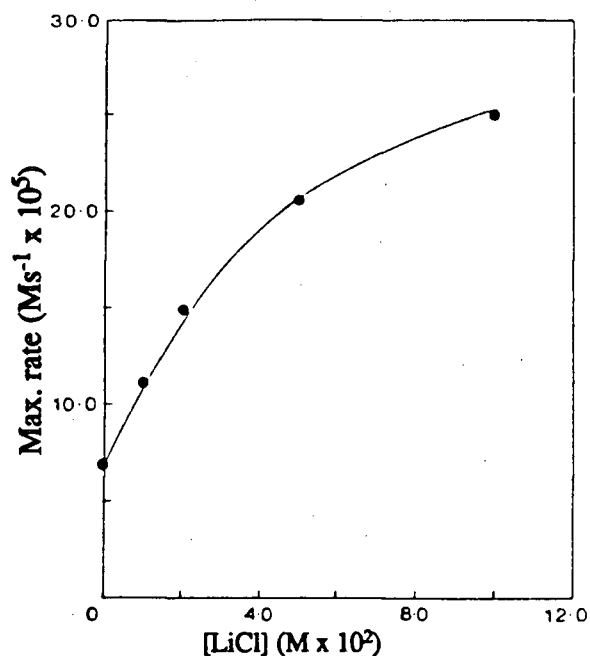


Figure 4.9 Dependence of maximum rate of hydrogenation on added lithium chloride concentration, in DMA at 30 °C with [hexene] = 0.2 M and $[Ru]_T$, as **1a**, = 2×10^{-3} M.⁷¹

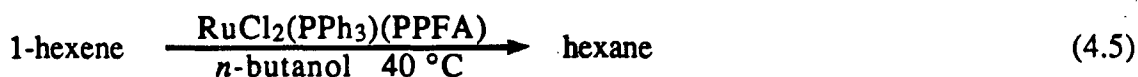
Hydrogenation systems catalyzed by 3a and 3b

A few comments on the choice of ligands in these studies are in order. As mentioned in Chapter 1, PPFA and isoPPFA (Fig. 1.1) are ferrocene based ligands, possessing both phosphine and amine functionalities. The ligands are thus chelating, mixed soft/hard PN donor systems, with both planar and central elements of chirality. For practical reasons, catalysts which are selective for substrate type, e.g. olefin versus ketone, are more desirable in organic synthesis than indiscriminate (non-selective) catalysts. Thus, the original interest²⁵ was to compare the known terminal olefin selectivity of, for example, $RuCl_2(PPh_3)_3$ with the selectivity of complex **3** systems. It had been noted that rhodium complexes, such as $Rh(bipy)_2^+$ can selectively catalyze hydrogenation of a ketone in a ketone/olefin mixture,¹⁰⁶ while similar systems using diphosphines selectively catalyzed the reduction of olefins.¹⁰⁷ Another reason for the choice of a PN ligand was the

possibility that the coordinated nitrogen donor might accept a proton and assist in the heterolytic activation of dihydrogen.²⁵ There was also a possibility that mechanistic studies on the **3a** and **3b** systems might shed light on the analogous $\text{RuCl}_2(\text{PPh}_3)_3$ systems, which are still not fully understood. Finally, because of the chirality of PPFA and isoPPFA, the systems offered the prospect of catalytic asymmetric hydrogenation.

Hydrogenation systems catalyzed by **3a**:

Previously, Rodgers *et al.*²⁵ reported a study of the catalytic hydrogenation system:



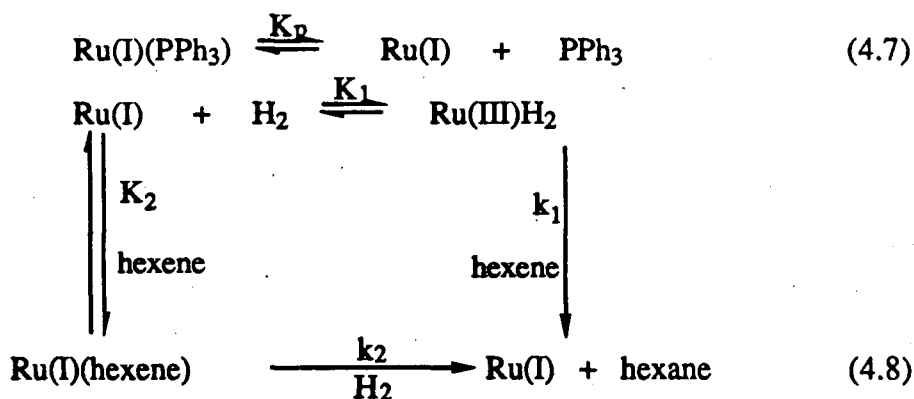
In an attempt to identify possible intermediates involved, reactions of **3a** with H_2 were carried out in the absence of substrate. Rodgers *et al.* reported that *n*-butanol solutions of **3a** absorbed slightly more than 0.5 mole H_2 per mole Ru at 40°C at several pressures, the solution colour changing from green to red; these reactions at constant hydrogen pressure followed pseudo first-order behaviour, and visible spectral changes (loss of intensity of a band at 628 nm and increasing absorption at 350 - 450 nm, replacing an initial 457 band) were said to reveal "isosbestic points". Hydrides were not detected in the butanol solutions, or in the solution with benzene as solvent, where reaction with H_2 was slow and incomplete. Attempts to isolate solids from the butanol solutions by solvent evaporation, even under H_2 , led to slow regeneration of the green colour of **3a**. No $^{31}\text{P}\{^1\text{H}\}$ NMR signals could be detected from the hydrogenated butanol solutions.

The system described by equation 4.5 effected efficient catalytic hydrogenation under mild conditions, with an activity comparable to that of $\text{RuHCl}(\text{PPh}_3)_3$, one of the most active catalysts known for the hydrogenation of terminal olefins. The hydrogenation rate was negligible for the internal alkene, 2-hexene, and for the substituted olefins, styrene and α -*N*-acetamidoacrylic acid. Rodgers *et al.* found no evidence for isomerization of 1-hexene during the hydrogenation.

The kinetics of the hexene system described in equation 4.5 were followed using a gas uptake apparatus as described in reference 7. The S-shaped H₂-uptake plots showed an initial autocatalytic type region before reaching a maximum rate at 200-800 s. The 'induction period' did not appear to be affected by 1-hexene concentration. The dependence on ruthenium in the absence of added PPh₃ (Fig. 4.10), as measured by maximum uptake rates, was first order at low concentrations, but became less than one at higher [Ru]. The dependence on 1-hexene (Fig. 4.11) and on H₂ pressure (Fig. 4.12) was first order, and the data also showed a direct inverse dependence on added PPh₃ (Fig. 4.13). Because a hydride was not detected in the reaction of 3a with hydrogen in the absence of substrate, a mechanism for the hexene hydrogenation was proposed that involved initial quantitative formation of a Ru(I) species by hydrogen reduction:



The lack of ³¹P{¹H} NMR signals from hydrogenated ruthenium solutions was taken as support for proposing a paramagnetic Ru^I species. A pre-equilibrium loss of phosphine was invoked to account for the inverse dependence on phosphine and the apparent approach to half-order dependence on ruthenium, as well as a direct first-order dependence on Ru in the presence of added PPh₃ (Fig. 4.10). The mechanism proposed to account for all these observations was:



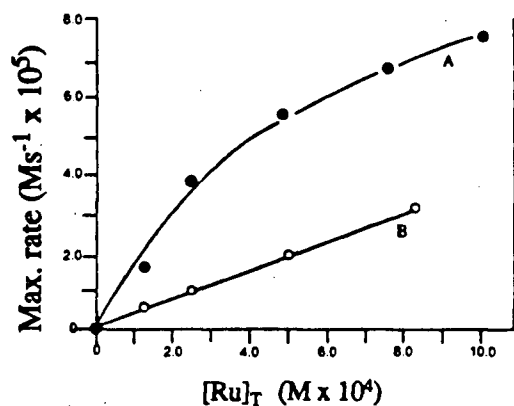


Figure 4.10 A: Dependence of maximum rate on total Ru concentration (3a) in *n*-butanol at 40 °C; 0.04 M 1-hexene and 1 atm total pressure. B: As for A, but in the presence of 11.9×10^{-4} M added PPh_3 .²⁵

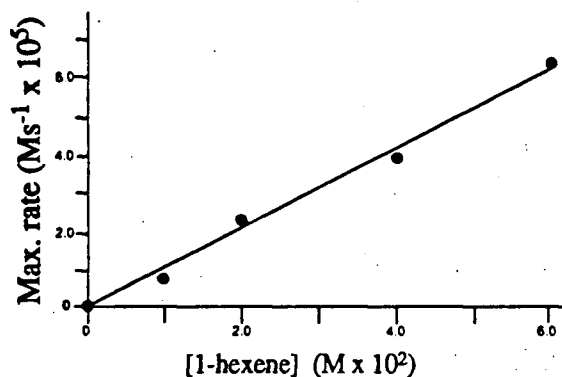


Figure 4.11 Dependence of maximum hydrogenation rate on 1-hexene concentration in *n*-butanol at 40 °C, 1 atm total pressure, and $[\text{Ru}]_T$, as 3a, = 2.47×10^{-4} M.²⁵

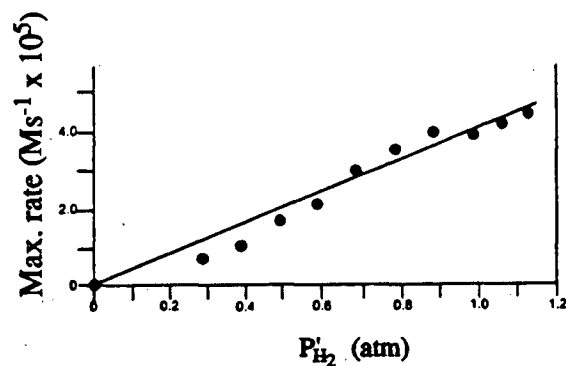


Figure 4.12 Dependence of maximum hydrogenation rate on partial pressure of H_2 in *n*-butanol at 40 °C, 0.04 M 1-hexene and $[\text{Ru}]_T$, as 3a, = 2.47×10^{-4} M. Pressure reading corrected for vapour pressure of *n*-butanol.²⁵

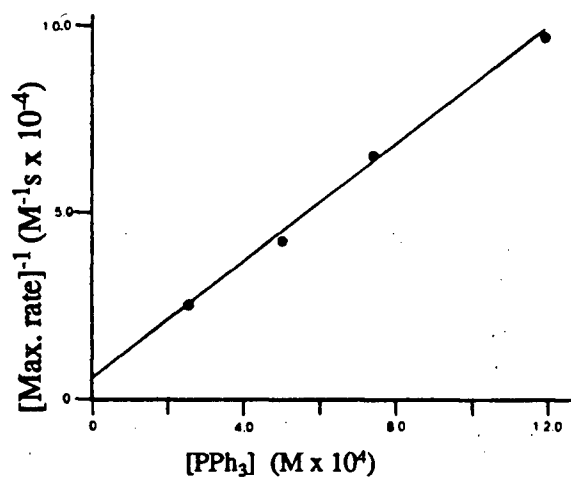


Figure 4.13 Inverse dependence of maximum hydrogenation rate on added phosphine concentration in *n*-butanol at 40 °C, 0.04 M hexene, 1 atm total pressure and $[\text{Ru}]_T$, as 3a, = 2.47×10^{-4} M.

with a rate-law of the form:

$$\frac{-d[\text{H}_2]}{dt} = \frac{(k_1K_1 + k_2K_2)K_p[\text{Ru}_T][\text{H}_2][\text{hexene}]}{K_p + [\text{PPh}_3]} \quad (4.9)$$

Thorburn⁶⁵ followed up this work with gas uptake experiments in other solvents, and he found the stoichiometry in DMA at 10 °C to be 0.56 mole H₂ per mole Ru, this decreasing with increasing temperature: 0.39 at 30°C, 0.19 at 50 °C. The uptake in DMA at 30 °C in the presence of Proton Sponge[®] was 0.57 mol H₂/Ru. Attempted visible spectrophotometric experiments to monitor the kinetics of the reaction in 1:1 toluene/methanol gave no clear indication of reaction order, and no clean isosbestic, but did give spectral changes similar to those reported by Rodgers *et al.* Also, after storage of the hydrogenated solution for one day under Ar, the spectrum exhibited changes representing possible partial reversion to the starting spectrum.

Butler⁶⁴ was later able to isolate a red solid from the H₂ reaction with 3a in toluene/methanol, and found a "paramagnetic hydride" with a very broad ¹H NMR signal at δ -17, that shifted "from sample to sample". Butler also found that there was no reaction between 3a and H₂ in toluene, and Thorburn⁶⁵ correspondingly reported zero uptake at 1 atm over 2 h in toluene, even in the presence of Proton Sponge[®].

Thus, at the time this present work was initiated, it appeared that a hydride was formed, at least in toluene/methanol; and there were suggestions of reversibility in the reactions in DMA and in butanol. It was certainly puzzling that there should be no reaction in toluene, and yet a slow reaction in benzene. It was clear, however, that the presence of a polar solvent such as DMA or an alcohol had a pronounced effect on the reactivity toward H₂.

Experiments were therefore undertaken in attempts to isolate and/or identify hydride(s), formed by the reaction of **3a** with dihydrogen, which might be active intermediates in the catalytic hydrogenation of 1-hexene.

Hydrogenation systems catalyzed by $\text{RuCl}_2(\text{PPh}_3)(\text{isoPFA})$, **3b**:

Ian Butler, from this department, first prepared **3b**, and obtained crystals for subsequent X-ray analysis.¹⁰⁸ The solid state structure of this molecule is analogous to that of $\text{RuCl}_2(\text{PPh}_3)_3$,^{26,109} and is best described as square pyramidal, with approximately *trans* chlorides, and the PPh_3 ligand being approximately *trans* to the NMe_2 moiety of the isoPFA ligand.

To complement work on the **3a**-catalyzed 1-hexene hydrogenation system of Rodgers *et al.*,²⁵ the study of 1-hexene hydrogenation catalyzed by **3b** was considered worthwhile, and out of mechanistic studies the need arose to search for hydrides or other intermediates which might be involved in the catalytic cycle. Unlike for the **3a** system, little work had been done at the outset of this present work on the reactions of **3b** with H_2 . Butler had studied⁶⁴ the reaction of a CH_2Cl_2 solution of this complex with H_2 , but as no hydride was detected, the use of a more polar solvent was tried in the present work, because such solvents are known to promote monohydride formation via heterolytic cleavage of H_2 .²⁻⁴

4.2 Experimental

*Reactions of $\text{RuCl}_2(\text{PPh}_3)(\text{PPFA})$, **3a**, with H_2 in toluene- d_8 , toluene- d_8 /butanol and butanol*

Some of complex **3a**, typically 0.10 g (0.11 mmol), was placed in a 5 mm NMR tube and undried toluene- d_8 was freeze/thaw-degassed and vacuum-transferred into the NMR tube. Hydrogen was then admitted at below 1 atm into the NMR tube which was sealed while partially immersed in liquid nitrogen; the hydrogen pressure on warming to

ambient temperature was estimated to be 2 - 3 atm . The ^1H NMR and $^{31}\text{P}\{^1\text{H}\}$ NMR spectra were recorded after leaving the solution for 12 h at ambient temperature in the dark.

In exactly corresponding experiments, some 2 - 3 drops of *n*-butanol were also added in an attempt to promote the reaction which occurred in neat butanol (described in the next paragraph); the small quantity of butanol was used to avoid swamping any possible ^1H NMR hydride signal(s). The amount of hydrogen available in these NMR tube experiments would be about 0.2 mmol (2 mL H_2 at 2 - 3 atm and 20 °C).

For the reaction in neat butanol at ambient temperature, the procedures described in section 2.1 were used. The complex 3a (0.5 g, 0.6 mmol) was reacted with 2 - 8 atm H_2 overnight in dry *n*-butanol (3 mL); complex 3a was largely undissolved initially, but the suspension gradually changed to give a brown solution and yellow precipitate, A. When the mixture was stirred, the final product had a very small particle size and was difficult to filter; this product with small particle size is hereinafter referred to as the yellow precipitate of A. Golden yellow crystals formed in the mixture if it was not stirred; this more crystalline product will be referred to as the yellow crystals of A. The yellow precipitate/crystals of A were washed with butanol, and then very small quantities of toluene (e.g., 3 x 0.2 mL). It should be noted that the volume of a vessel used for this reaction would hold 10 to 30 mmol H_2 at the pressures used.

The volume of gas evolved on dissolving the yellow precipitate of A was measured using a gas uptake/evolution apparatus under a 16.6 cm Hg nitrogen atmosphere, and with the solution at 28 °C. Also, elemental analyses, conductivity measurements, and further experiments to study gas evolution on dissolving in toluene- d_8 were performed on the yellow crystals of A. Conductivity measurements were performed on a 1:1 methanol/dichloromethane solution ($\sim 4 \times 10^{-4}$ M). The identity of the gas evolved was determined by GC, by sampling with a syringe the gas present in a small headspace (~ 0.5 mL) above a dry toluene solution of the yellow crystals of A under nitrogen at ambient pressure and temperature.

Reactions of RuCl₂(PPh₃)(isoPFA), 3b, with hydrogen in DMA, DMA/C₆D₆, and benzene/methanol

The reaction of **3b** with ~10 atm H₂ in DMA to give (η²-H₂)(PPh₃)₂Ru(μ-Cl)₂(μ-H)RuH(PPh₃)₂, **1a**, is described in section 2.4 using the apparatus shown in Figure 2.2. In standard Schlenk apparatus, complex **3b** (0.2 g, 0.25 mmol) and PPh₃ (1.3 g, 5 mmol) were stirred in 5 mL DMA under 1 atm H₂ for 2 days at ambient temperature. The resulting violet precipitate was washed three times with hexanes, dried, and identified by ¹H NMR spectroscopy.

The complex **3b** (0.032 g, 0.040 mmol) was stirred under H₂ (7 atm) in a 1:1 solvent mixture of DMA/C₆D₆ (2 mL) at ambient temperature for 6 h, and the solution then transferred under H₂ to an NMR tube which was subsequently sealed. No precipitate was observed. The ³¹P{¹H} NMR spectrum at 20 °C was recorded within a further 2 h.

The complex **3b** (0.24 g, 0.3 mmol) was placed in a glass tube with benzene (3 mL) and methanol (0.2 mL) under H₂ (0.9 atm), and the tube sealed while partially immersed in liquid nitrogen. When the tube was warmed to room temperature, the H₂ pressure would have been 2 - 3 atm. Although not very soluble initially, the green solid, **3b**, had reacted after ~3 days at ambient temperature to give a reddish-brown solution and a few reddish particles. When the "solution" was heated to 40-45 °C, the solution turned brown and ~0.1 g of green solid precipitated from the solution. The system was cooled to ambient temperature, and the green solid reacted slowly, over a period of 2 days, to give an orange solid that was isolated by decanting and removing the solvent under vacuum; the orange solid was analyzed by ¹H NMR spectroscopy. In a similar experiment, the supernatant solution was separated from the orange precipitate by decanting, and the solvent removed from the supernatant under vacuum. A CDCl₃ solution of the residue was analyzed by ¹H NMR spectroscopy.

Crystals for X-ray analysis were obtained from this methanol/benzene system.

Experiments were carried out, using the apparatus and procedure described in Figure 2.2

and section 2.1. In one case, **3b** (0.060 g, 0.074 mmol) was placed in the tube described, into which benzene (7.5 mL) and methanol (0.5 mL) were vacuum transferred. The tube was charged with 2 atm H₂ and the Teflon valve closed. The contents of the tube were then mixed and left for ~3 weeks at ambient temperature. During this time, the green **3b** complex gradually disappeared, yielding a brown solution and an orange precipitate. The mixture was filtered under hydrogen, as described in section 2.1, and the solid then transferred with the aid of a small stir bar, guided by an external magnet, back into section A of the tube. Benzene (9 mL) and dichloromethane (5 mL) were then vacuum-transferred into section C of the tube, keeping part B (containing the filtrate) immersed in liquid nitrogen. It was hoped that by exposing the components to vacuum only when the solvent was frozen, decomposition might be avoided. The orange precipitate was dissolved in the benzene/dichloromethane mixture, and hexane (20 mL) then vacuum-transferred into the tube with parts A, B and C immersed in liquid nitrogen. (While most of the hexane, dichloromethane and benzene was transferred to sections A or C, less than 10% may have been transferred through the frit to section B.) When the hexane and benzene/dichloromethane solutions were mixed in section A, no precipitate appeared, and some solvent (~2 mL) was then removed from the solution by pumping under vacuum, during which time section B was immersed in liquid nitrogen. The tube was then recharged with hydrogen (~1 atm), and the Teflon valve closed; crystals slowly formed on the walls of section A. When the crystals appeared to have ceased growing, the solution in section A was transferred, under hydrogen, to another tube through the opened Teflon valve by inverting the tube while the solution in section B was kept frozen. The pressure in the tube, containing the crystals and the frozen solution (section B), was then reduced to much less than 1 atm, the Teflon valve closed, and the section A arm sealed off using a torch. The crystals could thus be removed without having air contaminate the atmosphere present in section B. The crystalline compound was identified by ¹H and ³¹P{¹H} NMR,

and by X-ray crystallography, as the benzene solvate of $(\eta^2\text{-H}_2)(\text{isoPFA})\text{Ru}(\mu\text{-Cl})_2(\mu\text{-H})\text{RuH}(\text{PPh}_3)_2$, **4**, (see sects. 2.4 and 3.3).

Other crystals (some white, some black-red, the latter being diamond shaped) gradually grew in the benzene/methanol/ dichloromethane/hexane solution, under hydrogen in section B. These crystals were filtered off, at the frit above section B, by inverting the tube and applying a pressure differential across the frit, and then washed with hexane. The white crystals, which proved to be dimethylammonium chloride, and the unidentified black-red crystals of **Y** were analyzed by spectroscopy, and the spectra are reported in section 4.3.

*Catalytic hydrogenations of prochiral substrates using $\text{RuCl}_2(\text{PPh}_3)(\text{PPFA})$, **3a**, and $\text{RuCl}_2(\text{PPh}_3)(\text{isoPFA})$, **3b***

Catalytic hydrogenations of prochiral substrates were carried out using the optically active complexes (*S,R*)-**3**, at ambient temperature and 1000 psi H_2 , in 30 - 50 mL steel bombs equipped with pressure gauges and glass liners. Work-up of the hydrogenation products from prochiral olefins was done according to the procedure described in reference 20, and yields were determined by ^1H NMR spectroscopy. Gas chromatography of distillates of hydrogenated solutions was used to determine yields for hydrogenation of prochiral ketones.

*NMR studies of the catalytic hydrogenation of 1-hexene by **3a**, **3b** and $(\eta^2\text{-H}_2)(\text{PPh}_3)_2\text{Ru}(\mu\text{-Cl})_2(\mu\text{-H})\text{RuH}(\text{PPh}_3)_2$, **1a***

The following general procedure was used to obtain NMR spectra of catalytically hydrogenating solutions: hydrogen gas uptake was monitored as indicated in section 2.2 in a hydrogenation flask fitted with a F-145 septum plug (from Alltech Associates) for withdrawing samples. When the rate of hydrogen uptake appeared to be reaching a maximum, a ~0.8 mL sample was withdrawn using a syringe and injected into a 5 mm

NMR tube filled with 1 atm H₂ and capped with a rubber septum. The NMR tube was then placed into a Schlenk tube containing hydrogen, and the capped Schlenk tube placed into a dry ice/acetone bath; freezing of the solution in the NMR tube occurred slowly. Within 20 min of sampling, the solution in the NMR tube was carefully thawed and placed into the probe of the NMR spectrometer, and then the probe was cooled as quickly as possible to ~5 °C. The NMR spectra were then recorded, the acquisition being complete within ~2 h of starting the catalytic hydrogenation. The following systems, all under 1 atm H₂, were studied in this way:

a) The **1a** system with experiments at 0.04 M and 1.0 M 1-hexene in 4 mL 50:50

DMA/C₆D₆ with **1a** (0.02 g, 0.004 M), and another experiment at 1.0 M 1-hexene in 4 mL 1:7 DMA/toluene-d₈ at the same ruthenium concentration.

b) The **3a** system: 0.1 M 1-hexene in 0.5 mL *n*-butanol/3.5 mL C₆D₆ with **3a** (0.050 g, 0.014 M).

c) The **3b** system: 0.05 M 1-hexene in 4 mL of 50/50 DMA/C₆D₆ with **3b** (0.015 g, 0.005 M).

Hydrogen-uptake measurements for 1-hexene hydrogenation

All rates of hydrogenation of 1-hexene, using **3a**, the species **A** described below, **3b** and **1a** as catalysts were measured by means of hydrogen gas uptake experiments (sect. 2.2).

4.3 Results

*Reactions of RuCl₂(PPh₃)(PPFA), **3a**, with hydrogen in toluene-d₈, toluene-d₈/butanol and butanol*

The ^1H NMR spectrum of the toluene- d_8 reaction mixture formed after 12 h from mixing showed no upfield, hydride signals. The $^{31}\text{P}\{^1\text{H}\}$ NMR spectrum (Fig. 4.14) shows that no starting complex remained, and the main features were a pair of doublets at δ 42.7 and 45.7 with $^2J_{\text{PP}} = 40$ Hz, and a less intense singlet at δ 28.9.

No reaction occurred at ambient temperature in toluene- d_8 /butanol in the absence of H_2 , but after 6 h in this solvent in the presence of H_2 , several species were observed in the $^{31}\text{P}\{^1\text{H}\}$ NMR spectrum (Fig. 4.15). The starting complex **3a** was present (δ 77.4 d, 44.2 d, $^2J_{\text{PP}} = 38$ Hz), and there was also a species, **A**, (δ 71.1 d, 65.3 d, $^2J_{\text{PP}} = 40$ Hz), associated, via data from other experiments (see below), with a ^1H NMR triplet at δ -20.3 ($^2J_{\text{PH}} = 32$ Hz); there is also evidence for the presence of **1a** in the $^{31}\text{P}\{^1\text{H}\}$ NMR spectrum (δ 71 br s, under the "doublet" at 71.1, and δ 46 br s). Supporting evidence for this assignment comes from the observation of a broad ^1H NMR signal at δ -13.2 (Fig. 4.16; cf. δ -12.9 for **1a** in toluene- d_8 , sect. 3.3). The T_1 measurements, given below, at 6 °C and \sim 20 °C, indicating a dihydrogen complex, are also consistent with this assignment. In addition, low temperature $^{31}\text{P}\{^1\text{H}\}$ NMR data show that **1a** is formed in the reaction of **3a** with H_2 in butanol. Another major feature in the $^{31}\text{P}\{^1\text{H}\}$ NMR spectrum (Fig. 4.15) is an AB quartet with δ 69.8 d, 69.0 d, $^2J_{\text{PP}} = 40$ Hz (due to an unknown species, **B**) and a singlet at δ 63.8 of comparable intensity; there is also a strong, broad singlet due to Ph_3PO at 28.5, very similar to that appearing in the $^{31}\text{P}\{^1\text{H}\}$ spectrum for the reaction in pure toluene- d_8 , where no hydrides were detected. Also, after 6 h, four upfield resonances appeared in the ^1H NMR spectrum (Fig. 4.16): two resonances, at δ -13.2 (br s, 'ii'), due to **1a** and at δ -20.3 (t, 'iv'), due to **A**, are mentioned above, and the other two have the following characteristics: δ 11.5 br s, with $T_1 = 50$ ms at 300 MHz, and δ -18.5 t, with $^2J_{\text{PH}} = 30$ Hz. The $^{31}\text{P}\{^1\text{H}\}$ NMR AB quartet, 'c', at δ 69.8, 69.0 for the unknown species, **B**, is thought to be associated with this ^1H NMR triplet, 'iii', at δ -18.5 because:

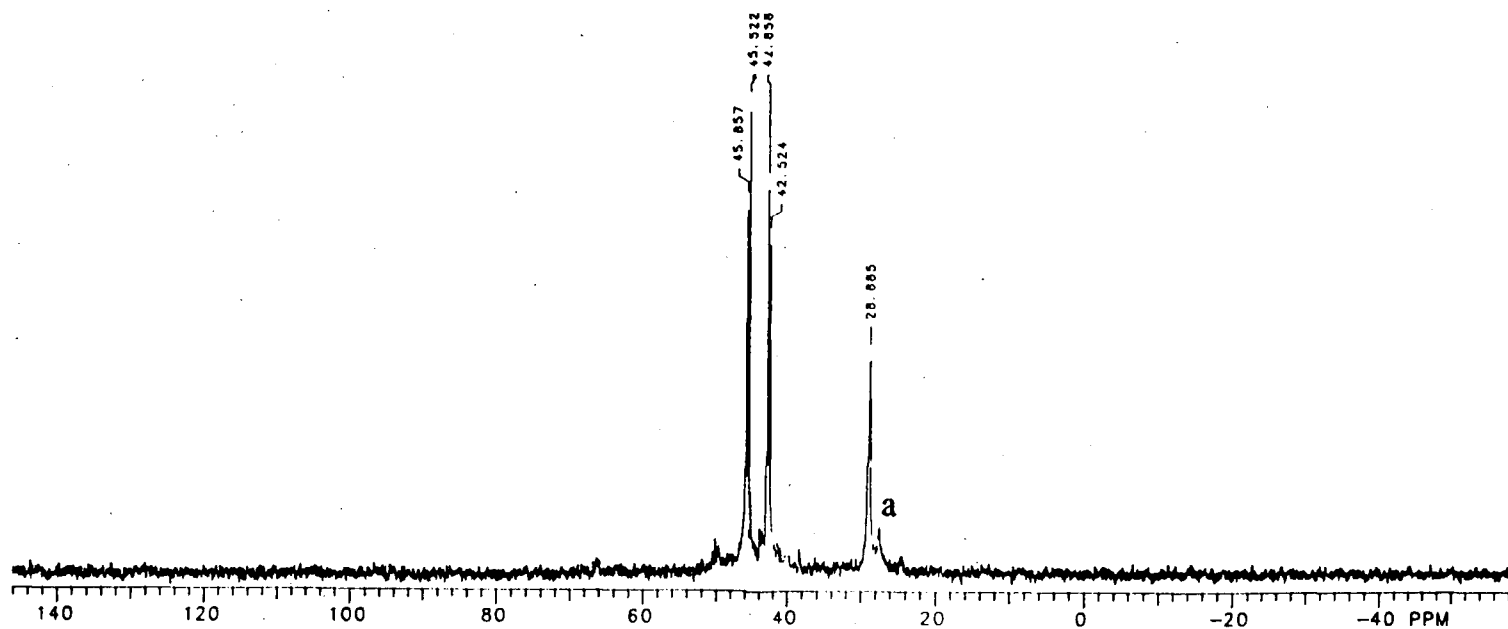


Figure 4.14 The $^{31}\text{P}\{^1\text{H}\}$ spectrum (121 MHz, toluene- d_8 , ambient temperature) of the *in situ* product(s) of the reaction of 3a with H_2 , after ~12 h from mixing; the peaks around 'a' are not identified, although one of these is probably due to Ph_3PO , present as an impurity in the sample of 3a used.

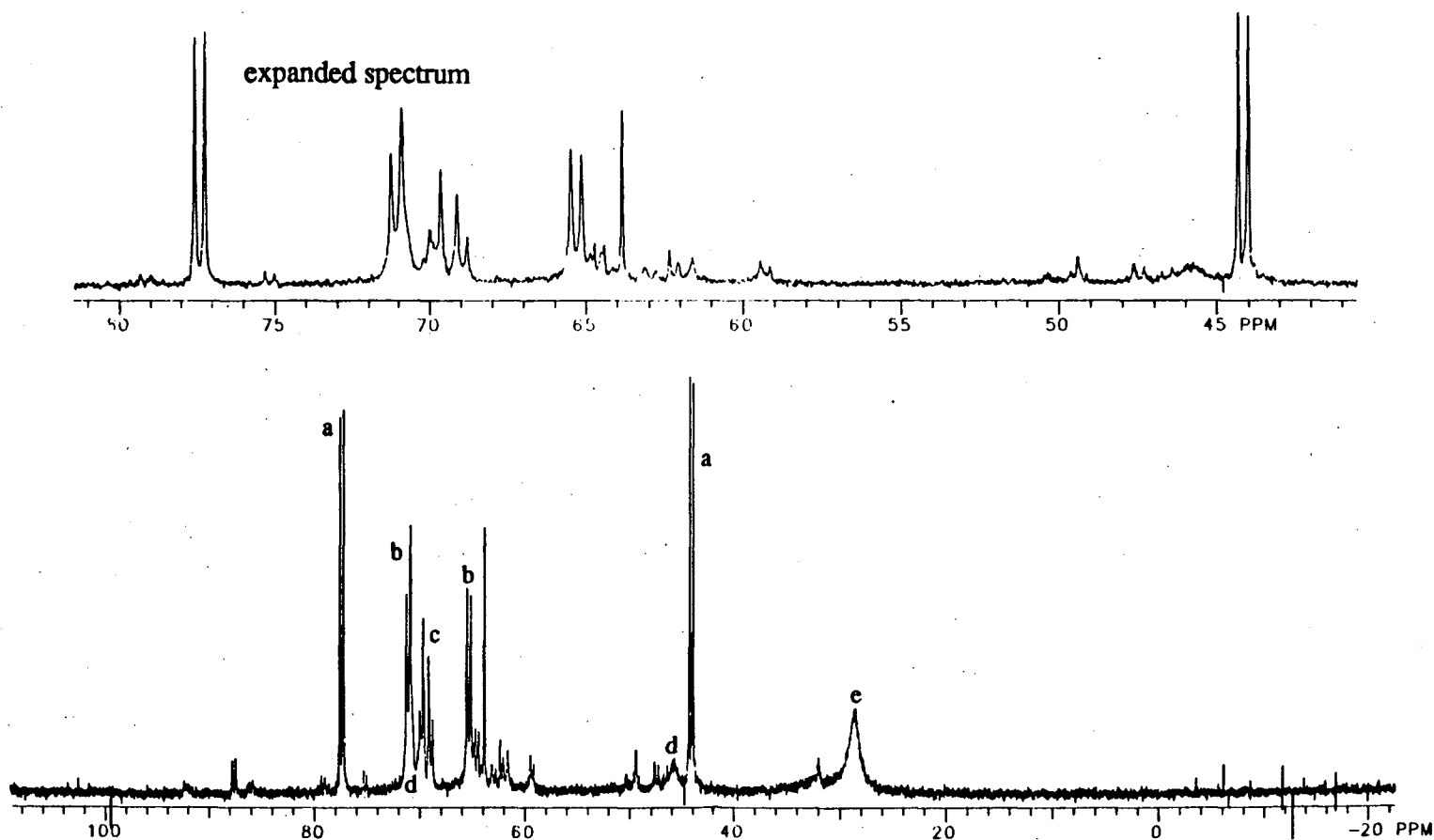


Figure 4.15 The $^{31}\text{P}\{^1\text{H}\}$ NMR spectrum (121 MHz, toluene- d_8 / n -butanol, ambient temperature) of the reaction mixture formed from the reaction of **3a** with H_2 , after ~6 h from mixing; peaks are identified as follows: 'a', due to **3a**; 'b', due to complex **A**; 'c' (AB quartet), due to complex **B**; 'd' (partially obscured by resonances due to **A**), complex **1a**; 'e', Ph_3PO ; unmarked peaks are unidentified.

(1) the ratio of the area under the $^{31}\text{P}\{^1\text{H}\}$ NMR resonances at δ 71.1 and 65.3, to the area under the AB quartet 'c', at δ 69.8, 69.0 is similar to the ratio for the integrations of the two ^1H NMR triplets, 'iii' and 'iv', at δ -20.3 and -18.5, respectively, and (2) the triplet 'iii', implying coupling to two equivalent phosphorus atoms, could result from coupling to the two, almost equivalent, phosphorus atoms giving rise to the AB quartet. It should be noted that in other experiments, the four ^1H NMR upfield resonances appeared to be independent of each other: numbering these resonances in order of increasing field

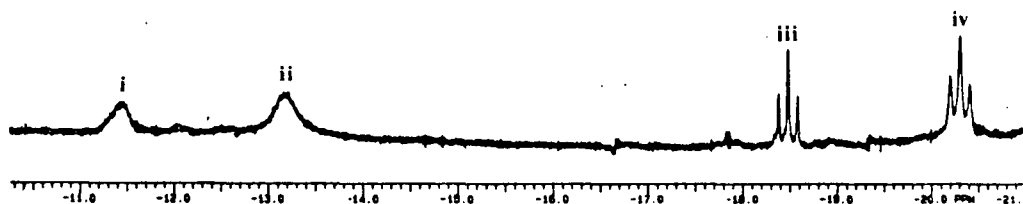


Figure 4.16 The upfield ^1H NMR spectrum (300 MHz, toluene- d_8 / n -butanol, ambient temperature) of *in situ* products from the reaction of 3a with H_2 , after 6 h from mixing; resonances 'i' - 'iv' are discussed in the text.

(Fig. 4.16), 'i', 'ii' (due to 1a) and 'iv' (due to A) appeared without 'iii'; 'ii' and 'iv' appeared without 'i' and 'iii'; and also, 'ii' appeared on its own. The T_1 values (Table 4.1) for 'i' - 'iv' indicate that 'i' and 'ii' are truly due to dihydrogen complexes, and 'iii' and 'iv' are due to classical hydride complexes. The ^1H and $^{31}\text{P}\{^1\text{H}\}$ NMR spectra, after two weeks, showed little change. Other minor species were also observed both after 6 h and after two weeks in the $^{31}\text{P}\{^1\text{H}\}$ NMR spectrum. On one occasion, in a similar experiment, other additional minor hydride resonances, observed at about 4 h, had disappeared after about a further 1 h, leaving only those upfield resonances shown in Fig. 4.16.

The golden yellow precipitate, obtained from the reaction of H_2 with 3a in neat n -butanol was not a pure compound. The NMR spectra (Figs. 4.17, 4.18) of solutions of the yellow precipitate in CD_2Cl_2 under hydrogen, even after careful washing, revealed, in

Table 4.1

T_1 (300 MHz) values, in ms, estimated by the inversion-recovery method, for upfield ^1H NMR resonances observed in the reaction of $\text{RuCl}_2(\text{PPh}_3)(\text{PPFA})$, **3a**, with H_2 in toluene- d_6 /butanol at ambient temperature

Recording temperature ($^\circ\text{C}$)	chemical shift (δ)			
	-11.5	-13.2	-18.5	-20.3
20	50(2)	21(1)	222(8)	145(5)
6	60(2)	19(2)	264(7)	164(5)

addition to resonances due to the yellow complex, **A**, resonances due to **3a** and **1a**:

For the new yellow species, **A**: $^{31}\text{P}\{^1\text{H}\}$ NMR (121 MHz) δ (20 $^\circ\text{C}$) 71.11 (d, $^2J_{\text{PP}} = 40$ Hz), 70.97 (d, $^2J_{\text{PP}} = 43$ Hz), 64.72 (d, $^2J_{\text{PP}} = 40$ Hz), 64.59 (d, $^2J_{\text{PP}} = 43$ Hz).

^1H NMR (300 MHz) δ -20.4 (t, $^2J_{\text{PH}} = 32$ Hz).

For **3a**: $^{31}\text{P}\{^1\text{H}\}$ (121 MHz) δ 76.18 (d), 42.18 (d), $^2J_{\text{PP}} = 38$ Hz. ^1H NMR (300 MHz) δ 1.57 (d, $^3J_{\text{HH}} = 7$ Hz, C- CH_3), 2.47, 2.68 (2s, N-(CH_3) $_2$), 3.60 (s, Fe- C_5H_5), 4.12, 4.34, 4.58 (3 s, Fe- C_5H_5), 6.22 (q, $^3J_{\text{HH}} = 6$ Hz, Fc- CH); integrations were hampered by overlap with other resonances from other species in the mixture, but the data are close to those given in the literature^{††} (see also sect. 2.4).

For **1a**: $^{31}\text{P}\{^1\text{H}\}$ NMR (121 MHz, δ (20 $^\circ\text{C}$) 70.8, 46.8 (br s); δ (-78 $^\circ\text{C}$) 79.5 (br s), 64.5 (underneath the resonance at 64.5 due to the yellow species, **A**), 61.6 (br s), 34.8 (br s); the data correspond to those quoted in sect. 3.4. ^1H NMR: δ -13.1

^{††}From reference 25: δ_{CDCl_3} 1.52 (d, 3H, $^3J_{\text{HH}} = 7$ Hz, C- CH_3), 2.44, 2.66 (2d, $J = 2.4$ Hz, N-(CH_3) $_2$), 3.56 (s, 5H, Fe- C_5H_5), 4.12, 4.27, 4.48 (s, t, s, 3H, $J = 2$ Hz, Fe- C_5H_5), 6.23 (q, 1H, $^3J_{\text{HH}} = 6.4$ Hz, Fc- CH), 6.9 - 7.8 (m, 25H, Ph).

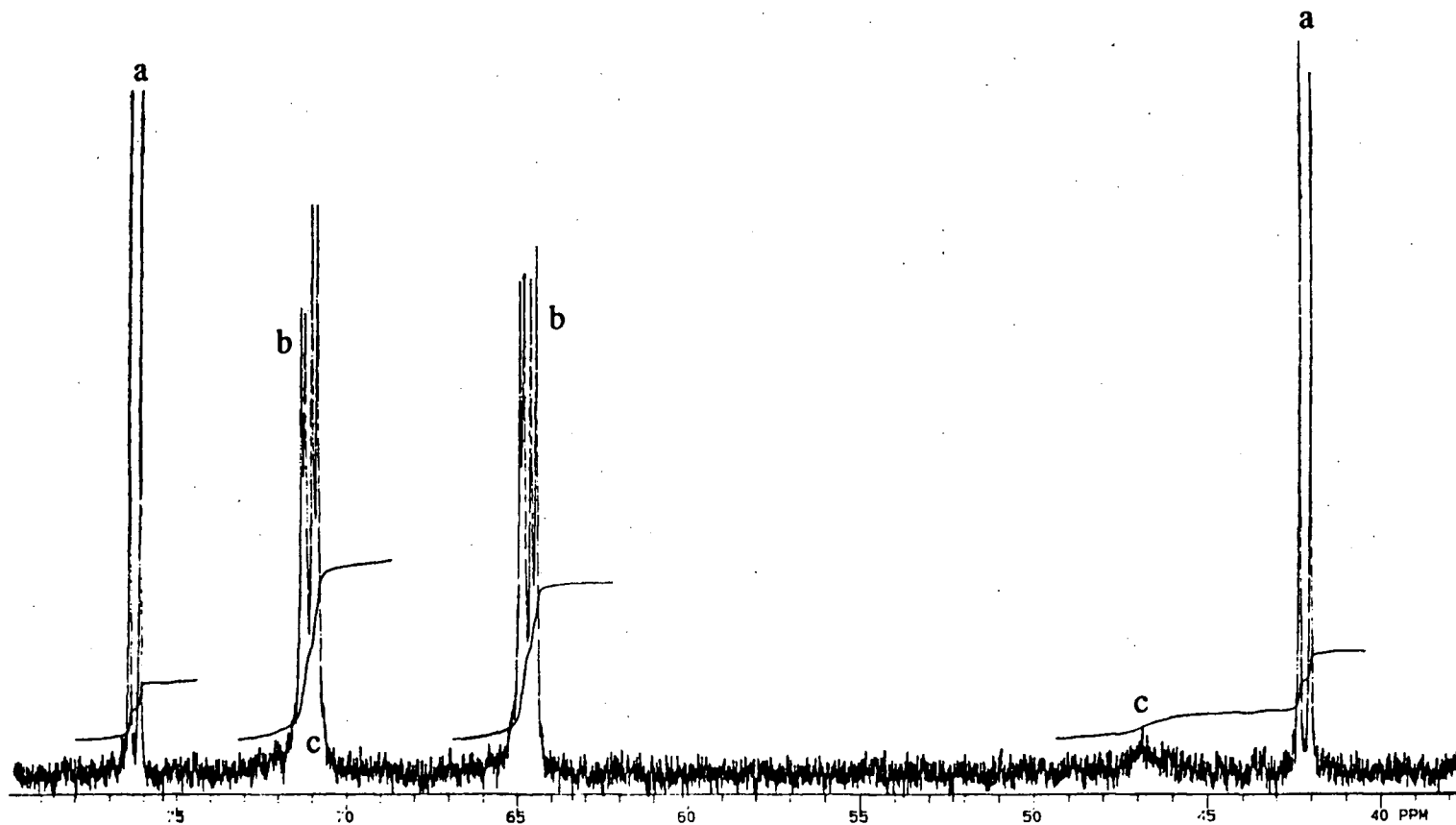


Figure 4.17 The $^{31}\text{P}\{^1\text{H}\}$ spectrum (121 MHz, CD_2Cl_2 , ambient temperature, under hydrogen) of the yellow precipitate from the reaction of **3a** with H_2 in *n*-butanol; peaks are assigned as follows: 'a', complex **3a**; 'b', complex **A**; 'c' (partially obscured by the 'b' resonances), complex **1a**. Resonances 'a' increased with time, and resonances 'b' decreased with time, as the solution turned greenish.

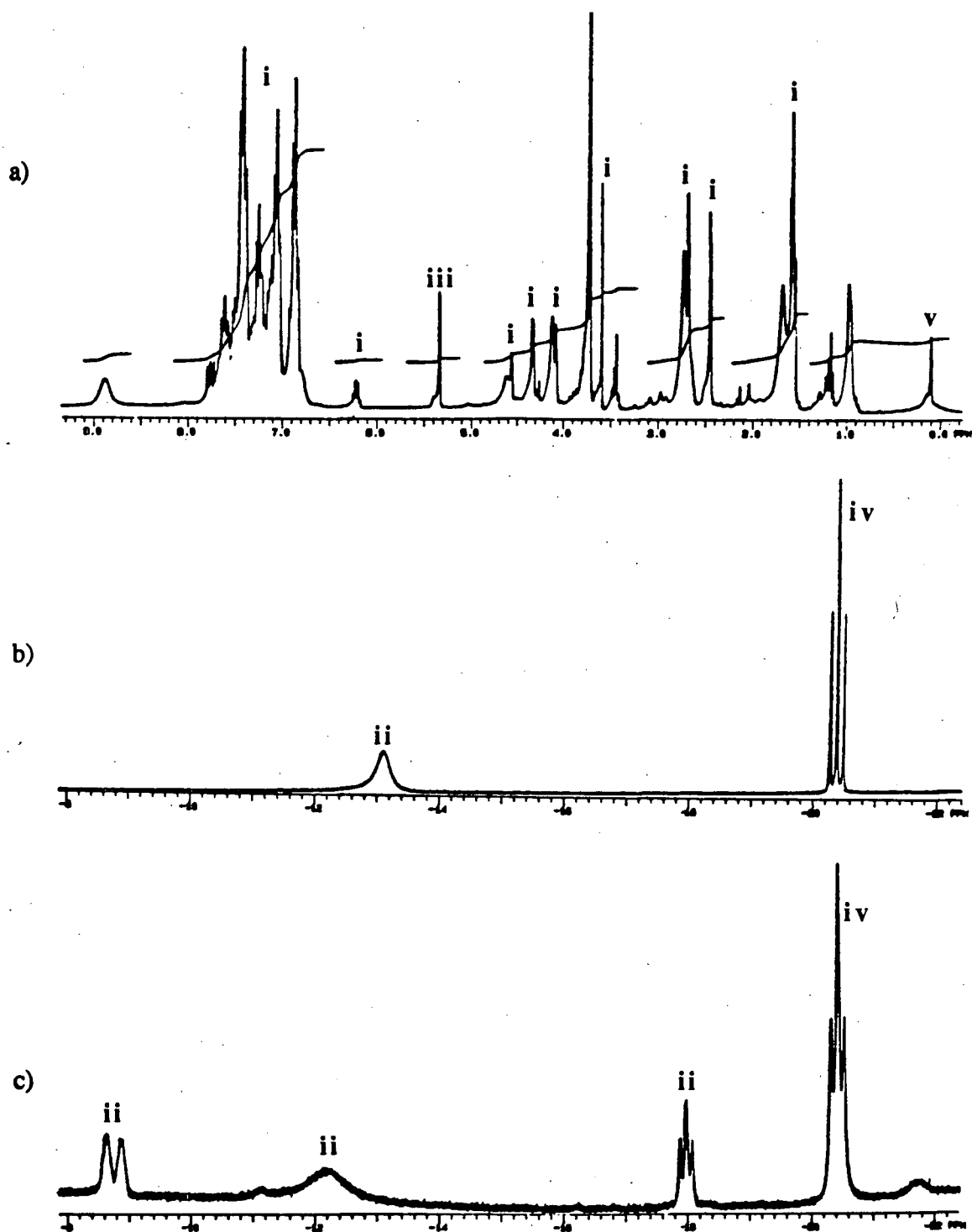


Figure 4.18 ^1H NMR spectra (300 MHz, CD_2Cl_2 , under hydrogen) of the yellow precipitate from the reaction of 3a with H_2 in *n*-butanol: a) downfield region at ambient temperature, b) upfield region at ambient temperature, and c) upfield region at -78°C . Peak assignments are: 'i', complex 3a; 'ii', complex 1a; 'iii', CH_2Cl_2 ; 'iv', complex A; 'v', silicone grease; unmarked peaks are unidentified.

(br s); cf. $\delta_{\text{toluene-d}_8}$ -12.9 (br s) (sect. 3.3).

Another broad singlet (δ 29.3), probably due to Ph_3PO , appeared in the $^{31}\text{P}\{^1\text{H}\}$ NMR spectrum of the solution of this mixture. This singlet also appeared in the spectrum of the *in situ* toluene- d_8 reaction solution of H_2 with **3a**, in the absence of butanol (see above), as well as in the spectrum of a **3a** catalyzed 1-hexene hydrogenation solution with 1:8 butanol/ C_6D_6 as solvent. It should also be noted that a peak at δ 24.9, due to Ph_3PO ,^{21,26} appeared in the spectrum of **3a** in C_6D_6 , and this peak was shifted to δ 27.4 when the spectrum was recorded in a solvent made up of 5 drops *n*-butanol/1 mL C_6D_6 .

The $^{31}\text{P}\{^1\text{H}\}$ NMR signals due to the yellow species, A, decreased with time, while the signals due to **3a** increased with time, even under H_2 . At the same time, the ^1H NMR spectra of this mixture show a decrease in the triplet associated with species A ('iv', Fig. 4.19, δ -20.3), relative to the broad singlet at δ -13.1 ('ii', Fig. 4.19). Figure 4.19 shows the ^1H NMR spectrum of a sample of the mixture within about one hour, and then after about 6 h. In addition to the above-mentioned upfield changes, corresponding changes can be seen downfield; changes in intensity can be related to the solvent resonance (CH_2Cl_2 , 'iii', at $\sim\delta$ 5.3) and another unassigned resonance at $\sim\delta$ 9. The resonance 'i' at $\sim\delta$ 6.2, due to the $\text{CH}(\text{CH}_3)$ in **3a**, is seen to increase markedly during this time, while the δ -13.1 peak 'ii' due to **1a** remains about the same. Further examination of the ^1H NMR spectrum (δ 0 - 5) confirms that the concentration of **3a** is increasing with time. The NMR data show that species A decomposes to regenerate **3a**.

The yellow solid remains as such if kept dry and under hydrogen. But instability, when moist and in solution, and the precipitation of other, additional species during the preparation, made work-up of the pure yellow product, A, difficult. Nevertheless, one sample of crystals was submitted for elemental analysis (Found: C 59.37, H 5.93, N 1.30, Cl 9.50). The yellow crystals were only slightly soluble in dry toluene- d_8 , but dissolved slowly with shaking under H_2 to give a pale yellow solution, which turned green

a)

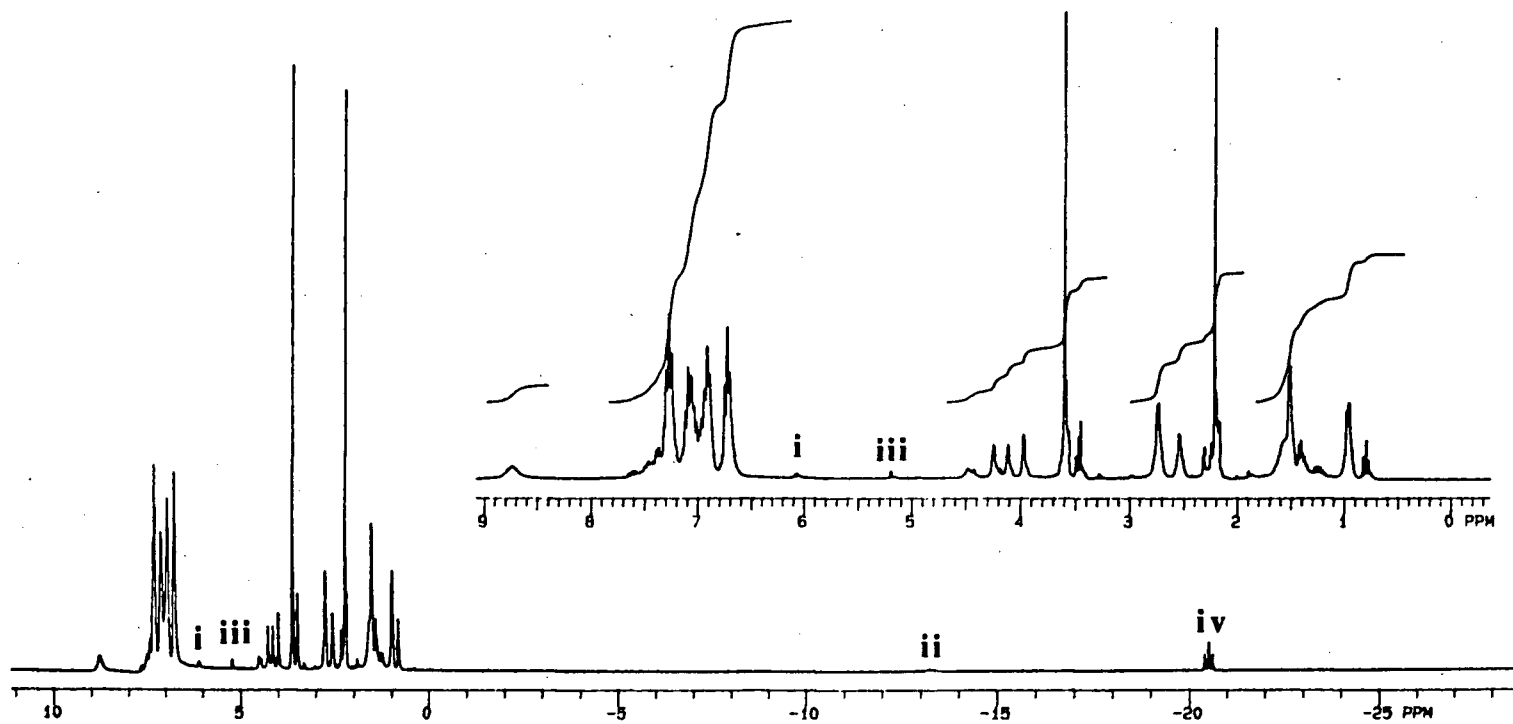


Figure 4.19 ^1H NMR spectra (300 MHz, CD_2Cl_2) of the yellow precipitate from the reaction of **3a** with H_2 in *n*-butanol, within a) 1 h, and b) 6 h of making up the solution; peaks to note are: 'i', due to **3a**; 'ii', due to **1a**; 'iii', due to CH_2Cl_2 ; 'iv', due to complex A. Peaks due to **3a** increase with time relative to those due to A.

b)

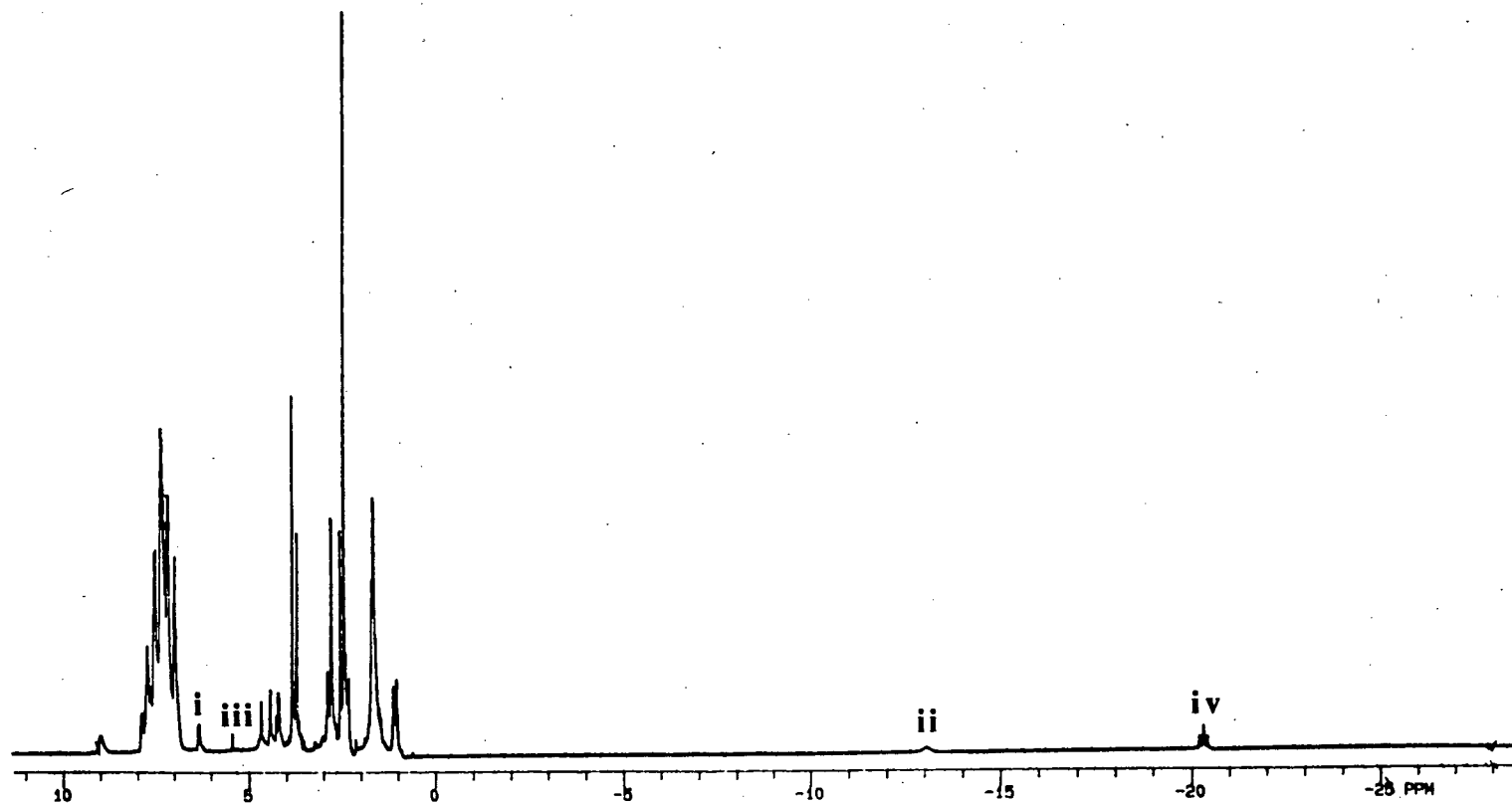
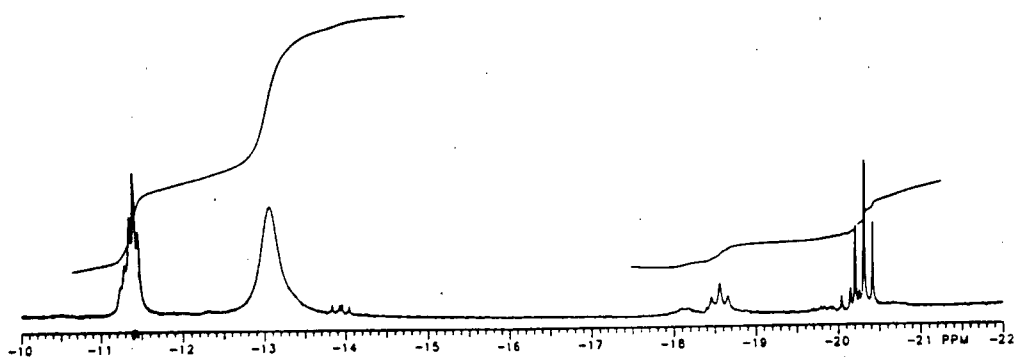


Figure 4.19b (see legend, previous page)

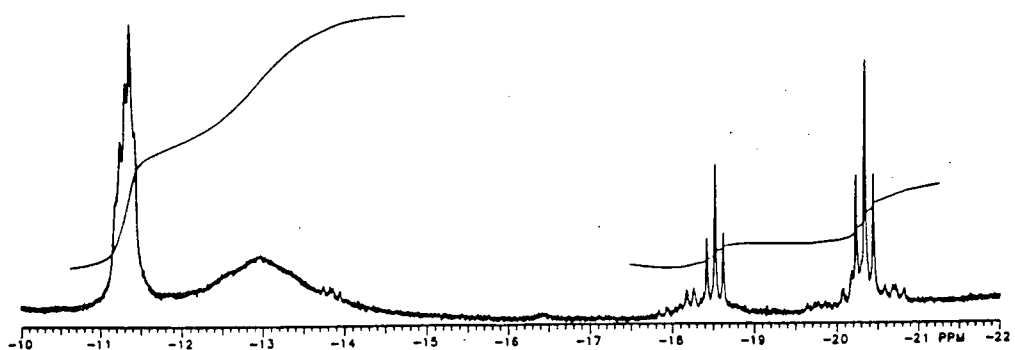
within 30 min. The ^1H and $^{31}\text{P}\{^1\text{H}\}$ NMR spectra of this green solution proved it to contain **3a**. Signals in the ^1H NMR spectrum at δ 0.82(t), 1.2 - 1.3 (m) and 3.3 (m) bore some similarity to butanol signals found in more concentrated solutions of butanol in toluene- d_8 (~2 drops in 0.7 mL) at δ 0.89 (t), 1.3 - 1.5 (m), 3.1 (br s), 3.6 (t), suggesting the presence of perhaps 1 equivalent of *n*-butanol/Ru in the yellow crystals of **A** (discussed in sect. 4.4). This latter spectrum also showed broad signals at δ 0.5 (s, ~5H) and 4.5 (s, ~3H). The $^{31}\text{P}\{^1\text{H}\}$ NMR spectrum showed that no **1a** was present, indicating that the washing of the yellow crystals of **A** had been successful in removing at least this impurity. This $^{31}\text{P}\{^1\text{H}\}$ NMR spectrum was the same as that of a solution of **3a**, except that the integral of the δ 60 - 70 region suggested that there were possibly some signals hidden in the baseline. The volume of gas evolved from 0.0146 g (0.0015 mmol, based on the suggested formulation given later, sect. 4.4) of the yellow precipitate corresponded to 0.0013 mmol of gas. The gas evolved from a toluene solution of the yellow crystals of **A** was identified by GC as H_2 . The equivalent conductance, Λ , of a sample of the yellow crystals of **A**, calculated on the basis of the formulation, was $30 \Omega^{-1}\text{mol}^{-1}\text{cm}^2$, which compares with $63 \Omega^{-1}\text{mol}^{-1}\text{cm}^2$ found for NEt_4Cl using the same solvent and molar concentration.

The reaction of **3a** with H_2 to give the yellow species was also carried out in benzene/hexane/methanol (6:7:2) and in benzene/methanol (~6:1) solvent systems. The variable-temperature ^1H NMR spectrum of an isolated solid mixture formed in benzene/hexane/methanol solution is shown in Figure 4.20. The main upfield resonances were: $\delta_{\text{CD}_2\text{Cl}_2}$ (18 °C) -11.4 (t, $J_{\text{PH}} = 17$ Hz), -13.1 (br s), -18.55 (t, $J_{\text{PH}} = 30$ Hz), -20.3 (t, $J_{\text{PH}} = 32$ Hz); this last noted triplet corresponds to species **A**, formed in the reaction in the presence of butanol.

a)



b)



c)



Figure 4.20 Variable temperature ¹H NMR spectra (300 MHz, CD₂Cl₂) of the yellow deposit from the reaction of 3a with hydrogen in 6:7:2 benzene/hexane/methanol; spectra were observed at: a) ambient temperature, b) -15 °C and c) -55 °C.

Reactions of RuCl₂(PPh₃)(isoPFA), 3b, with hydrogen in DMA, DMA/C₆D₆, and benzene/methanol

The ¹H NMR spectrum of RuCl₂(PPh₃)(isoPFA), 3b, is shown in Figure 4.21.

The violet precipitate, obtained from the reaction of 3b H₂ in DMA in the presence of PPh₃, was identified as RuHCl(PPh₃)₃ by ¹H NMR (80 MHz, CDCl₃, ambient temperature, under nitrogen): δ -17.4 (q, ²J_{PH} = 25 Hz, Ru-H) (*cf.* reference 81); the yield was 90%.

After 3b had reacted with H₂ for 2 h in DMA/C₆D₆, in the absence of added PPh₃, peaks due to the following four major species were observed in the ³¹P{¹H} NMR spectrum (Fig. 4.22):

- (i) unreacted 3b: identified by the two doublets at δ 35.7 and 94.7 with ²J_{PP} = 32 Hz. The spectrum compares closely with that given in section 2.2 and with that for a CDCl₃ solution containing 2 drops DMA per mL (δ 36.05 (d), 95.25 (d), ²J_{PP} = 32 Hz).
- (ii) (η²-H₂)(isoPFA)Ru(μ-Cl)₂(μ-H)RuH(PPh₃)₂, 4: identified by the resonances at δ 78.6 (dd), 76.8 (s), 64.5 (dd). These and the coupling constants compare closely with the values for the CD₂Cl₂ spectrum (sects. 2.4, 3.3).
- (iii) 1a: identified by the two broad singlets at δ 70.3 and 46.0 (*cf.* sects. 2.4 and 3.3).
- (iv) an unidentified species with a broad singlet at δ -13.9.

Also observed were:

- (v) RuHCl(PPh₃)(isoPFA), 7: identified by two doublets at δ 98.0 and 61.0 (*cf.* values given in sect. 2.4).
- (vi) RuHCl(PPh₃)₃: the singlet at δ 59.3 is close to that reported for the CH₂Cl₂ solution of this complex (δ 59.0).⁷⁴

and several unidentified minor resonances.

The unwashed orange solid deposited during the reaction of 3b with H₂ in methanol/benzene contained mainly 4, identified by ¹H NMR (sect. 2.4), and also another unidentified hydride Z, (¹H NMR: δ -12.8 (t)). The ¹H NMR (CDCl₃, 400 MHz)

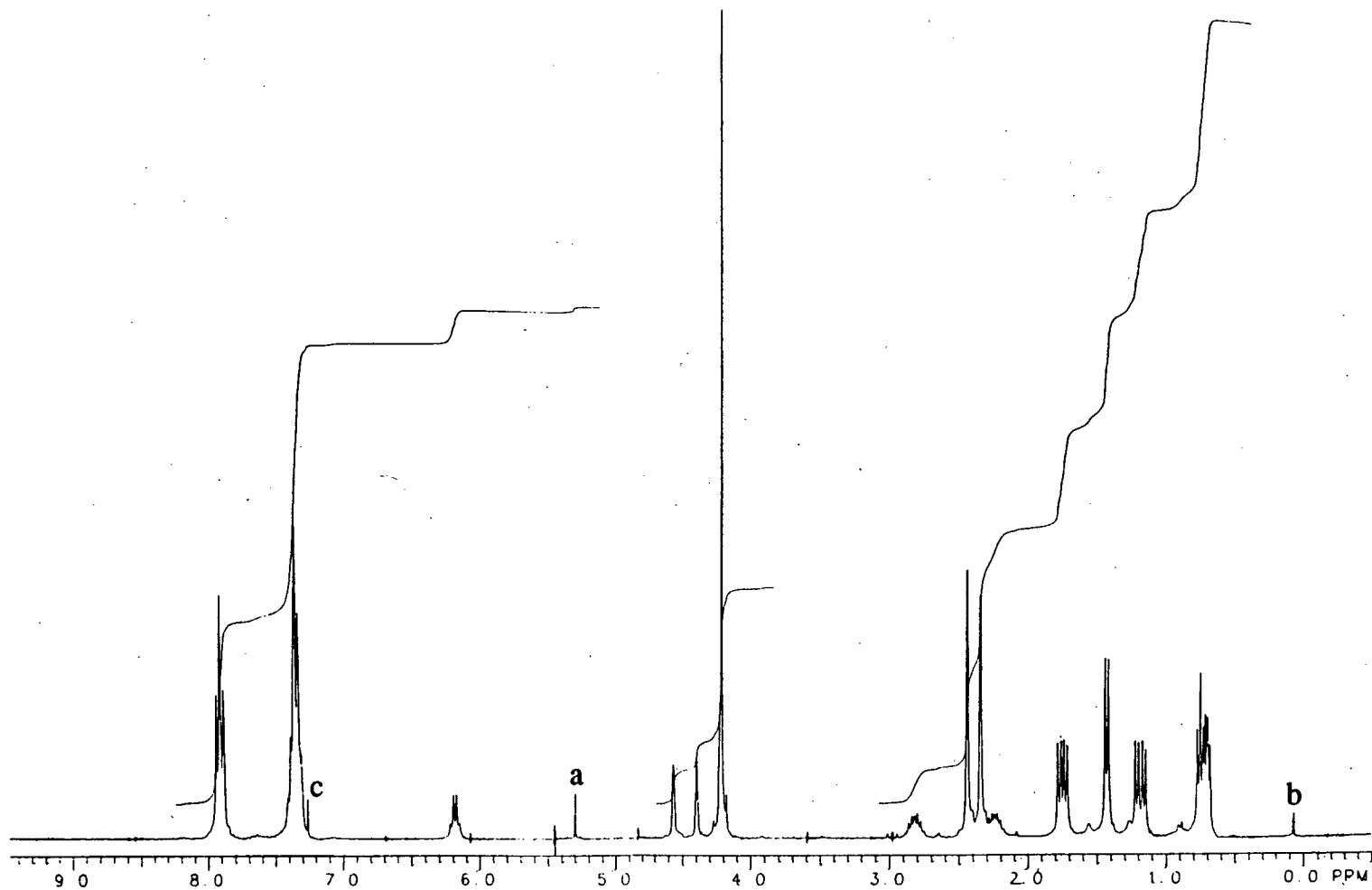


Figure 4.21 The ^1H NMR spectrum of complex 3b. Detailed assignments are given in sect. 2.2; peak 'a' is an unidentified impurity, 'b' is due to silicone grease and 'c' is due to CHCl_3 .

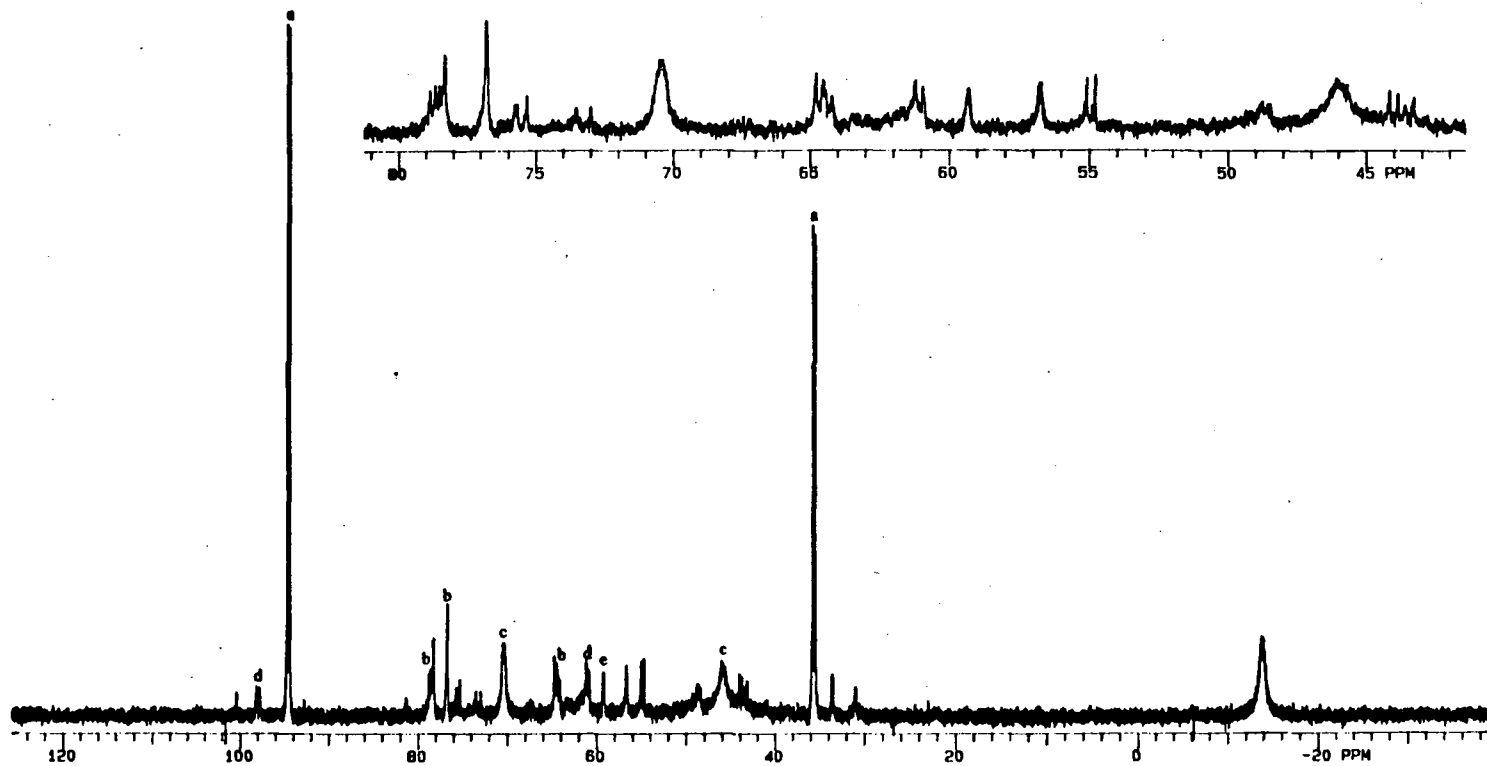


Figure 4.22 The $^{31}\text{P}\{^1\text{H}\}$ spectrum (121 MHz, ambient temperature) of a solution obtained after ~6 h from mixing 3b in 1:1 v/v $\text{C}_6\text{D}_6/\text{DMA}$ under H_2 ; peaks are assigned as follows: 'a', complex 3b; 'b', complex 4; 'c', complex 1a; 'd', complex 7; 'e', $\text{RuHCl}(\text{PPh}_3)_3$. Unmarked peaks are unidentified. An expansion of part of the spectrum is shown in the inset.

spectrum of the residue of the supernatant of the reaction of 3b with H₂ in methanol/benzene is shown in Figure 4.23. Although some decomposition undoubtedly

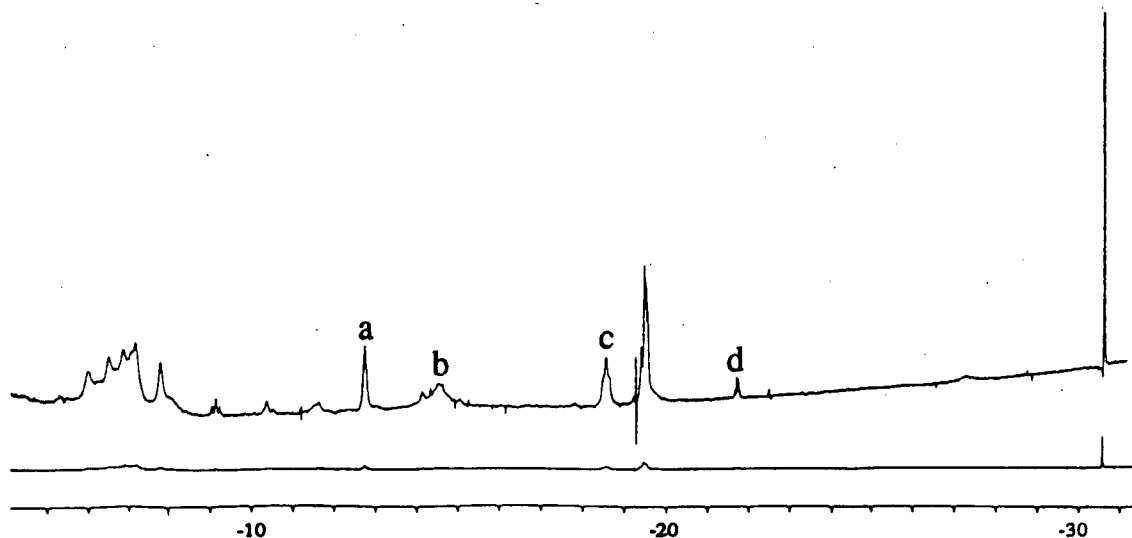


Figure 4.23 The ¹H NMR spectrum of the residue obtained by removal of solvent from the supernatant of the reaction of 3b with H₂ in 1:15 v/v methanol/benzene. Peak assignments are as follows: 'a', complex Z; 'b' and 'c', complex 4; 'd', complex Y. Unmarked peaks are unidentified. Some decomposition has probably occurred as a result of removing the H₂ atmosphere.

occurred as a result of loss of hydrogen pressure, some peaks are recognizable: the δ -14.5 (v br s) and -18.6 (t) peaks of 4 (see above), the δ -12.8 (t) peak of the unidentified hydride Z, and a δ -21.8 (q) peak of species Y, not yet identified but discussed more fully below.

The white crystals of dimethylammonium chloride, which grew in the benzene/methanol supernatant, to which some dichloromethane/hexane solvent had been transferred, exhibited a single ¹H NMR (CD₃OD, 80 MHz, ambient temperature) singlet at δ 2.75, the same as that of an authentic sample. The mass spectrum (Fig. 4.24) shows peaks at *m/z* 46, 45, 44, 38 and 36, 37 and 35; the mass spectrum of an authentic sample showed the same peaks, with the same relative intensities. The unidentified black-red, diamond-shaped crystals of Y exhibited the ³¹P{¹H} NMR spectrum shown in Figure

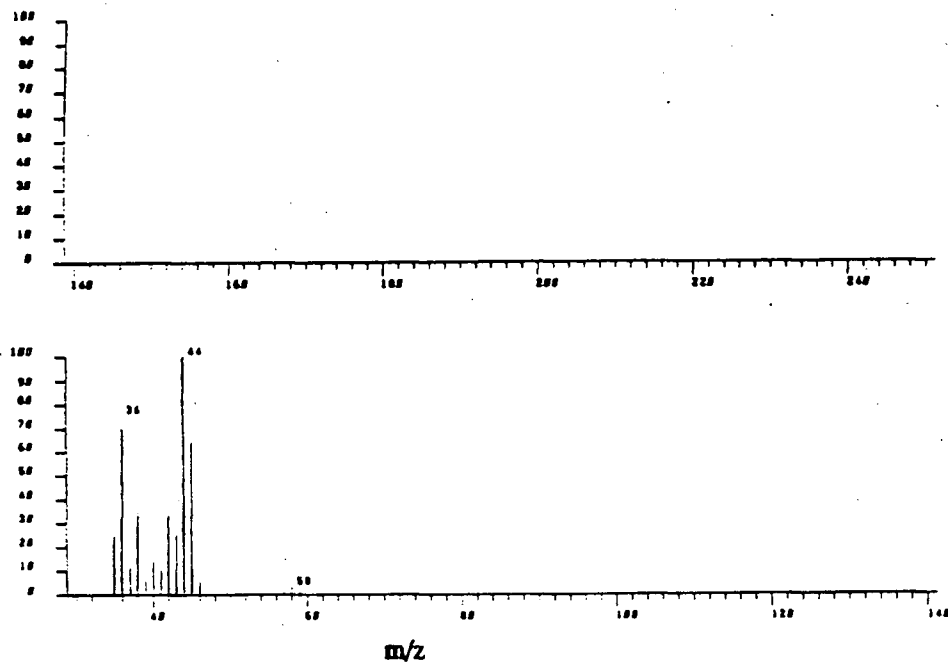


Figure 4.24 The EI mass spectrum of the white crystals of dimethylammonium chloride isolated from the reaction of 3b with H₂ in 1:15 v/v methanol/benzene.

4.25; the ¹H NMR spectrum shown in Figure 4.26 is partly obscured by hexane signals around δ 1. No signals were observable in the IR (KBr pellet) in the region 1700 to 2300 cm⁻¹.

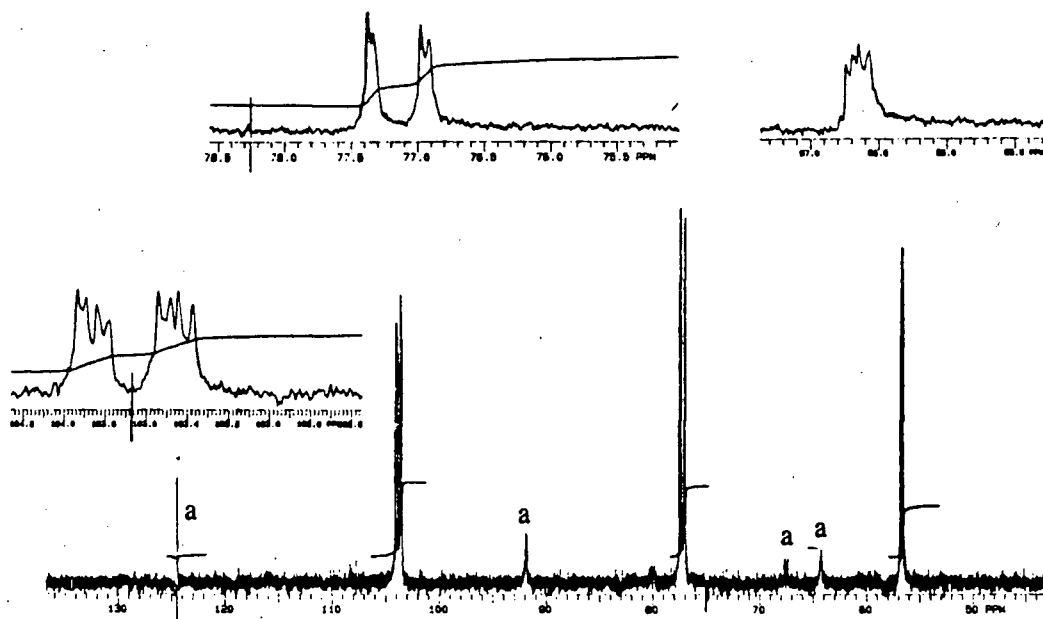


Figure 4.25 The ^{31}P (^1H) NMR spectrum (121 MHz, CD_2Cl_2 , ambient temperature, under hydrogen) of the blackish red crystals of complex **Y** isolated from the reaction of **3b** with H_2 in 1:15 v/v methanol/benzene. Expansions of the three peaks due to **Y** are shown in the insets; minor peaks marked with an 'a' are unidentified impurities.

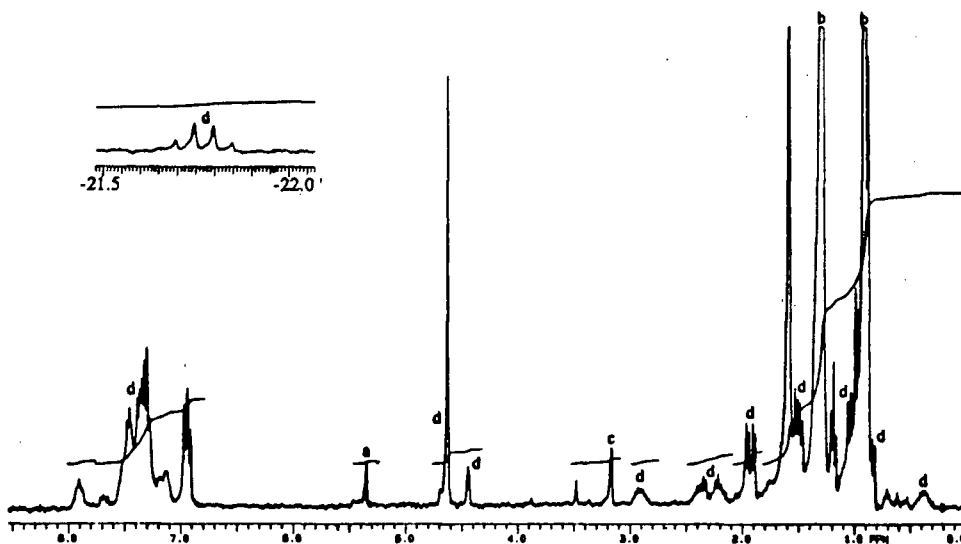


Figure 4.26 The ^1H NMR spectrum (300 MHz, CD_2Cl_2 , ambient temperature, under hydrogen) of **Y**. Peaks are assigned as follows: 'a', CH_2Cl_2 ; 'b', hexane; 'c', methanol; 'd', peaks tentatively assigned to complex **Y**.

Catalytic hydrogenations of prochiral substrates catalyzed by (S,R)-RuCl₂(PPh₃)(PPFA), 3a, and (S,R)-RuCl₂(PPh₃)(isoPPFA), 3b

Results of these studies are presented in Table 4.2.

NMR studies of the catalytic hydrogenation of 1-hexene by (η²-H₂)(PPh₃)₂Ru(μ-Cl)₂(μ-H)RuH(PPh₃)₂, 1a, RuCl₂(PPh₃)(PPFA), 3a and RuCl₂(PPh₃)(isoPPFA), 3b

The 1a system in DMA/C₆D₆:

a) at 0.04 M hexene, the ³¹P{¹H} NMR spectrum (Fig. 4.27) of the active hydrogenation solution, measured as described in section 4.3, showed the presence of mainly 1a. The minor peak at δ 24.2 is probably due to Ph₃PO,^{21,26} while other minor unassigned peaks are present at δ ~72.5, 65.5, 60.2 and 51.2.

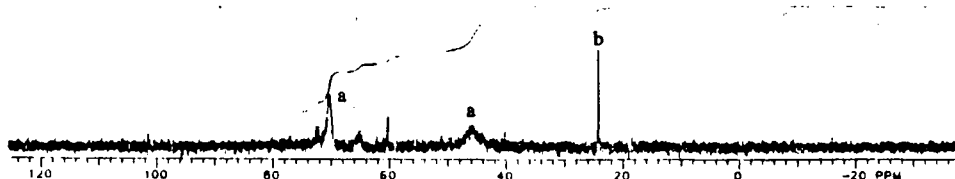


Figure 4.27 The ³¹P{¹H} NMR spectrum (121 MHz, 1:1 v/v DMA/C₆D₆, 5 °C, under hydrogen), acquired within 2 h of starting the reaction, of the 1a-catalytic hydrogenating solution containing initially 0.04 M 1-hexene. Peaks marked 'a' are due to 1a; peak 'b' is due to Ph₃PO; other peaks are unidentified.

b) at 1.0 M hexene, the total H₂ uptake after 2 min was 0.024 M and at this rapid reaction rate the capacity of the buret would have been exceeded in another 4 min.

Therefore, the uptake apparatus was adjusted to allow free, unmeasured flow of H₂ to the reaction solution. The ³¹P{¹H} NMR spectrum (Fig. 4.28) of this active hydrogenating solution showed no trace of 1a. There is a minor peak at δ 24.2 due to Ph₃PO, and a peak at δ 58.5 possibly due to RuHCl(PPh₃)₃; the other peaks in this spectrum at δ 72.5, 65.5, 60.2 and 51.2, which also appear in the 0.04 M

Table 4.2

Hydrogenation results for various substrates using (*S,R*)-RuCl₂(PPh₃)(PPFA), **3a**, and (*S,R*)-RuCl₂(PPh₃)(isoPFA), **3b**, as catalysts^a

With (*S,R*)-**3a** as catalyst:^b

catalyst (M x 10 ³)	substrate (M)	time (h)	solvent	yield (%)	ee ^c
1.4	CH ₂ =C(COOH)NHCOMe (0.11 M)	23	butanol	100 ^d	0
1.7	(<i>E</i>)-PhCH=C(COOH)NHCOMe (0.076 M)	23	methanol/ benzene (1:9)	90	0
1.6	CH ₂ =C(COOH)CH ₂ COOH (0.12 M)	27	methanol/ benzene (1:9)	100	0
1.6	EtC(O)Me (0.13 M)	23	methanol/ benzene (1:9)	0	
1.6	PhC(O)Me (0.17 M)	23	butanol	0	

With (*S,R*)-**3b** as catalyst:^b

1.1	CH ₂ =C(COOH)NHCOMe (0.10 M)	25	methanol/ benzene (1:9)	100	0
1.9	(<i>E</i>)-PhCH=C(COOH)NHCOMe (0.076 M)	23	"	100	
1.7	CH ₂ =C(COOH)CH ₂ COOH (0.12 M)	27	"	100	0
1.3	EtC(O)Me (0.13 M)	18	"	0	
0.9	PhC(O)Me (0.17 M)	22	"	0	

^aAt 1000 psi H₂.

^bThe optical purity of the chiral ligands (84%) for catalysts was based on rotation measurements on (*S,R*)-1-[α -*N,N*-dimethylaminoethyl]-2-diphenylphosphinoferrocene and (*S*)-1-[α -*N,N*-dimethylaminoethyl]ferrocene, giving optical purity = 84 %.

^cThe optical purity of the hydrogenated products was measured by rotation.

^dAt 10 atm H₂ for 24 h, yield = 80%.

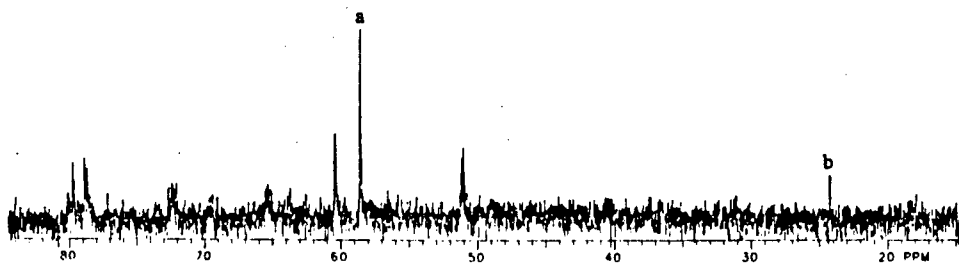


Figure 4.28 The $^{31}\text{P}\{^1\text{H}\}$ NMR spectrum (121 MHz, 1:1 v/v DMA/ C_6D_6 , 5 °C, under hydrogen) of the **1a**-catalytic hydrogenating solution containing 1.0 M 1-hexene, the NMR data being acquired within 2 h of starting the reaction. The peak marked 'a' is due to $\text{RuHCl}(\text{PPh}_3)_3$; peak 'b' is due to Ph_3PO ; other peaks are unassigned.

hexene spectrum, are unassigned; also unassigned is a broad resonance in the δ 78 - 81 range.

The **1a** system in DMA/toluene- d_8 :

After ten minutes of shaking under hydrogen and 0.013 M H_2 had been absorbed, some of the **1a** was still undissolved, showing that the amount of **1a** used in this experiment exceeded the solubility limit. The rate of uptake was approaching a maximum at this time, and the shaking of the flask was stopped to allow transfer of solution to the NMR tube. After the shaking had been stopped for about 1 min, the solution colour had changed from red to a brownish-maroon and the remaining solid then dissolved. Uptake of >0.08 M H_2 was also observed within 3 min of stopping the shaking; the exact amount of H_2 could not be measured as it exceeded the capacity of the buret. (Behaviour similar to that described above was also observed when shaking was stopped in other experiments at 1 M 1-hexene in 1:1 DMA/ C_6D_6 .) The $^{31}\text{P}\{^1\text{H}\}$ NMR spectrum (Fig. 4.29), acquired at 5 °C within 2 h of starting the DMA/toluene- d_8 reaction, showed the presence of Ph_3PO at δ 24.1, unidentified peaks at δ 52.1, -15.3 and -30.2, and possibly resonances, scarcely above noise level, in the δ 55 - 80 range. The ^1H NMR spectrum, acquired at 5°C after 2 h from the start of the reaction, showed only one upfield hydride resonance at δ -17.85 (q,

$^2J_{\text{PH}} = 26$ Hz) due to $\text{RuHCl}(\text{PPh}_3)_3$. Subsequent acquisition of the $^{31}\text{P}\{^1\text{H}\}$ NMR spectrum at -58 °C led to confirmation of the presence of $\text{RuHCl}(\text{PPh}_3)_3$ (δ 94.2 (t, 1P), 38.8 (d, 2P), $^2J_{\text{PP}} = 27$ Hz; *cf.* reference 81); the -58 °C spectrum also included peaks at δ 52.0 and 24.5, due to an unidentified species and Ph_3PO , respectively.

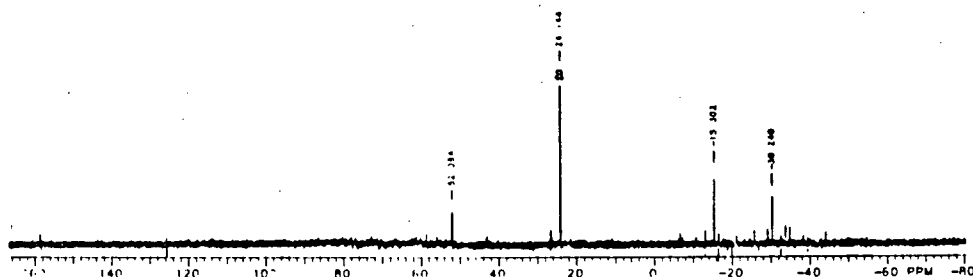


Figure 4.29 The $^{31}\text{P}\{^1\text{H}\}$ NMR spectrum (121 MHz, 1:7 v/v DMA/toluene- d_8 , 5 °C, under hydrogen) acquired during the second hour after the start of the **1a**-catalyzed hydrogenation reaction with 1.0 M 1-hexene. The peak marked 'a' is due to Ph_3PO ; other peaks are unassigned.

The **3a** system:

When, at 9.5 min from starting the reaction, the hydrogen-uptake part of the experiment was interrupted in order to obtain an NMR sample, the hexene-to-hexane turnover number had reached 3.3. The $^{31}\text{P}\{^1\text{H}\}$ NMR spectrum (Fig. 4.30) of this hydrogenation solution shows peaks indicating the presence of mainly **3a** and Ph_3PO , as well as a minor peak at δ 61.7, all of which were also observed at ambient temperature for a solution of **3a** in a solvent made up of 5 drops butanol and 1 mL C_6D_6 , without H_2 or hexene present; the Ph_3PO was also present in a C_6D_6 solution of **3a**. Unidentified peaks barely above noise level, appear at δ 42.1 and 57.9 in the spectrum in Figure 4.30. No upfield hydride signals were observed in the ^1H NMR spectrum, which was acquired at 5 °C two hours after starting the reaction.

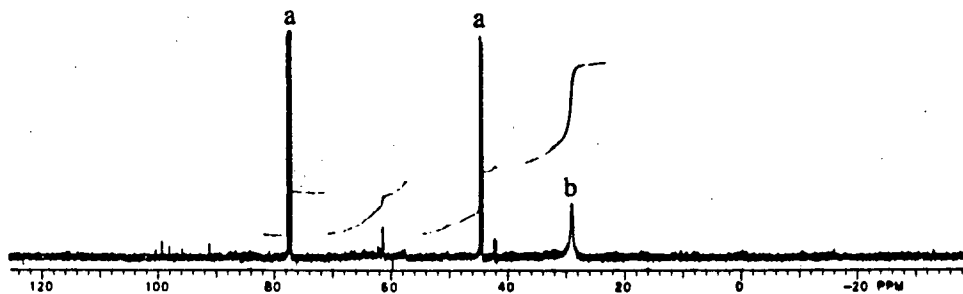


Figure 4.30 The $^{31}\text{P}\{^1\text{H}\}$ NMR spectrum (121 MHz, 1:7 v/v *n*-butanol/ C_6D_6 , 5 °C, under hydrogen), acquired within 2 h of starting the reaction, of a **3a**-catalytic hydrogenating solution containing 0.1 M 1-hexene and 0.014 M **3a**. The peaks marked 'a' are due to **3a**; peak 'b' is due to Ph_3PO ; other peaks are unassigned.

The **3b** system:

The $^{31}\text{P}\{^1\text{H}\}$ NMR spectrum (Fig. 4.31) of this hydrogenation solution shows the presence of mainly **3b** and Ph_3PO , as well as other unassigned minor peaks.

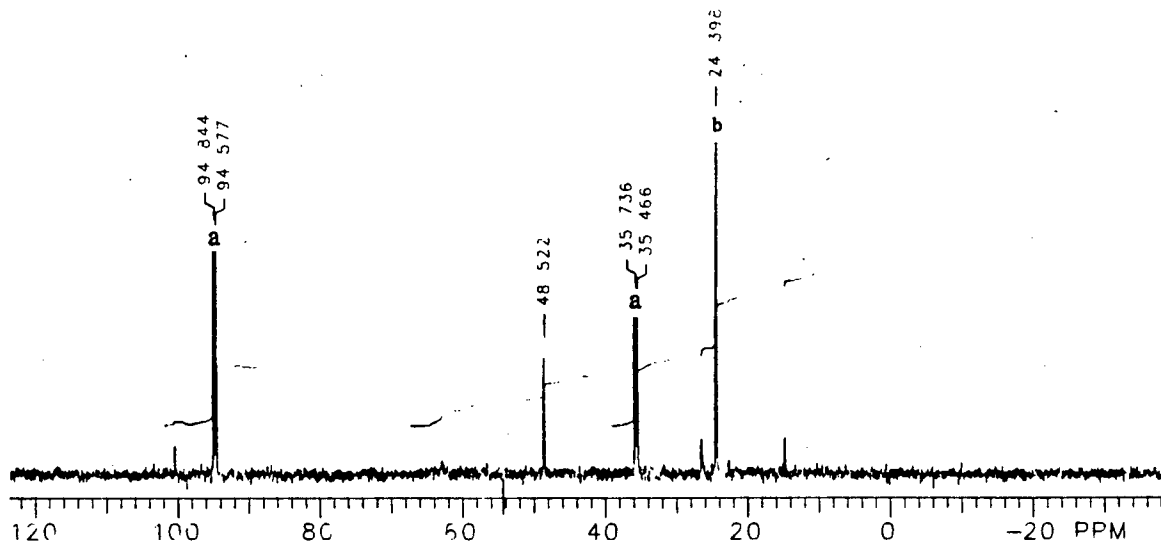


Figure 4.31 The $^{31}\text{P}\{^1\text{H}\}$ NMR spectrum (121 MHz, 1:1 v/v DMA/ C_6D_6 , 5 °C, under hydrogen), acquired within 2 h of starting the reaction, of a **3b**-catalyzed hydrogenating solution containing 0.05 M 1-hexene and 0.005 M **3b**. The peaks marked 'a' are due to **3b**; peak 'b' is due to Ph_3PO ; other peaks are unidentified.

Kinetic data from hydrogen-uptake measurements for 1-hexene hydrogenation

With $(\eta^2\text{-H}_2)(\text{PPh}_3)_2\text{Ru}(\mu\text{-Cl})_2(\mu\text{-H})\text{RuH}(\text{PPh}_3)_2$, **1a**, as catalyst at a total ruthenium concentration of 6.2×10^{-4} M and a 1-hexene concentration of 0.02 M in DMA at 30 °C under 1 atm H_2 , the maximum rate of uptake was 1×10^{-5} M s^{-1} .

With compound **A** as catalyst, employing 3×10^{-4} M compound **A** and 0.1 M 1-hexene in dry *n*-butanol under 1 atm H_2 , the total H_2 uptake after 2 h corresponded to <10% of a quantitative conversion of 1-hexene to hexane. The golden colour of the solution obtained on dissolution was retained overnight.

More extensive data were obtained using $\text{RuCl}_2(\text{PPh}_3)(\text{isoPFA})$, **3b** as catalyst. For a 1-hexene hydrogenation system in DMA at 30 °C, the total gas uptake corresponded to virtually complete reduction of the 1-hexene to hexane. Isomerization of the 1-hexene was not detected at stages prior to complete hydrogenation. The uptake plots (Fig. 4.32) show an initial autocatalytic period prior to reaching a maximum rate, usually after 500 to 4000 s; the rate then gradually falls off. The maximum rates were used to determine the

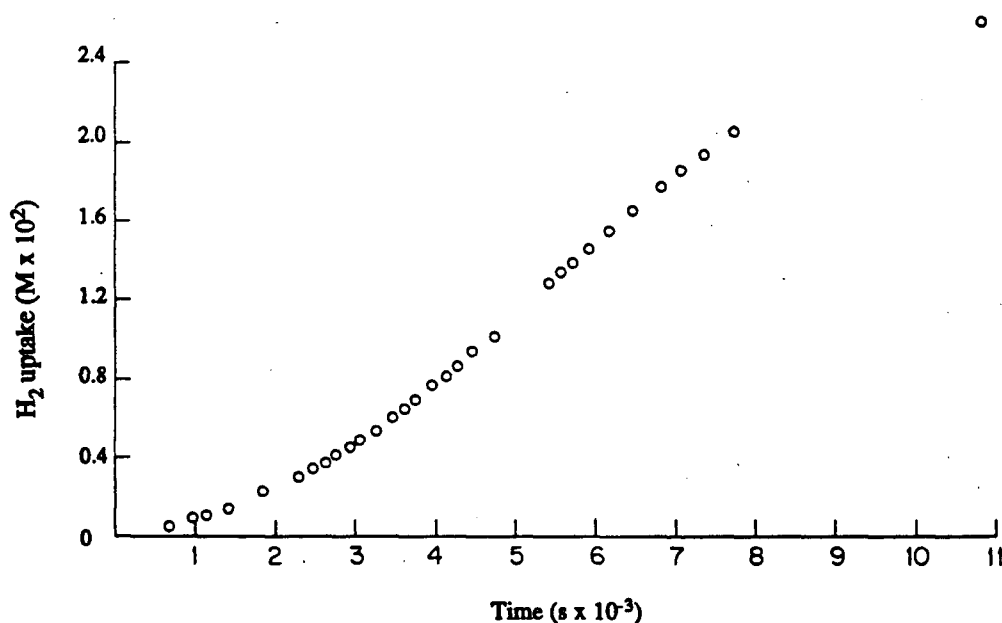


Figure 4.32 H_2 uptake plot for 1-hexene hydrogenation catalyzed by **3b**, with 1 atm H_2 , 0.030 M 1-hexene, 4.3×10^{-4} M PPh_3 and 5.2×10^{-4} M **3b** in DMA at 30 °C.

kinetic dependences. The data are summarized in Figures 4.33 to 4.37. The dependence on $[\text{Ru}]_{\text{total}}$ goes from first to half-order with increasing concentration; with added PPh_3 , the dependence is more nearly first-order (Figs. 4.33, 4.34). There is a first-order dependence on 1-hexene and on H_2 (Figs. 4.35, 4.36), and a complex dependence on added phosphine, with the rate initially increasing somewhat with phosphine concentration, and then becoming inhibited at $[\text{PPh}_3] > 1 \times 10^{-3} \text{ M}$ (Fig. 4.37). A colour change (from green to violet) of the hydrogenating solutions containing added phosphine was observed during gas-uptake measurements.

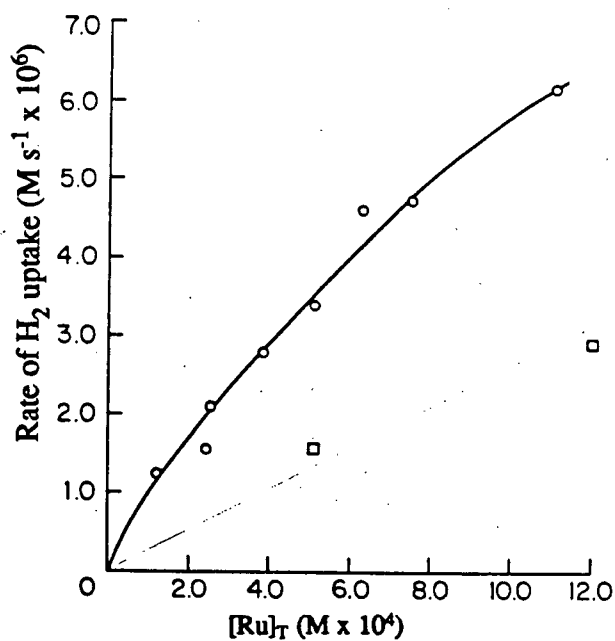


Figure 4.33 Dependence of maximum rate of hydrogenation of 1-hexene in DMA on total Ru concentration (3b): \circ , with no added PPh_3 ; \square , with $6.5 \times 10^{-3} \text{ M PPh}_3$ added.

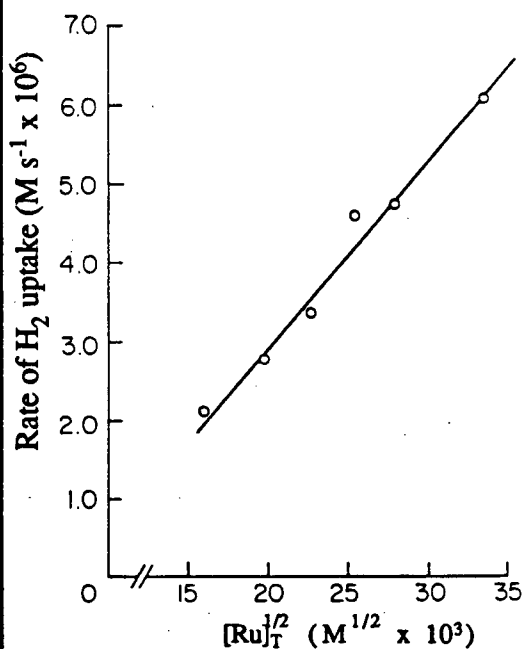


Figure 4.34 Dependence of maximum rate of hydrogenation of 1-hexene in DMA on the square root of the total Ru concentration (3b).

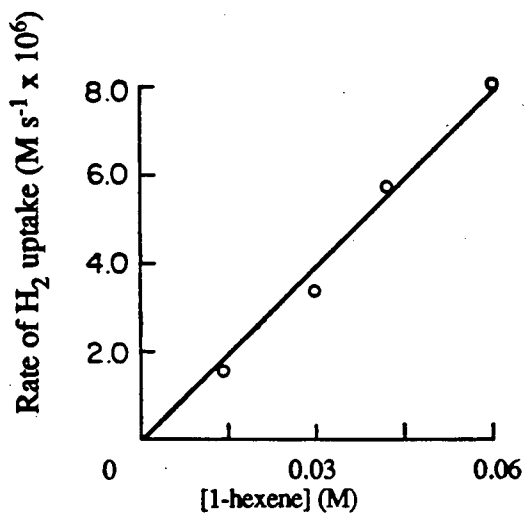


Figure 4.35 Hexene dependence of maximum rate of hydrogenation of 1-hexene in DMA at 30 °C, 1 atm total pressure and total Ru concentration (3b) = 5.1×10^{-4} M.

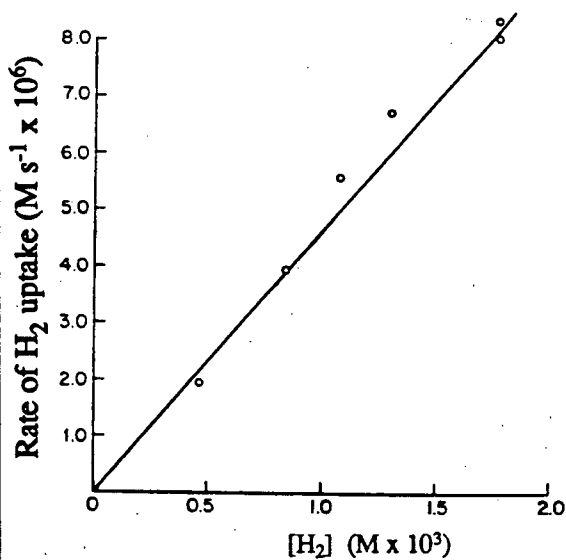


Figure 4.36 H₂ dependence of maximum rate of hydrogenation of 1-hexene in DMA at 30 °C, with total Ru concentration (3b) = 5.1×10^{-4} M and [1-hexene] = 0.06 M.

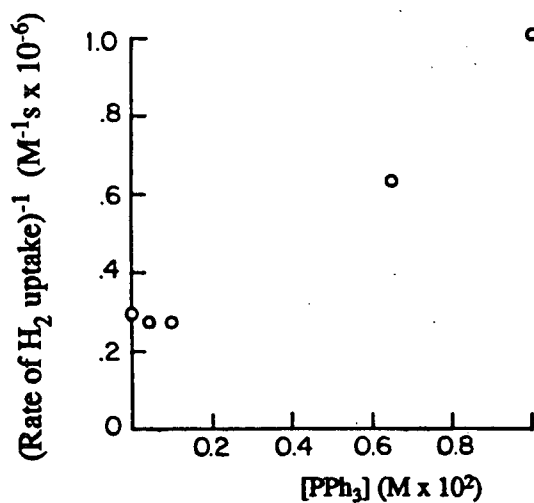


Figure 4.37 Phosphine dependence for the reciprocal of the maximum rate of hydrogenation of 1-hexene (0.03 M) in DMA at 30 °C and 1 atm total pressure, with total Ru concentration (3b) = 5.1×10^{-4} M.

With $(\eta^2\text{-H}_2)(\text{isoPFA})\text{Ru}(\mu\text{-Cl})_2(\mu\text{-H})\text{RuH}(\text{PPh}_3)_2$, **4** as catalyst, using a total ruthenium concentration of 3×10^{-4} M and a 1-hexene concentration of 0.02 M in DMA at 30 °C under 1 atm H_2 , the maximum rate of uptake was 8×10^{-6} Ms^{-1} .

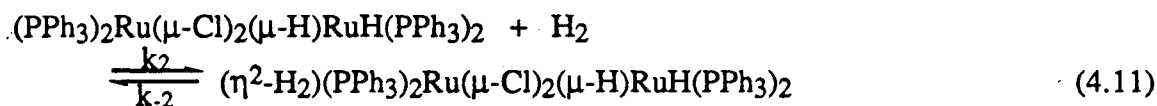
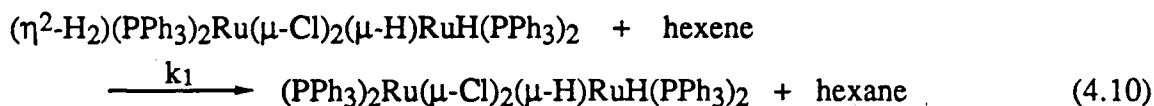
4.4 Discussion

*The $(\eta^2\text{-H}_2)(\text{PPh}_3)_2\text{Ru}(\mu\text{-Cl})_2(\mu\text{-H})\text{RuH}(\text{PPh}_3)_2$, **1a**, 1-hexene hydrogenation system*

At the relatively low hexene concentration of 0.04 M and at 1 atm H_2 , the hydrogenating solution exhibits a $^{31}\text{P}\{^1\text{H}\}$ NMR spectrum showing that **1a** is the main species present. This species was not observed at the high hexene concentration of 1 M; however, it must be remembered that stopping the shaking in order to sample this hydrogenating solution, even while under 1 atm H_2 , would result in depletion of dissolved H_2 . That this H_2 depletion actually perturbed the distribution of ruthenium species in solution is evidenced by the colour change from red to brownish-maroon (p. 117) and immediate dissolution of undissolved **1a**, present above its solubility limit in experiments at high hexene concentration. Furthermore, it was shown in section 3.3 that **1a** reacts, in the absence of hydrogen, with 1-hexene to give hexane and $\text{RuHCl}(\text{PPh}_3)_3$; thus, in the 1 M hexene hydrogenating solutions under 1 atm H_2 , the same reaction appears to occur, when shaking under hydrogen is stopped in order to sample, and the presence of $\text{RuHCl}(\text{PPh}_3)_3$ is, in fact, indicated by the $^{31}\text{P}\{^1\text{H}\}$ and ^1H NMR spectra of these solutions. That a somewhat altered catalytic system is present after stopping and then resuming the shaking is evidenced by the rapid uptakes observed and the fact the colour remains brownish-maroon (p. 117). It could be inferred then that, in the 1-hexene hydrogenation system present with continuous shaking, complex **1a** is catalytically reacting with 1-hexene both at high and low hexene concentration and is being regenerated by reaction of an intermediate with hydrogen. Other minor species are indicated by the $^{31}\text{P}\{^1\text{H}\}$ NMR spectra, but have not been identified; neither is it known whether these species are intermediates in the

catalytic cycle involving **1a**, or whether they are side-reaction products. The mechanisms for hexene coordination and hydride transfer are not known; however, breaking of a Ru-(μ -H) bond, which might occur during the rapid hydrogen ligand exchange process (sect. 3.3, 3.4), could provide a vacant site for coordination of hexene. Rapid transfer of η^2 -H₂ or hydride ligands to the hexene, elimination of the hexane and regeneration of **1a** could then occur. A possible intermediate might be the hypothetical species (PPh₃)₂Ru(μ -Cl)₂(μ -H)RuH(PPh₃)₂, discussed in section 3.4, which is thought to react rapidly with H₂ to regenerate **1a**, and may not be easily observed under H₂.

Thus, in explanation of the near first-order dependence on [Ru]_T, the first- to zero-order dependence on 1-hexene, the mainly first-order dependence on hydrogen at high substrate concentration, and the first- to zero-order dependence at lower substrate concentration, the following mechanism is proposed:



where k_1 , k_2 and k_{-2} are rate constants. Evidence for the equilibrium 4.11 is obtained from a study^{21,23} of the reaction of **1a** with PPh₃ (discussed in sect. 3.4), and the k_{-2} step is therefore written into the mechanism proposed here.

Applying a steady-state treatment to the intermediate, (PPh₃)₂Ru(μ -Cl)₂(μ -H)RuH(PPh₃)₂, gives the rate equation:

$$\text{Rate} = \frac{d[\text{H}_2]}{dt} = \frac{k_1 k_2 [\text{hexene}] [\text{H}_2] [\text{Ru}_2]_T}{k_{-2} + k_2 [\text{H}_2] + k_1 [\text{hexene}]} \quad (4.12)$$

$$\begin{aligned} \text{where } [\text{Ru}_2]_T &= [(\eta^2\text{-H}_2)(\text{PPh}_3)_2\text{Ru}(\mu\text{-Cl})_2(\mu\text{-H})\text{RuH}(\text{PPh}_3)_2] + \\ &\quad [(\text{PPh}_3)_2\text{Ru}(\mu\text{-Cl})_2(\mu\text{-H})\text{RuH}(\text{PPh}_3)_2] \\ &= \frac{1}{2} [\text{Ru}]_T \end{aligned} \quad (4.13)$$

The initial induction period (Fig. 4.1) preceding the maximum rate of H₂ uptake is probably due to the dissolution of the complex.

The rate equation (4.12) can be written as:

$$\text{Rate} = k'[\text{Ru}]_T \frac{1}{2}k_1k_2[\text{hexene}][\text{H}_2] \quad (4.14)$$

$$\text{where } k' = \frac{1}{k_{-2} + k_2[\text{H}_2] + k_1[\text{hexene}]} \quad (4.15)$$

Thus, the above mechanism would produce a first-order order dependence on [Ru]_T. The data in Figure 4.2, obtained by Thorburn,⁷¹ follow approximately first-order behaviour, at least at lower [Ru]_T (≤ 2 × 10⁻³ M, the concentration used in most of Thorburn's uptake experiments). The somewhat less than first-order Ru dependence at higher [Ru]_T, however, is probably real and is unexplained by this mechanism. A possible reason, admittedly speculative, for this fall-off in rate with increasing Ru concentration would be an interaction between one of the dinuclear complexes in equations 4.10 and 4.11, with a mononuclear species in solution to give a Ru₃ species. In any case, the fall-off in rate at higher [Ru]_T does not rule out the mechanism described above, at least when Ru_T ≤ 2 × 10⁻³ M.

At lower hexene concentrations, the k₁[hexene] term in the denominator of equation (4.12) could possibly become small compared to (k₋₂ + k₂[H₂]), and the rate equation approximates to equation 4.16, which shows a first-order dependence on hexene:

$$\text{Rate} = \frac{\frac{1}{2}k_1k_2[\text{Ru}]_T[\text{hexene}][\text{H}_2]}{k_{-2} + k_2[\text{H}_2]} \quad (4.16)$$

At higher hexene concentrations (>1 M), the k₁[hexene] term becomes the most important in the denominator, and equation 4.12 approximates to:

$$\text{Rate} = k_2[\text{Ru}]_T[\text{H}_2] \quad (4.17)$$

which shows independence of hexene concentration. Rearrangement of equation 4.12

gives:

$$\frac{1}{\text{Rate}} = \frac{k_{-2} + k_2[\text{H}_2]}{\frac{1}{2}k_1k_2[\text{H}_2][\text{Ru}]_T} \cdot \frac{1}{[\text{hexene}]} + \frac{1}{\frac{1}{2}k_2[\text{Ru}]_T[\text{H}_2]} \quad (4.18)$$

In fact, in accordance with equation 4.18, a plot of $1/\text{Rate}$ versus $1/[\text{hexene}]$ at constant $[\text{Ru}]_T$ and $[\text{H}_2]$ yields a straight line (Fig. 4.4), the intercept of which is used to calculate a k_2 value of $160 \text{ M}^{-1}\text{s}^{-1}$.

At the lower olefin concentration conditions where the rate equation approximates to 4.16, the proposed mechanism requires that the dependence on hydrogen should go from first- toward zero-order as the $[\text{H}_2]$ increases, as seen experimentally (see data for 0.3 M hexene experiments, Fig. 4.5). When the olefin concentration is high ($>1 \text{ M}$), the rate equation approximates to 4.17, and the mechanism requires that the rate should show a first-order dependence on hydrogen over the complete range of hydrogen concentrations. While experiments on H_2 dependence at $[\text{hexene}] > 0.7 \text{ M}$ have not been carried out, the data for experiments at 0.7 M hexene do show the increased tendency toward first-order behaviour.

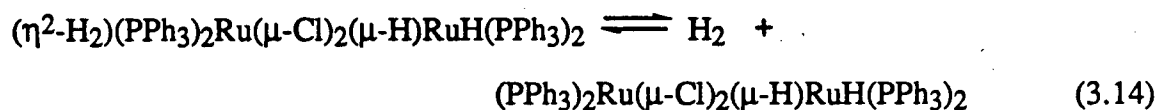
Values for rate constants can be obtained using a rearranged form of equation 4.12:

$$\frac{1}{\text{Rate}} = \frac{k_2 + k_1[\text{hexene}]}{\frac{1}{2}k_1k_2[\text{hexene}][\text{Ru}]_T} \cdot \frac{1}{[\text{H}_2]} + \frac{1}{\frac{1}{2}k_1[\text{Ru}]_T[\text{hexene}]} \quad (4.19)$$

In accordance with equation 4.19, plots of $1/\text{Rate}$ against $1/[\text{H}_2]$ at constant $[\text{Ru}]_T$ and $[\text{hexene}]$ at both hexene concentrations yield straight lines (Fig. 4.6), the intercepts of which are used to determine k_1 values of 0.56 and $0.58 \text{ M}^{-1}\text{s}^{-1}$. Since the value of k_2 is known (*vide supra*), these values of k_1 and k_2 can be used to derive the value of k_2 from the slope of one of the lines plotted according to equation 4.19 (Fig. 4.6), and hence the value of k_2/k_1 . Thus, for a hexene concentration of 0.2 M , a value for k_2 is calculated to be 0.020 s^{-1} , which yields a value for k_2/k_1 of $7.9 \times 10^3 \text{ M}^{-1}$. Calculation of k_2 could also be carried out, if necessary, for a hexene concentration of 0.7 M . Further, equation 4.18 and the slope of the line in Figure 4.4 could also be used to obtain a value for k_2 ; however, corresponding calculations carried out by Thorburn show that the data are self-consistent, and thus the alternate calculations are unnecessary in the present work. It is of

interest in connection with this value of K that work on the reaction of **1a** with PPh_3 yields an estimate of K of 5×10^4 .²³

For experiments at constant $[\text{Ru}]_T$, $[\text{H}_2]$ and $[\text{1-hexene}]$, the rate of hydrogenation decreases with increasing $[\text{PPh}_3]$. Addition of PPh_3 to **1a** is known to give a solution containing the monomeric $\text{RuHCl}(\text{PPh}_3)_3$ complex, with evolution of hydrogen.²³ The colour of the solution changes with increasing added PPh_3 from the red of **1a** to the violet colour of $\text{RuHCl}(\text{PPh}_3)_3$ and is now thought to proceed by an initial equilibrium involving loss of the $\eta^2\text{-H}_2$ ligand, followed by reaction with PPh_3 :



Added PPh_3 also suppresses the rate of hydrogenation catalyzed by $\text{RuHCl}(\text{PPh}_3)_3$;² thus, although $\text{RuHCl}(\text{PPh}_3)_3$, one of the most active platinum metal catalysts known for the hydrogenation of terminal olefins (see section 4.1), is probably formed on addition of PPh_3 to the hexene hydrogenation system, its formation is not inconsistent with loss of activity.

The reason for the increase in rate with increasing $[\text{LiCl}]$ is still unknown, but the increased rate is probably due to reaction of one of the dimeric species in equations 4.10 and 4.11 with chloride to give a more active catalyst.

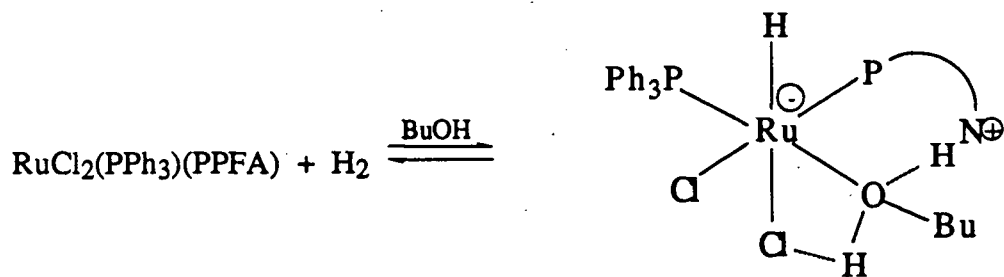
*Hydrogenations involving $\text{RuCl}_2(\text{PPh}_3)(\text{PPFA})$, **3a***

Reactions of **3a** with H_2 :

The complex **3a** reacts with hydrogen in toluene in the absence of alcohol to give non-hydridic species; hydride and dihydrogen species are presumably produced by the reaction of **3a** with H_2 in butanol. The hydrides were not observed *in situ* with 1 atm H_2 in the previous work,²⁵ and the reported absence of $^{31}\text{P}\{^1\text{H}\}$ NMR signals²⁵ must have

resulted from using solutions that were too dilute. The only product positively identified in the present work is the complex, $(\eta^2\text{-H}_2)(\text{PPh}_3)_2\text{Ru}(\mu\text{-Cl})_2(\mu\text{-H})\text{RuH}(\text{PPh}_3)_2$, **1a**, discussed in chapter 3, which must occur following a phosphine ligand redistribution reaction of **3a**.

The isolated golden yellow hydride, **A**, was not fully characterized, but must be closely related to **3a**, since it decomposes in CD_2Cl_2 , and in toluene- d_8 , even under H_2 , to regenerate **3a**, which was detected by its green colour and ^1H and $^{31}\text{P}\{^1\text{H}\}$ NMR spectra. Of importance, a butanol solution of the yellow hydride under 1 atm H_2 retained the yellow colour overnight (*vide supra*), suggesting that the alcohol solvent stabilizes the hydride. This behaviour is also consistent with the report of regeneration of the green colour of **3a**, even under H_2 , when work-up of hydrogenated butanol solutions was attempted.²⁵ Spectral changes in Thorburn's UV-vis experiment of subjecting hydrogenated solutions of **3a** to argon in toluene/methanol⁶⁵ (sect. 4.1) were consistent with regeneration of **3a**. Also, in the *in situ* experiments in toluene- d_8 /butanol, the reaction between and H_2 did not go to completion even though hydrogen was still available. These findings, coupled with Thorburn's H_2 uptake experiments which showed decreasing H_2 :Ru stoichiometries with increasing temperature,⁶⁵ suggest that an equilibrium exists between **3a** and the yellow hydride complex, **A**. Based on the above observations, a possible formulation for **A** is shown within a suggested equilibrium (eq. 4.20). The proposed structure involves a zwitterionic species stabilized by coordinated butanol of some type, either as shown, or involving the hydride ligand. In CD_2Cl_2 or toluene- d_8 , loss of the coordinated butanol could result in destabilization, and subsequent reverse reaction between the hydride and nitrogen-stabilized proton to give H_2 and the reactant complex, **3a**, as observed in the gas evolution experiments. The presence of a hydride ligand, *cis* to two almost equivalent,



(4.20)

mutually *cis* phosphine ligands is consistent with the observed highfield pseudo-triplet ($^2J_{\text{PH}} = 32$ Hz) in the ^1H NMR spectrum, and the magnitude ($^2J_{\text{PP}} = 40$ Hz) of the $^{31}\text{P}\{^1\text{H}\}$ NMR coupling constants.⁸⁹⁻⁹¹ The pale yellow colour of this hydride is consistent with a six-coordinate complex; five-coordinate Ru(II) hydrides are typically intensely red-coloured,⁹⁰ an observation born out in the present thesis work (sect. 5.3). The elemental analysis for A is generally reasonable, but the carbon analysis is low, and the chlorine analysis is high: Calcd. for $\text{C}_{48}\text{H}_{53}\text{ONCl}_2\text{FeP}_2\text{Ru}$: C 60.44, H 5.56, N 1.47, Cl 7.44. Found: C 59.37, H 5.93, N 1.30, Cl 9.50. The $^{31}\text{P}\{^1\text{H}\}$ NMR spectrum indicated that some Ph_3PO was present. Also, the conductivity measurement corresponds to half a mole of a 1:1 electrolyte; this might be due to 0.5 mole of an ionic chloride impurity, consistent with the chloride analysis which is high by roughly 1/2 Cl. The proposal implies a reaction showing heterolytic cleavage of H_2 promoted by the amine functionality of the coordinated PPFA ligand; indeed, one goal of the original P-N ligand work²⁵ was to determine if such a reaction might occur. There is limited direct data to support heterolytic cleavage of H_2 at a metal centre,¹¹⁰ and the subject is particularly important at Ru(II) centres where monohydride formation within a mononuclear species would otherwise have to invoke Ru(IV) dihydride intermediates.²⁵ Involvement of the

amine group in the reaction of the analogous complex, $\text{RuCl}_2(\text{PPh}_3)(\text{isoPFA})$, **3b**, with H_2 in benzene/methanol (15:1) is demonstrated above (sect. 4.3), where protonation of the $-\text{NMe}_2$ group, results in the formation of $\text{H}_2\text{NMe}_2^+\text{Cl}^-$. The yellow complex formed in the present PPFA system may represent an arrested intermediate in a reaction analogous to that in the isoPFA system.

The presence of two overlapping doublets in the $^{31}\text{P}\{^1\text{H}\}$ NMR spectra of **A** at δ 71.11 and 70.97, and also at δ 64.72 and 64.59 may be due to the presence of diastereomers in solution: the PPFA ligand may be *R,S* or *S,R*, and the ruthenium centre in the above structure is also chiral.

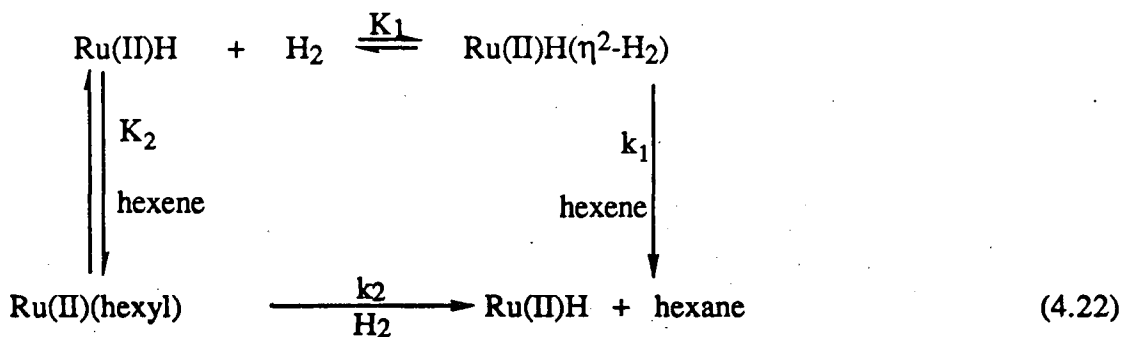
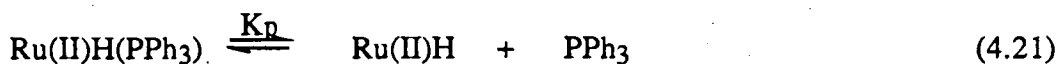
Hydrogenation systems catalyzed by **3a**:

Complex **A** was found to be relatively inactive as a 1-hexene hydrogenation catalyst in *n*-butanol under 1 atm hydrogen. It is therefore not a possible intermediate in the 1-hexene hydrogenation system catalyzed by **3a** in neat butanol, nor is it observed in the $^{31}\text{P}\{^1\text{H}\}$ NMR spectrum, observed within two hours of starting the reaction, of a hexene-hydrogenating solution with 1:7 *n*-butanol/ C_6D_6 as solvent (Fig. 4.30).

The complex $(\eta^2\text{-H}_2)(\text{PPh}_3)_2\text{Ru}(\mu\text{-Cl})_2(\mu\text{-H})\text{RuH}(\text{PPh}_3)_2$, **1a**, formed by the reaction of **3a** with several atmospheres H_2 , is also not observed in the spectrum shown in Figure 4.30, and the activity of **1a** is not high enough for traces of it to account for the activity of the **3a** system.

The complex **3a** is the main ruthenium species clearly indicated in the spectrum shown in Figure 4.30, the period of acquisition being from 0.5 to 2 h from the start of the 1-hexene hydrogenation reaction. Although the appearance of the ^{31}P NMR spectrum is very similar to that of the butanol/ C_6D_6 solution of the starting complex **3a**, there is a very low intensity broad resonance in the δ 58 - 68 range, in addition to weak resonances at δ 58 and 42, and any of these may be associated with intermediates in the catalysis. There is no indication of the presence of PPh_3 to support the proposal (sect. 4.1) of a pre-equilibrium loss of PPh_3 to account for the inverse dependence on added PPh_3 , the approach toward

half-order in ruthenium dependence at higher ruthenium concentrations, and the first-order ruthenium dependence in the presence of added phosphine. However, the dissociated PPh_3 may undergo a subsequent reaction; or it may be that free phosphine is not observed because concentrations of catalytically active species are low and also unobserved. No hydrides were observed in the ^1H NMR spectrum of a hexene-hydrogenating solution with 1:7 butanol/ C_6D_6 as solvent. But the fact that Ru(II) hydrides and dihydrogen complexes are formed in the presence of butanol under 2 - 3 atm H_2 , makes it likely that they are also formed under 1 atm H_2 , though perhaps at concentrations too low to be observed. It is therefore proposed that an intermediate Ru(II) hydride is initially formed, which can undergo a reversible phosphine dissociation, and that the dissociated ruthenium species is involved in the catalytic hexene hydrogenation cycle. A modification of the mechanism outlined in equations 4.7 and 4.8 is therefore proposed:



The question was raised earlier concerning the accessibility of Ru(IV) in catalysis at Ru(II) centres. The general tendency of Ru(II) to form $\eta^2\text{-H}_2$ complexes (sect. 3.1), the tendency in particular of **3a** to form such complexes, at least under 2 - 3 atm H_2 (Fig. 4.3, Table 4.1), and the work discussed above on the $(\eta^2\text{-H}_2)(\text{PPh}_3)_2\text{Ru}(\mu\text{-Cl})_2(\mu\text{-H})\text{RuH}(\text{PPh}_3)_2$, **1a**, hexene hydrogenation system, where a $\eta^2\text{-H}_2$ complex seems to be involved in a

hexene hydrogenation cycle, suggest that a $\text{Ru(II)H}(\eta^2\text{-H}_2)$ intermediate is more likely than a classical Ru(IV)H_3 species.

*Hydrogenations involving $\text{RuCl}_2(\text{PPh}_3)(\text{isoPFA})$, **3b***

The reactions of **3b** with H_2 in DMA, DMA/toluene- d_8 or methanol/benzene are complex, each giving several products, at least partly owing to phosphine ligand redistribution. Not all the products have been identified. Two products, which are considered in chapter 3, are well-established as **1a** and $(\eta^2\text{-H}_2)(\text{isoPFA})\text{Ru}(\mu\text{-Cl})_2(\mu\text{-H})\text{RuH}(\text{PPh}_3)_2$, **4**, and are among the products formed in the presence of DMA; **4** is also formed in methanol/benzene, along with $\text{H}_2\text{N}(\text{CH}_3)_2^+\text{Cl}^-$ and other products, one being a black-red phosphine ruthenium hydride, **Y**. In this reaction, the amine functionality of the isoPFA almost certainly accepts a proton, as judged by the formation of $\text{H}_2\text{NMe}_2^+\text{Cl}^-$, and promotes a 'heterolytic' H_2 reaction. It is important to note that, in the absence of base, the complexes **3a** and **3b** react with hydrogen in butanol or methanol/benzene to give, among other products, the dinuclear $\eta^2\text{-H}_2$ complexes **1a** and **4**, respectively. In contrast, the reactions with hydrogen of the complexes, $\text{Ru}_2\text{Cl}_4(\text{PR}_3)_4$ ($\text{R} = \text{Ph}$, *p*-tol), **2** (**a**, **b**), to give such dinuclear $\eta^2\text{-H}_2$ complexes, require Proton Sponge[®], a stronger base than DMA. This difference in reactivity toward H_2 between the complexes of type **3**, and the complexes of type **2**, must be in part related to involvement of the isoPFA amine functionality in promoting reaction with H_2 . This isoPFA amine involvement probably occurs in DMA as well, although isoPFA fragments were not identified in this system.

Hydrogenation of 1-hexene catalyzed by $\text{RuCl}_2(\text{PPh}_3)(\text{isoPFA})$, **3b**:

The $^{31}\text{P}\{^1\text{H}\}$ NMR spectrum (Fig. 4.31) of a hydrogenating system with 1:1 DMA/ C_6D_6 as solvent, shows **3b** to be the main ruthenium species present, with minor resonances at δ 100.1, 48.2, 26.2, 15, and possibly a weak, broad resonance at $\delta \sim 63$. The minor signals may be related to intermediates in the catalytic cycle, but have not been identified. The similarities in reactivity toward H_2 , between **3a** and **3b**, and the similarity

of $[Ru]_T$, $[H_2]$ and [hexene] dependences of the rates of 1-hexene hydrogenation for these complexes, suggest a mechanism similar to that proposed for **3a** in equations 4.21 and 4.22. Again, free Ph_3PO , but no free PPh_3 , is seen to be present (Figure 4.31).

*Hydrogenation of prochiral substrates catalyzed by $RuCl_2(PPh_3)(PPFA)$, **3a**, and $RuCl_2(PPh_3)(isoPFA)$, **3b***

The catalytic hydrogenation experiments on prochiral substrates, using the complexes of type **3**, were undertaken at elevated pressures, because the earlier studies²⁵ had found the **3a**/butanol system to be ineffective at 40 °C under 1 atm H_2 for the hydrogenation of disubstituted olefins, including α -*N*-acetamidoacrylic acid. At 1000 psig H_2 , the systems summarized in Table 4.2 catalyze the hydrogenation of the prochiral terminal olefins, itaconic acid, $CH_2=C(COOH)CH_2COOH$, α -*N*-acetamidoacrylic acid, $CH_2=C(COOH)NHCOMe$, and also the internal olefin, (*E*)- α -*N*-acetamidocinnamic acid, $CHPh=C(COOH)NHCOMe$. Although the number of substrates tried was limited, the lack of any chiral induction in olefinic acid systems is not encouraging. One obvious possible reason for lack of asymmetric induction is that the active species is not chiral. Experiments described earlier on the reactions of the complexes of type **3** with 2 - 10 atm H_2 in the absence of substrates showed that redistribution of phosphine ligands occurs in butanol or benzene/methanol solutions, leading to the formation of dinuclear η^2-H_2 complexes. The formation of $(\eta^2-H_2)(PPh_3)_2Ru(\mu-Cl)_2(\mu-H)RuH(PPh_3)_2$, **1a**, for example, in the olefinic acid hydrogenation systems, could account, in whole or in part, for the lack of chiral induction. In section 4.1 and elsewhere,³ questions were raised concerning the selectivity of catalytic hydrogenation systems containing P-N chelating ligands, compared to P-P and N-N systems. The systems show a decided preference for hydrogenation of disubstituted olefinic acids over sterically similar ketones, which are, by definition, disubstituted. Because of the degree of phosphine ligand redistribution that can occur in the reactions of

the complexes of type **3** with hydrogen in the absence of substrate, however, the evident selectivity of these systems for olefins over ketones must be interpreted with caution; it is possible that P-N ligands are not bonded to the catalytically active metal centre.

Chapter 5

Reactions of $\text{RuCl}_2(\text{PPh}_3)(\text{isoPFA})$ and derivatives with methanol

5.1 Introduction

The homogeneous dehydrogenation of alcohols by ruthenium, and other transition metal complexes, has been known for over twenty years.^{111,112,113,114} Indeed, reviews²⁻⁴ have listed many solvents, including water, glycols, aldehydes, amides, carboxylic acids, ethers and amines, that have been shown to undergo dehydrogenation by reaction with transition metal complexes. Dehydrogenation of these hydrogen donors is often facilitated by the presence of unsaturated organic substrates, acting in the role of hydrogen acceptors; the above-mentioned reviews²⁻⁴ list many examples of such catalytic hydrogen transfer systems. The acceptors, or substrates, have been most often carbonyl-containing compounds, but alkenes, imines⁴ and alkynes¹¹⁵ have also been used.

There are also many examples of decarbonylation of solvents by metal complexes, and this subject has been reviewed.¹¹⁶ Generally, in their reactions with alcohols, metal halides or halide complexes, often of platinum metals and containing also phosphine or arsine ligands, generate metal hydrido and hydrido-carbonyl complexes.³ These reactions are often base-assisted, with the base neutralizing the hydrohalic acid formed in the reaction. For example:¹¹⁷



Examples of catalytic dehydrogenation of alcohols, to generate H_2 and the corresponding ketone without the need for added base or hydrogen acceptor, are those catalyzed by $[\text{M}(\text{OCOR})_2(\text{CO})(\text{PPh}_3)_2]$, where $\text{M} = \text{Os}, \text{Ru}$; $\text{R} = \text{CF}_3, \text{C}_2\text{F}_5, \text{C}_6\text{H}_5$.¹¹³

Because the present work is mainly concerned with methanol reactions, we now turn to a brief review of developments in this more specific area. Reactions of methanol with metal complexes include dehydrogenation to give hydrogen and formaldehyde (eq.

5.2) and/or related products, and decarbonylation, in which methanol is converted just into CO and hydrogen.



These processes may involve heterogeneous or homogeneous systems, may or may not be base-assisted and/or photoassisted, and may be catalytic or stoichiometric.

Before looking at details of the dehydrogenation reactions, it is useful to consider some products which are sometimes associated with the formaldehyde formed according to equation 5.2. A comprehensive review of the chemistry of formaldehyde has been compiled by Walker.¹¹⁸ Processes which lead to associated products are briefly:

(i) dimethyl acetal formation:



(ii) methyl hemiacetal formation:



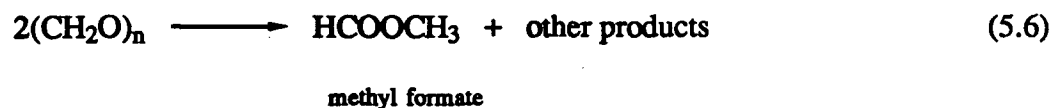
Under alkaline or neutral conditions, only the hemiacetal forms.

(iii) polymerization:

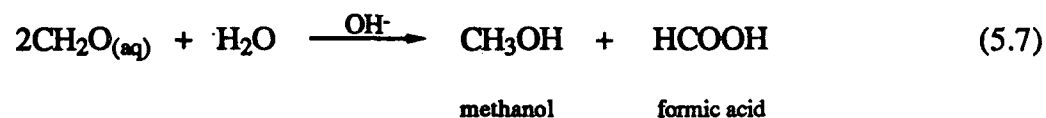
At room temperature, dry gaseous CH_2O polymerizes slowly; however, trace water promotes rapid polymerization:



(iv) thermal decomposition of paraformaldehyde:



(v) the Cannizzaro reaction:



which occurs via:



(vi) Condensation to give glycolic aldehyde:



glycolic aldehyde

In turn, process (vi) can lead to other products and even sugar-like derivatives; this process, however, is favoured more by the weaker alkaline earth bases, whereas the Cannizzaro reaction is favoured by a stronger base, such as KOH. Many of these processes listed under (i) - (vi) were considered in the present work during the search for organic products of the methanol dehydrogenation reactions.

Heterogeneous dehydrogenation of methanol to give formaldehyde, by means of high temperature air-oxidation over a metal catalyst has been known for 120 years;¹¹⁹ production of methyl formate by passing methanol vapour over copper metal at 250 °C was reported in 1916.¹²⁰ The air-oxidation of methanol, however, results in the formation of water:



and, as seen from equation 5.5, formaldehyde and water can react to form polymeric formaldehyde. These processes are similar to heterogeneously catalyzed dehydrogenation reactions of higher alcohols.

The interests in the homogeneous, solution, dehydrogenation of methanol according to equation 5.2 are that relatively mild conditions can be used, and also the formaldehyde product can be water-free and therefore stable against polymerization.

It was only recently, in 1985, that the first reports of homogeneous catalytic dehydrogenation of methanol appeared. At that time, there appeared reports of

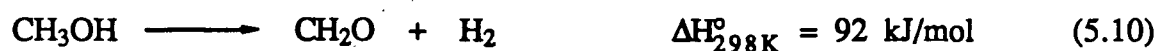
photocatalytic dehydrogenation of methanol, initially to formaldehyde, using rhodium and palladium catalysts,^{115,121} and in the same year from the same group¹¹⁴ came the first reports of thermal dehydrogenation of methanol to formaldehyde using homogeneous catalysts, formed from $[\text{Ru}_2(\text{OAc})_4\text{Cl}]$ and the tertiary phosphines, PR_3 ($\text{PR}_3 = \text{PPh}_3$, PEtPh_2 , PEt_2Ph). The thermal dehydrogenations were carried out in anhydrous methanol at 66 °C. Addition of acetic acid enhanced the rate, giving at best initial turnover frequencies of about 1 h^{-1} for the first 17 h. The initial organic product was formaldehyde and its dimethyl acetal, but this was gradually converted into secondary products including methyl formate. Deactivation of the PPh_3 -containing catalyst was associated with formation of the carbonyl complex $\text{RuHCl}(\text{CO})_2(\text{PPh}_3)_2$.

Maitlis' group¹²² reported the dehydrogenation of methanol, again in the absence of base or hydrogen acceptor, catalyzed by $\text{RuCl}_2(\text{PPh}_3)_3$, but at a higher temperature than used by Saito's group.¹¹⁴ The main ruthenium species identified in this case¹²² at the end of the catalysis was the dinuclear cation, $[\text{Ru}_2(\mu\text{-H})(\mu\text{-Cl})_2(\text{CO})_2(\text{PPh}_3)_4]^+$, with small amounts of other species being tentatively identified as $\text{RuHCl}(\text{CO})(\text{PPh}_3)_3$ and $\text{RuCl}_2(\text{CO})_2(\text{PPh}_3)_2$. In contrast to the results from Saito's group,¹¹⁴ the predominant organic product was methyl formate. However, the apparent selectivity of Maitlis' group's system for methyl formate may be due more to the higher temperature (150 °C versus 66 °C) than to the difference in catalyst.

The most recent report¹²³ of catalytic hydrogen production from methanol employed $\text{RuH}_2(\text{N}_2)(\text{PPh}_3)_3$, $\text{RuH}_2(\text{PPh}_3)_4$, $\text{RuH}_2(\text{H}_2)(\text{PPh}_3)_3$ or $\text{K}[\text{RuH}_3(\text{PPh}_3)_3]$, at 150 °C, or $[\text{Rh}(\text{bipy})_2]\text{Cl}$ at 120 °C. The reactions required the presence of NaOH base, and illumination enhanced the rate. Without illumination, turnover rates were $6 - 8 \text{ h}^{-1}$ for the first two hours. Surprisingly, the organic products were not reported, nor were the ruthenium products specifically, although Morton *et al.*¹²³ reported that the decarbonylation product, $\text{RuH}_2(\text{CO})(\text{PPh}_3)_3$, was observed after the catalysis, in the case of higher alcohols. Both this group and that of Halpern¹²⁴ have reported the formation of the

dihydrogen complex, $\text{RuH}_2(\text{H}_2)(\text{PPh}_3)_3$ via abstraction of hydrogen from higher alcohols by the $[\text{RuH}_3(\text{PPh}_3)_3]^-$ ion, and this may well occur in the case of methanol as well.

Reports of transfer hydrogenation, using methanol as the hydrogen source, preceded the discovery of methanol dehydrogenation by many years. The earliest report¹²⁵ of homogeneous methanol hydrogen transfer was in 1967, using platinum metal complexes as catalysts. There are a few other reports,¹²⁶ most recently those of Smith and Maitlis.^{127,128} The dehydrogenation of methanol, in the absence of a hydrogen acceptor, is highly endothermic:¹²⁷



Only the low solubility of hydrogen, leading its easy removal from solution, and the increase in entropy of the process, make the homogeneous dehydrogenation of methanol feasible. The participation of a hydrogen acceptor, however, makes the dehydrogenation considerably more favourable. The enthalpies for the process:



for several alcohols have been calculated:¹²⁸

alcohol	$\Delta H_{298\text{K}}^\circ$ (kJ/mol)
2-propanol	-25.9
ethanol	-3.8
1-propanol	+1.3
methanol	+21

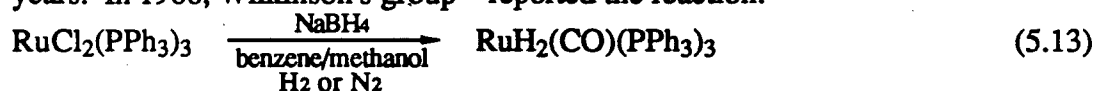
Thus, the participation of cyclohexanone as a hydrogen acceptor makes the dehydrogenation of methanol less endothermic by ~70 kJ/mol; yet, compared with these other alcohols, methanol is not a promising hydrogen source. The rates of transfer hydrogenation from methanol are also much lower than corresponding rates for higher alcohols.^{125, 129} For example,¹²⁹ for the reduction of cycloheptene by various alcohols in toluene, catalyzed by $\text{RhH}(\text{PPh}_3)_4$, the relative rates were 2-propanol (200) > ethanol (8) >

methanol (1). Similar trends are observed for dehydrogenation of alcohols in the absence of a hydrogen acceptor.¹²³ While higher alcohols have thus received more attention as hydrogen sources, Smith and Maitlis¹²⁷ have maintained that methanol still holds certain advantages over gaseous hydrogen and other alcohols, namely:

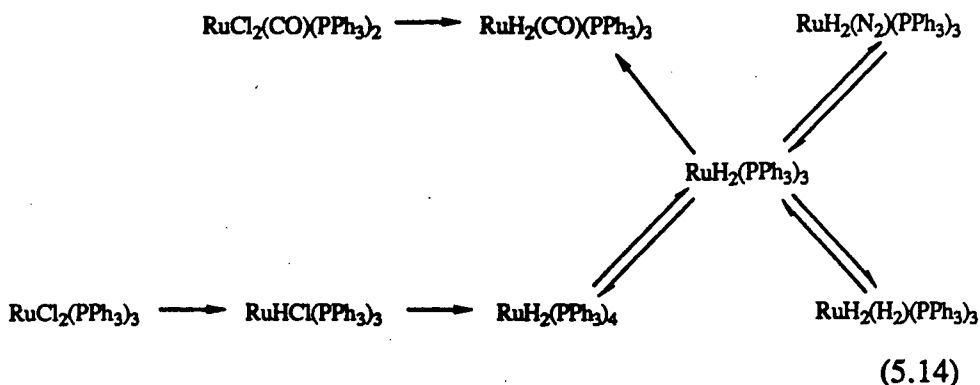
- (i) methanol is more easily handled than H₂.
- (ii) the local concentration of reductant is several orders of magnitude higher for methanol than for H₂. Thus, while the solubility of hydrogen gas in organic solvents is typically $\sim 3 \times 10^{-3} \text{ M atm}^{-1}$ at 20 °C, methanol contains, potentially, 49.4 mol H₂/L based on the reaction:

$$\text{CH}_3\text{OH} \longrightarrow \text{CO} + 2\text{H}_2 \quad (5.12)$$
- (iii) there are potentially 2 mol H₂/mol CH₃OH, compared with 1 mol H₂ for other alcohols, and
- (iv) methanol is relatively cheap (per mol H₂), and is likely to remain so.

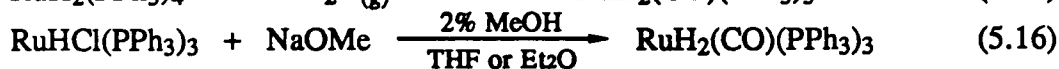
Examples of decarbonylation of methanol are scant, but have been known for many years. In 1968, Wilkinson's group⁶⁸ reported the reaction:



This same dihydrido-carbonyl has been produced from several different reactions between methanol and ruthenium complexes (as discussed below), and was mentioned above as appearing in alcohol dehydrogenation systems catalyzed by several ruthenium hydrides (e.g., RuH₂(N₂)(PPh₃)₃ in NaOH/alcohol solution).¹²³ Smith and Maitlis have related a series of complexes by the reaction scheme shown below for his RuCl₂(PPh₃)₃/methanol system in the absence of base:



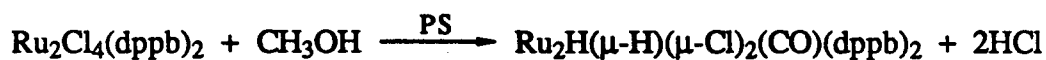
The $\text{RuH}_2(\text{CO})(\text{PPh}_3)_3$ species is also formed by stirring $\text{RuH}(\text{C}_6\text{H}_4\text{PPh}_2)(\text{PPh}_3)_2(\text{Et}_2\text{O})$ in methanol at room temperature for several hours,⁹¹ and also in the following reactions:⁹⁰



Other examples of reactions generating $\text{RuH}_2(\text{CO})(\text{PPh}_3)_3$ are given elsewhere.^{130,131} The ubiquity of this dihydrido-carbonyl complex suggests it is a ruthenium sink in these alcohol reactions, as indicated by its irreversible formation in equation 5.14.

Another common hydrido-carbonyl formed in methanol systems is

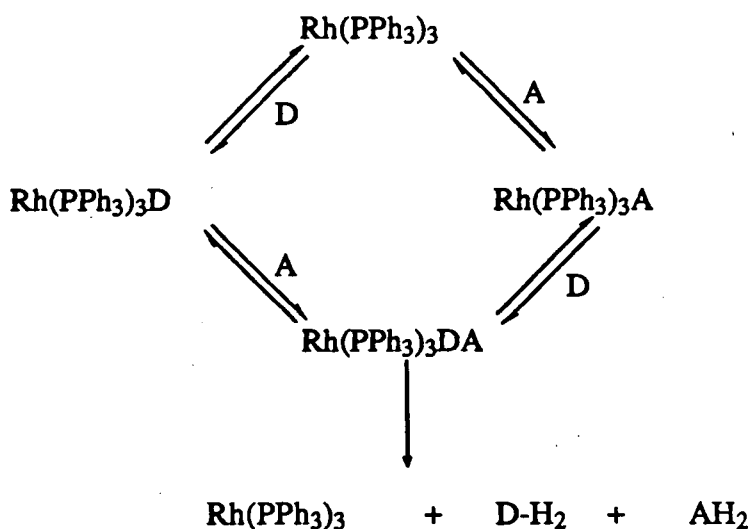
$\text{RuHCl}(\text{CO})(\text{PR}_3)_3$; for example, Saito's group¹¹⁴ reported that $\text{RuHCl}(\text{CO})(\text{PEtPh}_2)_3$ was formed quantitatively from $\text{Ru}(\text{OAc})\text{Cl}(\text{PEtPh}_2)_3$ solutions that had lost their catalytic activity for methanol dehydrogenation. As mentioned previously, the analogous $\text{RuHCl}(\text{CO})(\text{PPh}_3)_3$ species, along with $\text{RuCl}_2(\text{CO})_2(\text{PPh}_3)_2$, was tentatively identified by Maitlis' group¹²² as being formed from $\text{RuCl}_2(\text{PPh}_3)_3$ in methanol at 150 °C, along with the dinuclear, cationic complex, $\text{Ru}_2(\mu\text{-H})(\mu\text{-Cl})_2(\text{CO})_2(\text{PPh}_3)_4^+$. The reaction of $\text{RuCl}_2(\text{PPh}_3)_3$ with alcohols to give $\text{RuHCl}(\text{CO})(\text{PPh}_3)_3$ via the intermediate $\text{RuHCl}(\text{PPh}_3)_3$ has also been reported.¹³² Thorburn¹³³ obtained a neutral, dinuclear hydrido-carbonyl by the action of Proton Sponge[®] and methanol on $\text{Ru}_2\text{Cl}_4(\text{dppb})_2$. He proposed the following stoichiometry:



(5.17)

Mechanistic Studies

Many papers have appeared on the subject of the mechanism of transfer hydrogenation, and this subject will now be reviewed briefly. The mechanism of transfer hydrogenation is still poorly understood; for example, publications by Beaupere *et al.*^{134,135,136} have featured mechanistic studies on catalytic hydrogen transfer to α,β -unsaturated ketones using alcohols as the hydrogen source. Listed are 21 references, appearing between 1975 and 1983, which describe attempts to clarify the mechanism of transfer hydrogenation reactions using various acceptors, donors and catalysts. It is stated that¹³⁴ "usually, the equations describing the postulated reaction schemes are oversimplified and result only in the determination of product-formation rate constants." Details of the various steps depend on the catalyst, the donor (D), and acceptor (A) involved, but generally two main routes for hydrogen transfer from D to A, to give D-H₂ (i.e., D less 2 H atoms) and AH₂, have been proposed: the donor (D) route and the acceptor (A) route,² and are exemplified by a RhH(PPh₃)₄ system, studied by Beaupere *et al.* The active species in the cyclic part of the mechanism, after initial phosphine dissociation and transfer of hydride atoms from two RhH(PPh₃)₄ molecules to a single A,¹³⁷ is thought to be Rh(PPh₃)₃, and the D and A routes are outlined below:



The $\text{RhH}(\text{PPh}_3)_4$ catalyzed reduction of cyclohexenone, in the absence of base by 1-phenylethanol in toluene at 40 °C under argon, was sensitive to the mixing order.¹³⁸ The rate was fastest when alcohol and catalyst were mixed first, followed by addition of the acceptor, cyclohexenone; slowest when acceptor and catalyst were mixed first, followed by addition of the donor alcohol; and in between when the catalyst was mixed with a donor-acceptor mixture. With cyclohexenone, the D route was considered to be the faster one. Also, whereas transfer of the β -hydrogen of the alcohol has usually been considered rate determining in alcohol hydrogen transfer systems,^{139,140} O-H bond cleavage was the rate-determining step in the above system,^{137,141} and the hydroxyl H atom is transferred to the α -C atom of the ketone. This concerted H transfer, of course, requires the simultaneous coordination of both donor and acceptor. Spogliarich *et al.*¹⁴² later reported on the base-assisted transfer hydrogenation of cyclohexanone catalyzed by $[\text{Rh}(\text{COD})\text{dppe}]^+$, using 2-propanol as hydrogen source. The catalyst was refluxed in KOH/2-propanol solution, and then the substrate added—the same optimum order of addition found by Beaupere *et al.* In contrast, Kvintovics *et al.*¹⁴³ found that if the ketone was not added first, Rh metal precipitated in a similar transfer hydrogenation from 2-propanol to acetophenone catalyzed by an *in situ* rhodium catalyst containing *N*-acetyl-(*S*)-methionine-(*R,S*)-sulfoxide, in the presence of KOH. This comparison illustrates the contrasting dependence of optimal order of addition of reactants on catalyst, donor and acceptor; in the Rh-phosphine systems, the alcohol is presumed to form an active complex with the catalyst. In the rhodium-sulfoxide case, however, the interaction between basic 2-propanol and Rh complex gave reduction to metal.

In contrast to the concerted D \longrightarrow A hydrogen transfer proposed for the $\text{RhH}(\text{PPh}_3)_4$ system, hydrogen transfer via hydride formation from catalyst and alcohol has been inferred for other systems.^{131,132} In one system,¹⁴⁴ preference for hydride formation versus concerted hydrogen transfer depended on the choice of hydrogen

acceptor. With hydrogen transfer from 1-phenylethanol to the α,β -unsaturated ketone, benzylideneacetophenone, the following steps were inferred:

- (i) phosphine dissociation,
- (ii) coordination of acceptor,
- (iii) coordination of the alcohol and formation of a metal alkoxide,
- (iv) a rate-determining hydrogen transfer from the alkoxide ligand to the coordinated ketone
and
- (v) release of product via protonation.

With dibenzylketone as acceptor, however, kinetic studies indicated that while steps i to iii were similar to those of the previous case, step iv appeared to involve hydrogen transfer from alkoxide ligand to the metal. The coordinated hydride was then thought to attack the coordinated ketone with the lower reduction potential.

The above discussion has been limited to a description of general proposals and scattered results from studies on hydrogen transfer from higher alcohols. There are no examples of mechanistic studies on methanol hydrogen transfer. Smith and Maitlis have speculated on possible intermediates in the $\text{RuCl}_2(\text{PPh}_3)_3$ /methanol hydrogen transfer system, but lacked data to distinguish between the possibilities.¹²⁸

For the dehydrogenation of methanol catalyzed by $\text{Ru}(\text{OAc})\text{Cl}(\text{PPh}_3)_3$, the proposed mechanism¹⁴⁵ is analogous to that described for higher alcohols using $\text{M}(\text{OCOR}_F)_2(\text{CO})(\text{PPh}_3)_2$ ($\text{M} = \text{Ru}, \text{Os}$; $\text{OCOR}_F =$ a perfluorocarboxylate):¹¹³

- (i) solvolysis of the catalyst (alkoxide formation):



- (ii) β -elimination from the alkoxide ligand:



- (iii) acid attack on the hydride intermediate:



where R, R' = alkyl; L = ligands; L' = carboxylate. The methanol case is depicted in Figure 5.1.¹⁴⁵ As mentioned earlier, HOAc addition enhanced the dehydrogenation rate, while carbonyl formation was associated with catalyst deactivation. Addition of paraformaldehyde also deactivated the catalyst to the hydrido-carbonyl, by accelerating the process:



It was therefore concluded that facile liberation and difficult coordination of CH_2O was required to increase turnover frequency to H_2 and CH_2O , and, at the same time, avoid deactivation to the hydrido-carbonyl via decarbonylation of the formaldehyde (see Fig. 5.1). If incipient metal-carbon bond formation is allowed to occur, then CH_2O would

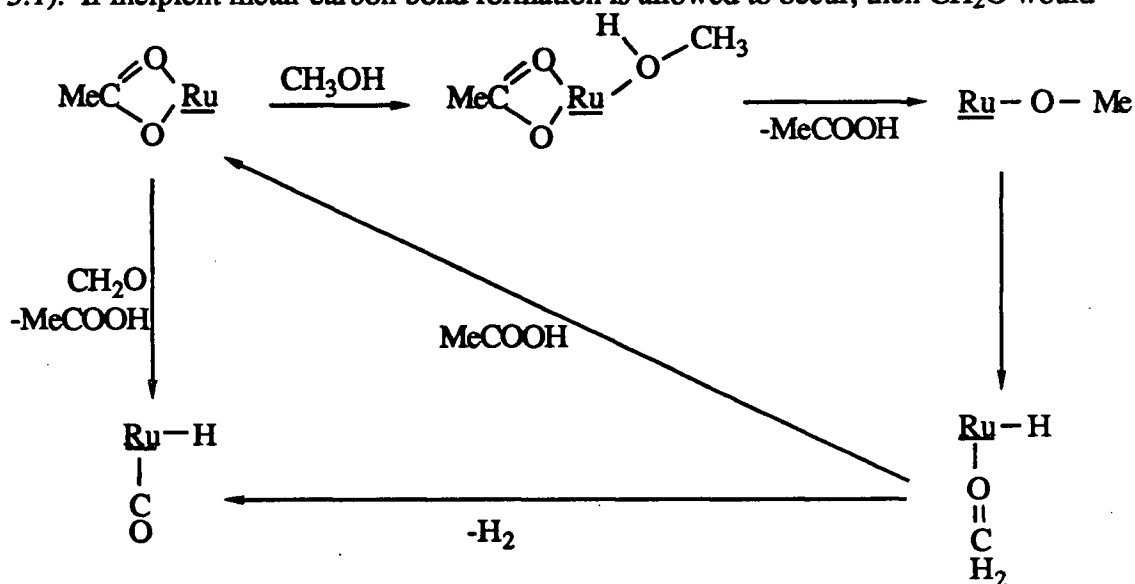


Figure 5.1 Scheme proposed in reference 145 for the dehydrogenation of methanol catalyzed by $\text{RuCl}(\text{OAc})(\text{PPh}_3)_3$.

probably react via coordination of the CH₂O through the carbon atom, followed by hydrogen transfers to the metal to give, finally, the hydrido-carbonyl and H₂.

Intermediates for the process:



were not specifically suggested. Some MO calculations were carried out to determine the relative tendencies toward metal-carbon bond formation for the CH₂O moieties coordinated to ruthenium in [RuHCl(CH₂O)(PH₃)₃] and for rhodium in *trans*-[Rh(CH₂O)(PH₃)₂].¹⁴⁵ As the Ru-O-C angle was decreased from 180°, initially repulsive M-C interactions gradually gave way to attractive M-C interactions. The Ru-C repulsive interactions were greater than the corresponding Rh-C repulsive interactions. Thus, theoretical calculations indicate that the rhodium complex would have the greater tendency toward carbonyl formation and concomitant loss of catalytic dehydrogenation activity. Furthermore, the calculations showed that $p\pi(\text{C}) \leftarrow d\pi(\text{M})$ interactions were important in promoting the formation of the M-CO bond, and this was considered to be favoured for Rh(I) compared to Ru(II). These calculations were consistent with the generally observed higher methanol dehydrogenation activity for ruthenium(II) versus rhodium(I) complexes.^{114,122,123,145}

These studies on methanol dehydrogenation and decarbonylation are also of interest in connection with mechanistic work on the Fischer-Tropsch reaction:



Germane to all these reactions, organometallic chemistry has provided structural precedents, which act as models for the proposed catalytic intermediates. Thus, examples of methanol-containing complexes of ruthenium have been characterized,^{90,146} as have η^2 -CH₂O and formyl complexes of osmium,¹⁴⁷ iron¹⁴⁸ and more tentatively, ruthenium,⁹⁰ and methoxo complexes of ruthenium^{149,150,151} as well as other alkoxo complexes of the iron triad.^{152,153}

5.2 Experimental

Experiments on the effects of various solvents, added PPh₃, and air, respectively, on visible spectra of RuCl₂(PPh₃)(isoPFA), 3b, in solution

The visible spectrum was recorded for a solution made up of **3b** (2.7 mg, 0.0033 mmol) in ~3 mL of CHCl₃ under Ar. Added PPh₃ (20 mg, 0.076 mmol) was then dissolved in this solution and the visible spectrum recorded again. The visible spectrum of an identical solution, but without added phosphine, was also recorded before and after exposure to air for a few minutes at ambient temperature.

The visible spectrum of **3b** in THF was recorded as follows: the complex **3b** (17 mg, 0.020 mmol) was dissolved in freeze/thaw-degassed THF (1 mL) by heating to reflux temperature under nitrogen in the anaerobic cell shown in Figure 2.4, and the visible spectrum recorded within 0.5 h at ambient temperature. A similar experiment was carried out with the differences being that the solution was made up of **3b** (6.9 mg, 0.0085 mmol) in THF (1.5 mL)/MeOH (0.5 mL).

Experiment on the effect of styrene on 3b in solution

Complex **3b** (~30 mg, 0.035 mmol) and nitrogen-purged styrene (0.035 mmol) were dissolved under nitrogen in ~1 mL nitrogen-purged CDCl₃ at ambient temperature in a 5 mm NMR tube, and the ³¹P{¹H} NMR spectra recorded. A similar experiment was carried out with a higher styrene:Ru ratio: **3b** (~60 mg, 0.070 mmol), styrene (0.90 mmol).

Reactions of RuCl₂(PPh₃)(isoPFA), 3b, and the derivative, RuHCl(CO)(PPh₃)(isoPOF), 5, with methanol in the absence of added base

The preparation of the product, **5**, from the reaction of **3b** with methanol, was as described in section 2.4. The same product was obtained when the reaction was carried out with 0.005 mmol **3b** in 2 mL methanol in a sealed tube under vacuum at 100 °C for 1.5 h in the presence of 0.4 mmol 1-hexene.

The preparative reaction was also carried out in methanol-d₄ under otherwise the same conditions as described in section 2.4. The distillate from the methanol-d₄ preparation was tested for formaldehyde using the Ee griwe test¹¹⁸ and a sample submitted for GCMS analysis.

A single crystal X-ray diffraction study of the isolated complex **5** from the methanol-d₀ reaction was carried out by the crystallographic group at SFU, Burnaby, Canada.¹⁵⁴

Catalytic activity of **5** and **3b**:

(i) isomerization of 1-hexene

The complex **5** (0.004 g, 0.005 mmol) was heated overnight at 105 °C with 0.4 mmol 1-hexene in 2 mL dry methanol under vacuum; at the beginning of this experiment, liquids were freeze/thaw degassed, then vacuum transferred onto the catalyst contained in a glass tube, which was then sealed. The distillate obtained after reaction was analyzed by gas chromatography using a packed column, packed with tricresylphosphate on chromosorb.

An almost identical procedure was used for the corresponding experiment with **3b** and various substrates, with the specific substrates and reaction conditions given later in Table 5.3 within the Results section (sect. 5.3). Distillates obtained after reaction were analyzed as indicated in the table.

(ii) hydroformylation of 1-hexene

The complex **5** (0.012 g, 0.015 mmol) was heated at 100 °C for 2 d with 1-hexene (0.16 mmol) in 2 mL CH₂Cl₂ under 1500 psig 1:1 H₂/CO. At the beginning of this experiment, the liquid reagents were placed in a glass liner, which was then inserted into a steel bomb, and these liquids then purged with a flow of nitrogen gas prior to addition of the solid catalyst; the bomb was then sealed, flushed at least twice with H₂/CO and filled with this gaseous mixture to the pressure indicated above. The distillate obtained after reaction was analyzed by gas chromatography using an OV-17 column for identification of alcohol and aldehyde products, and a tricresylphosphate column for identification of hexane and hexenes.

*Reactions of RuCl₂(PPh₃)(isoPFA), **3b**, and derivatives with methanol in the presence of added base*

With Proton Sponge[®] as base:

A typical reaction at room temperature is described in section 2.4 under synthesis of **7**. Single crystal X-ray diffraction studies on two of the products of this reaction were carried out; the structure of RuHCl(CO)(PPh₃)(isoPFA), **6**, was determined by S. Rettig of this department, and the structure of RuHCl(PPh₃)(isoPFA), **7**, by J. Simpson of the University of Otago, New Zealand.⁵⁵ Distillates of reaction mixtures obtained after reaction were analyzed by the Eegriwe test¹¹⁸ and by GCMS.

The gas evolved during a similar reaction was monitored in a gas evolution experiment using the standard procedure and apparatus indicated in chapter 2. Some of complex **3b** (0.037 g, 0.046 mmol) was shaken with Proton Sponge[®] (0.040 g, 0.19 mmol) in methanol (10 mL) under ~800 mm Hg nitrogen at 30 °C for more than 4 h, and the gas evolution measured at intervals.

With KOH as base:

A typical reaction of **3b** with methanol in the presence of KOH, with KOH:Ru = 1.0, to give **6** as the main ruthenium species, is described in section 2.4.

Some reactions employing a KOH:Ru mole ratio of >1:1 were carried out in a similar manner. Wine-coloured supernatants obtained from such reactions were analyzed by column chromatography, in experiments such as follows: the complex **3b** was heated at 80 °C under nitrogen in previously freeze/thaw-degassed KOH/methanol solution (3 mL of 1.8 M \equiv 5 mmol KOH) till the green, insoluble **3b** had completely reacted, and a wine-coloured solution was produced, along with a white precipitate, which was filtered off and shown to be $\text{RuH}_2(\text{CO})(\text{PPh}_3)_3$. The filtrate was vacuum-pumped and, as the solvent decreased, more white precipitate was deposited and this was filtered off to increase its yield. When the solvent volume reached about 0.5 mL, a red deposit was visible and so the remaining red supernatant, containing a high concentration of KOH, was decanted and discarded. The red solid was dissolved in methanol (~3 mL), and nitrogen-purged, deionized water (~50 mL) added to deposit the dissolved red material. This red deposit was washed with nitrogen-purged deionized water and dried under vacuum, before dissolving in a minimal amount of acetone prior to chromatography, initially in air; conditions were optimized using TLC (silica). Yellow band(s) could be eluted with acetone, but methanol was required to move red materials—a total of four red bands. The first eluted red methanol solution increased in intensity with increasing exposure of the initial acetone solution to air. Therefore, subsequently the column was prepared by removing air from the silica by vacuum-pumping, and thereafter keeping the silica under nitrogen. All solvents were purged with nitrogen and all column operations were conducted under nitrogen. The column was packed with silica and methanol (spectro-grade). An acetone solution of the red solid was transferred to this column; two yellow bands were first eluted with acetone, then three red bands with methanol, then two 'weak' yellow bands (which were discarded), then finally a fourth red band was collected. The

solvent was removed from these fractions by evaporation under vacuum and spectroscopic data recorded for the CDCl_3 extracts of the residues.

On recrystallization of the white precipitate of $\text{RuH}_2(\text{CO})(\text{PPh}_3)_3$ from dichloromethane/methanol, a few single crystals of the dichloromethane solvate of $\text{RuH}_2(\text{CO})(\text{PPh}_3)_3$ suitable for X-ray analysis were obtained on one occasion.

Also, a series of similar reactions, but with styrene also present, were carried out to show variations in appearance and styrene-hydrogenating activity with increasing KOH concentration, and the procedure in detail was as follows: Some of complex **3b** (0.006 g, 0.007 mmol), and a freeze/thaw degassed mixture of dry methanol, KOH/methanol solution (to give a total of 1 mL methanol) and styrene (0.087 mmol) were mixed under nitrogen in a Carius tube equipped with a septum for GC sampling. The tube, with the Teflon valve closed, was partially immersed in a thermostatted oil bath at about 80 °C; the clock was started, and the reaction mixture samples were injected at intervals directly into a Varian A-90 GC equipped with trap for dissolved and suspended solids, and a carbowax or SE-30 packed column.

*Experiments on the reaction of $\text{RuCl}_2(\text{PPh}_3)(\text{isoPFA})$, **3b**, with KOH/methanol, in THF in the presence or absence of styrene*

The KOH/methanol solution was made by dissolving KOH (7 g) in dry methanol (35 mL) under nitrogen and the suspended carbonate was filtered off. The KOH concentration of the filtrate was determined by titration of an aliquot (typically, 180 μL of KOH/methanol solution dissolved in 40 mL water) against potassium hydrogen phthalate (12-20 mg.) dissolved in water. The KOH/methanol solution thus prepared (~3 M) was stored under nitrogen and the titration repeated occasionally to monitor any change in concentration. Generally the concentration remained unchanged, at least over a couple of weeks, and even slight yellowing of the solution did not noticeably affect either the KOH concentration or the consistency of subsequent kinetic experiments.

A ^1H NMR experiment was carried out to determine if there is any reaction between methanolic KOH and THF at ambient temperature, as follows: THF (3 mL), 0.1 mL of 3 M KOH/MeOH and 0.9 mL of MeOH were mixed at ambient temperature under air. The ^1H NMR spectrum of this mixture in C_6D_6 was recorded after 2 h, and again after 4 d.

The title reactions were set up using one of the tubes shown in Figures 2.3 and 5.2 connected to a double-manifold vacuum system. The reactions were conducted in 3:1 THF/methanol, the two components being separately prepared according to the following general procedure: a weighed amount of **3b** was dissolved in section "B" of the specially designed tube (Fig. 2.3 or 5.2, Teflon valve closed) by refluxing, with a hot-air gun as heat source, under nitrogen in freeze/thaw-degassed THF (or in a THF/styrene mixture, when styrene was involved; the reactions involve dehydrogenation of methanol and styrene

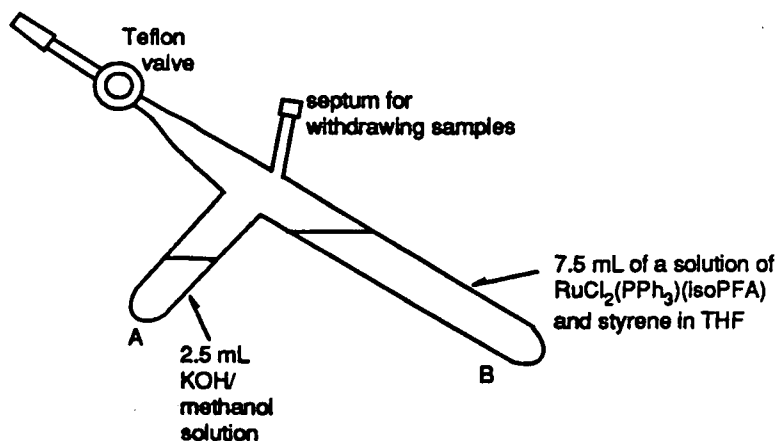


Figure 5.2 Glass tube used to monitor changes in the styrene/ethylbenzene ratio during transfer hydrogenation of styrene. Solutions are shown as they would appear before mixing.

was used as an appropriate substrate, being converted to ethylbenzene). To the THF solution thus formed, phosphine (PPh_3 or isoPFA) could be added, if necessary, through the Teflon valve opening. The tube was clamped at approximately the angle indicated (Figs. 2.3, 5.2), the THF solution was then frozen in section "B" of the tube and the required volume of KOH/methanol solution was introduced through the Teflon valve opening into section "A" of the tube. Solid potassium chloride or methanolic lithium

nitrate could also be introduced through the same opening, and also washed into section "A" with the volume of methanol required in order to bring the methanol/THF volume ratio up to 1:3. The methanol solution in section "A" was then degassed by means of three freeze/pump/thaw-cycles. The freeze/thaw cycles were applied to both sections "A" and "B" together to minimize premature mixing of the two solutions. Finally, the tube, still at the angle indicated, was brought to the desired temperature under nitrogen by immersing in a water bath, and the Teflon valve closed. The tube was removed from the vacuum line, and the reaction(s) initiated by tilting the tube to mix the two solutions.

Where styrene was used, it was important to mix the styrene with the solution of **3b** before adding the KOH/methanol solution if maximum hydrogenation was desired. Mixing the solution of **3b** with the KOH/methanol solution first, followed by addition of styrene, resulted in decreased hydrogenation rates and conversions.

Monitoring changes in the $^{31}\text{P}\{^1\text{H}\}$ NMR spectrum:

The reaction of **3b** with methanolic KOH and styrene, in methanol/THF (1:3 v/v), was carried out as described above, initially utilizing the tube shown in Figure 5.2; however, as soon as all reagents were mixed, about 1 mL of the yellow, reaction solution was transferred by a nitrogen-flushed syringe to a 5 mm NMR tube fitted with a septum and previously filled with nitrogen. The NMR tube was placed immediately into the Varian XL300 probe and the $^{31}\text{P}\{^1\text{H}\}$ NMR spectra recorded at intervals.

Monitoring changes in the visible spectrum:

Changes in the visible spectrum during the reaction were monitored using the tube shown in Fig. 2.3. Typically complex **3b** (3 mg, 0.004 mmol) was dissolved in THF, or THF/styrene (12 mL), thereby keeping the reactant concentration low to avoid subsequent clouding of the solution by the KCl that is produced in this reaction. For the same reason, the KOH concentration had to be ≤ 0.25 M (typically ≤ 1.5 mL of the 3 M KOH/methanol solution plus 2.5 mL methanol) or clouding of the solution made visible absorption measurements impossible. Even at these concentrations, a few tiny crystals of KCl did

grow in the quartz cell during the reaction, but their presence did not affect the spectral changes; their refractive index appeared to be identical to that of the reaction solution, since the crystals were completely invisible when immersed in the solution.

The reaction was monitored by setting the spectrophotometer at 605 nm, the absorption maximum of 3b, and starting the reaction (*vide supra*) and the chart drive simultaneously. When the two solutions were thoroughly mixed, the cell was placed in the thermostatted cell holder in the spectrophotometer, usually within 10 to 15 seconds of mixing at time = 0. If spectra were to be recorded at various times during a run, the spectrophotometer could be zeroed before the run, with the above cell in place, but containing merely the 3:1 THF/methanol solvent mixture. This zero-correction was done for the data of Figure 5.25, but not for the data of Figure 5.26 (sect. 5.3).

Monitoring changes in the styrene/ethylbenzene ratio:

In order to use GC to monitor the hydrogenation of styrene in some of the reactions, it was necessary to quench the reaction at various points, to allow for distillation; minimized evaporation from each sample withdrawn from the reaction mixture was also necessary, otherwise the samples gave erratic GC analyses.

The reaction was carried out in the tube shown in Figure 5.2 as described above. Typically, 3b (25 mg, 0.03 mmol) in 7.5 mL THF/styrene, containing up to 1 mL styrene (with dissolved phosphine, where applicable), in section "B" of the tube, and the KOH/methanol solution (≤ 0.8 mL of 3 M KOH/methanol solution with dry methanol added to raise the volume to 2.5 mL) in section "A", were brought to the desired temperature in a thermostatted bath, the reaction started by tipping the tube to mix the two solutions, and the timer started. Samples (~ 0.6 mL) of the reaction solution were withdrawn, by means of a syringe, through the septum with the Teflon valve closed, or through the opened Teflon valve which was subsequently closed, and immediately expelled into a small heap of solid boric acid (~ 1.5 g) in a small flask; the mixture was then swirled to quench the reaction. The flask was immediately stoppered, or sealed with Parafilm, and

chilled to minimize evaporation. The volatile fraction of the reaction mixture was vacuum transferred to another small flask and then stored in a stoppered vial until the sample could be analyzed by GC.

Monitoring gas evolution:

Depending on conditions, reactions of **3b** in basic methanol can lead to gas evolution (H_2), and this was monitored as described elsewhere^{19,20} with a flask and procedure that was modified as follows:

a) For experiments requiring a small volume ($< 100 \mu\text{L}$) of KOH/methanol solution:

First, the desired volume of THF ($\sim 6 \text{ mL}$) was introduced into the round part of the flask ("A", Fig. 5.3a.) Then a glass bucket containing the desired amount of **3b** was placed on a hook attached to a ground glass stopper, and inserted into the lower arm ("B") of the two-arm flask (Fig. 5.3a). An empty bucket was then placed on another hook attached to a ground glass stopper, this being inserted into the upper arm ("C") of the flask. The flask was then attached to the gas uptake/evolution apparatus by a narrow, spiral glass tube ("E", Fig. 5.3a), as described elsewhere.²⁰ The THF in the flask (part "A") was degassed by three freeze/pump/thaw cycles, and the flask then filled with nitrogen ($\sim 1 \text{ atm}$), and isolated from the main part of the apparatus by closing the stopcock on the narrow glass tube ("E") which connects the flask to the rest of the apparatus. The bucket containing the complex **3b** was then dropped into the THF, and portion "A" of the flask was heated, almost to reflux temperature, to dissolve the complex. When the flask was cooled to room temperature, the stopcock on the narrow tube ("E") was opened and the rest of the apparatus adjusted to allow free flow of nitrogen into the flask. The upper hook-and-stopper was then partly withdrawn from arm "C", and the required amount of freeze/thaw-degassed KOH/MeOH solution was injected by syringe into the upper bucket; the hook-and-stopper, still holding the bucket containing KOH/MeOH solution, was then

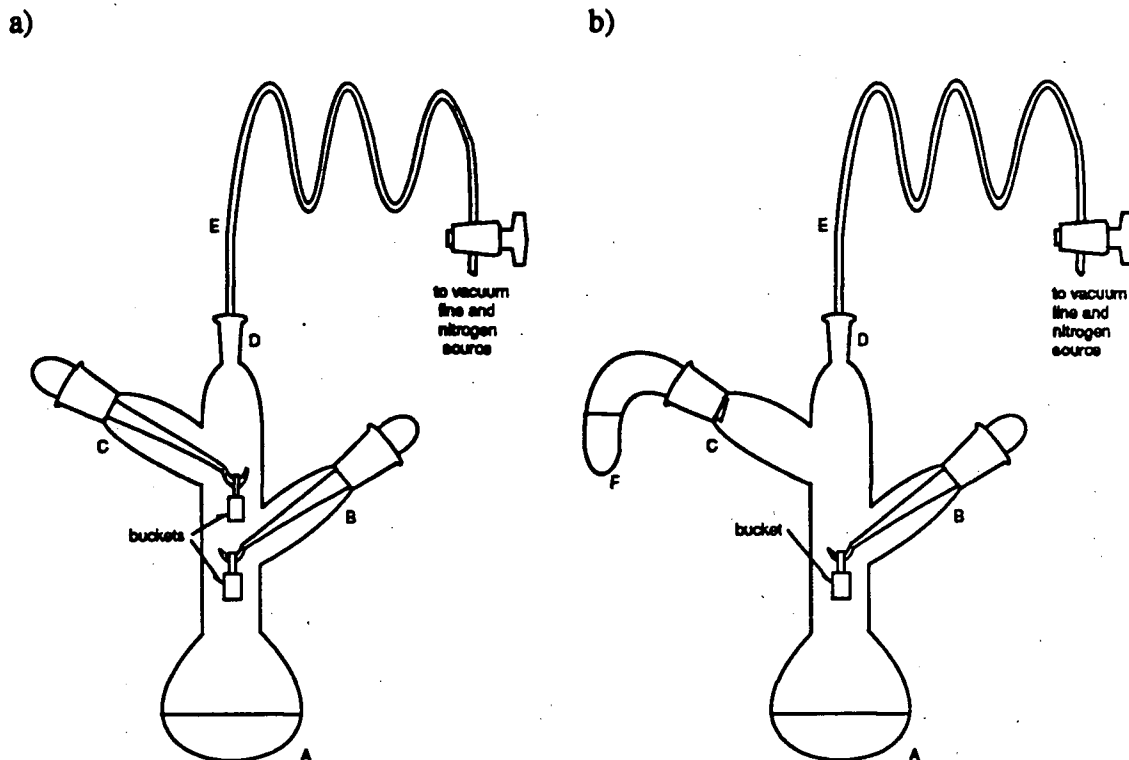


Figure 5.3 a) A 25 mL, modified gas evolution flask for following reactions between $\text{RuCl}_2(\text{PPh}_3)(\text{isoPFA})$, **3b**, in THF, and a small volume of KOH/methanol solution. b) Similar apparatus, for use with larger volumes of KOH/methanol solution.

reinserted into arm "C". The reaction was initiated by dropping the upper bucket, with its contents, into the **3b**/THF solution. The gas evolution was then followed in the usual manner.

b) For experiments requiring a larger volume (1 - 2 mL) of KOH/methanol solution:

As in (a), the desired volume of THF, and the complex **3b**, were introduced into the flask (Fig. 5.3b) at "A" and "B", respectively. A small, closed, bent tube ("F"), fitted with a ground-glass joint, and containing the desired volume of KOH/methanol solution, was then inserted into the upper arm ("C") of the flask. Next, the THF in "A", and the KOH/methanol solution in "F", were simultaneously freeze/thaw-degassed. After being degassed, the flask was filled with nitrogen (~1 atm) as in (a). The bucket containing **3b** was then dropped into the THF, and the complex dissolved by heating as in (a). The

procedure then followed closely that described in (a), the reaction being initiated by rotating the bent tube ("F") containing the KOH/methanol solution.

Procedure (a) was used for monitoring the gas evolution (H_2) for experiments in which the KOH:Ru ratio was ~ 1 . Gas evolution was monitored in one such experiment at $27^\circ C$, in the absence of styrene, in THF (6 mL)/MeOH (2 mL) with 3b (68 mg, 0.084 mmol) and KOH (0.096 mmol). After gas evolution had ceased, ruthenium complexes were isolated from this solution as described below, and the NMR spectra of the associated residue in $CDCl_3$ recorded.

Procedure (a) was also used in a related experiment at $27^\circ C$, where the KOH:Ru mol/mol ratio was 0.84, and styrene was present (styrene:Ru = 11).

Procedure (b) was used to monitor gas evolution in an experiment at $27^\circ C$ with high base and styrene concentrations (3b (28 mg, 0.035 mmol), KOH (3.8 mmol), styrene (8.7 mmol)) in THF (6.5 mL)/MeOH (2.5 mL); total volume: 10 mL. After gas evolution had ceased (time = ~ 40 min), analysis for ethylbenzene production was carried out by injecting the reaction solution directly into a GC with Carbowax column and a solute trap. A formaldehyde determination was carried out using the Hantzsch reaction and is described in a later section.

These methanol/THF reaction solutions, which had contained initially ~ 50 mg 3b in 8 - 10 mL solution, were worked up by mixing them with ~ 80 mL nitrogen-purged, deionized water. In the absence of styrene, precipitation of ruthenium-containing products occurred, and these were then filtered, dried under vacuum and analyzed in $CDCl_3$ by $^{31}P\{^1H\}$ and 1H NMR spectroscopy. Precipitation did not occur when this procedure was used for reaction solutions containing styrene; instead, separation of ~ 0.2 mL of a styrene phase less dense than the aqueous phase occurred, which was adsorbed on Celite[®] by passing the two phases through ~ 2 cm (~ 10 mL) Celite[®] in a Schlenk filter apparatus. Solvent was then removed from the adsorbed phase under vacuum, and the adsorbed residue extracted with $CDCl_3$ for analysis by $^{31}P\{^1H\}$ and 1H NMR spectroscopy.

Detection of KCl produced in the reaction of $\text{RuCl}_2(\text{PPh}_3)(\text{isoPFA})$, **3b**, with KOH/MeOH:

i) in THF:

The reaction was carried out in the general manner described above for monitoring changes in the visible spectrum, but in the tube shown in Figure 2.3. Conditions used were: $[\text{3b}] = 0.019 \text{ M}$, $[\text{KOH}] = 0.45 \text{ M}$, THF (1.0 mL), MeOH (0.33 mL), under nitrogen at ambient temperature. The reagents were mixed and the reaction monitored by recording the decay of the 605 nm band of **3b** by visible spectrophotometry. When a white precipitate, which had formed during the reaction, had settled (time = 72 min), the visible spectrum of the solution was recorded. The supernatant was decanted and the precipitate washed with acetone and dissolved in deionized water; addition of AgNO_3 solution resulted in a white precipitate, whose solubility in dilute HNO_3 was tested.

ii) in CH_2Cl_2 :

The reaction was carried out as follows: 1 mL of a $5 \times 10^{-3} \text{ M}$ solution of **3b** in degassed CH_2Cl_2 was mixed at ambient temperature under nitrogen with 2 mL of a 1.8 M KOH/MeOH solution. A white precipitate, which had precipitated within a minute after mixing, was isolated by decanting the yellow supernatant which had also formed in the first minute, recrystallized from water/acetone, dried under vacuum and submitted for elemental analysis. Anal. Calcd. for KCl: Cl, 47.6. Found: 45.8. An aqueous solution of the white solid (16 mg/100 mL) was analyzed for potassium by atomic emission at 766 nm, and the reading was compared with readings obtained for 10 and 20 mg/100 mL KCl solution standards. Solvent was removed from the decanted yellow supernatant under vacuum, and the NMR spectra recorded for the associated residue in CDCl_3 .

Formaldehyde detection:

i) in the distillate from a reaction of **3b** with KOH/MeOH in THF:

The reaction of **3b** with KOH/MeOH was carried out as follows: some of complex **3b** (30 mg, 0.037 mmol) was mixed with styrene (1.8 mmol), 0.5 mL of a 1.8 M

KOH/MeOH solution and 1.3 mL THF under nitrogen in a Carius tube, and the Teflon valve closed. The tube was heated for a couple of minutes at ~ 70 °C to dissolve the 3b complex, and then the temperature maintained at 50 °C for 5 d. The volatile components were then isolated from the reaction mixture by vacuum transfer; the Hantzsch reaction¹¹⁷ was carried out on this distillate, and the visible absorbance of the product solution at 412 nm compared with that of appropriate standards.

ii) of non-volatile CH_2O in a reaction mixture formed from a reaction of 3b with KOH/MeOH in THF:

The reaction mixture formed in the gas evolution experiment described above, with high base and styrene concentrations, was analyzed for formaldehyde content as follows: the reaction mixture was mixed with deionized water to give ~ 40 mL solution which was passed through Celite[®]; a portion (17 mL) of this aqueous solution, after several days, was filtered and neutralized with aqueous HCl. The Hantzsch reaction was carried out on this solution, and the visible absorbance (412 nm) of the yellow product solution compared with that of appropriate standards.

Experiment to detect gas phase CO by GC:

Some of complex 3b (26 mg, 0.032 mmol) was mixed under nitrogen with styrene (0.88 mmol) and a solution of KOH in methanol (2 mL, 1.8 M), in THF (5 mL) in a Carius tube equipped with a septum, and the Teflon valve closed. The complex was dissolved by heating briefly at 100 °C and then the tube was maintained at 45 °C for 25 min. A sample of the gas phase above the cooled solution was syringed onto a molecular sieves GC column (TCD detector), and the gas chromatogram compared to that for a CO gas standard.

²D NMR experiments on distillates from reactions of 3b with KOH/MeOH- d_4 and MeOH- d_1 :

These experiments were carried out to confirm that methanol was the true hydrogen source in the title reactions. The procedure was as follows: some of complex 3b (14 mg,

0.017 mmol) was mixed under nitrogen with THF (0.71 mL), styrene (0.88 mmol) and KOH/MeOH-d₄ or MeOH-d₁ (0.25 mL, 1.5 M) in the same apparatus as for the 'CO detection experiment'. Reaction was allowed to continue for 40 h at ambient temperature, and then the entire 1 mL reaction mixture was injected, in portions of 0.1 - 0.2 mL, into a Varian A-90 GC instrument equipped with a solute trap and a TCD detector. The ethylbenzene fraction was collected in a trap cooled with liquid nitrogen, and mixed with 1 mL acetone, before recording the ²D NMR (46 MHz) spectrum. The extents of hydrogenation of styrene in the MeOH-d₄ and MeOH-d₁ reactions were determined at the same time.

For reference purposes, the ²D NMR spectra of a 1:1 styrene/acetone mixture and a 1:1 ethylbenzene/acetone mixture were also recorded.

An experiment to determine what would happen to CH₂O generated in a solution similar to those used for the reactions of 3b with KOH/MeOH

Formalin solution (~50 mL of 37% CH₂O in methanol water) was mixed with KOH/MeOH solution (~50 mL, 1.5 M) and THF (~30 mL) at ambient temperature, and then the mixture neutralized with HCl_{aq}; acetone was then added until a considerable amount of white solid precipitated. About 0.5 g of this was collected, washed with water, acetone and diethylether and dried. The white solid was submitted for elemental analysis and mass spectrometric analysis.

Reactions of RuHCl(CO)(PPh₃)(isoPFA), 6, with methanol

The title complex, 6, (0.030 g, 0.037 mmol) was heated with methanol (1 mL) under nitrogen in a Carius tube at 80 - 85 °C overnight in the absence of base. Most of the yellow 6 remained undissolved. The yellow solid present after reaction was filtered off,

dried under vacuum and the ^1H NMR (300 MHz, CDCl_3 , ambient temperature, under nitrogen) of the dried solid was recorded.

Some of complex **6** (0.009 g, 0.011 mmol) was heated with KOH (0.01 mmol) in methanol (~1 mL) under nitrogen in a Carius tube partially immersed in a 80 °C oil bath overnight. The supernatant decanted from the reaction mixture was then analyzed by UV-vis spectrophotometry, and the remaining solids dried under vacuum and analyzed in CDCl_3 solution by ^1H NMR spectroscopy.

Finally, complex **6** (18 mg, 0.022 mmol) and styrene (0.88 mmol) were heated under nitrogen in freeze/thaw-degassed methanol (1.0 mL) at ~80 °C for 3 d and the solution analyzed by GC to determine the amount of hydrogenation of styrene to give ethylbenzene.

5.3 Results

Figure 5.4 shows the visible spectrum of **3b** ($\lambda_{\text{max}} = 455, 605 \text{ nm}$) under nitrogen in CHCl_3 in the absence (spectrum 'a') and presence (spectrum 'b') of added PPh_3 ; the solution of **3b** is air-sensitive (Fig. 5.5). The visible spectrum of **3b** in THF or a 3:1 v/v THF/MeOH solution shows: $\lambda_{\text{max}} 605 \text{ nm}$, $\epsilon = 500 \text{ M}^{-1}\text{cm}^{-1}$; $\lambda_{\text{max}} = 455 \text{ nm}$, $\epsilon = 1200 \text{ M}^{-1}\text{cm}^{-1}$.

The $^{31}\text{P}\{^1\text{H}\}$ NMR spectrum of **3b** was unaffected by the presence of up to a 10-fold excess of styrene.

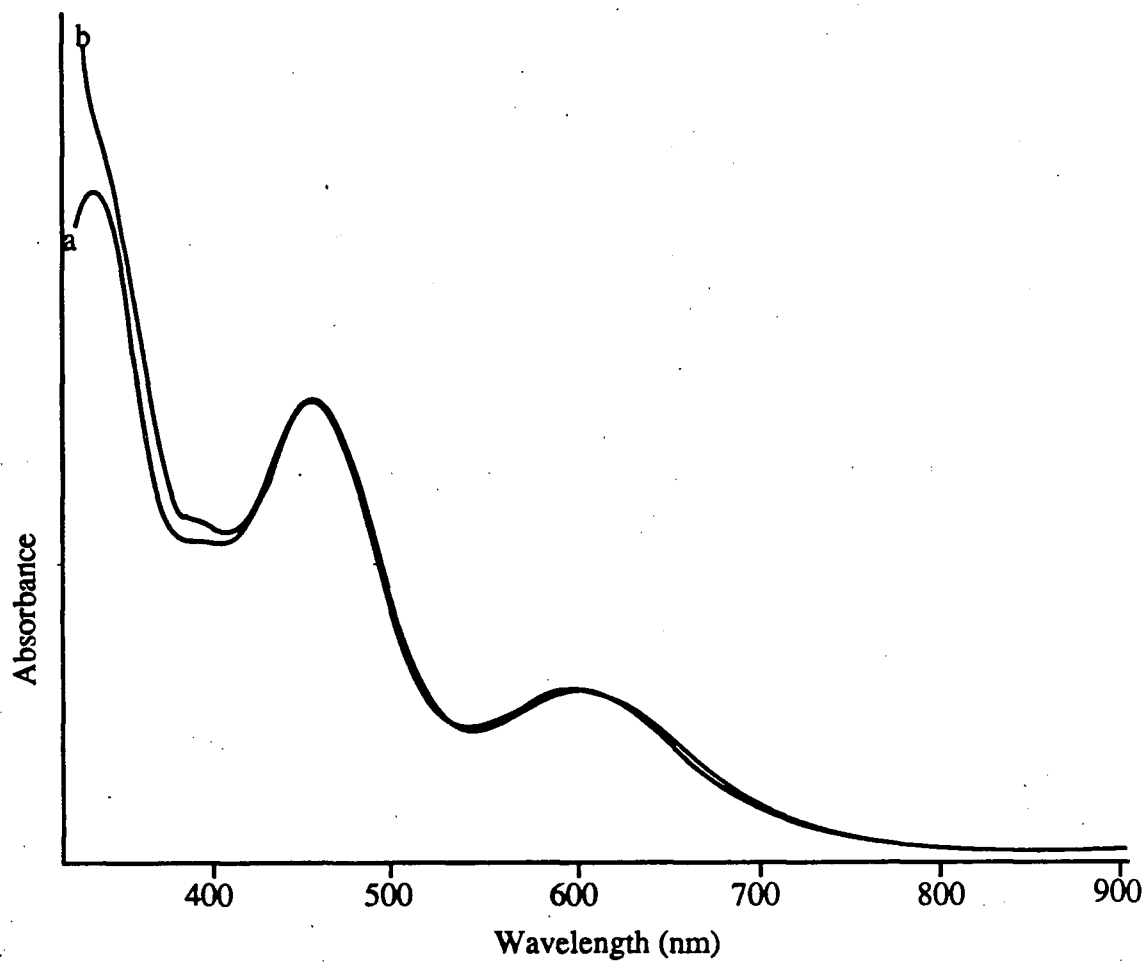


Figure 5.4 The visible spectrum of 3b (1.1×10^{-3} M) in CHCl_3 solution under nitrogen: 'a', in the absence of PPh_3 ; 'b', in the presence of a 23-fold excess of PPh_3 .

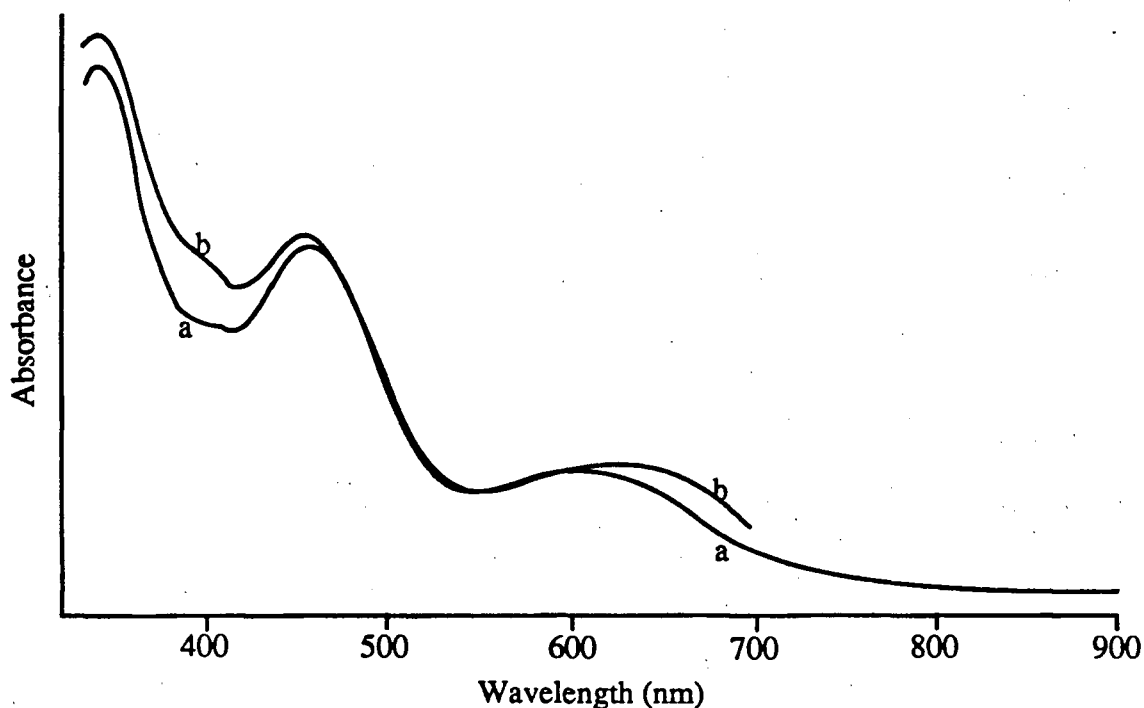


Figure 5.5 The visible spectrum of $\text{RuCl}_2(\text{PPh}_3)(\text{isoPFA})$, **3b**, in CHCl_3 solution: 'a', under nitrogen; 'b', on exposure to air.

*Reactions of $\text{RuCl}_2(\text{PPh}_3)(\text{isoPFA})$, **3b**, and $\text{RuHCl}(\text{CO})(\text{PPh}_3)(\text{isoPOF})$, **5**, with methanol in the absence of base*

The distillate from the methanol- d_4 preparation of **5** in the absence of hexene was analyzed using the Ee griwe test and 2 - 5% of a stoichiometric amount of formaldehyde was detected. Most gas chromatogram peaks obtained from the GCMS analysis of the same distillate could not be identified; however, one fraction, that gave a highest mass fragment with $m/z = 64$, indicates of the order of 30% of a stoichiometric amount of methyl formate- d_4 .

The formulation of **5** based on spectroscopic and analytical data was confirmed by the crystal structure; the amine functionality of the isoPFA ligand had been replaced by a

methoxy group during the reaction of **3b** with methanol at reflux temperature under nitrogen. The crystal structure of **5** is shown in Figure 5.6, and selected bond distances and angles are given in Tables 5.1 and 5.2. Disorder of the unsubstituted cyclopentadienyl ring was satisfactorily accounted for by including two orientations of this group in the refinement. All hydrogens were found in Fourier difference maps except for those in the disordered rings. The final residuals were $R = 0.033$ and $R_w = 0.037$. Other crystal data for the structure will be published elsewhere.¹⁵⁴

The spectroscopic and analytical data for **5** as prepared from methanol- d_0 are given in section 2.4, and the ^1H NMR spectrum is shown in Figure 5.7. The ^1H NMR spectrum

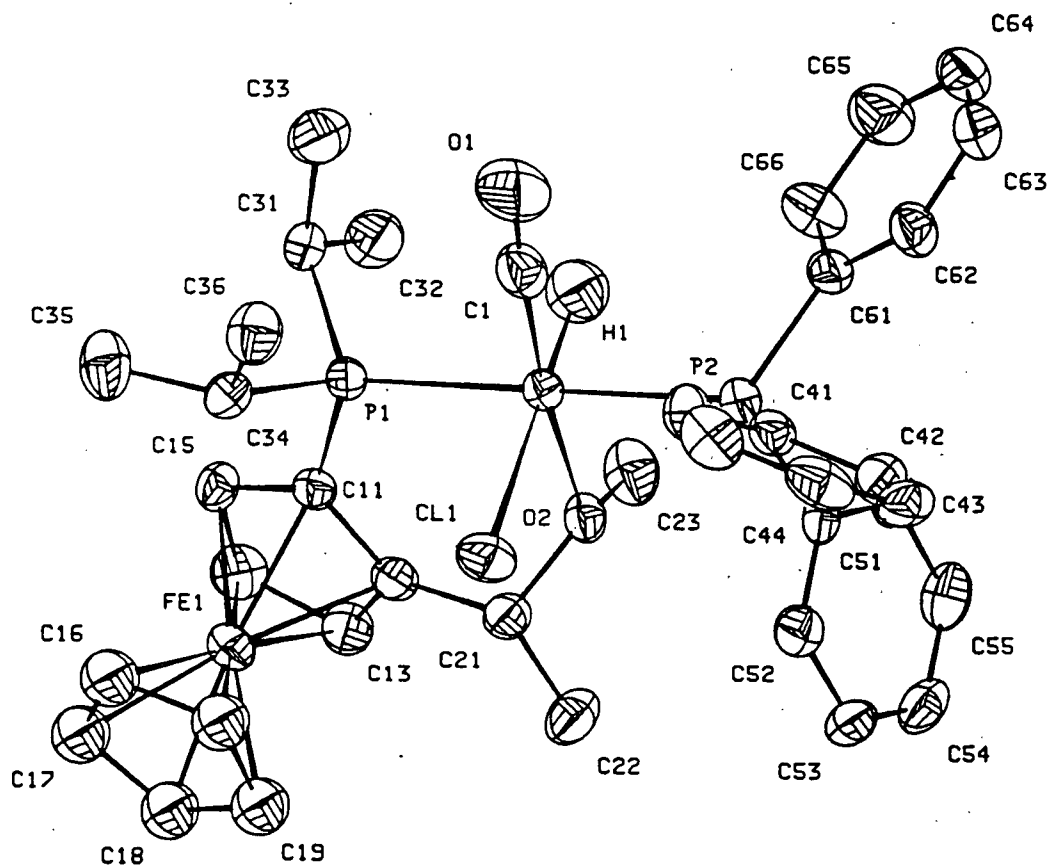


Figure 5.6 The X-ray structure of $\text{RuHCl}(\text{CO})(\text{PPh}_3)(\text{isoPOF})$, **5**.

Table 5.1

Selected bond distances (Å) obtained from X-ray diffraction data for three ruthenium products that have been isolated from the reactions of $\text{RuCl}_2(\text{PPh}_3)(\text{isoPFA})$, **3b**, with methanol

Bond type ^a			
	6^b	5^c	7^d
Ru-Cl	2.441(2)	2.521(2)	2.441(1)
Ru-H	1.53(6)	1.57	1.52
Ru-P(Pr^i) ₂	2.329(2)	2.358(2)	2.178(1)
Ru-PPh ₃	2.383(2)	2.354(2)	2.250(1)
Ru-NMe ₂	2.420(6)	-	2.265(5)
Ru-OMe	-	2.262(4)	-
Ru-(CO)	1.820(8)	1.793(8)	-
C-O _(carbonyl)	1.142(9)	1.161(8)	-
O-Me	-	1.439(7)	-
N-Me	1.469(9)	-	1.488(7)
N-Me	1.49(1)	-	1.483(7)

^aCorresponding distances are listed side by side for comparison.

^b $\text{RuHCl}(\text{CO})(\text{PPh}_3)(\text{isoPOF})$ (Fig. 5.6): six-coordinate, approximately octahedral.

^c $\text{RuHCl}(\text{CO})(\text{PPh}_3)(\text{isoPFA})$ (Fig. 5.9, 5.10): six-coordinate, approximately octahedral.

^d $\text{RuHCl}(\text{PPh}_3)(\text{isoPFA})$ (Fig. 5.12): five-coordinate, approximately trigonal bipyramidal.

of the sample prepared using methanol- d_4 is shown in Figure 5.8. The OMe signal at δ 2.38 of the 'proton-containing' sample (Fig. 5.7) is not present in the spectrum shown in Figure 5.8, and the underlying PCHCH_3 broadened multiplet at δ 2.36 (integrating at 1 proton) is clearly revealed. The hydride signal at δ -13.9, however, is still present in the spectrum shown in Figure 5.8, but integrates to about half a proton. The *ortho*-phenyl protons meanwhile are reduced from 6 protons to about 1, giving an *ortho/meta/para* ratio of 1:9 instead of 2:3 as in the non-deuteriated sample.

Table 5.2

Crystallographically determined bond angles associated with the bond distances shown in

Table 5.1

6 ^b		5 ^c		7 ^d	
Angles (°) ^a					
P ₁ -Ru-P ₂	158.67(6)	P ₁ -Ru ₁ -P ₂	177.55(6)	N ₁ -Ru ₁ -P ₂	157.1(1)
N-Ru-P ₁	92.8(1)	O ₂ -Ru ₁ -P ₁	88.8(1)	N ₁ -Ru ₁ -P ₁	97.9(1)
N-Ru-P ₂	108.3(1)	O ₂ -Ru ₁ -P ₂	89.5(1)	P ₁ -Ru ₁ -P ₂	101.5(1)
C ₃₉ -Ru-P ₁	94.1(2)	C ₁ -Ru ₁ -P ₁	92.9(2)		
C ₃₉ -Ru-N	96.6(3)	C ₁ -Ru ₁ -O ₂	170.1(2)		
C ₃₉ -Ru-P ₂	86.3(2)	C ₁ -Ru ₁ -P ₂	88.6(2)		
Ru-C ₃₉ -O	176.1(6)	Ru ₁ -C ₁ -O ₁	176.4(6)		
C ₃₉ -Ru-H ₁	89(2)	C ₁ -Ru ₁ -H ₁	82.5		
C ₃₉ -Ru-Cl	177.7(2)	C ₁ -Ru ₁ -Cl ₁	101.4(2)		
P ₁ -Ru-H ₁	68(2)	P ₁ -Ru ₁ -H ₁	88.9		
N-Ru-H ₁	161(2)	O ₂ -Ru ₁ -H ₁	87.7		
Cl-Ru-H ₁	89(2)	Cl ₁ -Ru ₁ -H ₁	175.9		
P ₂ -Ru-H ₁	90(2)	P ₂ -Ru ₁ -H ₁	89.4		
N-Ru-Cl	85.3(1)	O ₂ -Ru ₁ -Cl ₁	88.4(1)	N ₁ -Ru ₁ -Cl ₁	86.8(1)
P ₁ -Ru-Cl	87.11(6)	P ₁ -Ru ₁ -Cl ₁	89.61(6)	P ₁ -Ru ₁ -Cl ₁	124.9(1)
P ₂ -Ru-Cl	91.76(6)	P ₂ -Ru ₁ -Cl ₁	92.03(6)	P ₂ -Ru ₁ -Cl ₁	91.9(0)

^aCorresponding angles are listed side by side for comparison. Atom numberings are those given by the crystallographers.

^bRuHCl(CO)(PPh₃)(isoPFA) (Fig. 5.6).

^cRuHCl(CO)(PPh₃)(isoPOF) (Fig. 5.9, 5.10).

^dRuHCl(PPh₃)(isoPFA) (Fig. 5.12).

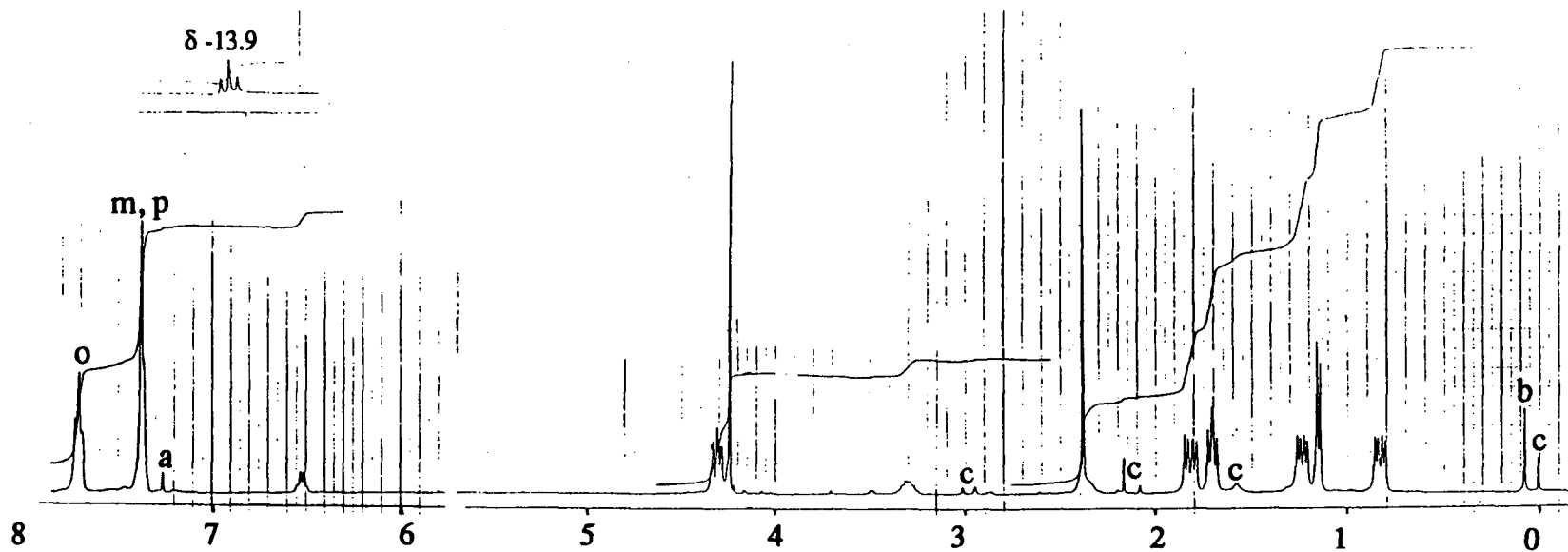


Figure 5.7 The ^1H NMR spectrum (300 MHz, CDCl_3 , ambient temperature, under nitrogen) of complex 5. Peaks for complex 5: 'o', *ortho* phenyl H atoms; 'm, p', *meta* and *para* phenyl H atoms; other peak assignments for 5 are given in sect. 2.4. Other peak assignments are: 'a', CHCl_3 ; 'b', silicone grease; peaks marked 'c' are due to unidentified impurities.

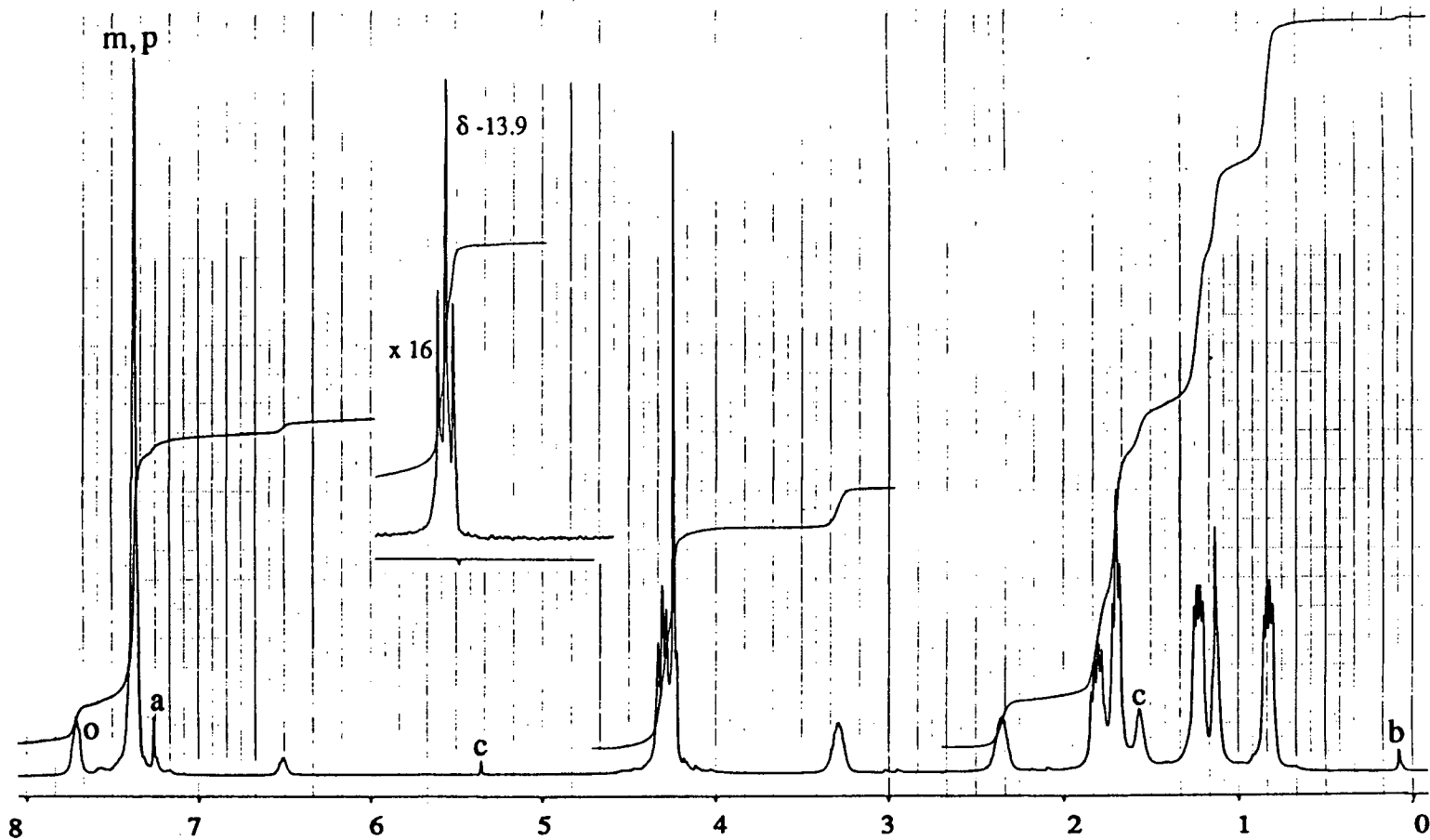


Figure 5.8 The ^1H NMR spectrum (300 MHz, CDCl_3 , ambient temperature, under nitrogen) of deuteriated complex **5**, prepared using methanol- d_4 . Peaks for complex **5**: 'o', *ortho* phenyl H atoms; 'm, p', *meta* and *para* phenyl H atoms; other peak assignments for **5** are given in sect. 2.4. Other peak assignments are: 'a', CHCl_3 ; 'b', silicone grease; peaks marked 'c' are due to unidentified impurities.

In the experiment on isomerization of 1-hexene catalyzed by **5**, the gas chromatograph of the distillate of the reaction mixture after reaction showed ~95% isomerization, mainly to *cis* and *trans*-2-hexene in a 1:4 ratio, with ~2% hydrogenation, presumably by methanol hydrogen transfer, to give hexane.

In the experiment on the hydroformylation of 1-hexene catalyzed by **5**, the reaction mixture after reaction had a strong smell that was certainly typical of either *n*-heptanol or *n*-heptaldehyde or a mixture of these. Comparison of the gas chromatogram, obtained using a tricresylphosphate column, of the distillate of this reaction mixture with standards showed that most of the 1-hexene was either isomerized or converted to other products.

Comparison of the OV-17 gas chromatogram of this distillate with standards indicated the presence of heptaldehyde, heptanol and other minor products. A quantitative estimate of the product distribution, assuming all products of 1-hexene conversion were detected on the columns used, and an estimated 90% conversion of 1-hexene to products, was: *trans*-2-hexene (0.03 mmol), *cis*-2-hexene (0.01 mmol), heptaldehyde (0.03 mmol), heptanol (0.03 mmol) and other minor products.

The results of the experiments on transfer hydrogenation catalyzed by **3b** are summarized in Table 5.3. It is seen that **3b** shows significant catalytic activity at 105 °C for the transfer of hydrogenation from methanol to ketones or activated olefins, while cyclohexene and hexene were reduced in only trace amounts under corresponding conditions. The hydrogen transfer to styrene was accelerated by the presence of KOH, but these data will be presented later.

Table 5.3

Catalytic hydrogen transfer from methanol, catalyzed by $\text{RuCl}_2(\text{PPh}_3)(\text{isoPFA})$, **3b**, in neat methanol at 105 °C in the absence of base

[Ru] (M x 10 ³)	time (h)	substrate (M)	product(s) ^a
2.5	overnight	1-hexene (0.20)	hexane ^{b,c} (3)
3.0	88	acetophenone (0.21)	α -methylbenzyl alcohol ^c (26)
3.0	88	cyclohexene (0.24)	cyclohexane ^c (3)
2.4	20	styrene (0.22)	ethylbenzene ^c (4)
3.2	97	vinylmethylketone (0.30)	2-butanol ^{c,d} (70) 2-butanone ^e (50)

^aIn parentheses is the total number of turnovers = moles hydrogenated substrate per mol Ru.

^bAccompanied by 93% isomerization, which corresponds to a turnover of 74.

^cEstimated from GC data.

^dEstimated from ¹H NMR data.

^eThus, the turnover number for the hydrogenation of the vinyl group was 120.

Reactions of $\text{RuCl}_2(\text{PPh}_3)(\text{isoPFA})$, **3b**, with methanol in the presence of added base

With Proton Sponge[®] as added base:

The spectroscopic and analytical data for the main ruthenium-containing products, $\text{RuHCl}(\text{CO})(\text{PPh}_3)(\text{isoPFA})$, **6**, and $\text{RuHCl}(\text{PPh}_3)(\text{isoPFA})$, **7**, of a typical reaction at ambient temperature are described in section 2.4.

The solid state structure of **6** (Figs. 5.9, 5.10) contains approximately *trans* disposed phosphorus atoms, with the hydride located *trans* to the nitrogen atom of the isoPFA ligand, and the CO *trans* to Cl. Selected bond distances and angles are tabulated in Tables 5.1 and 5.2, respectively, along with parameters for $\text{RuHCl}(\text{CO})(\text{PPh}_3)(\text{isoPOF})$, **5**, and **7** (to be discussed below). The ¹H NMR spectrum (300 MHz, CDCl₃, under

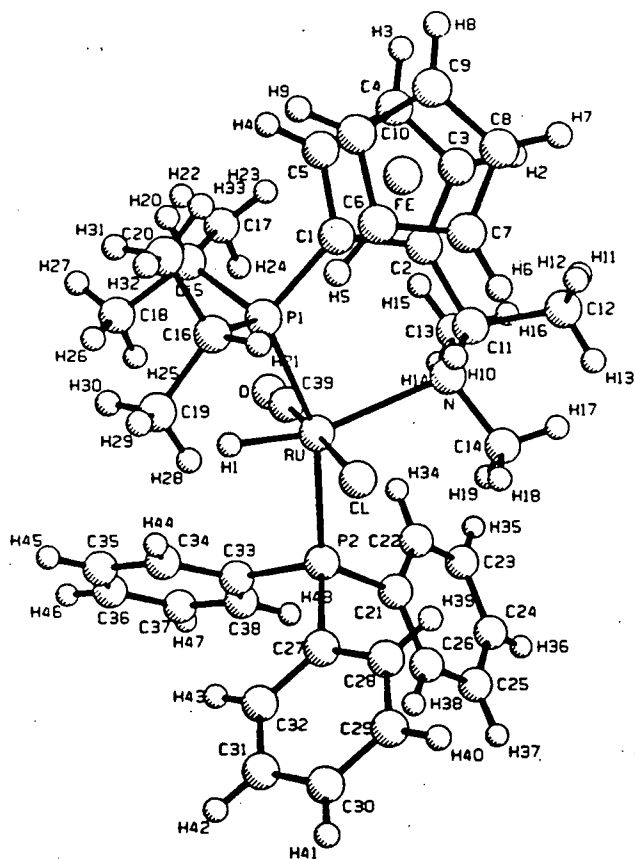


Figure 5.9 The X-ray structure of $\text{RuHCl}(\text{CO})(\text{PPh}_3)(\text{isoPFA})$, 6.

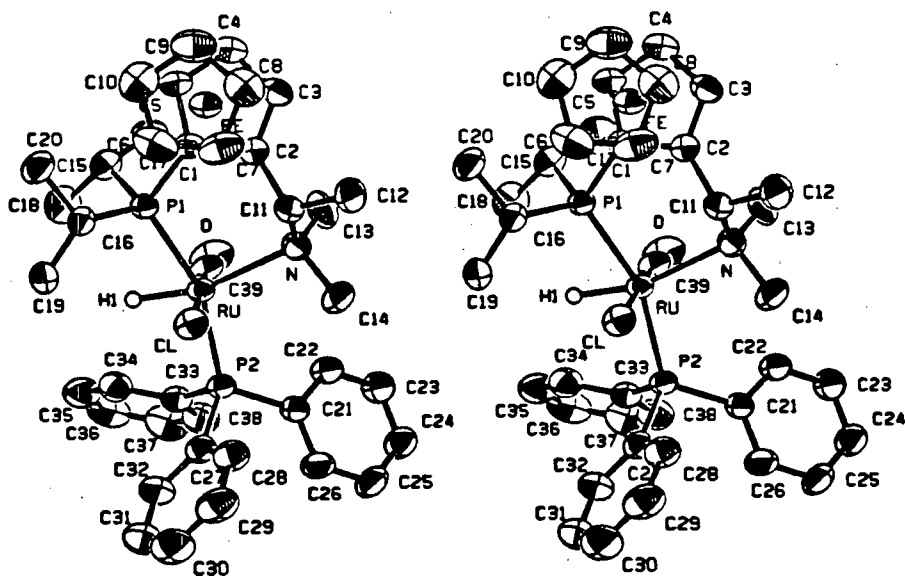


Figure 5.10 A stereoscopic view of the structure of 6.

nitrogen) of **6** is shown in Fig 5.11a (ambient temperature) and Fig. 5.11b (20 ° to -50 °C); detailed assignments are given in section 2.4. The -NMe₂ resonances show a temperature dependence (Fig. 5.11b), the single peak, δ 2.3 at ambient temperature, being resolved into two singlets at ≤ 0 °C. Besides the hydride quartet at δ -15.3 due to **6**, an additional hydride at δ -15.8 (t) is always present in very minor concentration (<10%) and increases with exposure to air. The ³¹P{¹H} NMR (121 MHz, ambient temperature, under nitrogen) data for **6** are given in section 2.4, and spectra including resonances due to this complex, prepared using KOH as base, are shown later in Figs. 5.13 and 5.14. These spectra will be discussed in connection with the KOH reaction. A very weak infrared peak at ν^{KBr} 1852 cm⁻¹ on the shoulder of the carbonyl peak at 1897 cm⁻¹ is always seen and is possibly due to the presence of the same oxidation product detected by the weak hydride triplet in the ¹H NMR at δ -15.8. The yellow complex **6** exhibits a weak band in the

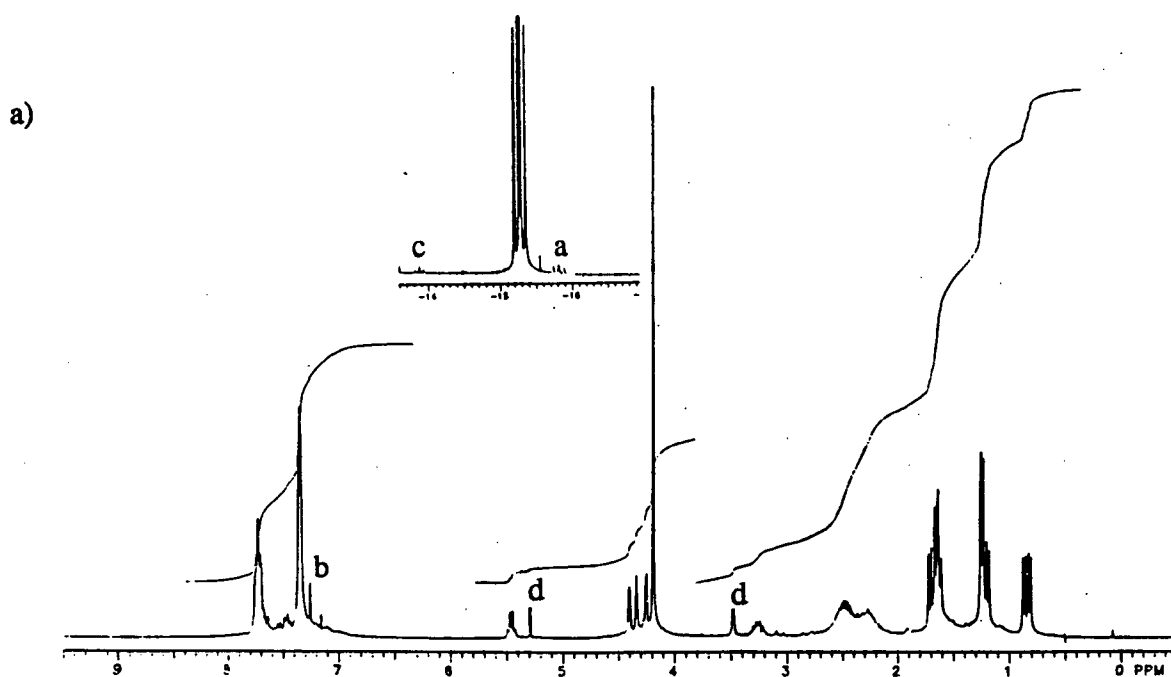
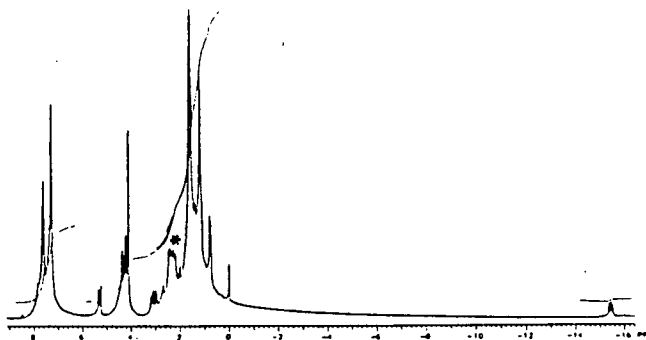
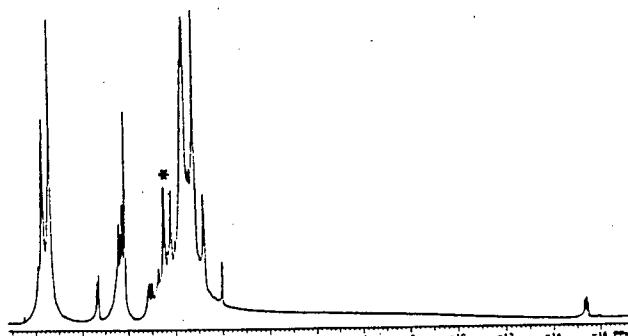


Figure 5.11 a) The ¹H NMR (300 MHz, CDCl₃, ambient temperature, under nitrogen) spectrum of RuHCl(CO)(PPh₃)(isoPFA), **6**; peaks for **6** are assigned in section 2.4. Other peak assignments are as follows: 'a', hydride oxidation product impurity which always accompanies **6**; 'b', CHCl₃; 'c', complex **5**; 'd', unidentified impurities. b) Variable temperature ¹H NMR spectra (300 MHz, CDCl₃, under nitrogen) for **6**. The peaks marked with an '*' are due to the NMe₂ protons; the two NMe₂ resonances are resolved at low temperature, but coalesce at room temperature.

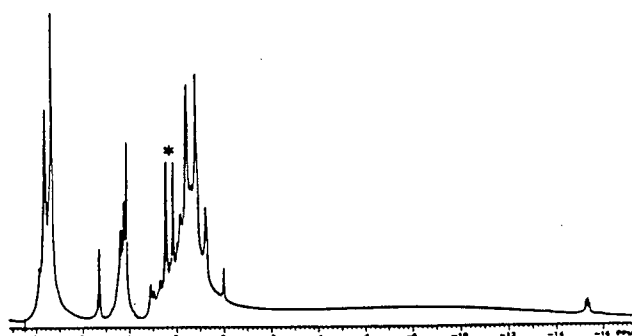
b)

ambient
temperature:

0 °C



-30 °C



-50 °C

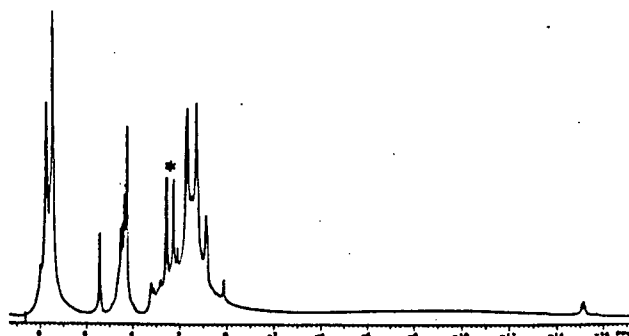


Figure 5.11b (see legend on previous page)

visible region at ~ 450 nm.

The crystal structure of $\text{RuHCl}(\text{PPh}_3)(\text{isoPFA})$, **7**, shows that the molecule is five-coordinate and has a structure that is best described as a distorted trigonal bipyramid (Fig. 5.12). Structural parameters are shown in Tables 5.1, 5.2, and 5.4 in a manner designed to facilitate comparison of corresponding features of similar complexes. Fortunately, the hydride was located, and a Ru-H bond distance of 1.52 \AA was obtained. The spectroscopic and analytical data for this complex are given in section 2.4.

In addition to the ruthenium-containing products described above, other unidentified crystals were isolated on one occasion from a reaction mixture where the Ru:PS ratio was 1:1; the solution of these crystals in CDCl_3 revealed a ^1H NMR triplet at $\delta -4.8$ with $J = 21$ Hz. Also, on another occasion, where a 1:1 mole ratio of Ru:PS at a higher temperature of 72°C , a ^1H NMR triplet at $\delta -13.9$ for the isolated solids dissolved in

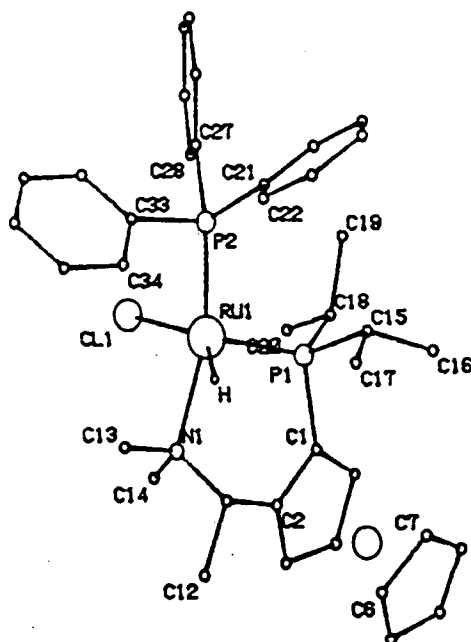


Figure 5.12 The X-ray structure of $\text{RuHCl}(\text{PPh}_3)(\text{isoPFA})$, **7**.

CDCl_3 indicated the formation of some **5**, in addition to the main product **6** showing a doublet-of-doublets at δ -15.3 (see sect. 2.4).

In attempts to identify gaseous and volatile products, in an experiment similar to that described in section 2.4 for the preparation of **7**, **3b** (0.044 g, 0.057 mmol) was allowed to react with dry methanol (4 mL) in the presence of Proton Sponge[®] at ambient temperature. Reaction occurred slowly and was complete only after four days, at which time there was no remaining solid starting complex, **3b**, which is only sparingly soluble in methanol. An Eegriwe, chromotropic acid test on the distillate from this reaction mixture revealed 0.76 mg (0.026 mmol) of CH_2O . Methyl formate could not be detected in the distillate using GC. The gas evolution experiment, using the gas uptake/evolution apparatus, showed that in the reaction of **3b** with methanol at 30 °C in the presence of Proton Sponge[®], the maximum gas evolution, reached after 3.7 h, corresponded to ~1 mol gas/mol **3b**.

With KOH as base:

A typical reaction of **3b** with dry methanol with KOH:Ru = 1.0, as described in section 2.4, yields mainly the complex **6**. Attempts to purify **6** by recrystallization from dichloromethane/methanol were unsuccessful and a satisfactory elemental analysis was never obtained. However, the merely filtered and washed precipitate of **6**, which deposited during the 1:1 KOH:Ru reaction, appeared reasonably pure by ^1H and $^{31}\text{P}\{^1\text{H}\}$ NMR spectroscopy. Some of complex **6** was also formed when this KOH reaction was carried out in the presence of styrene. The spectroscopic data for **6** have already been presented (above and in sect. 2.4), but more explanation is required for the $^{31}\text{P}\{^1\text{H}\}$ NMR spectrum. Figure 5.13 shows the spectrum of a CDCl_3 solution which has stood in a NMR tube under nitrogen for a week before the spectrum was recorded (the impurity at δ 29.2 is Ph_3PO). The interesting feature is the presence of minor peaks surrounding the two main

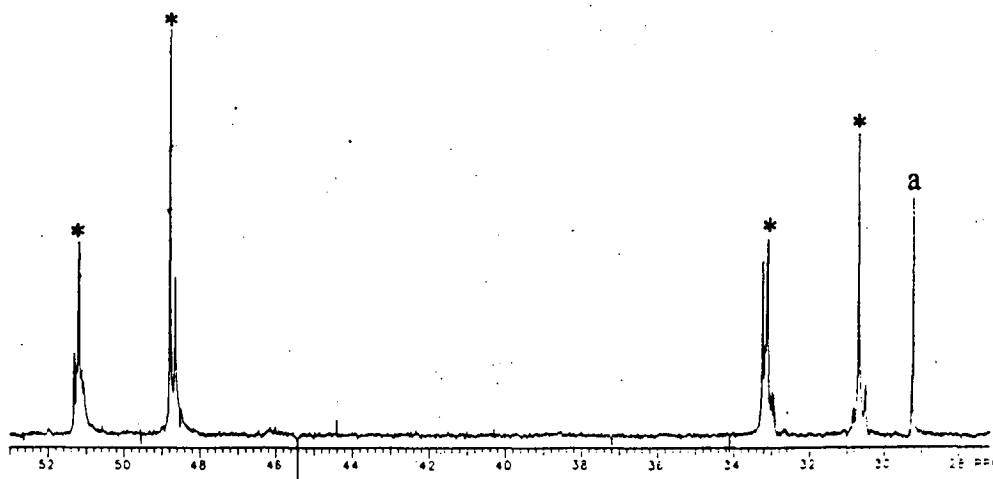


Figure 5.13 The $^{31}\text{P}\{^1\text{H}\}$ NMR spectrum (121 MHz, CDCl_3 , ambient temperature, under nitrogen) of **6** after ~ 1 wk; member peaks of the 'two main doublets' mentioned in the text are marked with an '*'. A peak due to Ph_3PO is marked with an 'a'.

doublets centred at δ 50.0 and 31.9, with $^2J_{\text{PP}} = \sim 290$ Hz; these may be due to geometric isomers or diastereomers of **6** with similarly *trans* disposed phosphorus atoms.

The results of experiments in neat methanol to show variations in appearance and styrene-hydrogenating activity of solutions of **3b** with increasing KOH concentration are summarized in Table 5.4. The colour changes observed depended both on time and KOH concentration, and a light white-yellow precipitate was always deposited. Table 5.4 also conveys some approximate rate data. In all cases, an initial, relatively rapid hydrogenation activity slowed markedly after about the first half-hour, which was approximately the time required for most of the insoluble, green **3b** complex to react.

No inorganic products were characterized from the yellow solutions obtained at higher [KOH] in the presence or absence of styrene, except for KCl (evidenced by an ill-chosen crystal structure determination!!). The wine-coloured supernatants, in appearance the same in the presence or absence of styrene, all exhibited a strong UV-vis band at 542 nm. Figure 5.14 shows the $^{31}\text{P}\{^1\text{H}\}$ NMR spectrum of the supernatant of a KOH/methanol reaction mixture with KOH:Ru = 2.0, but in other respects similar to that

Table 5.4

Colour changes of reaction mixtures^a and turnover numbers for hydrogen transfer from methanol to styrene to give ethylbenzene as a function of time and initial [KOH] using **3b** as catalyst

total turnovers^b (with solution colour given in parentheses)

[KOH] (M)	time: 0.5 h	10 h	20 h	30 h	2 d	1 wk
0.2	2.6 (pink-cherry red)	5.0 (wine)		6.2 (wine)		(red)
0.4	2.6 (pink-cherry red)	5.7 (wine)		7.2 (wine)		9.2 (pink)
0.7	(pink-cherry red)	7.7 (wine)		8.8 (wine)		
0.9	3.5 (pink-cherry red)		8.7 (wine)		9.1 (yellow)	
1.4	3.9 (reddish orange)		(pale orange)			
1.8	3.4 (yellow orange)					

^aConditions: 80 °C; neat methanol (1 mL); under nitrogen in a closed Carius tube; RuCl₂(PPh₃)(isoPFA), **3b**, (~6 mg, 0.007 mmol); initial styrene (0.087 mmol).

^bTotal turnovers = total number moles ethylbenzene produced per mole Ru.

described in section 2.2 for the preparation of **6**. The pairs of doublets centred at δ 50.7 and 33.5, and at δ 50.5 and 33.3, both with $^2J_{pp} = \sim 290$ Hz, if expanded, clearly indicate two equally dominant isomers of **6** along with other products present ~4 h after starting the reaction. Singlets at δ -4.8 and -5.8 are probably due to free isoPFA, also

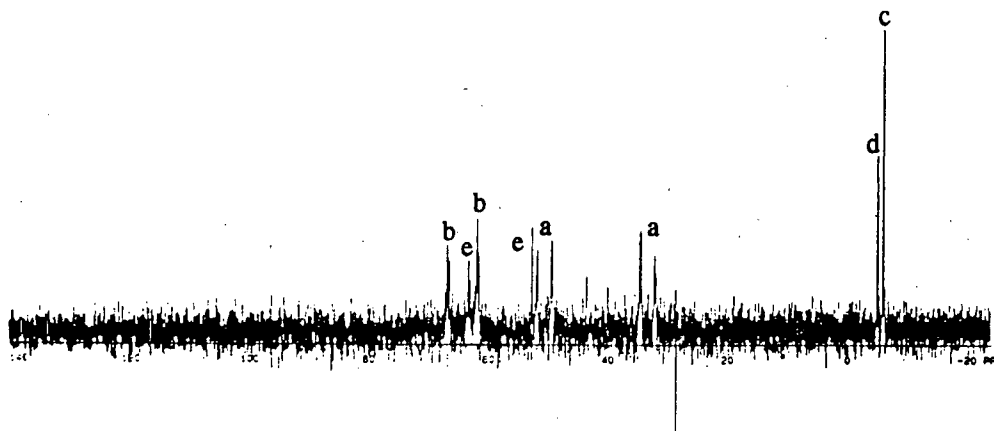


Figure 5.14 The $^{31}\text{P}\{^1\text{H}\}$ NMR spectrum (121 MHz, CH_3OH , ambient temperature, under nitrogen, unlocked) of the supernatant of a reaction mixture formed by heating $\text{RuCl}_2(\text{PPh}_3)(\text{isoPFA})$, **3b**, (58 mg, 0.072 mmol) in dry methanol (2 mL) in the presence of KOH (0.1 mL of a 1.8 M solution) at -80°C for 3 - 4 h under nitrogen. Peak assignments are: 'a', complex **6**; 'b', complex **X**, formulated in section 5.4; 'c', PPh_3 ; 'd', isoPFA; 'e', unidentified species.

isolated by chromatography in a similar reaction (described later, p. 181), and free PPh_3 , respectively. (The $^{31}\text{P}\{^1\text{H}\}$ NMR resonance (109 MHz, CD_2Cl_2) for free isoPFA occurs at $\delta -3.3$; the PPh_3 resonance, often used as a ^{31}P NMR standard, occurs at $\delta \sim -5.6$.) Peaks in the range $\delta 61$ to 67 are probably associated with the hydride resonances exhibited by the residue obtained by removal of solvent from this supernatant. The ^1H NMR (300 MHz, CDCl_3) spectrum of the soluble components of this residue is shown in Figure 5.15. The doublet-of-doublets at $\delta -15.3$ and -15.9 correspond to **6** and an oxidation product, respectively (*vide supra*); the other hydride resonances in the range $\delta -17.5$ to -19 were always observed in ^1H NMR spectra of the wine-coloured supernatants. A visible spectrum of this same CDCl_3 solution is shown in Figure 5.16; the wine-coloured solutions always exhibited the intense band shown at 542 nm. The ^1H NMR (300 MHz, CDCl_3) spectrum of the methanol-washed white precipitate from the same reaction (Fig. 5.17) showed the distinctive hydride pattern of $\text{RuH}_2(\text{CO})(\text{PPh}_3)_3$: $\delta -6.8$ (tdd, $^2J_{\text{PH}} = 16$, 30 Hz, $^2J_{\text{HH}} = 8\text{Hz}$), -8.8 (dtd, $^2J_{\text{PH}} = 31$, 78 Hz, $^2J_{\text{HH}} = 8\text{Hz}$), very similar to the

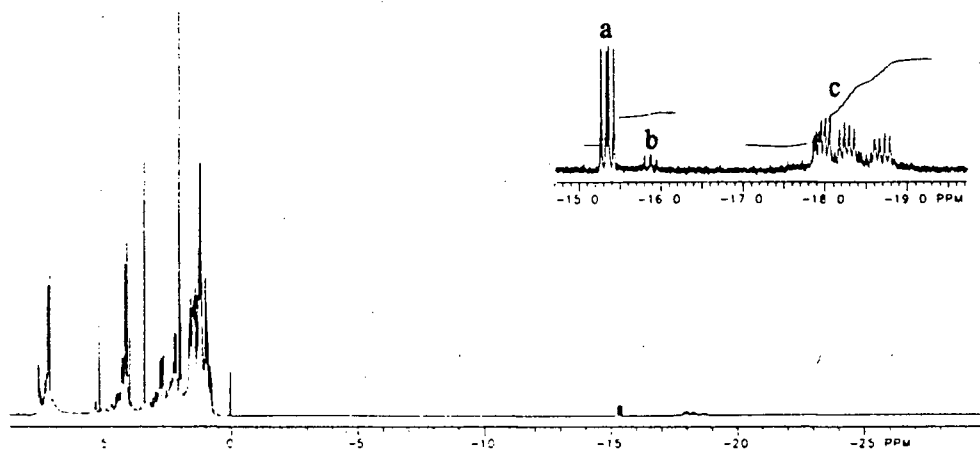


Figure 5.15 The ^1H NMR spectrum (300 MHz, CDCl_3 , ambient temperature, under nitrogen) of the residue obtained from the solution used for the $^{31}\text{P}\{^1\text{H}\}$ NMR spectrum given in Figure 5.14; upfield peak assignments are as follows: 'a', complex 6; 'b', a hydride oxidation product always accompanying 6; 'c' (a pair of doublets-of-doublets centred at $\delta \sim 18.1$), complex X, formulated in section 5.4; other upfield resonances are unidentified.

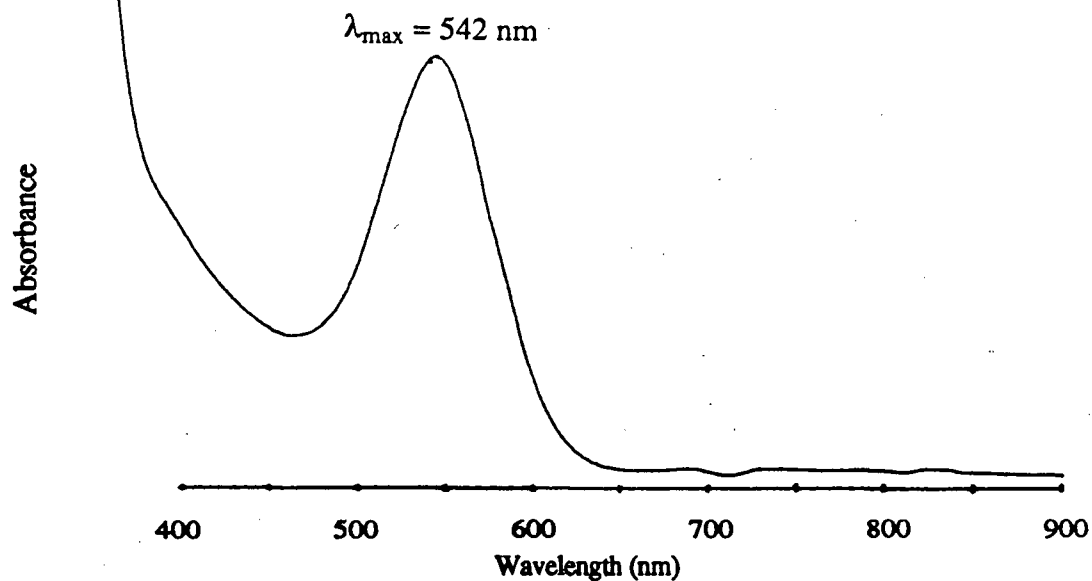


Figure 5.16 The visible spectrum of the CDCl_3 solution used for the ^1H NMR spectrum given in Figure 5.15.

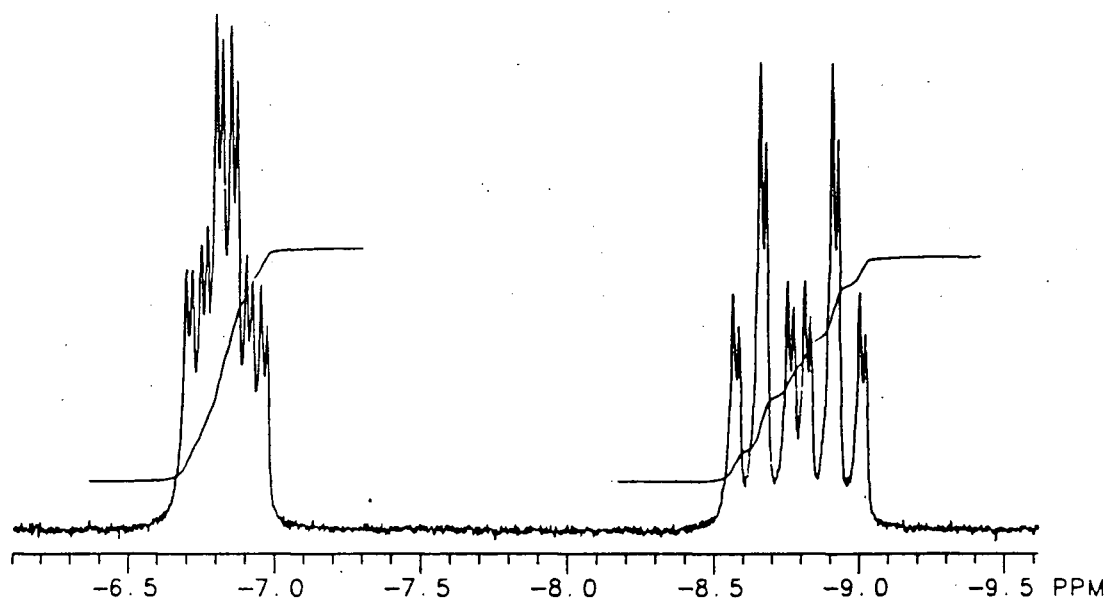


Figure 5.17 The upfield ^1H NMR spectrum (300 MHz, CDCl_3 , ambient temperature, under nitrogen) of $\text{RuH}_2(\text{CO})(\text{PPh}_3)_3$.

literature data.⁶⁸ An X-ray diffraction study on the single crystals of $\text{RuH}_2(\text{CO})(\text{PPh}_3)_3 \cdot \text{CH}_2\text{Cl}_2$ obtained on recrystallization from dichloromethane/methanol confirmed the structure proposed based on spectroscopic data.^{90,91} The structure²⁸ is shown in Figure 5.18, and selected bond angles and distances are listed in Table 5.5. The hydrides were not located; CH_2Cl_2 was found to be present in the crystal as a monosolvate.

In the chromatography of the wine-coloured supernatants of reaction mixtures with $\text{KOH}:\text{Ru} \gg 1:1$, litres of solvent were required to elute each of the last three bands, and dissolved silica, which is very slightly soluble in methanol, was a contaminant in these fractions. The small sample sizes obtained on removal of methanol gave poor quality NMR spectra because of the low concentration obtained when the residues were dissolved in the NMR solvent. However, the ^1H NMR spectrum of the first fraction (in CDCl_3) showed a multiplet at δ -17.6; the second yellow fraction was a mixture, the ^1H NMR spectrum exhibiting several hydride signals that were not in the spectrum of Figure 5.15, but 6 was

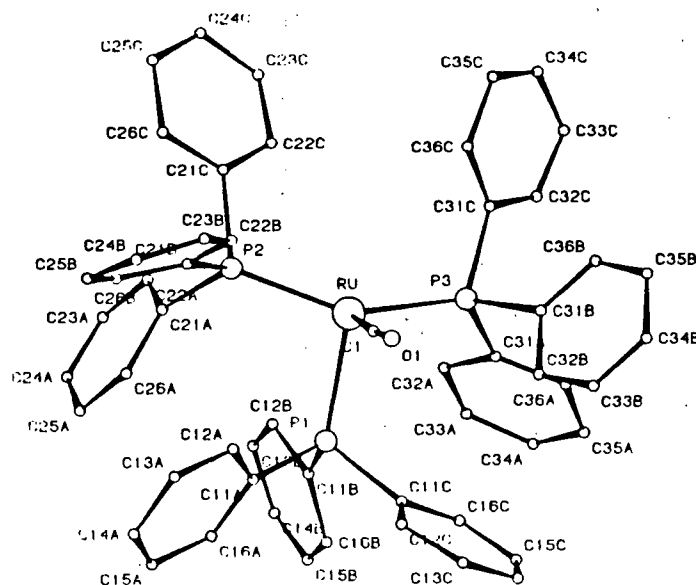
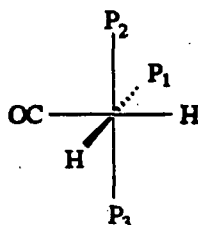


Figure 5.18 The X-ray structure of $\text{RuH}_2(\text{CO})(\text{PPh}_3)_3$.

identified by the resonance at δ_{CDCl_3} -15.3 (dd). The ^1H NMR spectrum of the residue from the first red band showed two hydride resonances, the more intense being at δ -18.7 (dd, $J = 36, 18$ Hz). The second red residue, X, exhibited spectral features (Fig. 5.19: δ -17.9 (dd, 1H, $^2J_{\text{PH}} = 36, 20$ Hz), -18.2 (dd, 1H, $^2J_{\text{PH}} = 36, 20$ Hz)) which were very similar to certain features of the spectra shown in Figure 5.15 (δ -17.95 (dd, $J = 36, 20$ Hz), -18.25 (dd, $J = 36, 20$ Hz)). Also shown in Fig. 5.19, in the range δ 1.0 - 5.2, are resonances typical of a coordinated isoPFA ligand, perhaps of two types present in equal

Table 5.5

Selected molecular structure parameters for $\text{RuH}_2(\text{CO})(\text{PPh}_3)_3^a$ 

Bond type	Bond name	distance (Å)
Ru-PPh ₃	Ru-P ₂	2.321(7)
Ru-PPh ₃	Ru-P ₃	2.301(7)
Ru-PPh ₃	Ru-P ₁	2.419(7)
Ru-CO	Ru-C ₁	1.97(3)
carbonyl C-O	C ₁ -O ₁	1.09(4)

Angles (°)

P ₂ -Ru-P ₃	148.23(25)
P ₁ -Ru-P ₂	101.01(23)
P ₁ -Ru-P ₃	103.33(23)
C ₁ -Ru-P ₂	103.3(8)
C ₁ -Ru-P ₁	91.0(7)
C ₁ -Ru-P ₃	96.4(8)
Ru-C ₁ -O ₁	174.9(25)

^aParameters arranged in order to compare with corresponding distances for $\text{RuHCl}(\text{CO})(\text{PPh}_3)(\text{isoPFA})$ in Table 5.1. Hydride positions were not crystallographically located; their positions in the diagram are based on spectroscopic data.⁶⁸

amounts. These resonances are tentatively assigned as follows: δ 5.21 (q, 1H, $^3J_{\text{HH}} = 7$ Hz, FcCHMe), 4.80 (q, 1H, $^3J_{\text{HH}} = 7$ Hz, FcCHMe); 4.48, 4.44, 4.39, 4.35, 4.30 (16H, for two C_5H_3); 4.23, 4.17 (2s, 10H, for two C_5H_5); 2.87, 2.76 (2s, 6H, $\text{N}(\text{CH}_3)_2$); 2.28, 2.06 (2s, 6H, $\text{N}(\text{CH}_3)_2$); 1.7 - 1.0 (m, >30H, two $\text{P}(\text{CH}(\text{CH}_3)_2)_2$ and two FcCHCH_3 ,

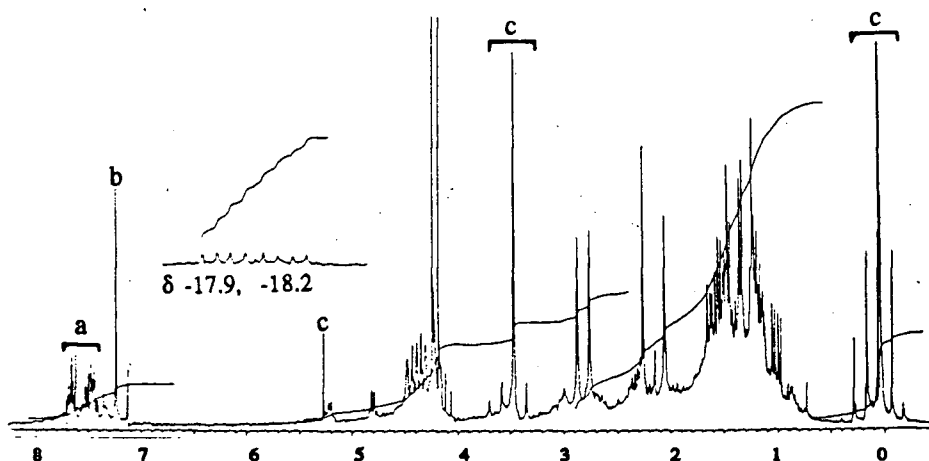


Figure 5.19 The ^1H NMR spectrum (270 MHz, CDCl_3 , ambient temperature, under nitrogen) of the residue obtained from the eluted second red band, containing complex X, obtained on chromatography of a worked-up supernatant from a $\text{RuCl}_2(\text{PPh}_3)(\text{isoPFA})$, **3b**/KOH/methanol reaction mixture. Detailed assignments for X are given in the text; other assignments are: 'a', unidentified phenyl-containing species; 'b', CHCl_3 ; 'c', unidentified species.

and probably some 'impurity' signals). Other signals around δ 0 (~25H), 4.5 (~6H) and 7 - 8 (~8H), are not assigned. The same solution exhibited a $^{31}\text{P}\{^1\text{H}\}$ NMR (121 MHz) spectrum dominated by two broad singlets of equal intensity at δ 60.7 and 66.1, as well as two minor peaks of insufficient area (5 - 10% of the total) for the presence of a PPh_3 ligand in the dominant hydride complex present; the low intensity under the ^1H NMR peaks between δ 7 and 8 supports this. The infrared spectrum in KBr showed two weak peaks (ν (Ru-H) 2055, 2027 cm^{-1}) and one very strong peak (ν (CO) 1932), tentatively assigned as indicated; the strong peak had a weak shoulder at 1910 cm^{-1} .

The third red residue gave ^1H NMR signals in the range δ 0.8 to 5, possibly due to a coordinated isoPFA ligand; no clear hydride signal was observed. The IR spectrum ν^{KBr} showed weak peaks at 2055, 2022 and a strong peak at 1940 cm^{-1} (with a weak shoulder at 1983 cm^{-1}). The fourth red residue yielded a $^{31}\text{P}\{^1\text{H}\}$ NMR singlet at δ_{CDCl_3} (121 MHz) 60.2, and strong IR peaks at ν^{KBr} 1957 (with a shoulder at 1921) and 1730 cm^{-1} . No hydride signal was seen in the ^1H NMR spectrum.

In another experiment, in which a wine coloured reaction mixture was generated, but on four times the scale of the previous reaction, a yellow band was eluted in sufficient intensity to be identified as free isoPFA ligand by the ^1H NMR (300 MHz, CDCl_3) spectrum: δ 0.85 - 1.05 (m, PCHCH_3); 1.2 (m, PCHCH_3) 1.38 (dd, $J = 7, 14$ Hz, PCHCH_3), 2.18 (m, PCHCH_3), 3.98 (q (?), FcCHCH_3), 4.05 (s, C_5H_5); 4.10, 4.22, 4.27 (3s, C_5H_3); the data corresponded roughly to those in the literature.⁸

Reactions of $\text{RuHCl}(\text{CO})(\text{PPh}_3)(\text{isoPFA})$, 6, with methanol in the absence and presence of base

The ^1H NMR spectrum of the yellow solid mixture obtained in the absence of base showed upfield hydride resonances at δ -13.9 (t) and -15.3 (dd), indicating the presence of 5 and 6, respectively, in a ratio of $\sim 1:9$.

In the reaction in the presence of KOH, a solution colour change to red and decolouration of the undissolved solid in the tube could be observed during the first hour. The visible spectrum of the final red solution exhibited an intense 542 nm band, typical of the wine coloured solutions. The ^1H NMR (300 MHz, CDCl_3) spectrum of solids isolated from the red solution by decanting indicated that at least $\sim 50\%$ of the 6 had reacted. No 5 was formed in this case, but $\text{RuH}_2(\text{CO})(\text{PPh}_3)_3$ was a major product, as indicated by its distinctive hydride resonances described above. There was also a minor hydride resonance at δ -17.93 (dd, $J = 18, 35$ Hz), which resembles one observed in Figure 5.15 for products obtained by the reaction of 3b with KOH/methanol.

The reaction of 6 with methanol and styrene in the absence of base for 5 d at 80°C resulted in $\sim 3\%$ hydrogenation of the styrene present, as indicated by GC analysis. The ethylbenzene produced is therefore 0.026 mmol, compared to the 0.027 mmol 6 present.

Experiments on the reaction of RuCl₂(PPh₃)(isoPFA), 3b, with KOH/methanol, in THF in the presence or absence of styrene

In an experiment to determine the reactivity of THF with methanolic KOH, a KOH/MeOH/THF/C₆D₆ solution, after 2 h of standing at ambient temperature, showed ¹H NMR signals due only to C₆D₆ (δ 7.23), THF (δ 3.62 (t, 1H), 1.48 (quintet, 1H)) and MeOH (δ 3.25 (s, 3H), 1.64 (s, 1H)). (For a MeOH/C₆D₆ solution: C₆D₆ (δ 7.23), MeOH (3.19 (d, 3H), 2.03 (q, 1H)), and adding KOH to this solution gave rise to a spectrum showing MeOH singlets with δ values identical to those given above; for a THF/C₆D₆ solution: C₆D₆ (δ 7.23), THF (δ 3.64 (t, 1H), 1.49 (quintet, 1H).)

Figure 5.20 shows the ³¹P{¹H} NMR spectra acquired during various time intervals for the reaction mixture formed from 3b, KOH, and styrene, using the method described in section 5.2 for methanol/THF reactions, at ambient temperature and other conditions shown in the figure legend. Spectrum i (Fig. 5.20) reveals some unreacted 3b (δ 95.2 (d), 36.0 (d)), as well as a relatively strong peak due to PPh₃ (δ -5.6). Two pairs of AB doublets are seen at δ 52.01 (d), 42.43 (d) (both with ²J_{PP} = 318 Hz), and δ 51.88 (d), 42.22 (d) (both with ²J_{PP} = 318 Hz), and these intensify with increased reaction time (ii - iv, Fig. 5.20) although the spectrum does not change very much after 1 h. The PPh₃ resonance decreases in intensity with time relative to that in spectrum i, and this decrease is roughly paralleled by a decrease in a resonance at δ 69; decreases in the PPh₃ and δ 69 resonances roughly parallel the increase in the AB pattern. Also, a weak resonance at δ ~58.5 persists for about the first 45 min and then decreases, while weak resonances at δ 56, 60.2, 64.2, and 66 persist throughout the experiment; after ~2 h a weak resonance at δ ~29.5 due to Ph₃PO appears. Figure 5.21 shows the effect on the spectrum, after it had become time-independent, of lowering the temperature. The AB pattern shifts downfield by almost 1 ppm, on lowering the temperature from ambient to -18 °C (spectra i - iii, Fig. 5.21), and then back upfield on warming back to about 20 °C (spectrum iv). Figure 5.21 also shows that, as the temperature is lowered, the integration ratio of the AB pattern to that

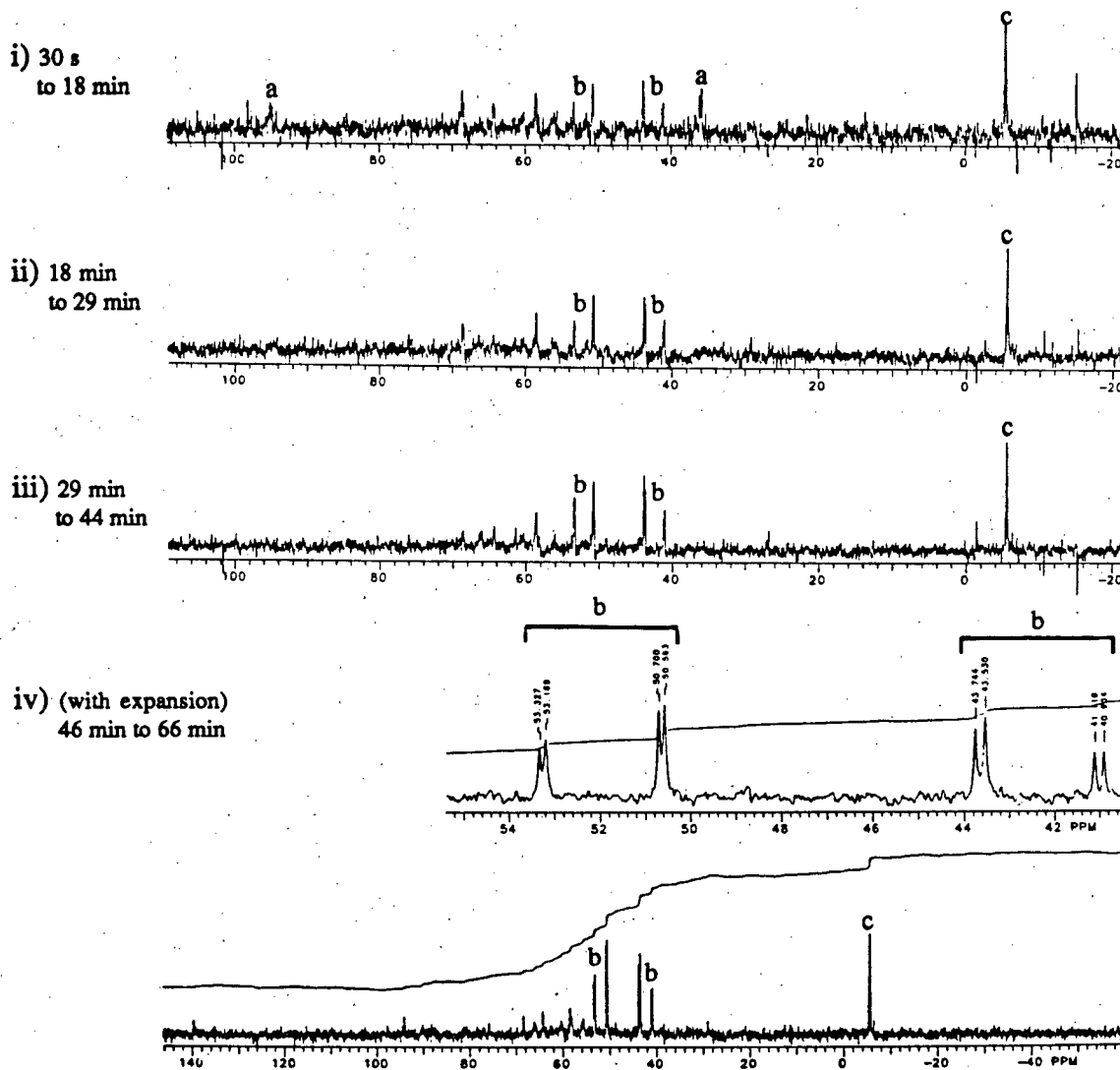
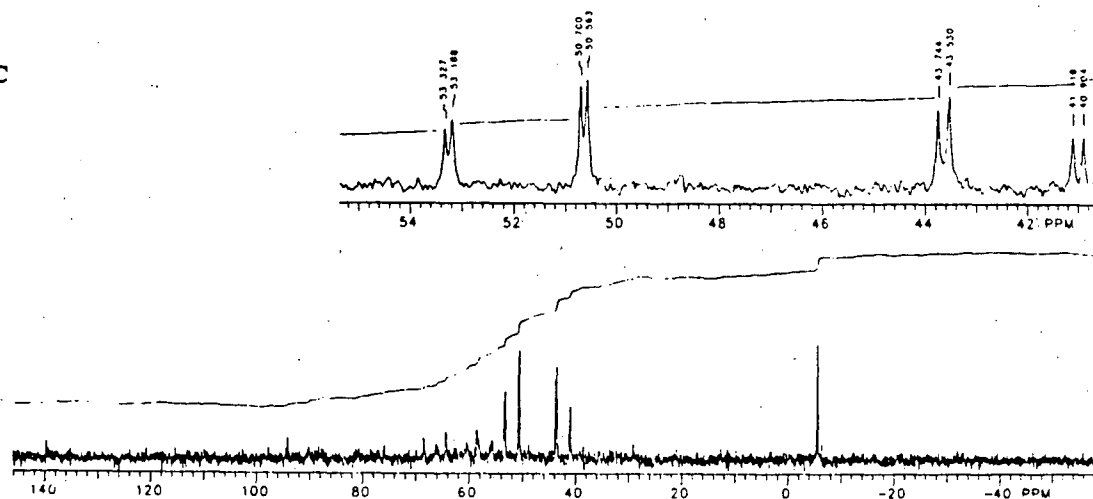
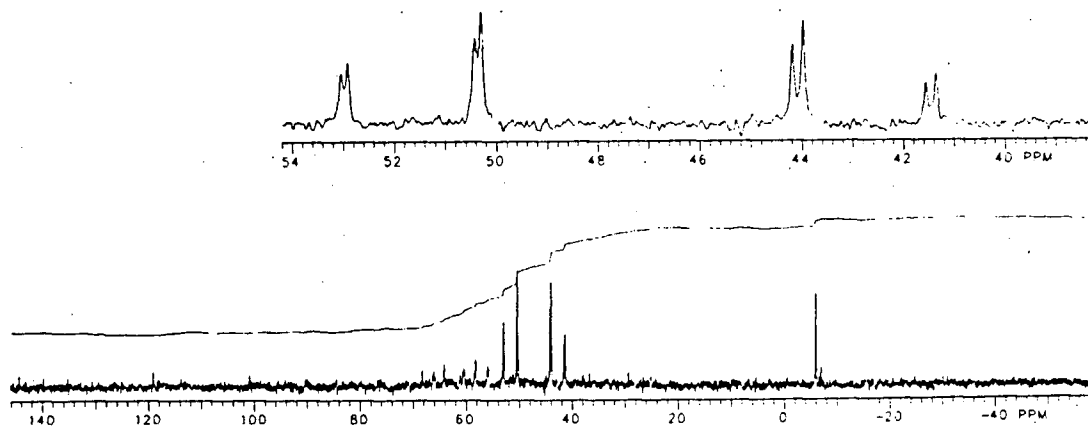


Figure 5.20 The $^{31}\text{P}\{^1\text{H}\}$ NMR spectrum (121 MHz, $\text{CH}_3\text{OH}/\text{THF}$ (1:3), ambient temperature, under nitrogen, unlocked) of the yellow reaction solution formed from mixing a $\text{RuCl}_2(\text{PPh}_3)(\text{isoPFA})$, **3b**/styrene/THF solution with a KOH/methanol solution at ambient temperature under nitrogen. Initial conditions on mixing: $[\text{RuCl}_2(\text{PPh}_3)(\text{isoPFA})]$ (0.0095 M), $[\text{KOH}]$ (0.075 M), $[\text{styrene}]$ (0.43 M). Peak assignments are: 'a', complex **3b**; 'b', complex **6'**, discussed later in the text; 'c', PPh_3 ; other peaks are unidentified. Data acquisition periods are given at the left.

i) 20 °C



ii) 3 °C



iii) -18 °C

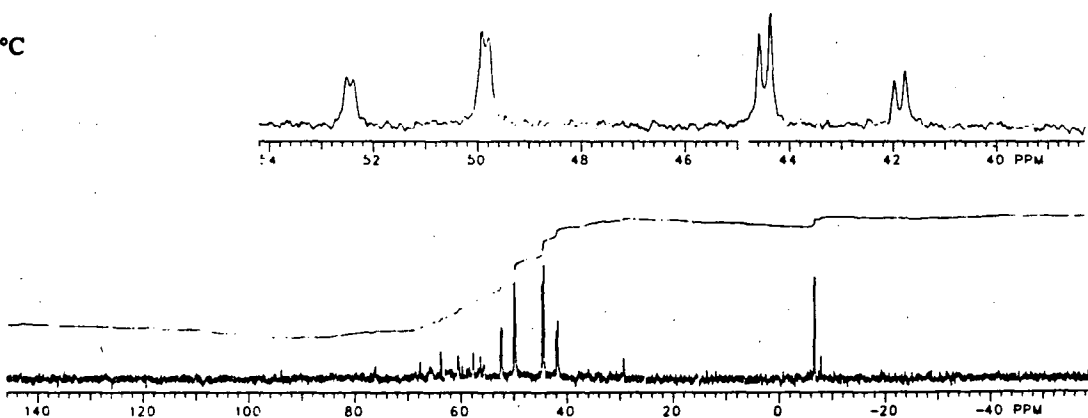


Figure 5.21 Variable temperature spectra for the same solution described for Figure 5.20, recorded after the spectrum had become time-independent. See Figure 5.20 for peak assignments. Expanded plots of the 'b' AB quartet are shown above each spectrum.

iv) 20 °C

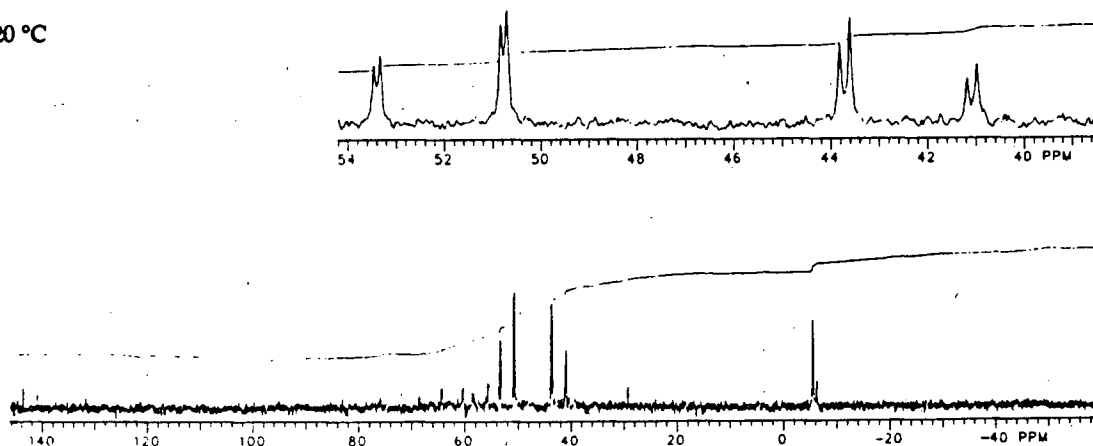


Figure 5.21 continued.

of the PPh_3 resonance clearly increases, and then decreases again on warming back to 20 °C.

In another ambient temperature reaction for 2 d, when the solution had turned bright red, the $^{31}\text{P}\{^1\text{H}\}$ NMR spectrum (Fig. 5.22) was dominated by peaks at δ 66, 62.4, 61, and the PPh_3 peak at δ -5.6. The peaks in the range δ 61 to 66 are similar to those seen in Figure 5.14 for a purely methanolic system in the absence of styrene. Weak resonances at δ 61 (obscured?) and 47 may be due to $\text{RuH}_2(\text{CO})(\text{PPh}_3)_3$ (see above). In none of these reactions in THF/MeOH were resonances due to **6**, *per se*, observed.

When these solutions, with styrene either absent or present, and with $\text{KOH}:\text{Ru} = 1.0$, were worked up (sect. 5.2), **6** was found to be present, as evidenced by ^1H and $^{31}\text{P}\{^1\text{H}\}$ NMR spectroscopy. It should be noted that the presence of ~ 1 equivalent of residual styrene after work-up did not affect the $^{31}\text{P}\{^1\text{H}\}$ NMR resonances due to **6**. Sometimes decomposition of **6** occurred because of exposure to air, the styrene solution of this complex being more air-sensitive than the solid precipitated sample. A colour change to greenish from the yellow colour of **6** in the worked-up residue accompanied aerobic

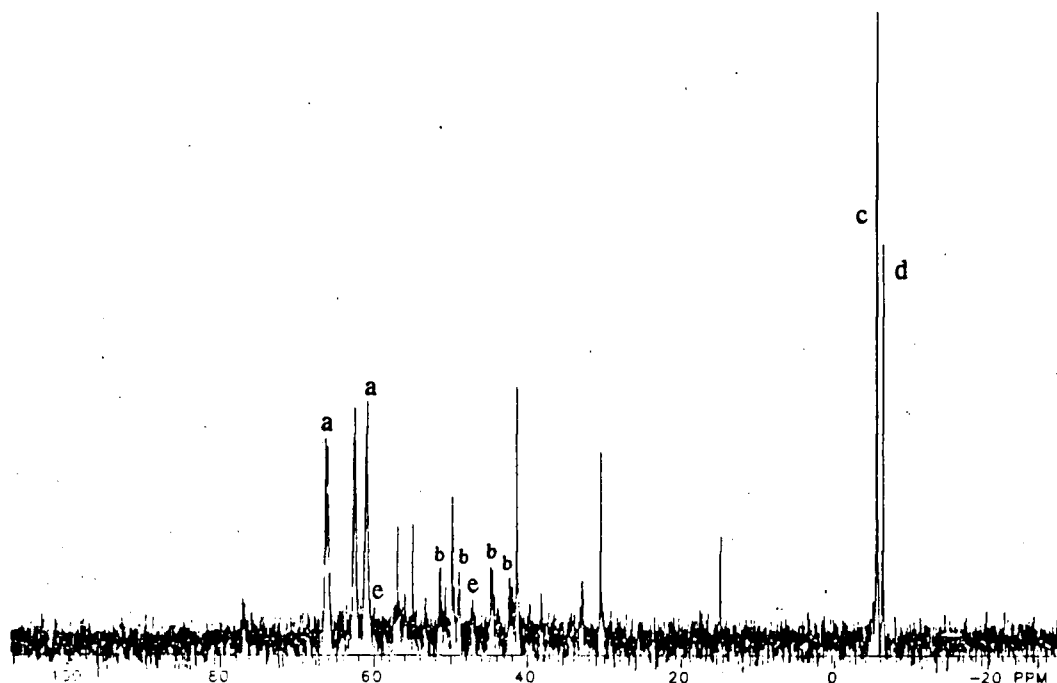


Figure 5.22 The $^{31}\text{P}\{^1\text{H}\}$ NMR spectrum (121 MHz, $\text{CH}_3\text{OH}/\text{THF}$ (1:3), ambient temperature, under nitrogen) spectrum of the red reaction solution formed, after 2 d, in the same way as that described for Figure 5.20, but with the following concentrations: $\text{RuCl}_2(\text{PPh}_3)(\text{isoPFA})$, **3b** (0.01 M), KOH (0.09 M) and styrene (0.86 M). Peak assignments are: 'a', complex X, formulated in section 5.4; 'b', complex **6'**, described later, in section 5.4; 'c', isoPFA; 'd', PPh_3 ; 'e', $\text{RuH}_2(\text{CO})(\text{PPh}_3)_3$; other peaks are unidentified.

decomposition, along with growth of a ^1H NMR hydride resonance at δ -15.8 (t, $^2J_{\text{PH}} = 24$ Hz).

In the H_2 evolution experiment, described in section 5.2, at 27 °C in the absence of styrene in THF (6 mL)/ MeOH (2 mL) with $\text{KOH}:\text{Ru} \approx 1$ (KOH , 0.096 mmol and **3b**, 0.084 mmol), the total gas evolved was 0.075 mmol. Ruthenium complexes were isolated as described in section 5.2 for such THF/MeOH solutions and spectra of this isolated material showed that about 0.064 mmol **3b** had reacted to give mainly **6** which showed characteristic $^{31}\text{P}\{^1\text{H}\}$ NMR resonances at δ 49.8 (d), 31.7 (d), ($^2J_{\text{PP}} = 290$ Hz) and a ^1H NMR upfield hydride resonance at δ -15.3 (dd); other weak ^{31}P resonances observed at δ 98.5 (d), 61 (d), ($^2J_{\text{PP}} \approx 40$ Hz) are assigned to the product $\text{RuHCl}(\text{PPh}_3)(\text{isoPFA})$, **7**, and other weak resonances at δ 51.0 (d), 31.7 (d), ($^2J_{\text{PP}} = 290$ Hz), which increased on

exposure to air, are assigned to an aerobic decomposition product of **6**. A ^{31}P singlet at δ 29.1 is attributed to Ph_3PO , while another weak resonance at δ 71 is unassigned. Of importance, the gas production corresponds to roughly 1 mol H_2 per mol Ru, the evolution being a first-order process (Figs. 5.23, 5.24), with $k_{\text{obs}} = 0.008 \text{ s}^{-1}$.

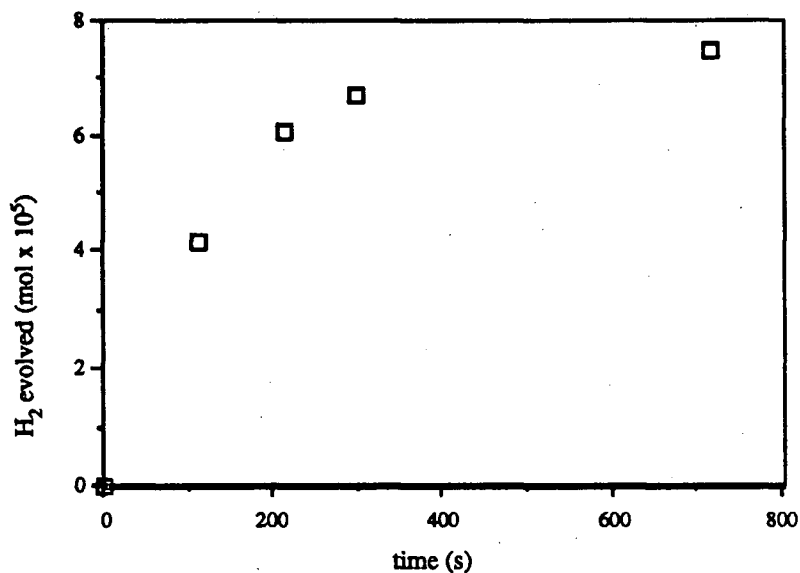


Figure 5.23 Gas evolution plot for a reaction between a solution of **3b** in THF and a KOH/MeOH solution: Reaction conditions: **3b** (0.0105 M), KOH (0.012 M), THF (6 mL), MeOH (2 mL), 27 °C, under nitrogen.

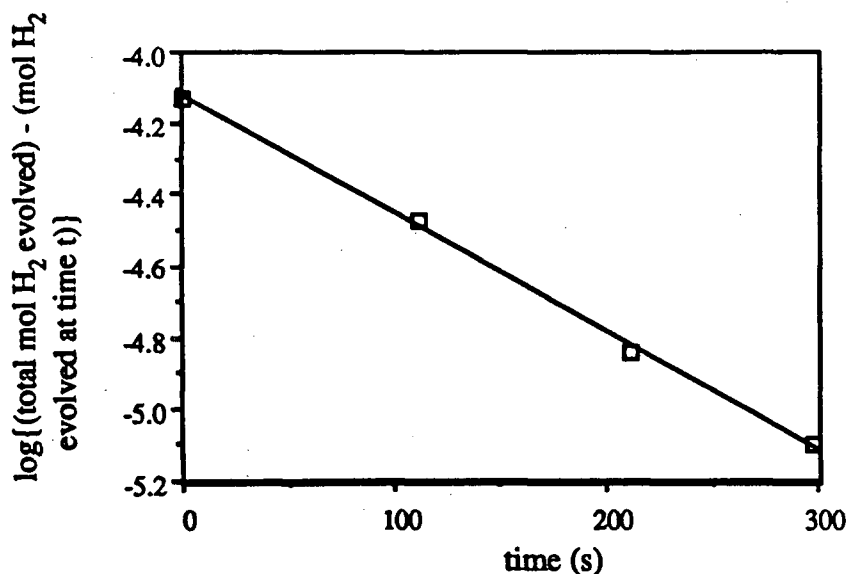


Figure 5.24 Straight-line semi-log plot for Figure 5.23 indicative of first-order gas evolution, based on total mol gas evolved.

In a related experiment, where the KOH/Ru ratio was 0.84, and styrene was present (styrene:Ru = 11), there was no gas evolution. In an experiment at 27 °C with high base and styrene concentrations ($[3b]_0 = 0.0035$ M, $[KOH]_0 = 0.38$ M, $[styrene]_0 = 0.87$ M, in THF (6.5 mL)/MeOH (2.5 mL), total volume: 10 mL), gas evolution was initially rapid and had virtually ceased at 40 min to give a total of ~ 0.12 mmol gas, *i.e.*, 3 mol gas per mol Ru. Gas chromatography indicated the formation of ethylbenzene (0.007 M) at this time. Formaldehyde (0.0027 M) was determined in this reaction solution using the Hantzsch reaction (sect. 5.2); this concentration corresponds to roughly 1 mol CH₂O per mol Ru.

Monitoring the THF/MeOH reaction by visible spectrophotometry:

The changes in the visible spectrum during a reaction of 3b with basic methanol in THF are shown in Figure 5.25. The visible bands of 3b decrease rapidly (a - d, $t_{1/2} = 400$ s), with an accompanying change in the solution colour from green to yellow. A slower secondary colour change from yellow to red then occurs, with the growth of an intense band at 542 nm (d - g, $t_{1/2} = \sim 14$ h).

Figure 5.26 shows the changes in visible spectrum during the secondary stage (intermediate [KOH], yellow \longrightarrow red) of a reaction under the same conditions as those shown for Figure 5.25, but with styrene absent. Similar general features are observed in both the presence and absence of styrene, although in the latter there are differences in

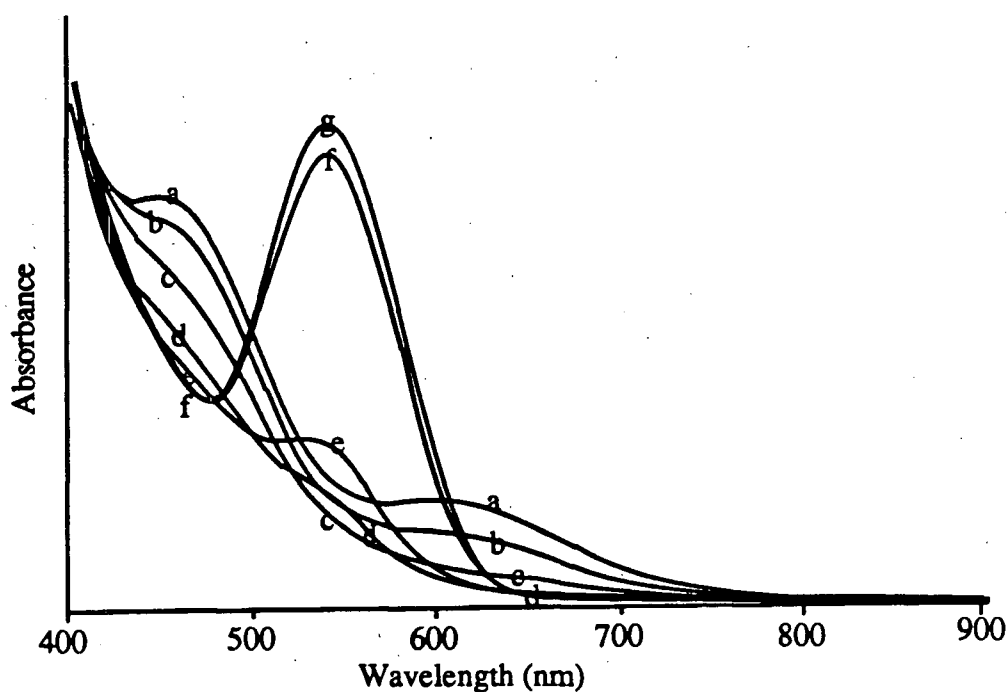


Figure 5.25 The changes in the visible spectrum during a 20 °C reaction of **3b** with basic methanol in THF under nitrogen: $[3b]_0 = 4.6 \times 10^{-3} \text{ M}$, $[\text{KOH}]_0 = 0.0041 \text{ M}$, $[\text{styrene}]_0 = 0.44 \text{ M}$; THF (15.2 mL), MeOH (4.0 mL). Spectra are labelled as follows: 'a', recorded at 3 min after starting the reaction, shows mainly the presence of **3b**, with $\lambda_{\text{max}} = 455, 605 \text{ nm}$; 'b', at 8 min; 'c', at 20 min; 'd', recorded at 1.5 h, shows mainly the presence of **6'**, with $\lambda_{\text{max}} = \sim 450 \text{ nm}$; 'g', recorded at $\sim 4 \text{ d}$, shows mainly the presence of red species with $\lambda_{\text{max}} = 542 \text{ nm}$.

absorbance in the region around 450 nm. Thus, in the first stage in the absence of styrene, the **3b** bands at 455 and 605 nm decrease rapidly, as the solution turns yellow. Then, in the second stage, shown in Figure 5.26, the **6'** absorbance at 450 nm decreases slightly at first, even though at this stage, nothing remains of the **3b** 605 nm band; the absorbance at 450 nm then gradually increases along with the red species band at 542 nm.

The first reaction, loss of **3b** to give **6'**, was monitored by following the loss of absorbance at 605 nm, the λ_{max} of **3b**. Typical continuous plots of the change in absorbance with time are shown in Figures 5.27 ($[\text{KOH}] = 0.066 \text{ M}$) and 5.28 ($[\text{KOH}] = 0.21 \text{ M}$); the derived plots of $\log(A_t - A_\infty)$ vs. t , where A_t = absorbance at time t and A_∞ is the final absorbance, are linear (Figs. 5.29 and 5.30), indicating that the reaction is first-

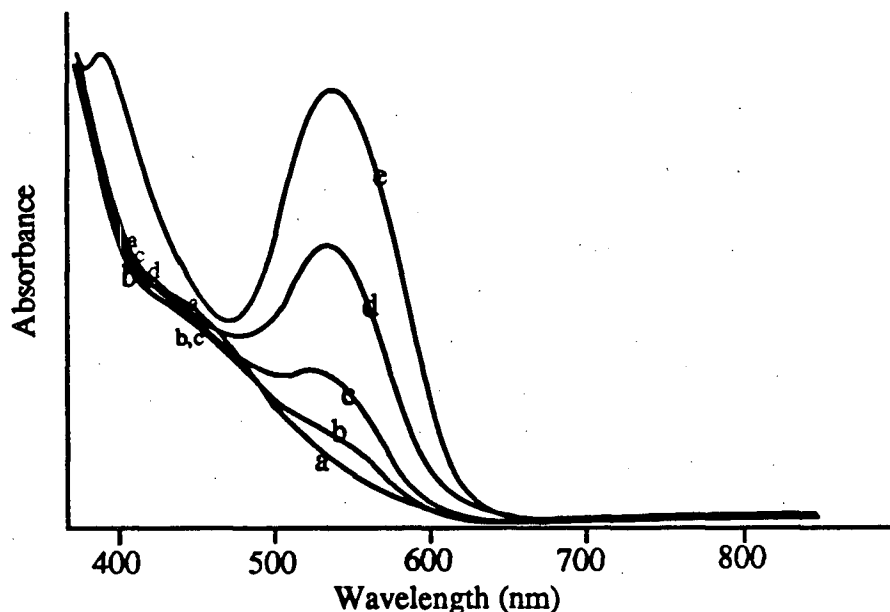


Figure 5.26 Changes in the visible spectrum during the second stage (intermediate [KOH], yellow \rightarrow red) of a reaction between **3b** and methanol in THF in the presence of KOH. Conditions were the same as for the reaction described in Figure 5.25, but with styrene absent. The spectra are: 'a', at 1 h 50 min, showing mainly a band at ~ 450 nm due to complex **6'**, discussed in section 5.4; 'b', at ~ 3 h, showing a decrease at ~ 450 nm and the slight growth of the band at 541 nm due to the red species (including complex **X**, discussed in sect. 5.4); 'c', at 6.5 h; 'd', at 14 h; 'e', at 3.8 d, showing the continued growth of bands at ~ 400 and 542 nm. The entire reaction was monitored at 605 nm, and based on an estimated A_{∞} at about 8 d, the spectrum 'e' represents $\sim 80\%$ completion of the reaction.

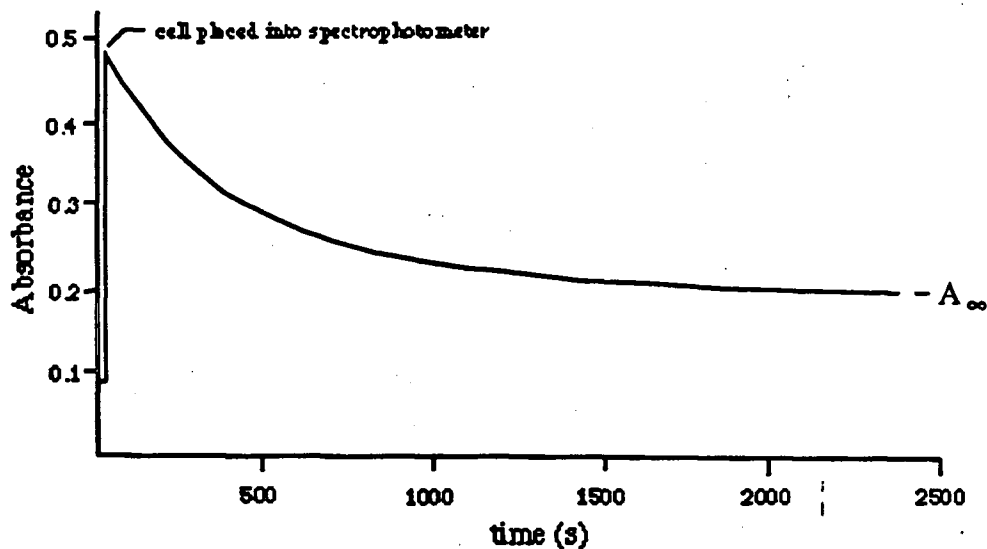


Figure 5.27 Plot of the change in absorbance (605 nm) with time during a reaction of **3b** with KOH/MeOH in THF at intermediate [KOH] (reaction 8, Table 5.6).

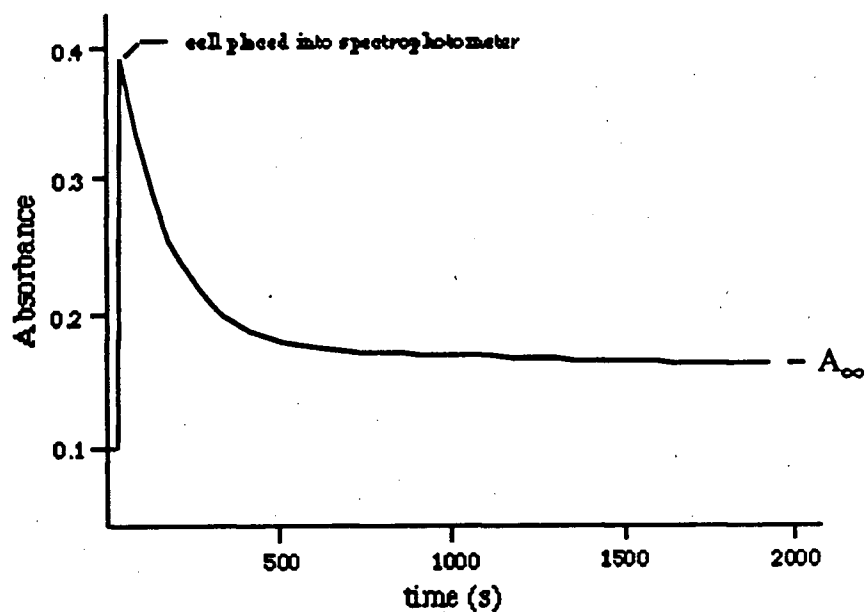


Figure 5.28 Plot of the change in absorbance (605 nm) with time during a reaction of 3b with KOH/MeOH in THF at high [KOH] (reaction 10, Table 5.6).

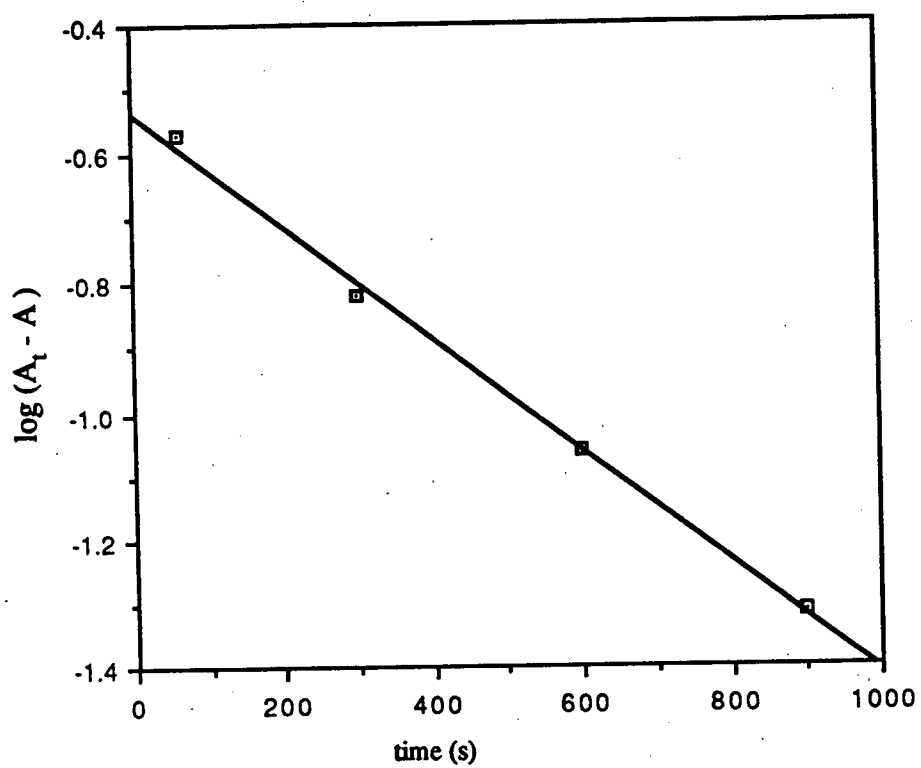


Figure 5.29 Plot of $\log(A_t - A_\infty)$ vs time (t) for the data of Figure 5.27, showing behaviour that is first-order in [3b].

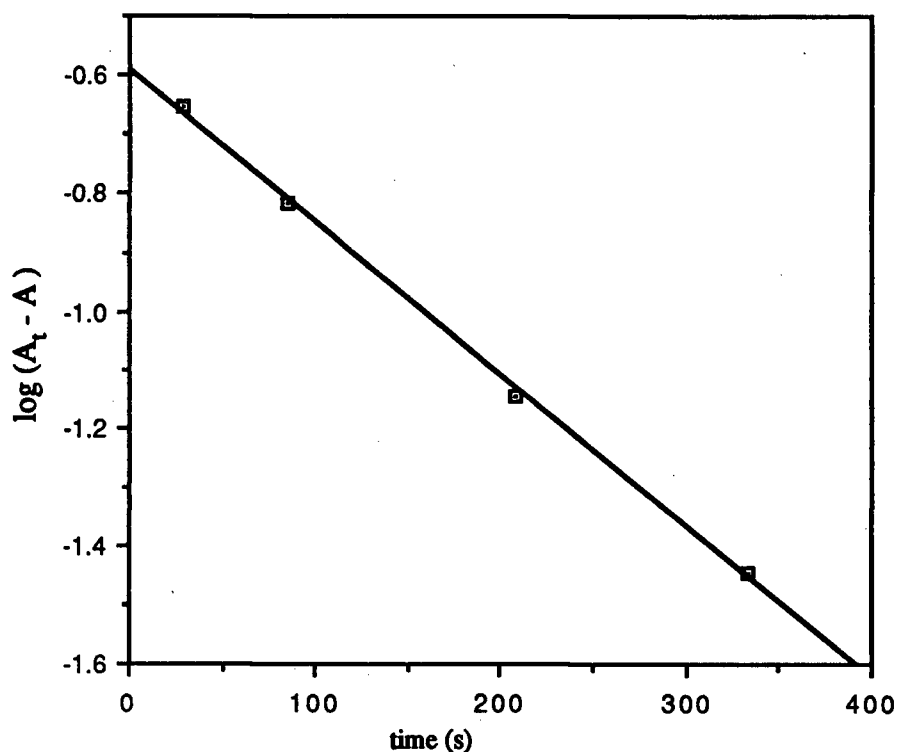


Figure 5.30 Plot of $\log(A_t - A_\infty)$ vs time (t) for the data of Figure 5.28, showing behaviour that is first-order in $[3b]$.

order in $3b$. Similar plots at other $[\text{KOH}]$ values were also linear over at least two half-lives, and the addition of styrene had little influence on the reaction rates. The kinetic data are summarized in Tables 5.6 and 5.7. The variations in k_{obs} with $[\text{KOH}]$ and with $[\text{styrene}]$ are shown in Figures 5.31 and 5.32, respectively.

The reaction was tested for a possible salt effect, in the absence of styrene, by carrying out two further reactions at low $[\text{KOH}]$ (0.001 M), but with added LiNO_3 at concentrations that corresponded to two of the higher $[\text{KOH}]$ values used to obtain the data of Figure 5.31, namely, 0.056 M and 0.18 M (reactions 13 and 14, respectively, Table 5.7). The data are also shown in Figure 5.33, in a standard salt-effect plot, where $k_{I=0}$ is taken as the value of k_{obs} at $[\text{KOH}] = 0.001$ M. There is only a slight positive salt effect (corresponding to a rate increase by a factor of ~ 1.3 over the range 0.00 - 0.18 M KOH M) and thus the shape of Figure 5.31 is largely due to a specific kinetic KOH-dependence.

Table 5.6

Some kinetic data for the reaction^a of $\text{RuCl}_2(\text{PPh}_3)(\text{isoPFA})$, **3b**, with KOH/MeOH in the absence of styrene

Reaction	[3b] (M x 10 ⁴)	[KOH] (M)	t _{1/2} (s)	k _{obs} (s ⁻¹ x 10 ³)
1	3.2	0.0017	570	1.21
2	4.7	0.0040	540	1.28
3	3.4	0.0048	520	1.33
4	5.1	0.0075	510	1.35
5	1.8	0.017	420	1.64
6	2.5	0.034	430	1.60
7	2.0	0.051	400	1.73
8	2.6	0.066	350	1.97
9	2.4	0.10	260	2.60
10	1.8	0.21	120	5.8
11	3.5	0.23	100	6.9
12	2.2	0.25	80	8.6
13	2.0	0.0010 ^b	510	1.35
14	2.8	0.0008 ^c	430	1.60
15	3.6	0.0035 ^d	520	1.32
16	3.4	0.0048 ^e	520	1.31
17	2.6	0.0048 ^f	520	1.33
18	2.6	0.0048 ^f	500	1.38
19	1.0	~0.03 ^g	380	1.8 ^h
20	0.8	~0.03	260	2.7 ^h

^aIn THF at 21 °C under nitrogen.

^b[LiNO₃] = 0.056 M.

^c[LiNO₃] = 0.18 M.

^dAdded [isoPFA] = 8.0 x 10⁻⁴ M.

^eAdded [PPh₃] = 19.8 x 10⁻⁴ M.

^fAdded [PPh₃] = 6.9 x 10⁻⁴ M.

^gAdded KCl (0.4 mg, 0.006 mmol).

^hThere were thermostating problems; however, the temperature drift was estimated to be ~1 °C/250 s, and therefore the difference between at least the initial rates of these reactions is considered significant.

Table 5.7

Some kinetic data for the reaction^a of $\text{RuCl}_2(\text{PPh}_3)(\text{isoPFA})$, **3b**, with KOH/MeOH showing dependence on $[\text{styrene}]$

Reaction	[3b] ($\text{M} \times 10^4$)	[styrene] (M)	[KOH] (M)	$t_{1/2}$ (s)	k_{obs} ($\text{s}^{-1} \times 10^3$)
	-	0	0.060	360	1.90 ^b
1	3.0	0.088	0.060	350	1.97
2	2.6	0.26	0.060	310	2.23
3	3.1	0.55	0.060	320	2.16
4	4.7	0	0.0040	540	1.28
5	3.8	0.22	0.0035	525	1.31
6	3.0	0.44	0.0035	520	1.33
7	4.0	0.66	0.0035	500	1.38
8	2.2	0	0.25	80	8.6
9	1.8	0.44	0.25	80	8.6

^aIn THF at 21 °C under nitrogen.

^bInterpolated from Figure 5.31.

Salt effect corrections for the data of Figure 5.31 were afforded by the line drawn in Figure 5.33. After these corrections were applied, a curve of the form shown in equation 5.24 was fitted to the $[\text{KOH}]$ dependence data within experimental error:

$$k_{\text{obs}} = 1.3 \times 10^{-3} + 0.082[\text{KOH}]^2 \quad (5.24)$$

and Figure 5.34 shows the plot of k_{obs} , corrected for salt effect, vs. $[\text{KOH}]^2$. The rates are essentially independent of the styrene (added as a hydrogen acceptor), Figure 5.32. The rates were also unaffected by addition of either isoPFA or PPh_3 (Table 5.6).

Experiments on the effect of added KCl were carried out, although solubility is limited. The amount used (0.44 mg KCl dissolved in 16 mL of ~0.03 M $\text{KOH}/(\text{MeOH}/\text{THF})$ solution, i.e., 0.0008 M), though not enough to cloud the solution, exceeded the solubility limit; as mentioned above, KCl precipitated out during the MeOH/THF reactions even in the absence of added KCl. The data are summarized in Table

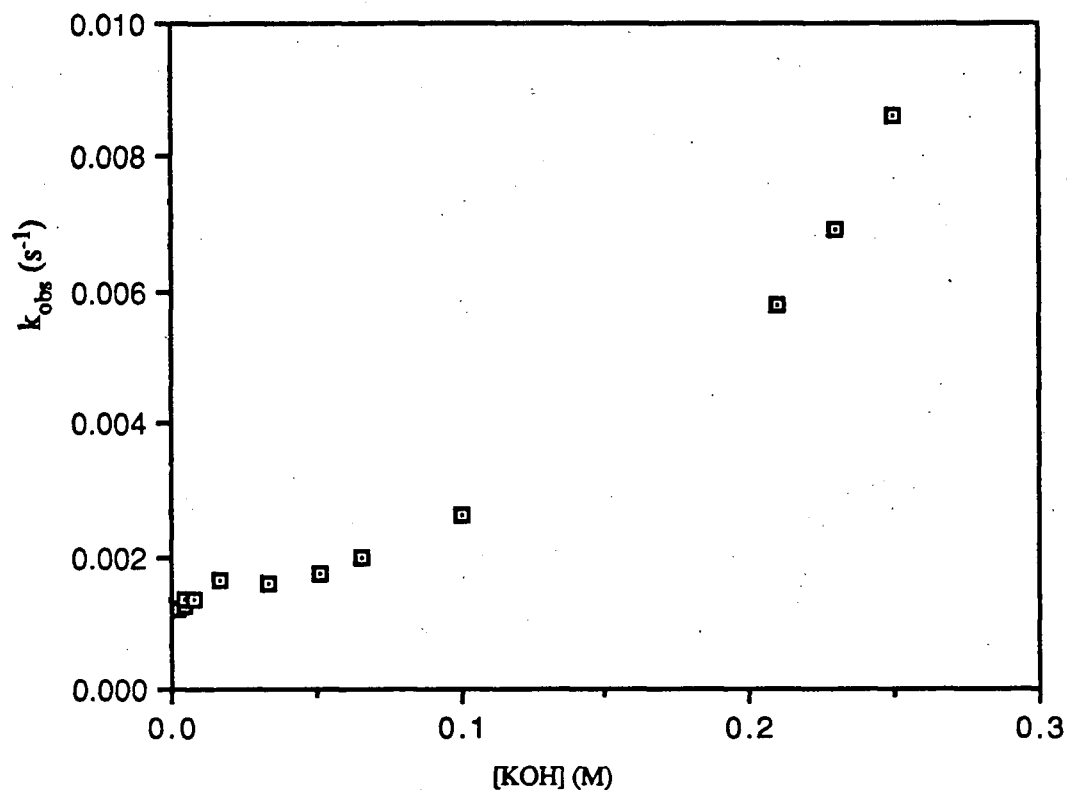


Figure 5.31 Dependence of k_{obs} , from visible spectrophotometric measurements, on $[\text{KOH}]$ for the reaction of **3b** with KOH/MeOH in THF (Table 5.6).

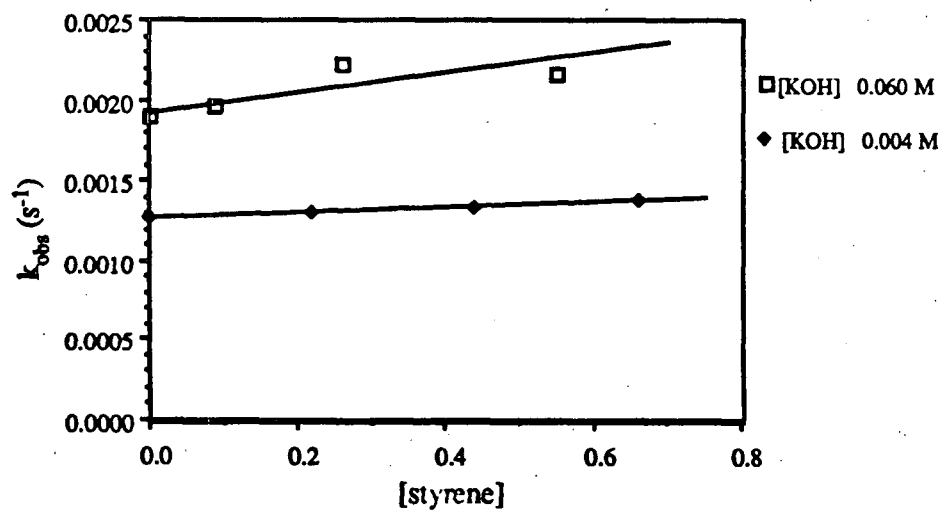


Figure 5.32 Plot of k_{obs} , from spectrophotometric measurements, versus $[\text{styrene}]$ at two different $[\text{KOH}]$ values (Table 5.7).

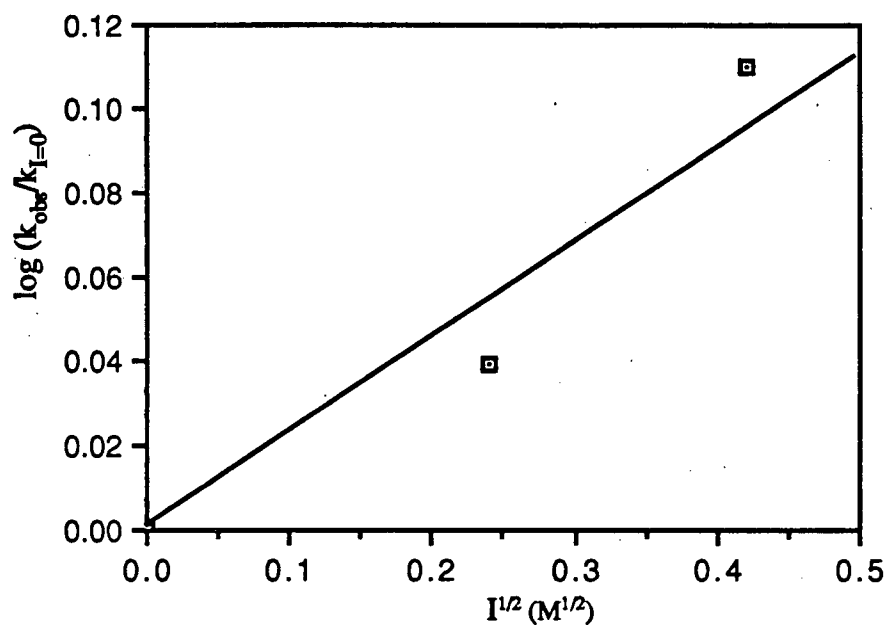


Figure 5.33 Conventional salt effect plot, showing the effect of LiNO_3 on the k_{obs} for the first step of the reaction of 3b with KOH/MeOH in THF (k_{obs} values are for reactions 13, 14, Table 5.6; $k_{I=0}$ is taken as the value of k_{obs} for reaction 1, Table 5.6).

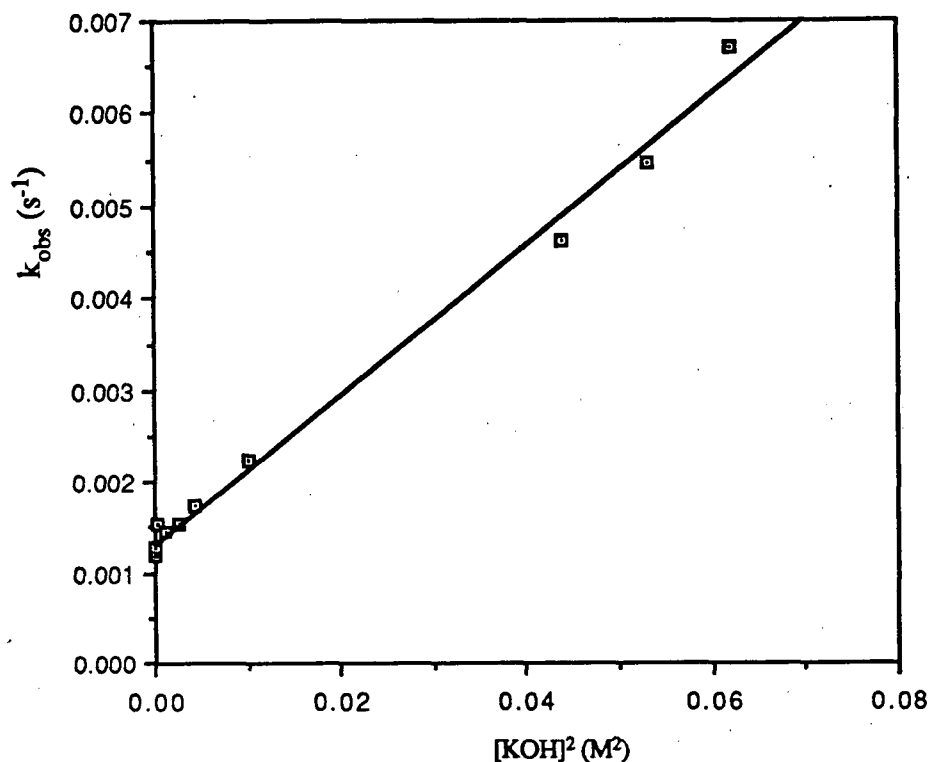


Figure 5.34 Plot of k_{obs} , from spectrophotometric measurements, and corrected for salt effect, versus $[\text{KOH}]^2$, for the reaction of 3b with KOH/MeOH in THF.

5.6. The difference in at least initial rates in the absence and presence of added KCl is significant, and the data are tentatively taken as indicating that added KCl suppresses the reaction rate.

In one of the kinetic experiments, the spectrophotometer light beam was blocked off for approximately half of one half-life after the reaction had commenced; there was no disruption in the exponential profile of the reaction, showing that light is, at least, not required to maintain reactivity.

Gas chromatographic analysis of styrene/ethylbenzene concentrations for these **3b**/KOH/MeOH reactions was carried out in the presence of styrene as a hydrogen acceptor. An example of a plot of $\{[\text{styrene}]_t/[\text{styrene}]_0\} \times 100\%$ vs. time is shown in Figure 5.35 (reaction 8, Table 5.8) and the corresponding semi-log plot is shown in Figure 5.36. The observed first-order process occurs with $k'_{\text{obs}} = 2.23 \times 10^{-3} \text{ s}^{-1}$. The decrease in hydrogenation activity of the system parallels well the disappearance of $\text{RuCl}_2(\text{PPh}_3)(\text{isoPFA})$, **3b**, as seen by comparison with the data of a similar reaction at almost the same $[\text{KOH}]$, monitored spectrophotometrically, where $k_{\text{obs}} = 1.97 \times 10^{-3} \text{ s}^{-1}$ (reaction 8, Table 5.6). Of note, the total amount of styrene hydrogenated, at the point where hydrogenation activity has virtually ceased, is 0.0032 M ($\sim 2\%$), equal to the amount

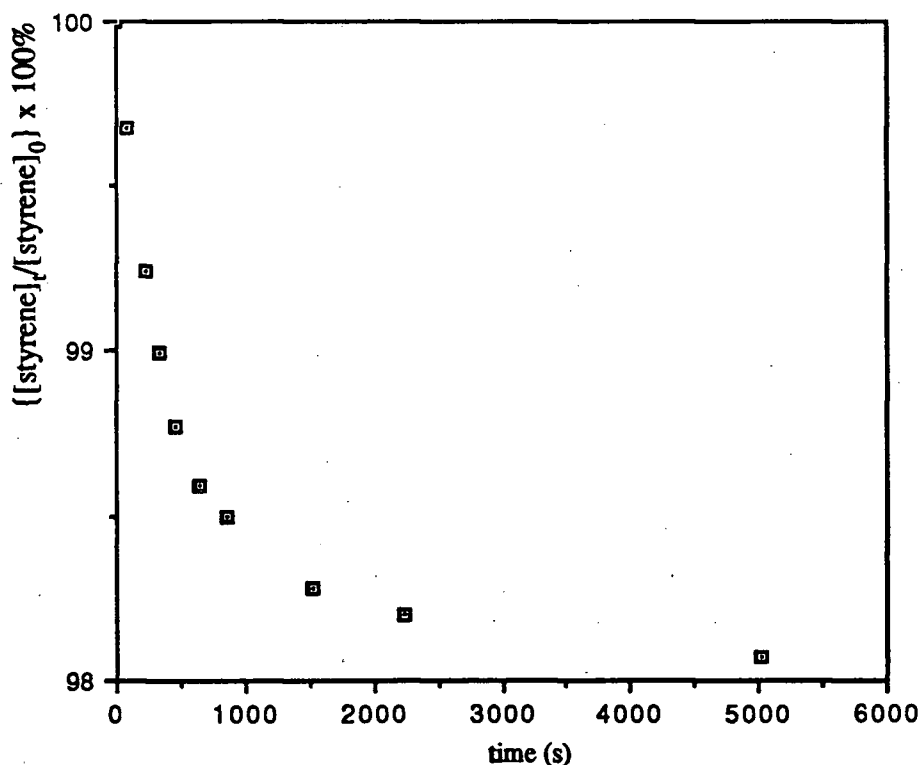


Figure 5.35 Plot of the percentage of styrene, $\{[\text{styrene}]_t/[\text{styrene}]_0\} \times 100\%$, present at time (t), during reaction 8, Table 5.8. The value of $[\text{styrene}]_0$ was taken as the sum of $[\text{styrene}]_t$ and $[\text{ethylbenzene}]_t$, the concentrations at time (t), which were obtained from the GC printout.

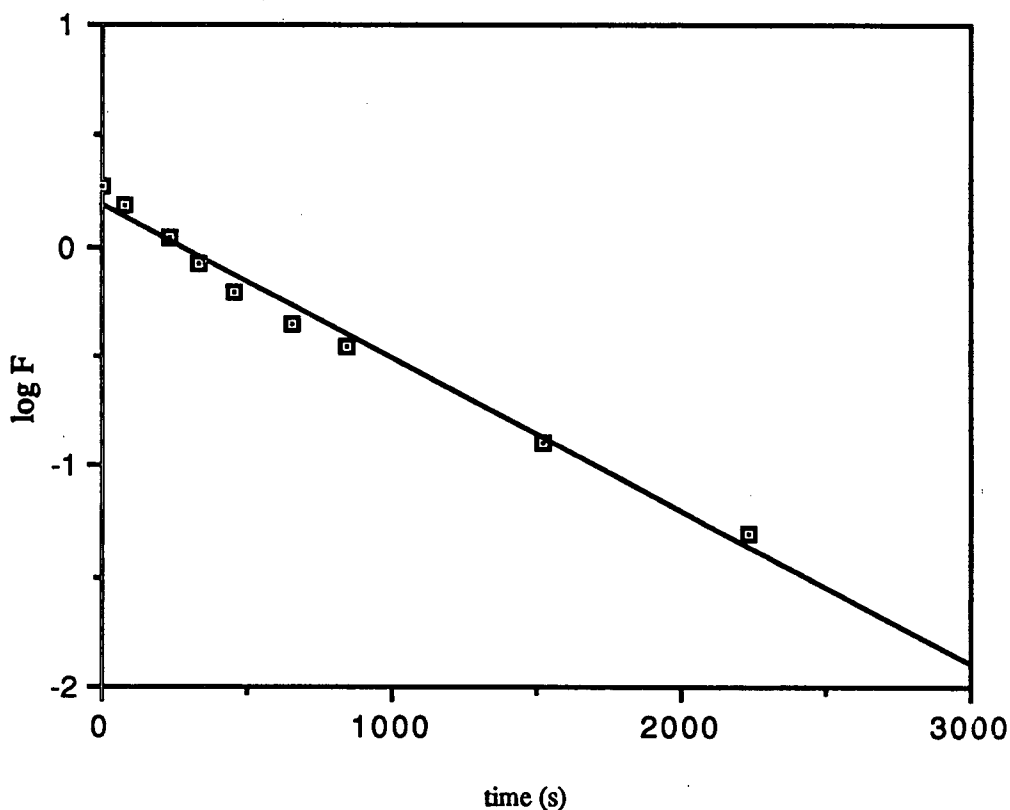


Figure 5.36 Plot of $\log F$ vs. time (t), derived from the data of Figure 5.35;

$F = \left\{ \frac{[\text{styrene}]_t}{[\text{styrene}]_0} - \frac{[\text{styrene}]_\infty}{[\text{styrene}]_0} \right\} \times 100\%$, where $\frac{[\text{styrene}]_t}{[\text{styrene}]_0}$ = the fraction of the original styrene remaining at time (t), and $\frac{[\text{styrene}]_\infty}{[\text{styrene}]_0}$ = the final fraction of the original styrene remaining.

of **3b** used. Thus, the hydrogenation of styrene is stoichiometric, with one mole of styrene hydrogenated per mole of **3b**. If the initial $[\text{KOH}]$ is increased above $\sim 0.060 \text{ M}$, a secondary hydrogenation process increases in importance and this is readily seen in the hydrogenation curves. Figures 5.37 and 5.38 show curves for reactions 6 and 7 (Table 5.8), respectively. In Figure 5.37, the rate decreases exponentially to about 2000 s, and then a second hydrogenation phase is evident until hydrogenation ceases after about 8000 s. This interpretation, of course, depends heavily on the positions of the two points at 1000 and 2000 s, but two other experiments, using the same concentrations and temperature, also exhibited the same 'inflection' in the hydrogenation curve after about 10 half-lives for the rate of disappearance of **3b** ($t_{1/2} = 90 \text{ s}$, from spectrophotometric

Table 5.8

Summary of kinetic data from the GC experiments used to follow styrene hydrogenation during the reaction^a of 3b with KOH/MeOH in the presence of styrene^{b,c}

Reaction	[3b] (M x 10 ³)	[styrene] (M)	[KOH] (M)	t _{1/2} (s)	k' _{obs} ^d (s ⁻¹ x 10 ³)
1	6.6	0.088	0.030	450	1.53
2	6.7	0.088	0.06	460	1.50
3	6.6	0.088	0.12	250	2.76
4	4.5	0.088	0.24	140	4.93
5	6.5	0.088	0.24	125	5.52
6	6.4	0.088	0.24 ^e	165	4.18
7	6.1	0.088	0.30	100	6.9
8	3.2	0.18	0.060	310	2.23
9	3.0	0.35	0.060	210	3.29
10	6.6	0.35	0.060	230	3.00
11	3.6 ^f	0.33	0.060	180	3.83
12	3.6 ^{f,g}	0.33	0.060	210	3.29
13	3.6 ^{f,h}	0.33	0.060	170	4.06

^aIn THF at 21 °C under nitrogen.

^b3b recrystallized from THF; samples recrystallized from CH₂Cl₂ gave variable hydrogenation rates.

^ck'_{obs} is defined in the text, and refers to the primary hydrogenation process.

^dLess frequent sampling (e.g., taking the first sample after ~10 min) consistently gave ethylbenzene concentrations ~20 - 30% higher than those detected using sampling every ~2 min.

^eTechnique in this run improved over that for other 0.24 M experiments.

^f3b recrystallized from CH₂Cl₂.

^gAdded [PPh₃] = 1.4 x 10⁻² M.

^hAdded [isoPFA] = 1.1 x 10⁻² M.

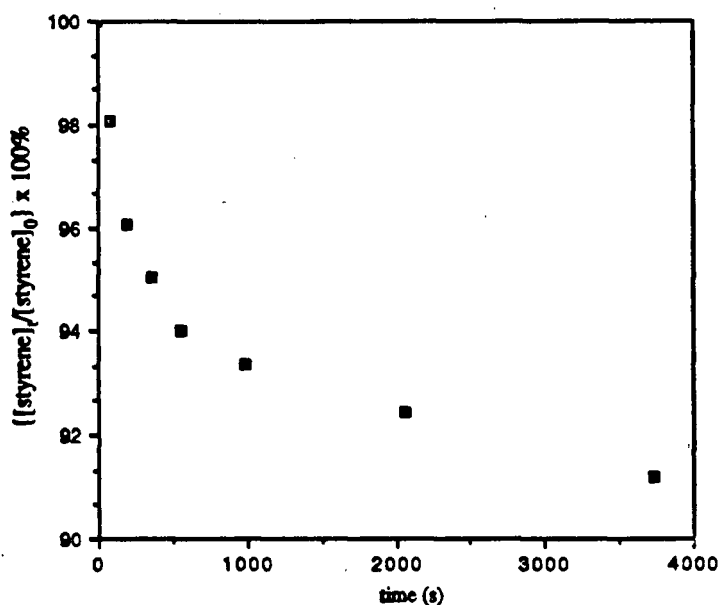


Figure 5.37 Plot of the percentage of styrene, $([\text{styrene}]_t/[\text{styrene}]_0) \times 100\%$, present at time (t), during reaction 6, Table 5.8. The value of $[\text{styrene}]_0$ was taken as the sum of $[\text{styrene}]_t$ and $[\text{ethylbenzene}]_t$, the concentrations at time (t), which were obtained from the GC printout.

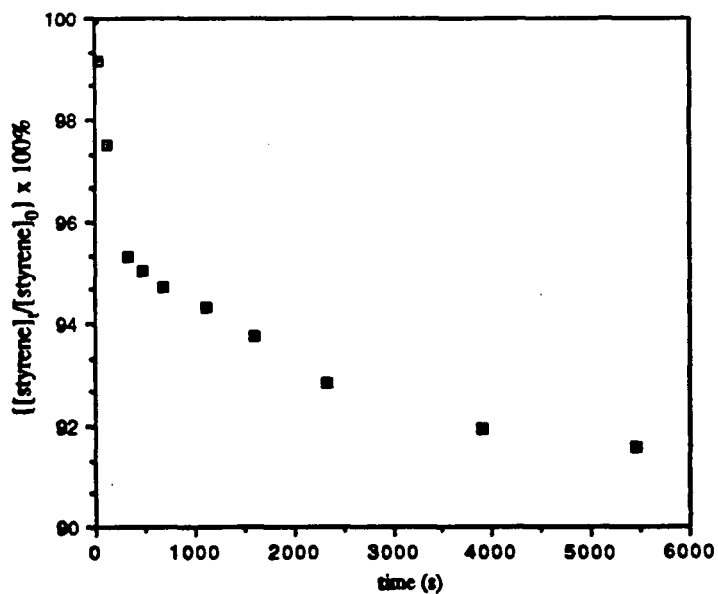


Figure 5.38 Plot of the percentage of styrene, $([\text{styrene}]_t/[\text{styrene}]_0) \times 100\%$, present at time (t), during reaction 7, Table 5.8. The value of $[\text{styrene}]_0$ was taken as the sum of $[\text{styrene}]_t$ and $[\text{ethylbenzene}]_t$, the concentrations at time (t), which were obtained from the GC printout.

measurements, Table 5.6). The ratio of ethylbenzene/Ru is 0.9 at 10 half-lives in this case. Further, the curve in Figure 5.38, at an even higher [KOH], shows a clearer demonstration of this two stage process, with the hydrogenation rate decreasing exponentially to about 1000 s, followed by relatively increased activity which slows markedly on approaching 6000 s. (Clouding of solutions at higher [KOH] interfered with visible absorption measurements, and no k_{obs} values for decay of 3b were obtained above 0.25 M KOH; however, $t_{1/2}$ for this reaction at [KOH] = 0.3 M is probably less than 60 s, based on data from Figure 5.34, including a correction for a salt effect estimated from Figure 5.33.) The stoichiometric hydrogenation associated with the primary reaction of 3b with KOH/MeOH would be virtually over after 10 half-lives; in this case, the ratio of ethylbenzene/Ru is 0.7 at $t = 10t_{1/2}$ by which time less than 0.1% of the activity resulting from the presence of 3b would be remaining. This is further reason to believe that the observed two-stage hydrogenation at higher [KOH] is real, since the first stage occurs within 10 half-lives for loss of 3b. Thus, for semi-log plots used to estimate k'_{obs} for these hydrogenations at higher [KOH] (Figs. 5.39, 5.40), the value for $[\text{styrene}]_{\infty}/[\text{styrene}]_0$ was taken as the value at time $(t) = 10t_{1/2}$, $t_{1/2}$ being estimated from spectrophotometric measurements; $[\text{styrene}]_0$ was taken as the sum of the [styrene] and [ethylbenzene] which were obtained from the GC printout. The variation of k'_{obs} with [KOH] and with [styrene], along with experimental conditions used, are summarized in Figs. 5.41 and 5.42, respectively, and in Table 5.8. The high value of k'_{obs} at 0.3 M (Fig. 5.41), is probably due to a contribution by the secondary hydrogenation process. The hydrogenation rates very approximately follow a first-order dependence on [KOH], with about the same intercept as obtained for the dependence on [KOH] for the decay of 3b. Figure 5.42 indicates a dependence on [styrene] that is at least close to first-order. The y-intercept of Figure 5.42

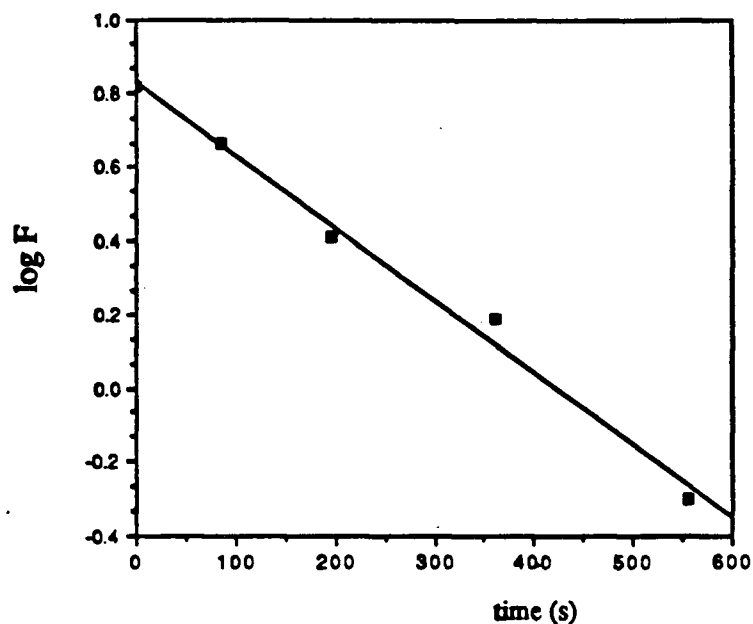


Figure 5.39 Semi-log plot, showing the first-order behaviour of the primary hydrogenation process, derived from the data of Figure 5.37 as described in the text. The function F is the same as defined for Figure 5.36.

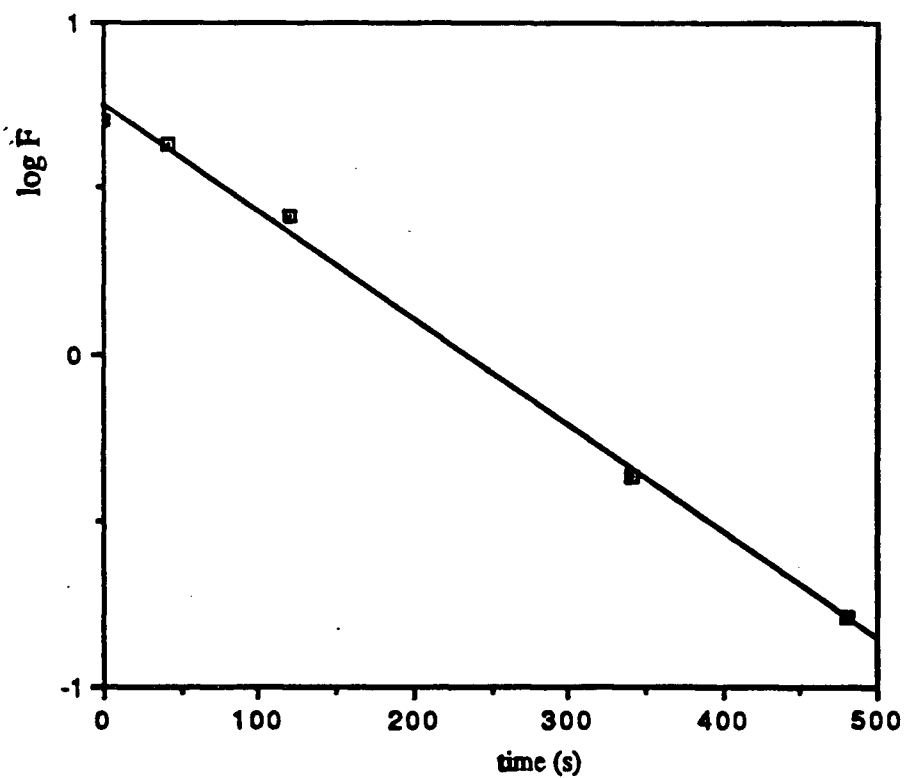


Figure 5.40 Semi-log plot, showing the first-order behaviour of the primary hydrogenation process, derived from the data of Figure 5.38 as described in the text. The function F is the same as defined for Figure 5.36.

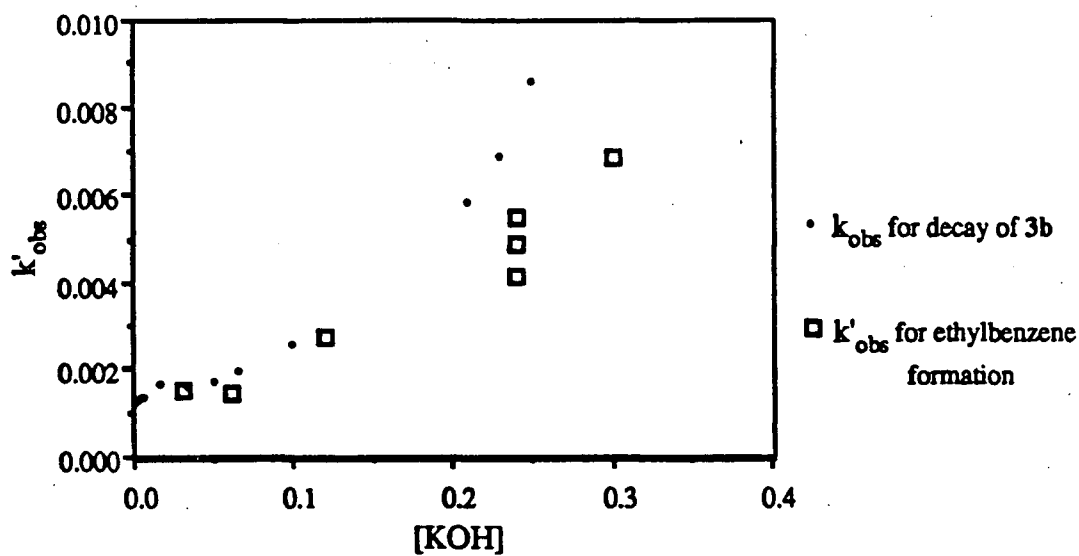


Figure 5.41 Plot showing $[\text{KOH}]$ dependence of k'_{obs} for styrene hydrogenation, in the reaction of 3b with methanol in the presence of styrene and KOH in THF (Table 5.8); data from Figure 5.31 are included for comparison.

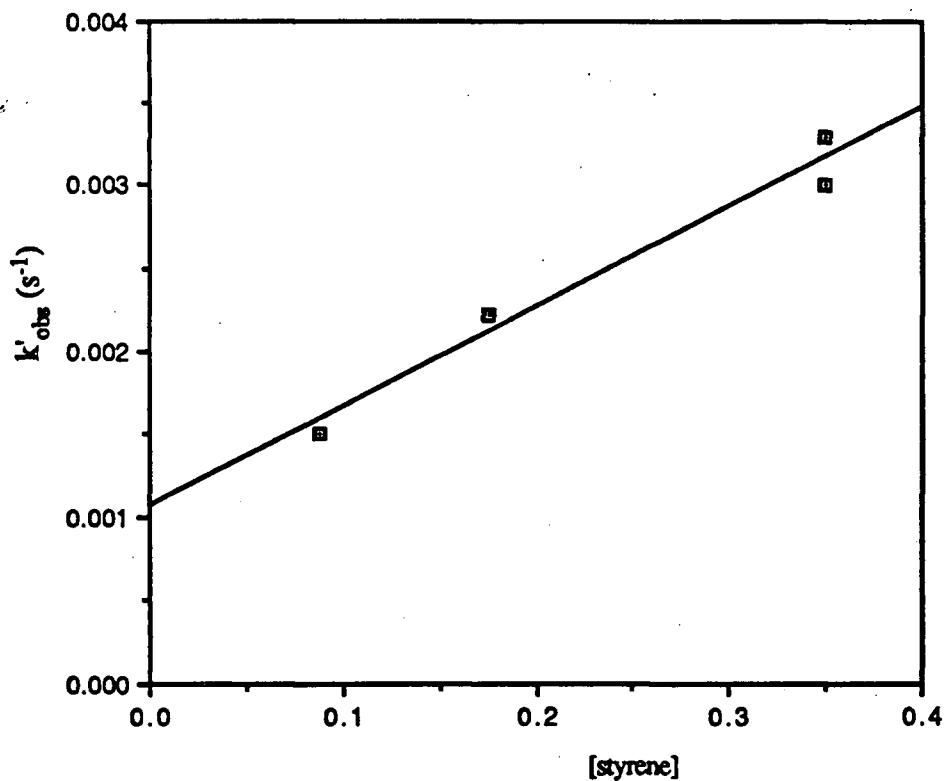


Figure 5.42 Plot showing $[\text{styrene}]$ dependence of k'_{obs} for styrene hydrogenation, in the reaction of 3b with methanol in the presence of styrene and KOH in THF (Table 5.8).

(0.0011 s^{-1}) is slightly lower than that (0.0017 s^{-1}) obtained by interpolation of the data of Figure 5.31 at this 0.060 M $[\text{KOH}]$ where the $[\text{styrene}] = 0$. (The data of Figure 5.32, which shows the $[\text{styrene}]$ dependence of k_{obs} determined from spectrophotometric measurements, give a k_{obs} value of 0.002 s^{-1} at corresponding conditions.) Values of k'_{obs} at higher $[\text{styrene}]$ ($> 0.18 \text{ M}$) are greater than k_{obs} at corresponding $[\text{styrene}]$.

In reaction 8 within Table 5.8, at 0.060 M KOH , the data show stoichiometric hydrogenation of styrene based on **3b**, as was generally the case in experiments with $[\text{KOH}]$ below 0.2 M .

Effects of adding excess PPh_3 or isoPFA in these GC kinetic experiments were relatively small (Table 5.8), and it should be noted that these experiments were carried out using **3b** recrystallized from CH_2Cl_2 and the measured styrene hydrogenations were some 25 - 30% more than stoichiometric based on $[\text{Ru}]$; but the calculation of k'_{obs} values for the three experiments (reactions 11 - 13, Table 5.8) was based on a stoichiometric limiting amount of hydrogenation for comparison with the previous results. (Use of CH_2Cl_2 -recrystallized **3b**, instead of the THF -recrystallized complex, did not significantly affect the k_{obs} values obtained from spectrophotometric experiments.)

Experiments were conducted for the detection of KCl , which deposited during the course of the primary reactions between $\text{RuCl}_2(\text{PPh}_3)(\text{isoPFA})$, **3b**, and $\text{KOH}/\text{MeOH}/\text{THF}$. When the white precipitate was dissolved in water and mixed with AgNO_3 solution, a white solid precipitated which was insoluble in dilute HNO_3 and presumed to be AgCl . The precipitate deposited during the Ru reaction must be KCl .

Product KCl was unambiguously identified when CH_2Cl_2 was used in place of THF . In the CH_2Cl_2 'KCl detection experiment' described in section 5.2, the isolated white precipitate formed in the first minute of the reaction of **3b** with KOH/MeOH analyzed correctly for KCl ; and atomic emission analysis of an aqueous solution of the white solid ($16 \text{ mg}/100 \text{ mL}$) gave a reading intermediate between those obtained for 10 and $20 \text{ mg}/100 \text{ mL}$ KCl solution standards, thus indicating the expected K content. The residue derived

from the yellow supernatant decanted off from the precipitate of KCl exhibited a $^{31}\text{P}\{^1\text{H}\}$ NMR spectrum which showed the residue was a mixture, including free PPh_3 (δ -5.6) and some $\text{RuHCl}(\text{CO})(\text{PPh}_3)(\text{isoPFA})$, **6**, (δ 50.0 (d), 31.9 (d), $^2J_{\text{PP}} = 290$ Hz) with associated isomers, as noted elsewhere. The ^1H NMR showed the associated upfield hydride resonance at $\delta \sim 15$. Other unidentified species were present, but the reaction seems similar to that in THF, and KCl is considered to be formed in the basic methanol reaction in both THF and CH_2Cl_2 .

In the experiment to determine the formaldehyde content of a distillate from a reaction of **3b** with KOH/MeOH in THF, a trace of CH_2O (0.00023 mmol) was detected, which corresponds to $\sim 1\%$ of a stoichiometric amount. In the experiment to determine the non-volatile formaldehyde content in the reaction mixture produced in the high [styrene], high [KOH] experiment for H_2 evolution, visible absorbance measurements on the yellow Hantzsch reaction product solution indicated a CH_2O concentration of ~ 19 $\mu\text{g}/\text{mL}$ in the 40 mL of worked up aqueous solution; thus, a total of ~ 750 μg (0.025 mmol) was produced in the reaction.

Sampling of the headspace gas above the **3b**/ $\text{KOH}/\text{MeOH}/\text{THF}$ reaction mixture in the 'CO detection experiment' revealed nitrogen but no CO.

Deuterium transfer experiments were conducted on reactions of **3b** with $\text{KOH}/\text{MeOH}-d_4$ and $\text{MeOH}-d_1$ in the presence of styrene. The extents of hydrogenation in the $\text{MeOH}-d_4$ and $\text{MeOH}-d_1$ reactions were 10 and 15% (by GC), respectively; i.e., ~ 5 and 7.5 turnovers based on Ru. The ^2D NMR spectra of the distillates of the reaction mixtures obtained after reaction are shown in Figures 5.43a and b, respectively. The reference spectra are shown in Figure 5.44a (styrene/acetone) and Figure 5.44b (ethylbenzene/acetone). All the spectra shown in Figures 5.43 and 5.44 show a peak due to deuterium in unenriched acetone at δ 2.03, which provided a useful reference peak. Both spectra in Figure 5.43 show peaks due to the deuteriated ethyl group of ethylbenzene, at δ 1.15 and 2.58, which are proof that methanol D atoms are transferred to styrene in the

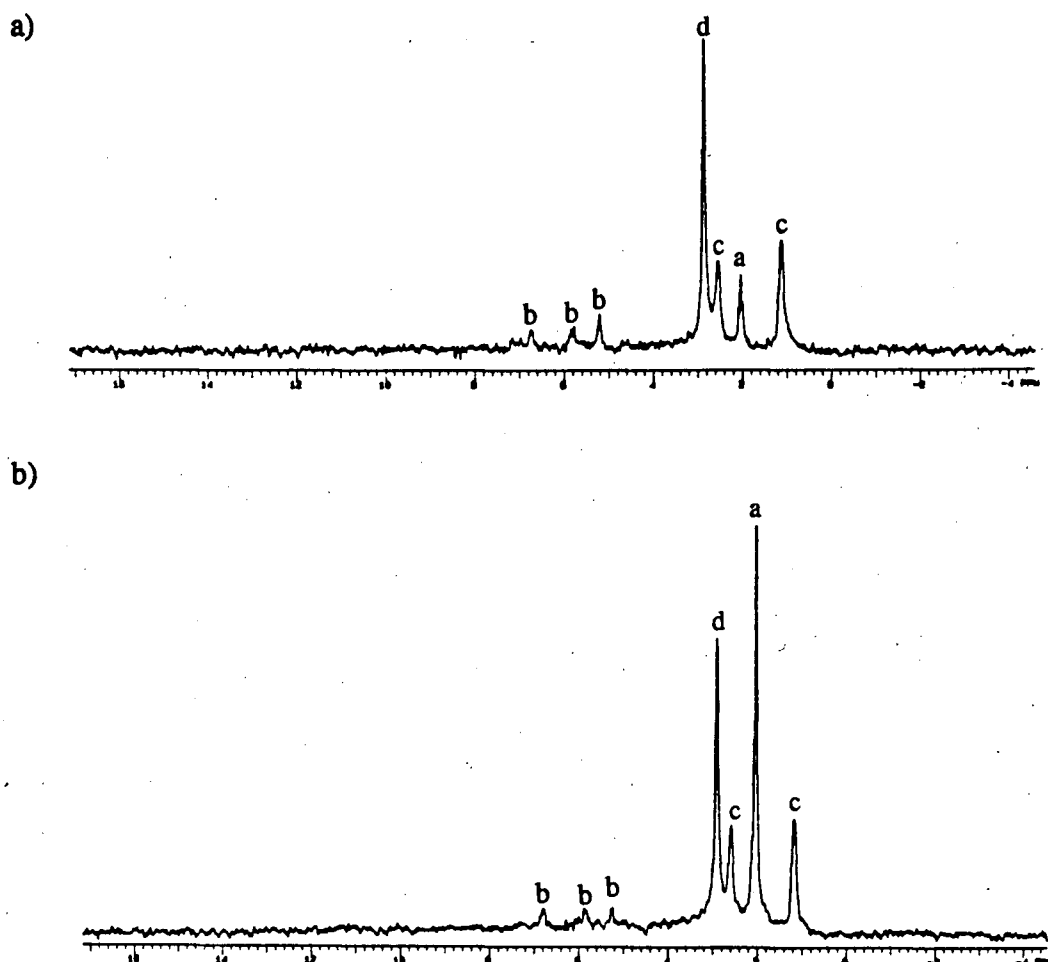


Figure 5.43 ^2D NMR (46 MHz, ambient temperature) spectra of deuterated ethylbenzene obtained by hydrogen transfer from (a) MeOH-d_4 and (b) MeOH-d_1 to styrene during the reaction of $\text{RuCl}_2(\text{PPh}_3)(\text{isoPFA})$, **3b**, with MeOH-d_4 and MeOH-d_1 , respectively, in the presence of KOH in THF . Peaks are assigned as follows: 'a', acetone; 'b', styrene; 'c', ethylbenzene; 'd', an unidentified impurity.

reaction, and also weak peaks due to the deuterated vinyl group of styrene at δ 5.2, 5.8 and 6.8, indicative of considerable exchange of vinyl hydrogen atoms with deuterium, because the NMR spectrum represents a GC fraction that contained perhaps 10% of the styrene present because of peak overlap with the ethylbenzene fraction. Both spectra also show an unidentified, strong peak at δ 2.9.

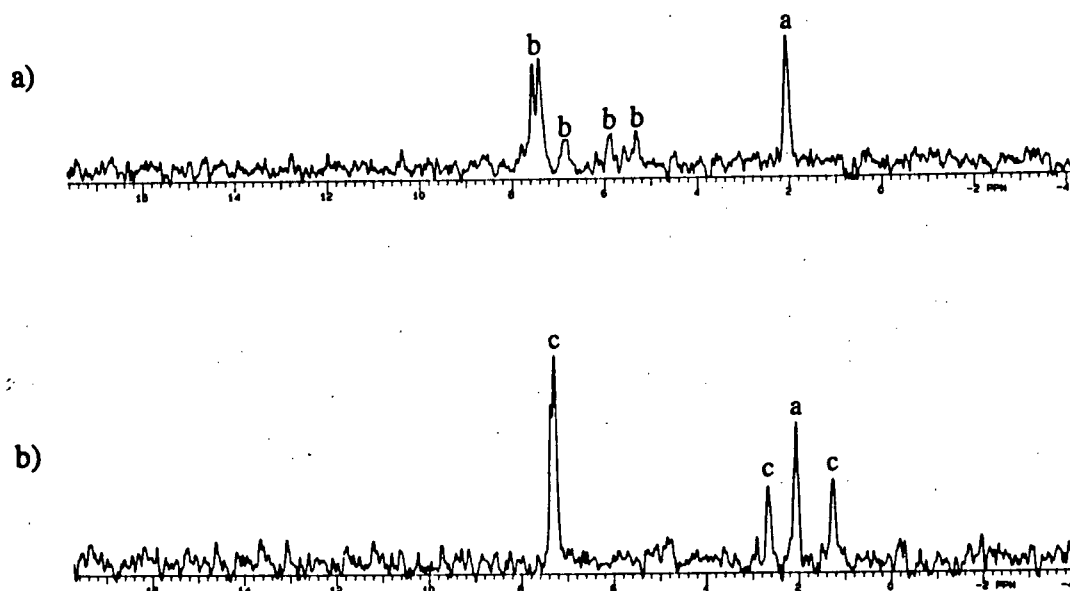


Figure 5.44 ^2D NMR (46 MHz, ambient temperature) spectrum of (a) a 1:1 unenriched acetone/styrene mixture and, (b) a 1:1 unenriched acetone/ethylbenzene mixture. Peaks are marked as described for Figure 5.43.

An experiment to determine what would happen to CH₂O generated in a solution similar to those used for the reactions of 3b with KOH/MeOH

When the formalin/KOH/MeOH/THF solution described in section 5.2 for the title experiment was neutralized, a white solid precipitated which was insoluble in HCl_{aq}, water, diethylether, acetone, methanol, benzene and dichloromethane, but was somewhat soluble in methanolic or aqueous KOH solutions. The mass spectrum showed mainly peaks at m/z = 30, 29, and 28, probably due to HCHO⁺, CHO⁺ and CO⁺. Anal. Calcd. for H(CH₂O)_nOH (n = 20 - 40): C, 38.83 - 39.41; H, 6.80 - 6.73. Found: C, 39.11; H, 6.90. Thus, the white solid is a polymerized form of formaldehyde, with an average of 20 - 40 carbons per chain, a range based on experimental errors in the analysis.

5.4 Discussion

Solution behaviour of RuCl₂(PPh₃)(isoPFA), 3b

There is no evidence for the dissociation of PPh₃ from **3b**, as the visible spectrum is unaffected by the presence of added PPh₃; nor is there any indication of the coordination of MeOH or THF to **3b**, since the visible spectrum is the same in THF, THF/MeOH or the non-coordinating solvent, CHCl₃. It appears that there is no observable coordination of styrene to **3b**, since the ³¹P{¹H} NMR spectrum of the starting complex, **3b**, in CDCl₃ was unchanged on addition of up to a 10-fold excess of styrene.

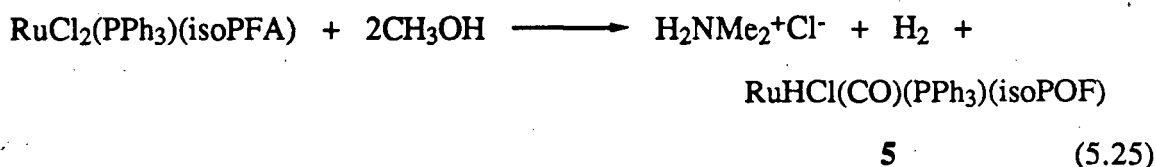
Reactions of RuCl₂(PPh₃)(isoPFA), 3b, and derivatives formed from methanol in the absence of added base

The RuHCl(CO)(PPh₃)(isoPOF), **5**, ³¹P{¹H} NMR coupling constants (²J_{PP} = 188 Hz) are in the range typical for coordinated *trans* phosphorus ligands.⁹¹ The ¹H NMR values of ²J_{PH} = 19 Hz for the upfield hydride triplet at δ -13.9 are in the range typical of a hydride *cis* to phosphorus atoms coordinated to ruthenium(II), and the position of the shift (δ upfield of -10) is typical of a hydride *trans* to a ligand of low *trans* influence, such as Cl.⁸⁹ The downfield shift (δ 6.52) of the proton on the carbon α to the ferrocene ring is typical of values (δ 5.0 - 6.5) obtained for coordinated isoPFA or PPFA (sect. 2.2), suggesting that the OMe group on the isoPOF ligand is coordinated in solution. The spectroscopic data are thus consistent with the crystal structure shown in Figure 5.6. In this structure, the arrangement of ligands is very close to octahedral, with a P₁-Ru₁-P₂ axis that is almost linear, ∠P₁-Ru₁-P₂ = 177.55(6). The ∠Cl-Ru-CO angle is 101.4(2), and the other three angles that are equatorial to the P₁-Ru₁-P₂ axis are slightly reduced from 90°: ∠H₁-Ru₁-CO = 82.5, ∠O₂-Ru₁-H₁ = 87.7, ∠O₂-Ru₁-Cl₁ = 88.4. The hydrido-carbonyl H-C distance is 2.2 Å, precluding any C-H interaction (there is precedent for intramolecular hydride transfer to a carbonyl on ruthenium).¹⁵⁵ The Ru-P distances of 2.358(2) and 2.354(2) are close to the Ru-P distances, ranging from 2.301 to 2.383(2),

obtained in the present work for other ruthenium(II) hydrido-carbonyls where Ru-P is approximately *trans* to another Ru-P bond (Tables 5.1, 5.2, 5.5). For the hydrido-chloro-phosphines without carbonyl groups (*cf.* Tables 5.1, 3.7 and 3.8), there is a tendency for the Ru-P distances to be slightly shorter, possibly because of greater electron density on the ruthenium atom due to the absence of back-bonding to a carbonyl, and consequently increased back-bonding to phosphines. The Ru-H distance of 1.57 Å for **5** is generally close to those of other ruthenium(II) terminal hydrides of complexes synthesized in the present work, which are in the range: 1.47(4) to 1.53(6) Å (Tables 5.1 and 3.8).

The formulation of **5** is analogous to that of the hydrido-carbonyls $\text{RuHCl}(\text{CO})(\text{PR}_3)_3$, formed from the reaction of other ruthenium phosphine complexes with methanol and reported in the literature (see sect. 5.1).

A possible stoichiometry for the formation of the complex **5** is:



No attempt was made to detect $\text{H}_2\text{NMe}_2^+\text{Cl}^-$ or H_2 in the product mixture. A suggested approach to isolate $\text{H}_2\text{NMe}_2^+\text{Cl}^-$ would be to induce its crystallization by addition of benzene and hexane, as was done in the isolation of $\text{H}_2\text{NMe}_2^+\text{Cl}^-$ from the reaction of **3b** with H_2 , where the same NMe_2 cleavage was noted (sect. 4.3). The mechanism for the formation of **5** could involve protonation of the $-\text{NMe}_2$ by coordinated CH_3OH , or from free proton following methoxide formation, to give non-coordinated $-\text{NMe}_2\text{H}^+$ and a coordinated methoxo group, followed by substitution, at the carbon atom α to the ferrocene, of the NMe_2H by the OMe group. This could occur after loss of Cl and formation of the hydrido-carbonyl, because **6**, $\text{RuHCl}(\text{CO})(\text{PPh}_3)(\text{isoPFA})$, can also react in neat methanol to give **5** (see below). More details on a possible mechanism are given below in connection with the mechanistic study on the reaction of **3b** with methanol in the presence of added base to give **6**.

Decarbonylation of alcohols by low valent phosphine complexes has been proposed to occur via alkoxide formation.^{90,133,156,157} It was stated in 1977⁹⁰ that this proposal had not been proved, and this is probably still the case. The present reaction of **3b** with methanol perhaps presents some indirect evidence for the proposal, since **5** may represent an "arrested methoxo intermediate" in which the methoxo ligand, before further dehydrogenation can take place, is transferred to the ferrocene ligand via substitution at the α -carbon position.

The ^1H NMR spectrum of **5** prepared from methanol- d_4 , with *ortho/meta*, *para* and *hydride/ferrocene* peak ratios reduced from the non-deuteriated values, indicates that exchange between hydride and *ortho*-phenyl hydrogens occurs in solution, although it is not clear whether this occurs in some intermediate, or in the final product, or both. There is clearly no exchange involving the methoxy group. The extent of deuteration observed at the *ortho*-phenyl position shows that other processes are also involved in this system. Detection of trace formaldehyde and methyl formate in the product mixture, along with other volatile components, is further evidence that other dehydrogenation processes, that can feed more deuterium atoms into the exchanging hydride/*ortho*-phenyl system, are also occurring in solution. The observed hydride/*ortho*-phenyl exchange is a further example of the well-established orthometallation reaction of ruthenium(II) phosphine complexes.^{91,158,159,160,161,162,163,164} The extent of catalytic methanol dehydrogenation, based on the preliminary search described above for organic products in the system, appears to be small. In the Ru acetate methanol dehydrogenation system investigated by Saito's group and described in section 5.1, precipitation of the hydrido-carbonyl $\text{RuCl}(\text{CO})(\text{PEtPh}_2)_3$ marked the deactivation of the catalytic methanol dehydrogenation. Thus, in the isoPFA system, deactivation by hydrido-carbonyl formation may just be more rapid than in the Ru acetate systems, perhaps owing to more facile Ru-C bond formation and, therefore, faster decarbonylation to give the hydrido-carbonyl. It should be noted that, although hydrido-carbonyl formation has been associated, by Saito's group, with catalyst

deactivation (sect. 5.1 and references 115 and 145), Smith and Maitlis came to the opposite conclusion: they observed no organic products until carbonyl formation had occurred.¹²⁸ Morton and Cole-Hamilton¹²³ saw somewhat decreased activity upon formation of $\text{RuHCl}(\text{CO})(\text{PPh}_3)_3$ in their methanol dehydrogenation system. The apparent contradictions may well be partly due to the differences in temperature used by the different groups. Both Smith and Maitlis¹²⁸ and Morton and Cole-Hamilton¹²³ carried out their reactions at 150 °C, at which temperature the hydrido-carbonyls do exhibit dehydrogenation activity. The experiments of Saito's group were done at 66 °C, which may just be too low for any significant activity from the hydrido-carbonyls in their system. Also, the $\text{RuH}_2(\text{PPh}_3)_3$ -based systems (Morton and Cole-Hamilton), and the $\text{Ru}(\text{OAc})\text{Cl}(\text{PR}_3)_3$ systems (Saito's group) are, in fact, more active than the respective hydrido-carbonyls formed in the systems. The $\text{RuCl}_2(\text{PPh}_3)_3$ complex as claimed may be less active than the hydrido-carbonyls produced in methanol.¹²⁸ But it must be noted that the solubility of $\text{RuCl}_2(\text{PPh}_3)_3$ in methanol is low, and the bulk of the ruthenium remains suspended as solid (hence incapable of homogeneous dehydrogenation catalysis) until the soluble hydrido-carbonyl $[(\text{CO})(\text{PPh}_3)_2\text{Ru}(\mu\text{-H})(\mu\text{-Cl})_2\text{Ru}(\text{CO})(\text{PPh}_3)_2]^\dagger$ is formed.¹²² Thus, the lack of significant activity prior to carbonyl formation, observed by Smith and Maitlis, may be due partly to a lack of significant solubility prior to carbonyl formation.

The single hydroformylation experiment described in section 5.2 was carried out partly because of the observation that many hydroformylation catalysts are complexes containing carbonyl groups,^{1b,165} and the recent success of a hydroformylation catalyst containing a P-O ligand^{1b} gives hope that **5** might also be effective for this purpose. The strong smell of hydroformylation products, coupled with the GC evidence, show that the complex **5** is an active hydroformylation catalyst, albeit a not very selective one.

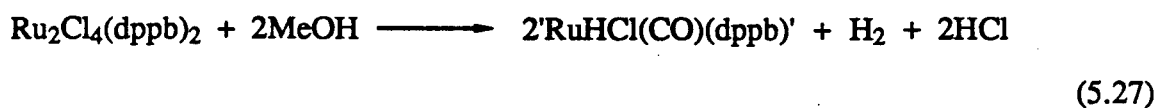
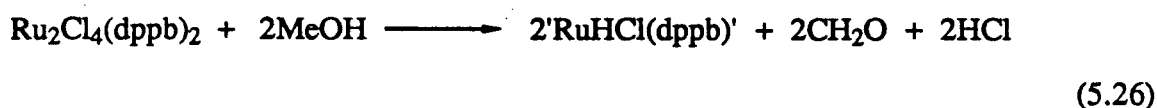
The transfer-hydrogenating activity of **3b** generally appears comparable to that of $\text{RuCl}_2(\text{PPh}_3)_3$ as reported by Maitlis' group.¹²² Unfortunately, these workers reported only the number of moles of reactants and did not give volumes or concentrations. Also,

the reaction conditions are different, Maitlis' group using higher temperature (150 °C) and shorter times. Nevertheless, $\text{RuCl}_2(\text{PPh}_3)_3$ also catalyzed the reduction of cyclohexene in only trace amounts, while the reduction of vinylmethylketone was much more efficient. As is common for hydrogen transfer from alcohols (sect. 5.1), reduction of the ketone acetophenone, and the α,β -unsaturated ketone vinylmethylketone, was more effective than reduction of olefins.

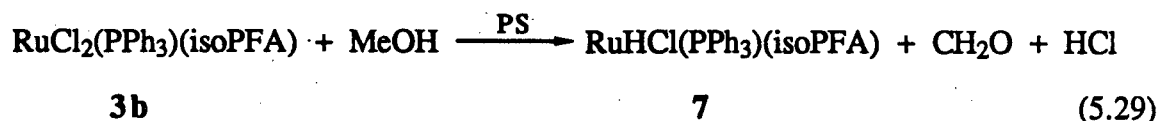
Reactions of $\text{RuCl}_2(\text{PPh}_3)(\text{isoPFA})$, 3b, with methanol in the presence of added base

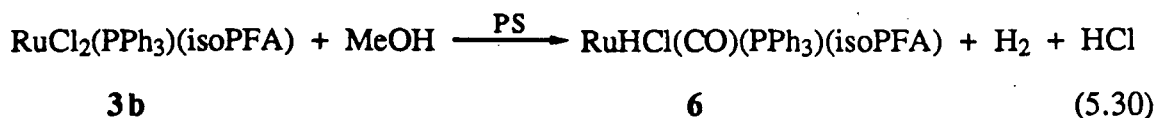
With Proton Sponge[®] as added base:

This investigation of the reaction of 3b with basic methanol was actually prompted by the observation, by Thorburn,¹³³ of a colour change, from green to yellowish, on stirring $\text{RuCl}_2(\text{PPh}_3)(\text{PPFA})$, 3a, under hydrogen in toluene/methanol in the presence of Proton Sponge[®] (see sect. 4.1); he had also discovered the reaction of $\text{Ru}_2\text{Cl}_4(\text{dppb})_2$ with methanol to give $\text{Ru}_2\text{H}(\mu\text{-H})(\mu\text{-Cl})_2(\text{CO})(\text{dppb})_2$. One mechanism considered¹³³ involved formation of both ' $\text{RuHCl}(\text{dppb})$ ' and ' $\text{RuHCl}(\text{CO})(\text{dppb})$ ' in sufficient amounts to be able to react together to give the observed yield of product:

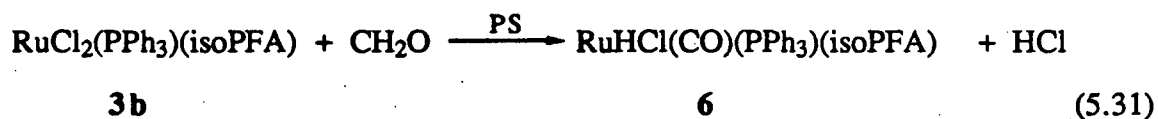


In the present reaction between $\text{RuCl}_2(\text{PPh}_3)(\text{isoPFA})$ and methanol in the presence of Proton Sponge[®], analogous stoichiometries could be proposed for the formation of 7 and 6, respectively:





These two hydrides appeared to be the major ruthenium products, but spectroscopic determination of the product distribution was not carried out. Formaldehyde was produced, and, where the reaction appeared to have gone to completion, the amount was 0.5 mol CH₂O per mol of **3b**. Gas evolution of ~1 mol/mol Ru was also detected and, considering that hydrogen is evolved in the reaction between **3b** and KOH/methanol (also, with the formation of **6**), the gas evolved in the present case is almost certainly H₂ as well. The alternative CO gaseous product is highly unlikely. Thus, there is some support for the stoichiometries of equations 5.29 and 5.30, although only 0.5 mol H₂ is expected if there is no other mechanism for H₂ production. In reaction 5.29, the formaldehyde is dissociated before it is decarbonylated, and therefore no CO ligand results; in reaction 5.30, decarbonylation of CH₂O would give **6** and H₂. The mechanisms for these reactions probably involve alkoxide, η²-CH₂O and, in the case of equation 5.30, formyl intermediates similar to those suggested for other examples of methanol decarbonylation.^{90,133} As noted in section 5.1, examples of such intermediate complexes have been characterized. More details on a probable mechanism are given later in connection with the mechanistic study on the reaction of **3b** with KOH/MeOH. A reaction between **3b** and CH₂O such as:



is also a possibility. Reactions of ruthenium complexes with CH₂O have been reported.^{90,145}

The present reaction is similar in some respects to the reaction of RuH(C₆H₄PPh₂)(PPh₃)(Et₂O) with methanol in diethylether at 0 °C to give a mixture of RuH₂(CO)(PPh₃)₃ and RuH₂(PPh₃)₄, as reported by Cole-Hamilton and Wilkinson.⁹¹

The structure of **6** should be compared particularly with that of **5**, $\text{RuHCl}(\text{CO})(\text{PPh}_3)(\text{isoPOF})$, because, as discussed later in this section, the former complex reacts with methanol, in the absence of base, to give the latter. In the crystal structures of both complexes, the coordinated P atoms are mutually *trans*. It seems clear from the NMR data that, in fact, all the observed geometric isomers of **6** have mutually *trans* phosphines. There appears to be only one isomer of **5** in solution; however, it should be noted that the $^{31}\text{P}\{^1\text{H}\}$ NMR resonances for this complex are ambiguous, and could be interpreted as two overlapping doublets with J larger than the difference in δ , or two close doublets with J smaller than the difference in δ . In addition to the possibility of geometric isomers, there is also the possibility of diastereomers for the isoPOF complex, **5**, as is also the case for the isoPFA complex, **6**; it should be noted that the isoPOF ligand may be *R,S*-, as in Figure 5.3, or *S,R*-, and the ruthenium atom is also a centre of chirality in the molecule. The temperature dependence of the ^1H NMR spectrum of **6** also has a bearing on the structural comparison with the isoPOF analogue. The most likely interpretation of this temperature dependence data is that the $-\text{NMe}_2$ functionality of the isoPFA ligand rapidly binds to, and dissociates from, the ruthenium at about 20°C , but remains coordinated below 0°C . Such lability of the $-\text{NMe}_2$ could provide a mechanism for the formation of other geometrical isomers. Thus, while in the crystal structure of **6** the hydride is *trans* to $-\text{NMe}_2$ and the CO is *trans* to Cl, dissociation of the $-\text{NMe}_2$ could allow the chloride to swing away from the hydride, to give mutually *trans* hydride and chloride (as observed in the crystal structure of **5** (Fig. 5.3)) upon re-coordination of the $-\text{NMe}_2$ of the isoPFA.

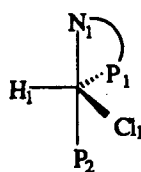
The structure of **7** is very similar to that of $\text{RuHCl}(\text{PPh}_3)_3$.¹⁶⁶ Both are best described as strongly distorted trigonal bipyramidal. In the case of $\text{RuHCl}(\text{PPh}_3)_3$, two phosphines are at the apices of this "trigonal bipyramid", with a " $\angle\text{P}_3\text{-Ru-P}_2$ " angle of 153.1° , with the other phosphine, the hydride and the chloride approximately equatorial. In the case of **7**, the PPh_3 and the nitrogen of isoPFA are at the apices (" $\angle\text{N}_1\text{-Ru}_1\text{-P}_2$ " =

157.1°) with the P atom of isoPFA, the chloride and the hydride approximately equatorial. Other parameters for these two structures are compared in Table 5.9, by listing side-by-side corresponding angles and distances. The angle of 121.4° between "the equatorial" P and Cl atoms in the case of $\text{RuHCl}(\text{PPh}_3)_3$ is close to the corresponding angle of 124.9° in 7. Skeletal bond distances in the two complexes also correspond quite closely. Slightly shorter Ru-P distances in 7 can be partly attributed to higher electron density on Ru due to the presence of more basic ligands, combined with fewer π -back-bonding ligands.

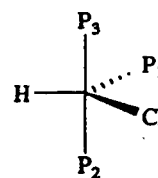
Comparison of the structure of 7 with that of its CO adduct, 6, reveals the effect of the carbonyl on the various bond distances. Table 5.1 lists the corresponding distances of these two structures. The generally longer skeletal bond distances in the case of 6 can be

Table 5.9

Comparison of structural parameters of $\text{RuHCl}(\text{PPh}_3)(\text{isoPFA})$, 7, and $\text{RuHCl}(\text{PPh}_3)_3$ ¹⁶⁶



7



$\text{RuHCl}(\text{PPh}_3)_3$

Bond distances (Å):

$\text{Ru}_1\text{-Cl}_1$	2.441(1)
$\text{Ru}_1\text{-H}_1$	1.52
$\text{Ru}_1\text{-P}_1$	2.178(1)
$\text{Ru}_1\text{-P}_2$	2.250(1)
$\text{Ru}_1\text{-N}_1$	2.265(5)

Ru-Cl	2.421
Ru-H	1.70(15)
Ru-P ₁	2.206
Ru-P ₂	2.361
Ru-P ₃	2.329

Angles (°)

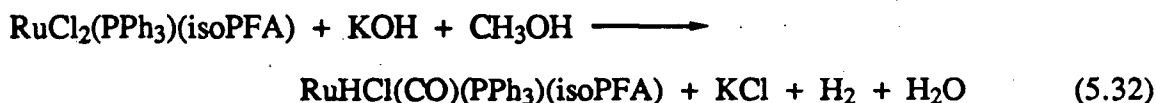
$\text{N}_1\text{-Ru}_1\text{-P}_2$	157.1(1)
$\text{P}_1\text{-Ru}_1\text{-Cl}_1$	124.9(1)

$\text{P}_3\text{-Ru-P}_2$	153.1
$\text{P}_1\text{-Ru-Cl}$	121.4
$\text{P}_1\text{-Ru-H}$	~89

attributed to decreased electron density on the ruthenium, and consequent decreased back-bonding to other ligands, caused by the high degree of back-bonding to CO.

With KOH as added base:

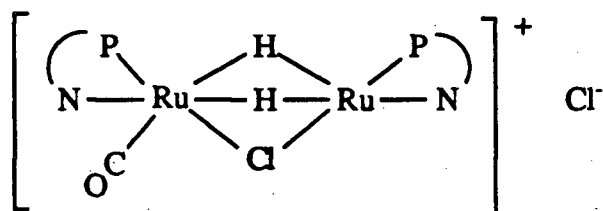
Reactions in the **3b**/KOH/methanol system are complex but some elucidation has been possible. The **6** complex is at least the main ruthenium product of the reaction when the KOH:Ru mole ratio is 1:1, and a possible stoichiometry is:



At higher KOH:Ru mole ratios, more complex product mixtures are obtained. In the experiments summarized in Table 5.4, no red solution was observed at any time during the reaction of **3b** with methanol with 1.8 M KOH (KOH:Ru = 240), whereas wine-coloured solutions persisted at KOH:Ru ratios below ~120. In the preparative scale experiments, wine-coloured solutions were produced when KOH:Ru mole ratios ranged from 10 to 50. The white dihydride $\text{RuH}_2(\text{CO})(\text{PPh}_3)_3$ is a major product present in these wine-coloured reaction mixtures. Redistribution of the coordinated phosphine ligands thus occurs in this system, as well as in the reactions of **3a** and **3b** with H_2 (chapter 4). The formation of a ruthenium complex with three PPh_3 ligands requires the dissociation of both isoPFA and PPh_3 ligands from other complexes present in the system; in fact, the presence of these ligands in the KOH/methanol system is indicated by NMR data, and, in one experiment, free isoPFA was isolated by column chromatography.

Other partially characterized complexes are also present in these wine-coloured reaction mixtures, which certainly contain Ru complexes with hydride, carbonyl, and isoPFA ligands. Column chromatography on silica results in some decomposition of the complexes, as judged by differences between the NMR spectra of the residues of some fractions and those of unseparated residues of supernatants of these KOH reactions. However, certain complexes eluted from the column, including a yellow hydride with $^1\text{H}_{\text{CDCl}_3}$ -18.7 (dd), and a red hydrido-carbonyl, **X**, containing two isoPFA ligands and

with $^1\text{H}\delta_{\text{CDCl}_3}$ 17.9 (dd), -18.2 (dd), survived the chromatography. The latter complex contains no PPh_3 ligands; no $\nu(\text{OH})$ was observed in the IR, and the intense red colour suggests a five-coordinate species.⁹⁰ The ^1H NMR integrations indicate that two hydrides are present. A tentative formulation of this complex, **X**, is:

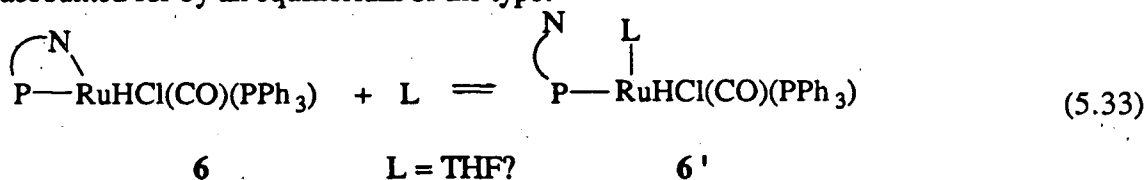


The hydride resonances of the two complexes (yellow and red species) resemble those observed (Fig. 5.15) for the residue of wine-coloured reaction mixtures after solvent removal only. Also, the $^{31}\text{P}\{^1\text{H}\}$ NMR spectrum of the red hydrido-carbonyl exhibits peaks resembling those of a wine-coloured **3b**/KOH/methanol *in situ* reaction mixture (Fig. 5.14). Formation of $\text{RuH}_2(\text{CO})(\text{PPh}_3)_3$ and a red species ($\lambda_{\text{max}} = 542 \text{ nm}$) from the reaction of **6** with KOH/methanol does occur, and this intermediate presumably provides the pathway for the secondary reactions observed when **3b** reacts with KOH/methanol.

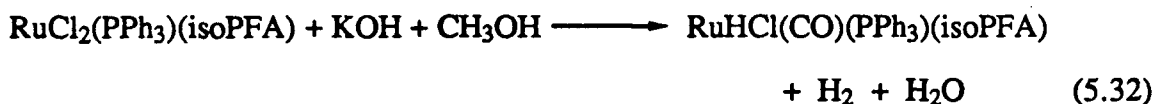
*Experiments on the reaction of $\text{RuCl}_2(\text{PPh}_3)(\text{isoPFA})$, **3b**, with KOH/methanol, in THF in the presence or absence of styrene*

The reaction of **3b** with KOH/MeOH was also conducted in 3:1 v/v THF/MeOH, since all ruthenium species in the system were soluble in this solvent, thus facilitating kinetic studies; fortunately, ^1H NMR data show that no reaction occurs between KOH/MeOH and THF at ambient temperature, in the absence of styrene and **3b**. In the **3b**/KOH/MeOH/THF reaction, no resonances due to the product **6**, $\text{RuHCl}(\text{CO})(\text{PPh}_3)(\text{isoPFA})$, were observed in the *in situ* $^{31}\text{P}\{^1\text{H}\}$ NMR spectra, although an AB pattern due to a species **6'** was observed. The $^{31}\text{P}\{^1\text{H}\}$ NMR spectra of residues

from these reactions, however, when stopped after the 'primary reaction' had occurred, showed the presence of **6**. (The work-up described in section 5.2 for the THF/MeOH styrene-containing reaction solutions is not recommended for isolation for Ru products, but it produced conclusive evidence that **6** can be recovered from these reaction mixtures.) Further evidence that **6** is present in some form **6'** (possibly with coordinated THF, see below) is obtained from the observation mentioned above (p. 162) that the reaction proceeds on to the formation of the red species ($^{31}\text{P}\{^1\text{H}\}$ NMR δ 61, 62.5, 66) which are also formed in the absence of THF and in the absence or presence of styrene. It should be remembered that the coordinated N atom of the isoPFA is labile (see the discussion of the temperature dependence of the ^1H NMR spectrum of **6**, above), and hence could be readily replaced by a ligand, L, such as THF, which, however, may be lost during work-up, when its concentration becomes low. Since the $^{31}\text{P}\{^1\text{H}\}$ NMR spectrum of a solution of **6** is unaffected by the presence of ~ 1 mole of styrene, L cannot be styrene. The data could be accounted for by an equilibrium of the type:



Thus, the reaction in the presence or absence of THF may well proceed along the same path, viz.:



but the form assumed by **6** is different in the 3:1 v/v THF/methanol solution. The temperature dependence of the ratio of the integration of the **6'** AB pattern to that of the PPh_3 resonance may represent an equilibrium involving loss of PPh_3 from the **6'** species:



The complex **6** in the form of **6'** (and its phosphine-dissociated equilibrium species) is probably the main product detected in the spectra of Figures 5.20 and 5.21.

The higher yield of $\text{RuH}_2(\text{CO})(\text{PPh}_3)_3$, from a secondary reaction in the neat methanol case could be rationalized in terms of low solubility in this solvent, and shifts in various equilibria.

The visible spectrophotometric experiment giving the spectra shown in Figure 5.25 is comparable to that giving the $^{31}\text{P}\{^1\text{H}\}$ NMR spectra shown in Figures 5.20 and 5.21; the **[3b]** and **[KOH]** are much lower in the 'visible' experiment, but the **[KOH]/[Ru]** ratio is about the same (9:1), and the **[styrene]** in the two experiments is about the same (~ 0.44 M). Thus, the main product at the end of the first stage of the **3b/KOH/MeOH/THF** reaction, indicated by the visible absorption spectrum 'd' in Figure 5.25, is perhaps the THF complex **6'**. The yellow complex, $\text{RuHCl}(\text{CO})(\text{PPh}_3)(\text{isoPFA})$, **6**, exhibits a weak visible band at 450 nm, and it is likely that the THF complex is also yellow and mainly responsible for the yellow colour observed. At intermediate **[KOH]**, generally < 0.1 M, a much slower secondary colour change to red occurs, as exemplified in Figure 5.25 (curves e - j). The growth in red colour is accompanied by an increase in an intense band at 542 nm ($t_{1/2} = \sim 14$ h), as observed for species **X** and possibly other red ruthenium hydrido-carbonyl species are formed which are also produced in the reaction in neat methanol.

It seems clear from NMR spectra (Figs. 5.14, 5.15, 5.22) that there are more than one species produced in secondary reactions in basic methanol, or basic methanol/THF. The **KOH** ratio is important in determining which secondary processes occur (see also Table 5.4, for the neat methanol reaction). At **[KOH]** higher than 0.2 M, for the THF/MeOH reactions, the formation of the red species is less readily observed, and instead, formation of a second yellow species is seen. This latter change is accompanied by a small decrease in absorbance at 605 nm (yellow \longrightarrow yellow); this reaction is also slower than the formation of **6'**, and both these secondary colour changes, at intermediate **[KOH]** (yellow \longrightarrow red), or at high **[KOH]** (yellow \longrightarrow yellow), can be

monitored at 605 nm, independently of the first reaction that gives **6'**. The behaviour of the spectrum at 450 nm during the yellow \longrightarrow red process with styrene absent (Fig. 5.26) is similar to that with styrene present; but with styrene absent there is an unexplained gradual increase (Fig. 5.26) at 450 nm that accompanies the growth of the 542 nm band. Kinetic studies on the secondary reactions were not attempted.

The formation of ~ 1 mol gas during the primary reaction of **3b** to give **6'** in the absence of styrene, and the lack of gas evolution, at a KOH:Ru ratio of ~ 1 , coupled with the formation of ~ 1 mol of ethylbenzene in the presence of styrene at [KOH] below ~ 0.06 M, indicate that ~ 1 mol H_2 /mol Ru is produced during this primary reaction. This, together with the detection of KCl produced during this stage, support the stoichiometry shown in equation 5.32 for the reaction in the absence of styrene; but in the THF case, **6** presumably further reacts to give **6'**, as in equation 5.33. The production of **6'** and KCl occurs whether styrene is present or absent, suggesting that the pathways for the styrene hydrogenation and uncoupled methanol dehydrogenation are very similar, perhaps differing only in a couple of steps, and having the same stoichiometry, except that the H_2 is transferred to styrene if styrene is present. It is noteworthy that this is perhaps the first time that KCl has been positively identified in a reaction of a platinum metal chloro complex with alcoholic KOH, although KCl formation has been proposed.¹⁴³

This reaction of **3b** to give **6**, or **6'**, is at least the dominant reaction in the primary process (sect. 5.3); this is in contrast to the relative complexity of reactions during the second stage (*vide supra*). Therefore, a kinetic study of the primary process both in the presence of styrene (Fig. 5.25, curves a - d) and in the absence of styrene, has been carried out. The rate of decay of **3b**, measured in terms of k_{obs} , is essentially independent of styrene, and essentially independent of added PPh_3 and isoPFA in the absence of styrene; the rate of styrene hydrogenation is essentially independent of added isoPFA but inhibited by $\sim 10\%$ in the presence of 1.4×10^{-2} M added PPh_3 (i.e., $PPh_3:Ru = 4$). Results on chloride dependence of the rate of decay of **3b**, hampered by insolubility of KCl,

tentatively indicate an inverse dependence of k_{obs} on added chloride (sect. 5.3).

Spectrophotometric studies (sect. 5.2, 5.3) monitoring the disappearance of **3b** in the presence of base showed that there is a pathway with a second-order dependence on $[\text{KOH}]$ for this first step in the reaction of **3b** with KOH/MeOH , as well as a base-independent pathway:

$$k_{\text{obs}} = 1.3 \times 10^{-3} + 0.082[\text{KOH}]^2 \quad (5.24)$$

Since KOH can react with MeOH to give OMe^- (eq. 5.35), attack on **3b** by OMe^- must be considered in proposing a mechanism for the second-order base dependent pathway. For the equilibrium in equation 5.35:



a value for the equilibrium constant, K , of 18 has been reported for the $\text{NaOMe}/\text{neat MeOH}$ system;¹⁶⁷ this value yields a plot of $[\text{OMe}^-]$ against $[\text{OH}^-]$ that is close to linear (Fig. 5.45), over the range of $[\text{OH}^-]$ used to determine the second-order $[\text{KOH}]$ dependence in THF/MeOH in the present work.

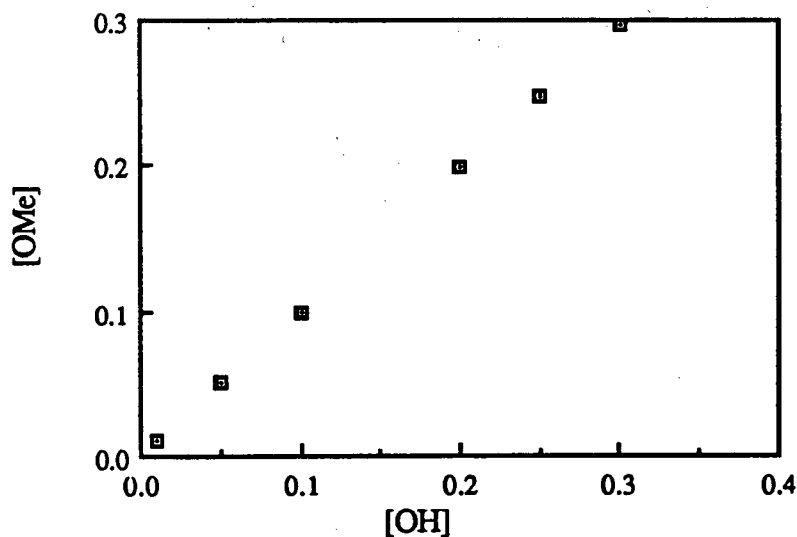


Figure 5.45 Plot of $[\text{OMe}^-]$ versus $[\text{OH}^-]$ based on the equilibrium constant, K (18), for the reaction of NaOH with MeOH at 20°C .¹⁶⁷ Determination of this equilibrium constant is discussed further in reference 168.

Measurements of K for equilibrium 5.35 in the THF/MeOH system are not available; however, based on the data for the NaOMe/MeOH system, a linear dependence of $[\text{OMe}^-]$ on $[\text{OH}^-]$ is assumed in the present work on the THF/MeOH reaction. Therefore, a second-order dependence on $[\text{KOH}]$ is accounted for by the mechanistic proposal shown

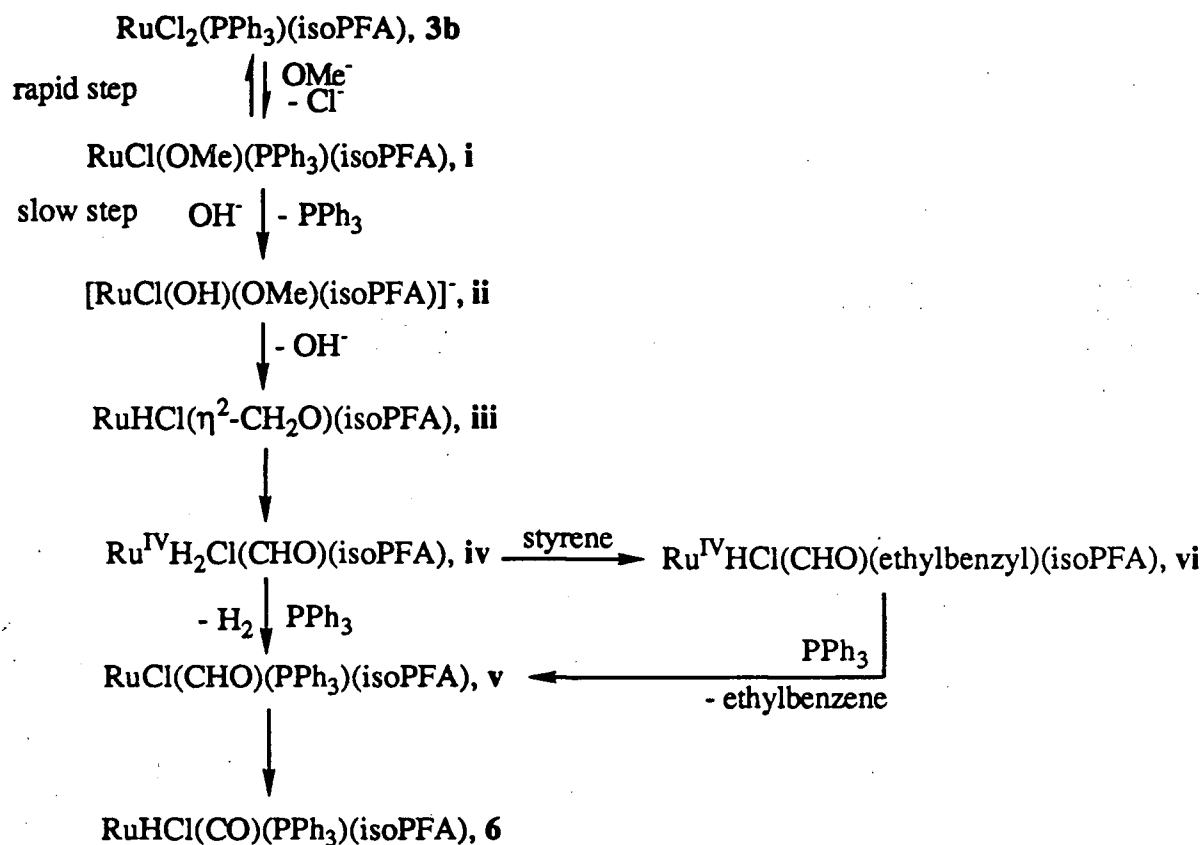
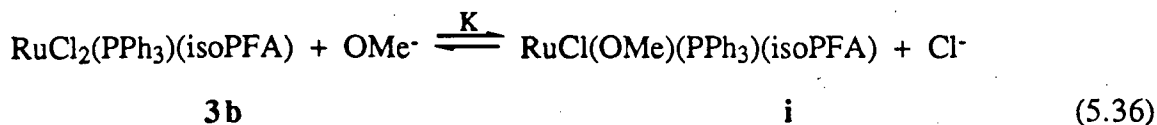
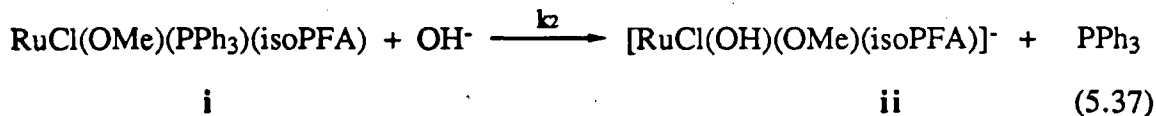


Figure 5.46 Proposed mechanism for the second-order base dependent pathway for reaction 5.30 via methoxide attack on **3b**.

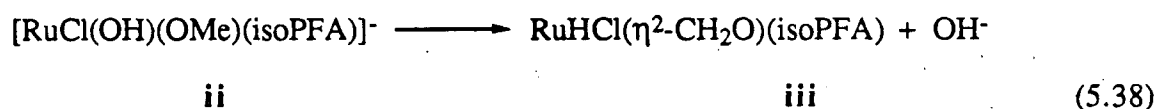
in Fig. 5.46 for the reaction of **3b** with KOH/MeOH in THF. To account for the second-order dependence on KOH, and for the inhibition of the rate by chloride, the initial step in the mechanism (Fig. 5.46) is proposed to be a rapid step involving replacement of Cl^- by OMe^- :



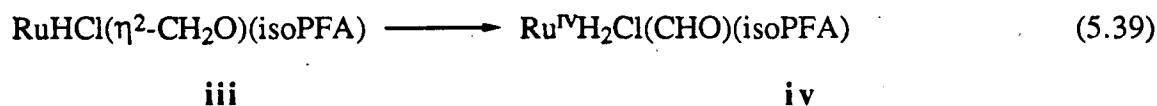
followed by the slow replacement of PPh_3 by OH^- :



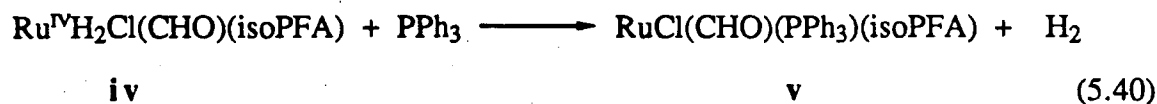
This step is supported by the observation, by $^{31}\text{P}\{^1\text{H}\}$ NMR spectroscopy (sect. 5.3), of PPh_3 dissociation early during the overall reaction (5.32). Hydride transfer to the vacant site, accompanied by dissociation of OH^- is next:



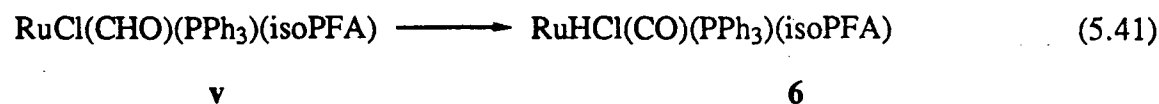
The coordinated formaldehyde is likely to be dihapto-coordinated, because it is further dehydrogenated (see discussion in sect. 5.1) and also there is structural precedent for $\eta^2\text{-CH}_2\text{O}$ ligands on members of the iron triad (sect. 5.1). Step 5.38 is followed by further migration of hydride from CH_2O to give a Ru(IV) dihydride with a carbon-bonded formyl ligand; in proposing this intermediate, consideration is given to the structural precedent for formyl complexes in ruthenium chemistry (sect. 5.1):



Reaction with available PPh_3 could then lead to a reductive elimination of hydrogen to give a Ru(II) species:



Finally, hydride transfer from the five-coordinated formyl intermediate gives the product, **6**:



In the presence of styrene, step 5.40 could be circumvented by reaction of the 16-electron intermediate **iv** with styrene (Fig. 5.46), followed by concerted reductive elimination of ethylbenzene and coordination of PPh_3 . The slightly inhibitive effect of added PPh_3 on the rate of styrene hydrogenation could be due to competition of PPh_3 with styrene for intermediate **iv**.

The parallel decreases in hydrogenation rate and **[3b]** decay rate during reactions at these KOH concentrations below 0.06 M, together with the chloride dependence data, show that the rate determining step for the formation of **6'** from **3b** occurs early in the mechanism of the styrene-hydrogenation-coupled pathway as well as in the methanol-dehydrogenation pathway in the absence of styrene. With the second step (eq. 5.37) in the mechanism (Fig. 5.46) slow and rate-determining, the reaction rate,

$$\frac{d[\mathbf{3b}]}{dt} = k_2 [\text{OH}^-][\mathbf{i}] \quad (5.42)$$

As the value of **[i]** depends on equilibrium 5.36:

$$[\mathbf{i}] = \frac{K[\mathbf{3b}][\text{OMe}^-]}{[\text{Cl}^-]} \quad (5.43)$$

and because $[\text{OMe}^-]$ is approximately proportional to $[\text{OH}^-]$:

$$[\text{OMe}^-] = C[\text{OH}^-] \quad (5.44)$$

where C is a constant, equation 5.43 becomes:

$$[\mathbf{i}] = \frac{KC[\mathbf{3b}][\text{OH}^-]}{[\text{Cl}^-]} \quad (5.45)$$

Thus the net rate of decay of **3b** is given by:

$$\frac{d[\mathbf{3b}]}{dt} = \frac{k_2 KC[\mathbf{3b}][\text{OH}^-]^2}{[\text{Cl}^-]} \quad (5.46)$$

This rate law is thus consistent with the observed second-order dependence on $[\text{KOH}]$, as well as the first-order dependence on $[\text{Ru}]_T$ and the inhibitive effect of added chloride; also, the mechanism allows for the observed phosphine-independent rate, and is consistent with the observed PPh_3 dissociation.

A possible mechanism for the base-independent pathway is shown in Figure 5.47. To account for the inhibitive effect of Cl^- on the rate, and the fact that **3b** shows little evidence of reaction with methanol in the absence of base at ambient temperature, the first step (**3b** \longrightarrow **i**, Fig. 5.47) is taken as a reversible one with a small K value, involving replacement of Cl^- by MeOH :

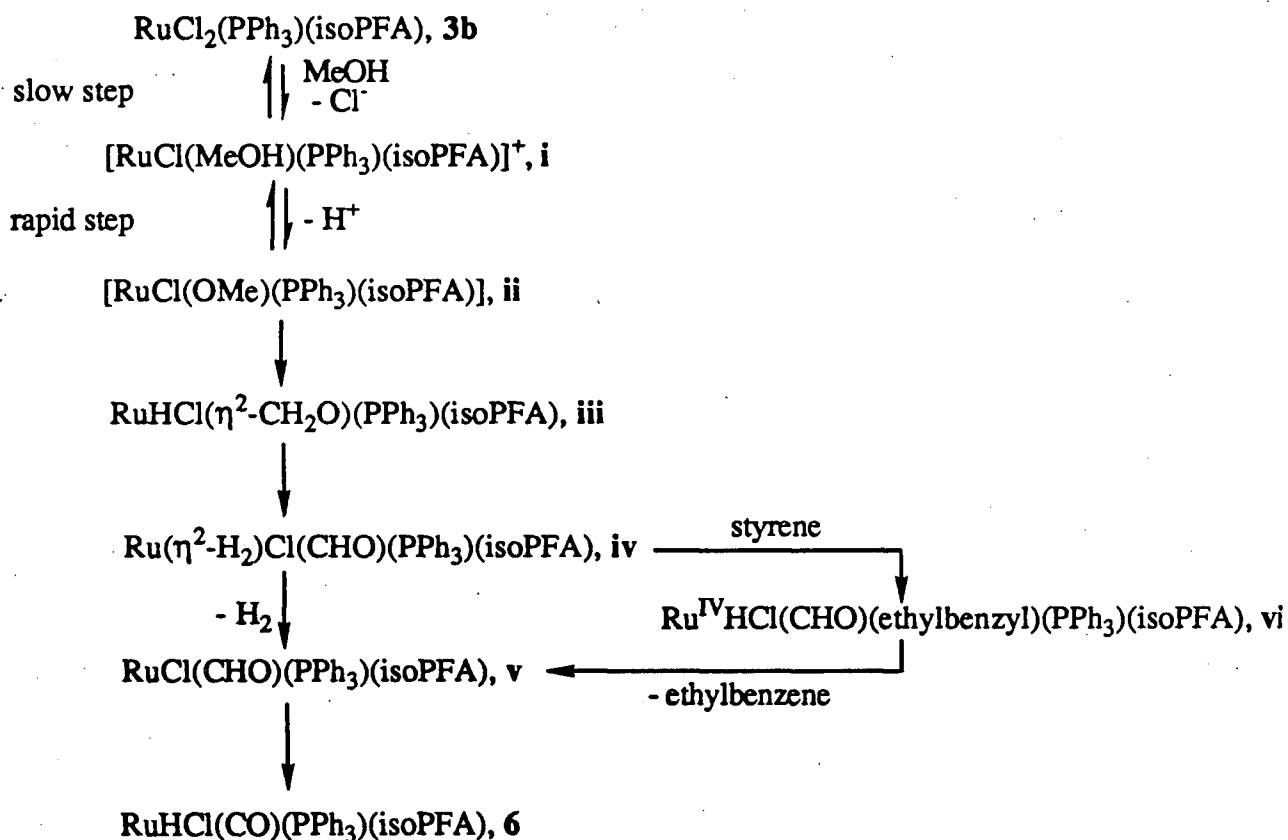
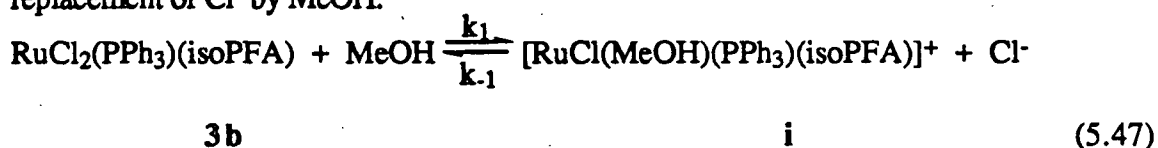
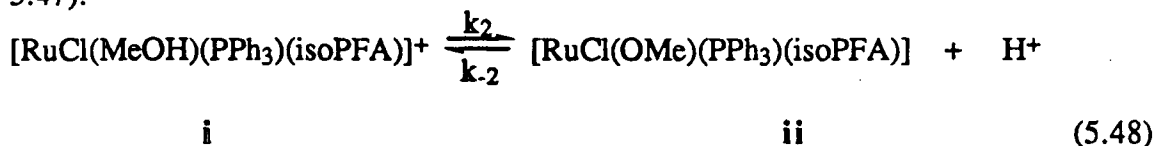


Figure 5.47 Proposed base-independent pathway for the reaction of **3b** with KOH/MeOH in THF.

The second step is reversible loss of a proton from coordinated MeOH (i \longrightarrow ii, Fig. 5.47):



Subsequent steps in Figure 5.47 describe the stepwise hydride migration and liberation of hydrogen associated with the dehydrogenation of the OMe⁻ ligand. Added base would rapidly neutralize the protons produced in the second reversible step (eq. 5.48), and thus shift the system toward formation of ii. Thus, if the neutralization is rapid, then the scheme allows for the rate of the overall process to be independent of [OH⁻], although at least 1 equivalent of added base (based on Ru) is required for formation of ii and final product formation. The rate for this base-independent pathway can be written as:

$$\frac{d[3b]}{dt} = k_1[3b][\text{MeOH}] - k_{-1}[i][\text{Cl}^-] \quad (5.49)$$

A steady state approximation for [i] gives:

$$k_1[3b][\text{MeOH}] + k_2[ii][\text{H}^+] = k_{-1}[\text{Cl}^-][i] + k_2[i] \quad (5.50)$$

while in the presence of OH⁻:

$$k_2[ii][\text{H}^+] \approx 0 \quad (5.51)$$

and therefore equation 5.50 becomes:

$$k_1[3b][\text{MeOH}] \approx k_{-1}[\text{Cl}^-][i] + k_2[i] \quad (5.52)$$

Rearranging gives:

$$[i] = \frac{k_1[3b][\text{MeOH}]}{k_{-1}[\text{Cl}^-] + k_2} \quad (5.53)$$

and substituting into equation 5.49 and rearranging finally gives:

$$\frac{d[3b]}{dt} = k_1[3b][\text{MeOH}] \left\{ 1 - \frac{k_{-1}[\text{Cl}^-]}{k_{-1}[\text{Cl}^-] + k_2} \right\} \quad (5.54)$$

This rate law is consistent with the observed first-order dependence of the rate of decay of 3b, as well as being independent of base, although the rate law only holds if at least 1 equivalent of base is present.

Intermediate **iv** is presented as an $\eta^2\text{-H}_2$ complex in view of the propensity of 18-electron Ru(II) complexes to stabilize this ligand (sect. 3.1). The step involving equilibrium loss of H_2 (the **iv** \longrightarrow **v** step, Fig. 5.47) is consistent with the typical reversibility of coordination of $\eta^2\text{-H}_2$ ligands (sect. 3.1). Styrene, if present, could react with **iv** to give the Ru(IV) hydrido-alkyl complex, **vi**, with reductive elimination of ethylbenzene giving **v** (Fig. 5.47).

Organic and gaseous products from high [KOH] reactions

The polymerized formaldehyde formed in the formalin/KOH/methanol/THF mixture is regarded as high grade.¹¹⁷ Such polymerization would account for the lack of formaldehyde detected in distillates from reactions of **3b** with KOH/MeOH in THF. Thus, at least in the presence of a large excess of KOH, these reactions generate approximately stoichiometric amounts of paraformaldehyde.

The dehydrogenation of methanol in these reactions of **3b** at high [KOH] appears to be 'catalytic', and the three moles of gas produced in such an experiment at [KOH] = 0.38, is probably H_2 , as CO was not detected by GC in a comparable experiment.

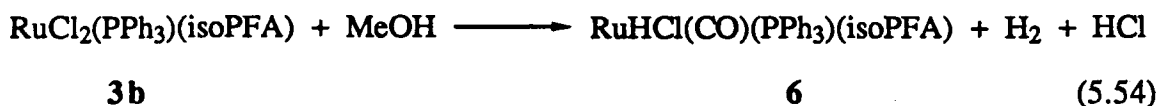
*The Figure 5.47 mechanism and the reaction of $\text{RuCl}_2(\text{PPh}_3)(\text{isoPFA})$, **3b** with methanol in the presence of Proton Sponge[®]*

Some discussion of a mechanism for the reaction of **3b** with methanol in the presence of Proton Sponge[®] was presented earlier (p. 219); the reaction scheme shown in Figure 5.47, proposed for the KOH reaction, provides details of a probable mechanism for the PS reaction. No kinetic studies were carried out on this reaction, but products $\text{RuHCl}(\text{CO})(\text{PPh}_3)(\text{isoPFA})$, **6**, and $\text{RuHCl}(\text{PPh}_3)(\text{isoPFA})$, **7**, were isolated and ~ 0.5 mol CH_2O /mol **3b** was produced. The reaction scheme in Figure 5.47 accounts for the

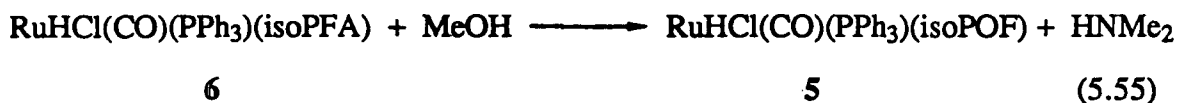
formation of **6**, while dissociation of CH_2O from intermediate **iii** would account for the formation of **7** and CH_2O .

*The Figure 5.47 mechanism and the reaction of $\text{RuCl}_2(\text{PPh}_3)(\text{isoPFA})$, **3b**, with methanol in the absence of base*

As discussed earlier, the complex **3b** reacts with methanol in the absence of base to give $\text{RuHCl}(\text{CO})(\text{PPh}_3)(\text{isoPOF})$, **5**, with complex **6** not being formed in detectable amounts; but as **6** reacts with methanol in the absence of base to give **5**, **6** is a possible intermediate in the **3b** \longrightarrow **5** reaction (5.25). Possible stoichiometries for these steps are:



proceeding via the mechanism in Figure 5.47, and:



proceeding via steps suggested on page 215. Reaction 5.55 would be followed by a neutralization:



Because **6** is not observed as a product in the absence of base, this proposal involving **6** as an intermediate requires step 5.54 to be slow and step 5.55 to be relatively fast. It should be remembered that the reaction of **3b** with methanol was very slow, requiring refluxing **3b** in methanol for several days (sect. 2.4); and the reaction scheme proposed in Figure 5.47 is expected to generate **6** (and therefore **5**) slowly if base is not present to shift the first two reversible reactions (eqs. 5.47 and 5.48) toward products.

Chapter 6

Summary and suggestions for further work

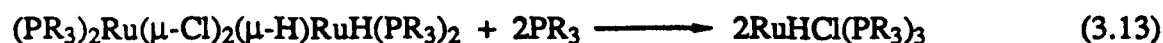
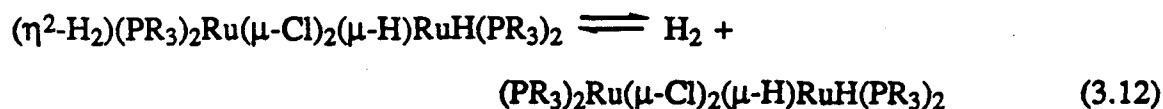
The previously known²³ complexes, $\text{Ru}_2\text{H}_4\text{Cl}_2(\text{PR}_3)_4$, have now been correctly reformulated as the $\eta^2\text{-H}_2$ species $(\eta^2\text{-H}_2)(\text{PR}_3)_2\text{Ru}(\mu\text{-Cl})_2(\mu\text{-H})\text{RuH}(\text{PR}_3)_2$ ($\text{R} = \text{Ph}$, ptol), **1a** and **1b**, and it is confirmed that in solution they are dimeric and undergo no ligand dissociation. The complexes **1a** and **1b** decompose under nitrogen or vacuum to give the corresponding $\text{RuHCl}(\text{PR}_3)_3$ complex, and, at least in the case of **1b**, a species with a four-spin ^{31}P NMR spectrum which had been noted previously by Dekleva.²¹ Also, a new analogue of complexes of type **1** is reported: the complex $(\eta^2\text{-H}_2)(\text{isoPFA})\text{Ru}(\mu\text{-Cl})_2(\mu\text{-H})\text{RuH}(\text{PPh}_3)_2$, **4**, is formed from the reaction of $\text{RuCl}_2(\text{PPh}_3)(\text{isoPFA})$, **3b**, with H_2 in methanol/benzene, and a crystal structure of **4** shows the $\eta^2\text{-H}_2$ ligand. Complexes **1a**, **1b** and **4** all react with 1-hexene to give hexane; the main ruthenium phosphine product in the case of **1** is the corresponding $\text{RuHCl}(\text{PR}_3)_3$ complex, while **4** reacts to give a complex mixture of ruthenium phosphine complexes, including **3b**. The amount of hexane formed from the reaction of **4** with hexene is quantified as 2 mol/mol **4**. The results summarized above are of particular interest and significance for the following reasons:

a) Dinuclear dihydrogen complexes are rare; besides the work described here, there is only one other report on such species.⁹⁶ Further, the ^1H NMR resonances for the hydrogen ligands are resolved only in the present work, fast exchange precluding direct T_1 measurements in the other system.⁹⁶

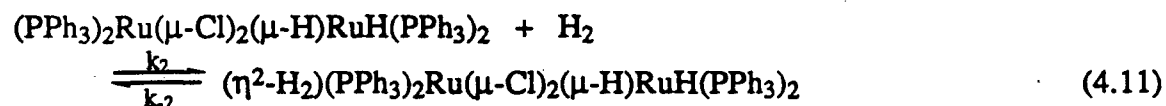
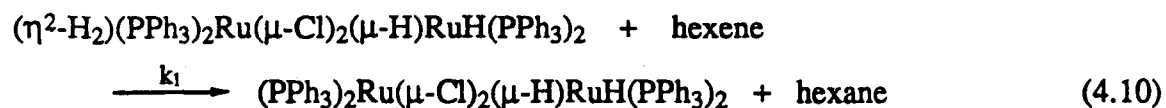
b) Crystal structures with a located $\eta^2\text{-H}_2$ ligand are rare (sect. 3.1). The crystal structure for **4**, presented in chapter 3, is the first such structure for a dinuclear complex.

c) There have been several previous studies²³ on systems involving these $\eta^2\text{-H}_2$ complexes, when their true formulation was not recognized, or a dihydrogen complex went unnoticed; thus, more detailed interpretation and, in some cases, reinterpretation of earlier

work is required. In the reactions of complexes of type 1 with the corresponding triarylphosphine, the demonstrated initial H₂ loss²³ is almost certainly the loss of the η^2 -H₂, i.e.:



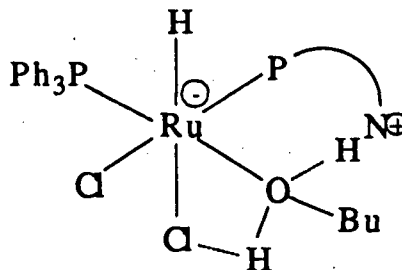
The hydrogenation of 1-hexene catalyzed by **1a** is now interpreted as occurring via the mechanism:



Wang's kinetic studies on the hydrogenation of acrylamide catalyzed by **1a** in DMA⁷⁸ have yet to be re-interpreted based on the re-formulation of **1a** given in the present work.

d) It is possible that complex **1a** is involved in hydrogenations catalyzed by the much studied^{2,3,66-68} complex, RuHCl(PPh₃)₃, which remains one of the most active catalysts known for the hydrogenation of terminal olefins.⁶⁶⁻⁶⁸ Thus, a reinterpretation of some unpublished data obtained by Hui¹⁰³ and Markham⁷² on hydrogenation catalyzed by RuHCl(PPh₃)₃ needs to be carried out.

Reactions of RuCl₂(PPh₃)(PPFA), **3a**, and RuCl₂(PPh₃)(isoPFA), **3b**, with H₂ have been further studied, in connection with earlier mechanistic studies on the hydrogenation of organic substrates catalyzed by complex **3a**.²⁵ The complex **3a** reacts with 2 - 8 atm H₂ in *n*-butanol to give ruthenium phosphine products including **1a** and a species A, possibly of the structure shown below; the species A is formed reversibly from **3a** as follows:



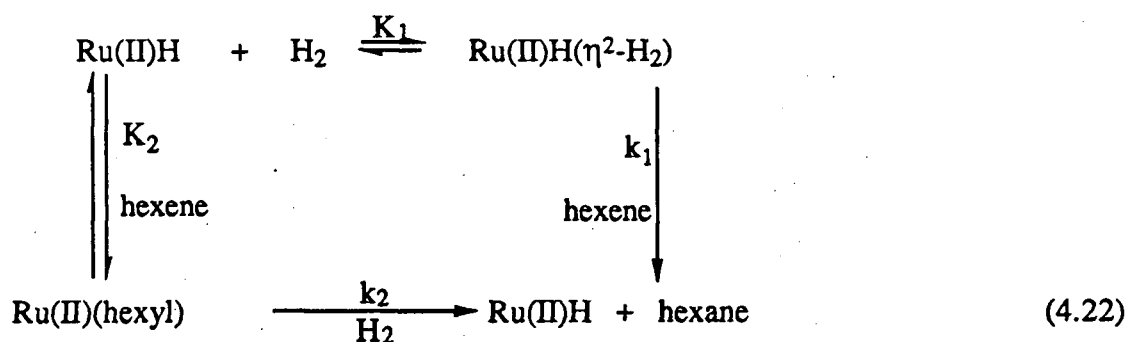
3a

A

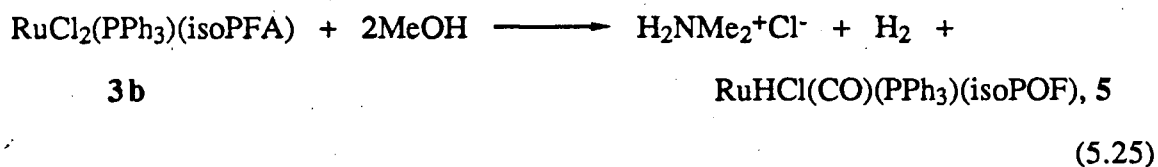
(4.20)

The complex **3b** reacts with H_2 in methanol/benzene to give **4**, as mentioned above, as well as a number of unidentified hydrides; in DMA, the reaction of **3b** with H_2 gives **1a**, **4**, **7**, $\text{RuHCl}(\text{PPh}_3)_3$ and other unidentified ruthenium phosphine complexes. The compound $\text{H}_2\text{NMe}_2^+\text{Cl}^-$ was another product isolated from the methanol/benzene reaction mixture, and, together with the formation of complex **A** from the **3a** reaction with H_2 , provides evidence that the amine functionality of the P-N ligands is involved in the promotion of the heterolytic cleavage of dihydrogen to give a proton and a hydride ($\text{H}_2 \longrightarrow \text{H}^+ + \text{H}^-$); in fact, one of the goals of the original P-N ligand work was to determine if such a reaction might occur.²⁵ Another goal²⁵ was to determine the accessibility of the Ru(IV) state during reactions of Ru(II) with H_2 , and the demonstrated propensity of complexes **3** for $\eta^2\text{-H}_2$ complex formation suggests the possible participation of Ru(II) $\eta^2\text{-H}_2$ complexes in catalytic hydrogenation. Kinetic studies on the hydrogenation of 1-hexene catalyzed by **3a**,²⁵ and by **3b** in the present work, are now interpreted according to the mechanism:

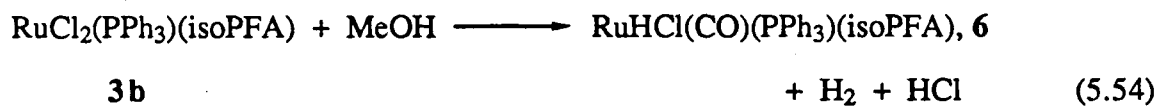




Reactions involving **3b** and methanol have also been studied, and **3b** is also active for the transfer hydrogenation (from methanol) of ketones and activated olefins. The reaction of **3b** with methanol in the absence of base is proposed to occur with the stoichiometry:

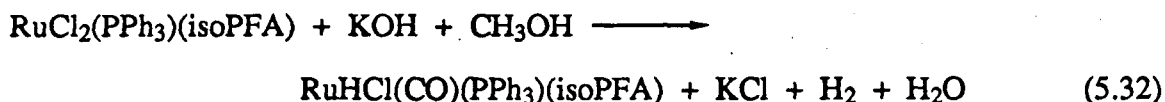


via the following steps:

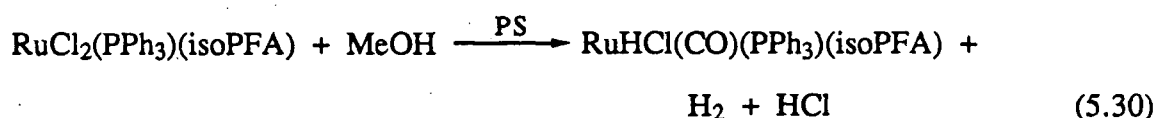
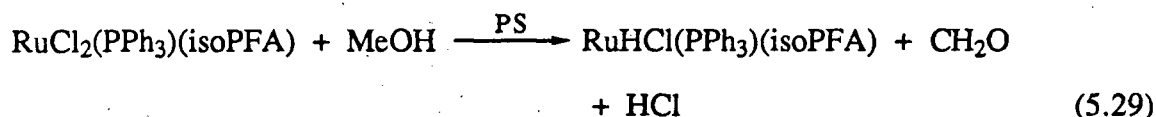


A mechanism for reaction 5.54 is presented (Fig. 5.47) and invokes reversible attack by MeOH, replacing Cl⁻, followed by reversible deprotonation of coordinated MeOH to give successively methoxo, formaldehyde and formyl intermediates, for which there is precedent in the literature,^{90,147-153} and finally the hydrido-carbonyl, **6**.

The reaction of **3b** with methanol in the presence of KOH is proposed to occur according to the stoichiometry:



and two pathways have been identified, one base-independent, identical to that proposed for reaction 5.54 (Fig. 5.47), and one showing a second-order dependence on KOH (Fig. 5.46). The latter pathway invokes initial reversible attack on $\text{RuCl}_2(\text{PPh}_3)(\text{isoPFA})$, **3b**, by MeO^- , replacing Cl^- to give $\text{RuCl}(\text{OMe})(\text{PPh}_3)(\text{isoPFA})$, and subsequent reversible replacement of PPh_3 by OH^- , followed by concerted loss of OH^- and hydride transfer from coordinated OMe^- to give a hydrido-formaldehyde complex $\text{RuHCl}(\eta^2\text{-CH}_2\text{O})(\text{isoPFA})$. A subsequently formed formyl intermediate reacts via intramolecular hydride transfer from the formyl to the metal, H_2 loss and phosphine coordination to give the hydrido-carbonyl **6**. The complex, $\text{RuHCl}(\text{PPh}_3)(\text{isoPFA})$, **7**, as well as **6**, is formed when Proton Sponge[®] rather than KOH is used as base; the Proton Sponge[®] reaction is tentatively accounted for by the stoichiometry:



Both reactions could occur via the pathway suggested for reaction 5.54, with Proton Sponge[®] promoting the deprotonation of coordinated MeOH. Unlike OH^- , Proton Sponge[®] does not coordinate to Ru to displace PPh_3 ; thus, in the PS reaction, an intermediate $\text{RuHCl}(\eta^2\text{-CH}_2\text{O})(\text{PPh}_3)(\text{isoPFA})$ (Fig. 5.47) dissociates CH_2O to give **7**. Thus, both KOH and Proton Sponge[®] act as proton acceptors, but differ in that, while OH^- displaces coordinated PPh_3 (Fig. 5.46), Proton Sponge[®] does not. In summary, the roles of KOH in reactions of **3b** with methanolic KOH solution are:

i) deprotonation of MeOH by OH^- to give H_2O , leading to methoxide attack on **3b**,

- ii) deprotonation of coordinated MeOH to give H₂O and a methoxo complex (Fig. 5.47),
- iii) supplying OH⁻ for the displacement of PPh₃ from an intermediate in the reaction (Fig. 5.46), and
- iv) supplying K⁺ for the formation of KCl, which is proven, perhaps for the first time, to be formed in a reaction involving a platinum metal chloro complex and alcoholic KOH.

The decarbonylation of methanol or other alcohols must involve several steps, even merely to break the four bonds associated with the CO group. In general, using platinum metal complexes, if a chloride is to be dissociated, and perhaps a phosphine as well, and also if two hydrogen atoms are to be transferred to a substrate, or alternately H₂ is eliminated, the total number of steps required for a mechanistic proposal becomes imposing. It is therefore desirable that the solution behaviour of the starting complex be simple, and RuCl₂(PPh₃)(isoPFA), **3b**, satisfies this requirement, as it is undissociated in solution, although dissociation is observed for analogous RuCl₂(PPh₃)(P-P) complexes.¹⁶⁹

Bibliography

- 1 Fieser, M.; Fieser, L.F. "Reagents for Organic Synthesis," Wiley, New York, vol. 1 - 12, 1967-.
- 1b Collman, J.P.; Hegedus, L.S.; Norton, J.R.; Finke, R.G. "Principles and Applications of Organotransition Metal Chemistry", University Science Books, Mill Valley, CA, 1987.
- 1c James, B.R. *Chem. Can.* 1978, 30, 13.
- 2 James, B.R. *Adv. Organomet. Chem.* 1979, 17, 319.
- 3 James, B.R. in "Comprehensive Organometallic Chemistry," vol. 8. Wilkinson, G., Stone, F.P.A., Abel, E.W., eds. Pergamon, Oxford, 1982. Chap. 51.
- 4 James, B.R. "Homogeneous Hydrogenation," J. Wiley and Sons, New York, 1973.
- 5 Ozin, G.A.; Garcia-Prieto, J. *J. Am. Chem. Soc.* 1986, 108, 3099.
- 6 Eisenschmid, T.C.; Kirss, R.V.; Deutsch, P.P.; Hommeltoft, S.I.; Eisenberg, R. *J. Am. Chem. Soc.* 1987, 109, 8089.
- 7 Eisenberg, R.; Kirss, R.U.; Eisenschmid, T. 3rd North American Chem. Congress, Toronto, 1988. Abstract No. 294.
- 7b Kirss, R.U.; Eisenschmid, T.C.; Eisenberg, R. *J. Am. Chem. Soc.* 1988, 110, 8564.
- 8 Butler, I.R.; Cullen, W.R.; Kim, T.-J. *Synth. React. Inorg. Met.-Org. Chem.* 1985, 15, 109.
- 9 Hayashi, T.; Mise, T.; Fukushima, M.; Kagotani, M.; Nagashima, N.; Hamada, Y.; Matsumoto, A.; Kawakami, S.; Konishi, M.; Yamamoto, K.; Kumada, M. *Bull. Chem. Soc. Jpn.* 1980, 53, 1138.

-
- 10 Yamamoto, K.; Wakatsuki, J.; Sugimoto, R. *Bull. Chem. Soc. Jpn.* 1980, 53, 1132.
- 11 Bishop, J.J.; Davison, A.; Katcher, M.L.; Lichtenberg, D.W.; Merrill, R.E.; Smart, J.C. *J. Organomet. Chem.* 1971, 27, 241.
- 12 Cullen, W.R.; Kim, T.-J.; Einstein, F.W.B.; Jones, T. *Organometallics* 1983, 2, 714.
- 13 McCulloch, B.; Ward, D.L.; Woolins, J.D.; Brubaker, Jr., C.H. *Organometallics* 1985, 4, 1425.
- 14 Aratani, T.; Gonda, T.; Nuzaki, H. *Tetrahedron Lett.* 1969, 2265.
- 15 Marquarding, D.; Kusacek, H.; Gokel, G.; Hoffmann, P.; Ugi, I. *J. Am. Chem. Soc.* 1970, 92, 5389.
- 16 Gokel, G.; Ugi, I. *J. Chem. Educ.* 1972, 49, 294.
- 17 Cullen, W.R.; Woolins, J.D. *Coord. Chem. Rev.* 1981, 39, 1.
- 18 Appleton, T.G.; Cullen, W.R.; Evans, S.V.; Kim, T.-J.; Trotter, J. *J. Organomet. Chem.* 1985, 279, 5.
- 19 Chalk, A.J.; Halpern, J. *J. Am. Chem. Soc.* 1959, 81, 5846.
- 20 Kim, T.-J. Ph.D. Thesis, University of British Columbia, Vancouver, 1984.
- 21 Dekleva, T.W. Ph.D. Thesis, University of British Columbia, Vancouver, 1983.
- 22 Cullen, W.R.; Einstein, F.W.B.; Huang, C.-H.; Willis, A.C.; Yeh, E.-S. *J. Am. Chem. Soc.* 1980, 102, 988.
- 23 Dekleva, T.W.; Thorburn, I.S.; James, B.R. *Inorg. Chim. Acta* 1985, 100, 49.
- 24 James, B.R.; Thompson, L.K.; Wang, D.K.W. *Inorg. Chim. Acta* 1978, 29, L237.
- 25 Rodgers, G.E.; Cullen, W.R.; James, B.R. *Can. J. Chem.* 1984, 61, 1314.
- 26 Hoffman, P.R.; Caulton, K.G. *J. Am. Chem. Soc.* 1975, 97, 4221.
- 27 Stephenson, T.A.; Wilkinson, G. *J. Inorg. Nucl. Chem.* 1966, 28, 945.

-
- 28 Charland, J.-P. Personal communication.
- 29 Kubas, G.J. *Acc. Chem. Res.* 1988, *21*, 120.
- 30 Ashworth, T.V.; Singleton, E. *J. Chem. Soc., Chem. Commun.* 1976, 705.
- 31 Kubas, G.J. *J. Chem. Soc., Chem. Commun.* 1980, 61.
- 32 Kubas, G.J.; Ryan, R.R.; Vergamini, P.J.; Wasserman, H. 185th Am. Chem. Soc. National Meeting, Seattle, 1983. Abstract INOR 229. Cited in reference 21.
- 33 *Chem. Eng. News*, 1983, *61(13)*, 4.
- 34 Crabtree, R.H.; Lavin, M. *J. Chem. Soc., Chem. Commun.* 1985, 794.
- 35 Morris, R.H.; Sawyer, J.F.; Shiralian, M.; Subkowski, J.D. *J. Am. Chem. Soc.* 1985, *107*, 5581.
- 36 Hamilton, D.G.; Crabtree, R.H. *J. Am. Chem. Soc.* 1988, *110*, 4126.
- 37 Bautista, M.T.; Earl, K.A.; Maltby, P.A.; Morris, R.H. *J. Am. Chem. Soc.* 1988, *110*, 4056.
- 38 Crabtree, R.H.; Hamilton, D.G. *J. Am. Chem. Soc.* 1986, *108*, 3124.
- 39 Henderson, R.A. *J. Chem. Soc., Chem. Commun.* 1987, 1670.
- 40 Jackson, S.A.; Upmacis, R.K.; Poliakoff, M.; Turner, J.J.; Burdett, J.K.; Grevels, F.-W. *J. Chem. Soc., Chem. Commun.* 1987, 678.
- 41 Bianchini, C.; Mealli, C.; Peruzzini, M.; Zanobini, F. *J. Am. Chem. Soc.* 1987, *109*, 5548.
- 42 Sweany, R.L.; Russell, F.N. submitted, quoted in reference 29.
- 43 Sweany, R.L.; Polito, M.A. 194th Am. Chem. Soc. National Meeting, New Orleans, LA; Am. Chem. Soc., Washington, D.C., 1987; quoted in reference 29.
- 44 Conroy-Lewis, F.M.; Simpson, S.J. *J. Chem. Soc., Chem. Commun.* 1987, 1675.
- 45 Hay, P.J. *J. Am. Chem. Soc.* 1987, *109*, 705.

-
- 46 Jean, Y.; Eisenstein, O.; Volatron, F.; Maouche, B.; Sefta, F. *J. Am. Chem. Soc.* 1986, *108*, 6587.
- 47 Burdett, J.K.; Phillips, J.R.; Pourian, M.R.; Poliakoff, M.; Turner, J.J.; Upmacis, R. *Inorg. Chem.* 1987, *26*, 3054.
- 48 Hampton, C.; Cullen, W.R.; James, B.R.; Charland, J.-P. *J. Am. Chem. Soc.* 1988, *110*, 6918.
- 49 Kubas, G.J.; Ryan, R.R.; Swanson, B.I.; Vergamini, P.J.; Wasserman, H.J. *J. Am. Chem. Soc.* 1984, *106*, 451.
- 50 Vergamini, P.J.; Wasserman, H.J.; Koetzle, T.; Kubas, G.J., manuscript in preparation, quoted in reference 51.
- 51 Kubas, G.J.; Unkefer, C.J.; Swanson, B.I.; Fukushima, E. *J. Am. Chem. Soc.* 1986, *108*, 7000.
- 52 Bautista, M.T.; Earl, K.A.; Maltby, P.A.; Morris, R.H.; Schweitzer, C.T.; Sella, A. *J. Am. Chem. Soc.* 1988, *110*, 7031.
- 53 Ricci, J.S.; Koetzle, T.F.; Bautista, M.T.; Hofstede, T.; Morris, R.H.; Sawyer, J.F. In preparation, quoted in reference 52.
- 54 Bianchini, C.; Mealli, C.; Peruzzini, M.; Zanobini, F. *J. Am. Chem. Soc.* 1987, *109*, 5548.
- 55 Simpson, J. Personal communication.
- 56 Hampton, C.; Dekleva, T.W.; James, B.R.; Cullen, W.R. *Inorg. Chim. Acta* 1988, *145*, 165.
- 57 Kubas, G.J.; Ryan, R.R.; Wroblewski, D.A.; *J. Am. Chem. Soc.* 1986, *108*, 1339.
- 58 Aresta, M.; Giannoccaro, P.; Rossi, M.; Sacco, A. *Inorg. Chim. Acta* 1971, *5*, 115.
- 59 Chinn, M.S.; Heinekey, D.M. *J. Am. Chem. Soc.* 1987, *109*, 5865.

-
- 60 Conroy-Lewis, F.M.; Simpson, S.J. *J. Chem. Soc., Chem. Commun.* 1987, 1675.
- 61 Bautista, M.; Earl, K.A.; Morris, R.H.; Sella, A. *J. Am. Chem. Soc.* 1987, *109*, 3780.
- 62 Crabtree, R.H.; Lavin, M.; Bonneviot, L. *J. Am. Chem. Soc.* 1986, *108*, 4032.
- 63 Bautista, M.T.; Earl, K.A.; Morris, R.H. *Inorg. Chem.* 1988, *27*, 1126.
- 64 Butler, I.R. Personal communication.
- 65 Thorburn, I.S. Personal communication.
- 66 Evans, D.; Osborn, J.A.; Jardine, F.A.; Wilkinson, G. *Nature* 1965, *208*, 1203.
- 67 Hallman, P.S.; Evans, D.; Osborn, J.A.; Wilkinson, G. *J. Chem. Soc., Chem. Commun.* 1967, 305.
- 68 Hallman, P.S.; McGarvey, B.R.; Wilkinson, G. *J. Chem. Soc. (A)* 1968, 3143.
- 69 James, B.R.; Rattray, A.D.; Wang, D.K.W. *J. Chem. Soc., Chem. Commun.* 1976, 792.
- 70 Wang, D.K.W. Ph.D. Thesis, University of British Columbia, Vancouver, 1978.
- 71 Thorburn, I.S. M. Sc. Thesis, University of British Columbia, Vancouver, 1980.
- 72 Markham, L.D. Ph. D. Thesis, University of British Columbia, Vancouver, 1973.
- 73 James, B.R.; Markham, L.D. *Inorg. Chem.* 1974, *13*, 97.
- 74 Hoffman, P.R.; Caulton, K.G. *J. Am. Chem. Soc.* 1975, *97*, 4221.
- 75 Caulton, K.G. *J. Am. Chem. Soc.* 1974, *96*, 3005.
- 76 Sasson, Y.; Blum, J. *J. Org. Chem.* 1975, *40*, 1887.
- 77 Poddar, R.K.; Agarwala, U. *Ind. J. Chem.* 1971, *9*, 1971; *J. Inorg. Nucl. Chem.* 1973, *35*, 567.
- 78 James, B.R.; Wang, D.K.W. *J. Chem. Soc., Chem. Commun.* 1977, 550.
- 79 Oki, M. "Applications of Dynamic NMR Spectroscopy to Organic Chemistry", vol. 4 of the series, "Methods in Stereochemical Analysis", Marchand, A.P., ed. VCH

Publishers, Deerfield Beach, FA, 1985. p. 407. The Eyring equation is given in the form: $\ln \frac{k}{T} = \ln \left(\kappa \frac{k_B}{h} \right) - \frac{\Delta H^\ddagger}{RT} + \frac{\Delta S^\ddagger}{R}$, where k is the rate constant, κ is the transmission coefficient, usually taken as unity, k_B is the Boltzmann constant, $1.381 \times 10^{-23} \text{ J K}^{-1}$, h is Planck's constant, $6.626 \times 10^{-34} \text{ Js}$, R is the gas constant, $8.314 \text{ J mol}^{-1}\text{K}^{-1}$ and T is absolute temperature.

- 79b Pople, J.A.; Schneider, W.G.; Bernstein, H.J. "High Resolution NMR", McGraw-Hill, New York, 1959.
- 80 Morris, R.H. Personal communication.
- 81 For $\text{RuHCl}(\text{PPh}_3)_3$, from reference 68, δ_{CDCl_3} (25 °C) -17.44 (q, $^2J_{\text{PH}} = 26 \text{ Hz}$).
From reference 21, δ_{CDCl_3} (30 °C) -17.78 (q, $^2J_{\text{PH}} = 26 \text{ Hz}$).
- 82 For $\text{RuHCl}(\text{P}(\text{p-tol})_3)_3$, from reference 21, $^1\text{H NMR } \delta_{\text{CDCl}_3}$ (30 °C) -17.78 (q, $^2J_{\text{PH}} = 26 \text{ Hz}$), $^{31}\text{P}\{^1\text{H}\} \text{ NMR } \delta_{\text{CD}_2\text{Cl}_2}$ (30 °C) 55.5. From references 21, 23, $^1\text{H NMR } \delta_{\text{C}_6\text{D}_6}$ (30 °C) -16.84.
- 83 Dekleva has noted a similar spectrum for a species he refers to as an "ABCD" complex. From reference 21, the $^{31}\text{P}\{^1\text{H}\} \text{ NMR}$ spectrum for this complex was $\delta_{\text{DMA/toluene-d}_8}$ (-60 °C) 58.9 (d, $J_{\text{PP}} = 22.5 \text{ Hz}$), 51.9 (d, $J_{\text{PP}} = 30 \text{ Hz}$), 41.7 (dd), 19.8 (dd).
- 84 Yawney, D.B.W.; Doedens, R.J. *Inorg. Chem.* 1972, 11, 838.
- 85 Mason, R.; Thomas, K.M.; Gill, D.F.; Shaw, B.L. *J. Organometal. Chem.* 1972, 40, C67.
- 86 Bennett, M.J.; Caulton, K.G.; Cotton, F.A. *Inorg. Chem.* 1969, 8, 1.
- 87 Mattson, B.M.; Heiman, J.R.; Pignolet, L.H. *Inorg. Chem.* 1976, 15, 564.
- 88 Dahl, L.F.; Rodulfo de Gil, E.; Feltham, R.D. *J. Am. Chem. Soc.* 1969, 91, 1653.
- 89 Kaesz, H.D.; Saillant, R.B. *Chem. Rev.* 1972, 72, 231.

-
- 90 Chaudret, B.N.; Cole-Hamilton, D.J.; Nohr, R.S.; Wilkinson, G. *J. Chem. Soc., Dalton Trans.* 1977, 1546.
- 91 Cole-Hamilton, D.J.; Wilkinson, G. *Nouv. J. Chim.* 1977, 1, 142.
- 92 Heinekey, D.M.; Payne, N.G.; Schulte, G.K. *J. Am. Chem. Soc.* 1988, 110, 2303.
- 93 Antinolo, A.; Chaudret, B.; Commenges, G.; Fajardo, M.; Jalon, F.; Morris, R.H.; Otero, A.; Schwetzer, C.T. *J. Chem. Soc., Chem. Commun.* 1988, 1210.
- 94 Chaudret, B.; Commenges, G.; Jalon, F.; Otero, A. *J. Chem. Soc., Chem. Commun.* 1989, 210.
- 95 Suzuki, H.; Omori, H.; Lee, D.H.; Yoshida, Y.; Moro-oka, Y. Proc. 6th Intern. Symp. on Homog. Catal., Vancouver, Canada, 1988. P-115.
- 95b A re-interpretation of the crystallographic data for this complex shows that all four bridging hydride ligands are, in fact, classical hydrides (see Marsh, R.E. *Organometallics* 1989, 8, 1583).
- 96 Arliguie, T.; Chaudret, B.; Morris, R.H.; Sella, A. *Inorg. Chem.* 1988, 27, 598.
- 97 Hauge, R.H.; Kafafi, Z.H.; Margrave, J.L. *Proceedings, The Physics and Chemistry of Small Clusters*, Richmond, VA, Oct. 1986. quoted in ref. 29.
- 98 Joshi, A. Personal communication.
- 99 Calvin, M. *J. Chem. Soc., Trans. Faraday Soc.* 1938, 34, 1181. Quoted in reference 3.
- 100 Roelen, O. U.S.Pat. 2 327 066 (1943). *Chem. Abstr.* 1944, 38, 550. Quoted in references 3, 101.
- 101 Halpern, J. *J. Organomet. Chem.* 1980, 200, 133.
- 102 Halpern, J.; Harrod, J.F.; James, B.R. *J. Am. Chem. Soc.* 1961, 83, 753.
- 103 Hui, B. C.-Y. Ph. D. Thesis, University of British Columbia, Vancouver, 1969.
- 104 Strathdee, G.; Given, R. *Can. J. Chem.* 1975, 53, 106.
- 105 Stolzenberg, A.M.; Muetterties, E.L. *Organometallics* 1985, 4, 1739.

-
- 106 Mestroni, G.; Zassinovich, G.; Camus, A. *J. Organomet. Chem.* 1977, 140, 63.
- 107 James, B.R.; Mahajan, D. *Can. J. Chem.* 1979, 57, 180.
- 108 Butler, I.; Hampton, C.; Cullen, W.R.; James, B.R.; Charland, J.-P. To be published.
- 109 LaPlaca, S.J.; Ibers, J.A. *Inorg. Chem.* 1965, 4, 778.
- 110 Fryzuk, M.D.; MacNeil, P.A. *Organometallics* 1983, 2, 682.
- 111 Charman, H.B.; *Nature* 1966, 212, 278.
- 112 Charman, H.B. *J. Chem. Soc., B* 1967, 629.
- 113 Dobson, A.; Robinson, S.D. *Inorg. Chem.* 1977, 16, 137.
- 114 Shinoda, S.; Itagaki, H.; Saito, Y. *J. Chem. Soc., Chem. Commun.* 1985, 860.
- 115 Yamamoto, H.; Shinoda, S.; Saito, Y. *J. Mol. Catal.* 1985, 30, 259.
- 116 Doughty, D.H.; Pignolet, L.H., in "Homogeneous Catalysis with Metal Phosphine Complexes" Pignolet, L.H., ed. Plenum Press, New York, 1983. Chap. 11.
- 117 Chatt, J.; Shaw, B.L.; Field, A.E. *J. Chem. Soc.* 1964, 3466.
- 118 Walker, J.F. "Formaldehyde," Reinhold, New York, 1964.
- 119 Noller, C.R. "Chemistry of Organic Compounds," 2nd ed. W.B. Saunders, London, 1957. p. 169.
- 120 Mannich, C.; Geilman, W. *Ber.* 1916, 49, 586.
- 121 Takahashi, T.; Shinoda, S.; Saito, Y. *J. Mol. Catal.* 1985, 31, 301.
- 122 Smith, T.A.; Aplin, R.P.; Maitlis, P.M. *J. Organomet. Chem.* 1985, 291, C13.
- 123 Morton, D.; Cole-Hamilton, D.J. *J. Chem. Soc., Chem. Commun.* 1988, 1154.
- 124 Linn, D.E.; Halpern, J. *J. Am. Chem. Soc.* 1987, 109, 2969.
- 125 Bailar, J.C.; Itatani, H. *J. Am. Chem. Soc.* 1967, 89, 1592. *Ibid.*, p. 1600.
- 126 Milstein, D. *J. Mol. Catal.* 1986, 36, 387.
- 127 Smith, T.A.; Maitlis, P.M. *J. Organomet. Chem.* 1984, 269, C7, and references therein.
- 128 Smith, T.A.; Maitlis, P.M. *J. Organomet. Chem.* 1985, 289, 385.
- 129 Imai, H.; Nishiguchi, T.; Fukuzumi, K. *J. Org. Chem.* 1976, 41, 665.

-
- 130 Chaudret, B.; Poilblanc, R. *J. Organomet. Chem.* 1979, 174, C51.
- 131 Speier, G.; Marko, L. *J. Organomet. Chem.* 1981, 210, 253.
- 132 Speier, G.; Marko, L. "Proc. Int. Conf. Coord. Chem., 16th" Dublin, Ire. 1974, 4.37.
- 133 Thorburn, I.S. Ph.D. Thesis, University of British Columbia, Vancouver, 1985.
- 134 Beaupere, D.; Nadjo, L.; Uzan, R. *J. Mol. Catal.* 1983, 20, 195, and references therein.
- 135 Beaupere, D.; Massoui, M.; Ralainirina, R.; Uzan, R. *Nouv. J. Chim.* 1986, 10, 493.
- 136 Massoui, M.; Beaupere, D.; Goethals, G.; Uzan, R. 1985, 33, 209.
- 137 Beaupere, D.; Nadjo, L.; Uzan, R.; Bauer, P. *J. Mol. Catal.* 1983, 20, 185.
- 138 Beaupere, D.; Nadjo, L.; Uzan, R.; Bauer, P. *J. Mol. Catal.* 1982, 14, 129.
- 139 Ohki, A.; Nishiguchi, T.; Fukuzumi, K. *Tetrahedron* 1979, 35, 1737.
- 140 Ohki, A.; Nishiguchi, T.; Fukuzumi, K. *J. Org. Chem.* 1979, 44, 766.
- 141 Beaupere, D.; Bauer, P.; Nadjo, L.; Uzan, R. *J. Organomet. Chem.* 1982, 238, C12.
- 142 Spogliarich, R.; Zassinovich, G.; Mestroni, G.; Graziani, M. *J. Organomet. Chem.* 1979, 179, C45.
- 143 Kvintovics, P.; James, B.R.; Heil, B. *J. Chem. Soc., Chem. Commun.* 1986, 1810.
- 144 Sasson, Y.; Blum, J. *J. Org. Chem.* 1975, 40, 1887.
- 145 Itagaki, H.; Saito, Y. *J. Mol. Catal.* 1987, 41, 209.
- 146 Dobson, A.; Moore, D.S.; Robinson, S.D.; Hawthorne, M.B.; New, L. *Polyhedron* 1985, 4, 1119.
- 147 Brown, K.L.; Clark, G.R.; Headford, C.E.L.; Marsden, K.; Roper, W.R. *J. Am. Chem. Soc.* 1979, 101, 503.

-
- 148 Collman, J.P.; Winter, S.R. *J. Am. Chem. Soc.* 1973, 95, 4089.
- 149 Nagao, H.; Aohagi, K.; Yukawa, Y.; Howell, F.S.; Mukada, M.; Kakihana, H. *Bull. Chem. Soc. Jpn.* 1987, 60, 3247.
- 150 Stasunik, A.; Malisch, W. *J. Organomet. Chem.* 1984, 270, C56.
- 151 Gillard, R.D.; Kaue-Maguire, L.A.P.; Williams, P.A. *J. Chem. Soc., Dalton Trans.* 1977, 1039.
- 152 Cole-Hamilton, D.J.; Stephenson, T.A. *J. Chem. Soc., Dalton Trans.* 1976, 2396.
- 153 Hayashi, Y.; Komiya, S.; Yamamoto, T.; Yamamoto, A. *Chem. Lett.* 1984, (8), 1363.
- 154 Jones, R.; Einstein, F.; Hampton, C.; Cullen, W.; James, B. To be published.
- 155 Dombek, B.D. *Ann. N.Y. Acad. Sci.* 1983, 415, 176.
- 156 Chatt, J.; Shaw, B.L.; Field, A.E. *J. Chem. Soc.* 1964, 3466.
- 157 Benedetti, E.; Bracci, G.; Shrana, G.; Solvetti, F.; Grassi, B. *J. Organomet. Chem.* 1972, 37, 361.
- 158 Bennett, M.; Milner, D.L.; *J. Am. Chem. Soc.* 1969, 91, 6983.
- 159 Parshall, G.W.; Knoth, W.H.; Schunn, R.A. *J. Am. Chem. Soc.* 1969, 91, 4990.
- 160 Cole-Hamilton, D.J.; Wilkinson, G. *J. Chem. Soc., Dalton Trans.* 1977, 797.
- 161 Hata, G.; Kondo, H.; Miyake, A. *J. Am. Chem. Soc.* 1968, 90, 2278.
- 162 Ainscough, E.W.; Robinson, S.D. *J. Chem. Soc. (D)* 1970, 863.
- 163 Valentine, J.S. *J. Chem. Soc., Chem. Commun.* 1973, 857.
- 164 Gosser, L.W. *Inorg. Chem.* 1975, 14, 1453.
- 165 Suess-Fink, G.; Reiner, J. *J. Mol. Catal.* 1982, 16, 231.
- 166 Skapski, A.C.; Troughton, P.G.H. *J. Chem. Soc., Chem. Commun.* 1968, 1230.
- 167 Tarasov, B.P.; Vergunova, N.G.; Belovodskii, V.P.; Blazhin, Yu.M.; Ogorodnikov, S.K. *Zh. Prikl. Khim.* 1986, 59, 1795.

-
- 168 Pavelek, Z. *Chem. Papers* 1988, 42, 299.
- 169 James, B.R.; Pacheco, A.; Rettig, S.J.; Thorburn, I.S. *J. Mol. Catal.* 1987, 41, 147.